

From the  
Comprehensive Pneumology Center (CPC) München  
of the Ludwig-Maximilians-Universität München  
Directors: PD Dr. Anne Hilgendorff and Dr. Ali Önder Yildirim



## **Molecular Analysis and Functional Profiling of SFRP1 as a Novel Regulator of Lung Fibrosis**

Dissertation zum Erwerb des Doctor of Philosophy (Ph.D.)  
an der Medizinischen Fakultät der Ludwig-Maximilians-Universität zu München

Submitted by

**Arunima Sengupta**

From Kolkata, India

2019



<b>Title of the thesis:</b>	Molecular Analysis and Functional Profiling of SFRP1 as a Novel Regulator of Lung Fibrosis
<b>Prepared in:</b>	Comprehensive Pneumology Center Max-Lebsche-Platz 31 81377 München
<b>PhD supervisors:</b> <b>(Helmholtz Zentrum München)</b>	Dr. Gerald Burgstaller Head of "Live Cell Imaging" core unit Comprehensive Pneumology Center Ph: +49 89 3187 4678 Email: <a href="mailto:gerald.burgstaller@helmholtz-muenchen.de">gerald.burgstaller@helmholtz-muenchen.de</a>  Dr. Ali Önder Yildirim Director of Institute Comprehensive Pneumology Center / Institute of Lung Biology and Disease Ph: +49 89 3187-4037 Email: <a href="mailto:oender.yildirim@helmholtz-muenchen.de">oender.yildirim@helmholtz-muenchen.de</a>
<b>First PhD supervisor:</b> <b>(LMU)</b>	Prof. Dr. Silke Meiners Head of research group "Proteasome Function in Chronic Lung Disease" Comprehensive Pneumology Center Ph: +49 89 3187-4673 Email: <a href="mailto:silke.meiners@helmholtz-muenchen.de">silke.meiners@helmholtz-muenchen.de</a>
<b>Second PhD supervisor:</b> <b>(LMU)</b>	PD Dr. Markus Rehberg Head of "In vivo imaging" Institute of Lung Biology and Disease - Comprehensive Pneumology Center Ph: +49-89-3187-49685 Email: <a href="mailto:markus.rehberg@helmholtz-muenchen.de">markus.rehberg@helmholtz-muenchen.de</a>
<b>Dean of medicine faculty:</b> <b>(LMU)</b>	Prof. Dr. med. dent. Reinhard Hickel
<b>Date of oral defense:</b>	30.04.2020



**“By our stumbling, the world is perfected.”**

-Sri Aurobindo





## Affidavit

Sengupta, Arunima

---

Surname, first name

CPC, Max-Lebsche-Platz 31, 81377 Munich, Germany

---

Address

I hereby declare, that the submitted thesis entitled

**“Molecular Analysis and Functional Profiling of SFRP1 as a Novel Regulator of Lung Fibrosis”**

is my own work. I have only used the sources indicated and have not made unauthorized use of services of a third party. Where the work of others has been quoted or reproduced, the source is always given.

I further declare that the submitted thesis or parts thereof have not been presented as part of an examination degree to any other university.

Bern, 13.07.2020

---

Place, Date

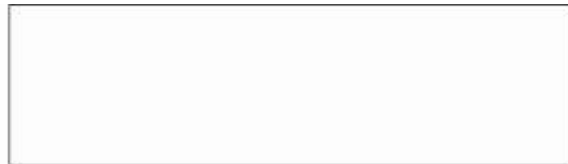
Arunima Sengupta

---

Signature doctoral candidate







## **Confirmation of congruency between printed and electronic version of the doctoral thesis**

Doctoral Candidate: **Arunima Sengupta**

Address: CPC, Max-Lebsche-Platz 31, 81377 Munich

I hereby declare that the electronic version of the submitted thesis, entitled is congruent with the printed version both in content and format.

Bern, 13.07.2020

---

Place, Date

Arunima Sengupta

---

Signature doctoral candidate



---

# TABLE OF CONTENTS

<b>Summary.....</b>	<b>1</b>
<b>1. Introduction</b>	
<b>1.1. Anatomy and physiology of the lung.....</b>	<b>3</b>
<b>1.2. Interstitial Lung Diseases (ILD).....</b>	<b>4</b>
<b>1.3. Idiopathic Pulmonary Fibrosis (IPF).....</b>	<b>4</b>
1.3.1. Diagnosis and treatment strategies of IPF.....	5
1.3.2. Histopathological features of IPF.....	7
1.3.3. IPF pathogenesis.....	8
1.3.4. Aberrant WNT signaling in IPF.....	11
1.3.5. Secreted Frizzled Related Proteins (SFRP's) in IPF.....	13
1.3.6. IPF disease models.....	13
<b>1.4. Lung fibroblasts.....</b>	<b>16</b>
1.4.1. Fibroblasts in wound healing.....	16
1.4.2. Activated fibroblasts in IPF.....	16
1.4.3. Transforming Growth Factor-beta (TGF $\beta$ ) signaling.....	18
<b>1.5. Extracellular matrix (ECM).....</b>	<b>20</b>
1.5.1. Aberrant ECM remodeling in IPF.....	21
<b>2. Objectives.....</b>	<b>22</b>
<b>3. Materials and Methods</b>	
<b>3.1. Materials.....</b>	<b>24</b>
3.1.1. Antibodies.....	24
3.1.1.1. Primary antibodies.....	24
3.1.1.2. Secondary antibodies.....	25
3.1.2. Primers.....	25
3.1.3. Small interfering RNA (siRNA).....	26
3.1.4. Cell lines.....	27

---

3.1.5.	Human cells and tissues.....	27
3.1.6.	Cell culture media.....	27
3.1.7.	Reagents and chemicals.....	27
3.1.8.	Buffer formulations.....	29
3.1.9.	Consumables.....	30
3.1.10.	Laboratory equipment and software.....	31
3.1.11.	Standards and Kits.....	33
<b>3.2.</b>	<b>Methods</b>	
3.2.1.	Cell biological methods	
3.2.1.1.	Isolation and culture of primary human lung fibroblast.....	34
3.2.1.2.	Cryopreservation of mammalian cells.....	34
3.2.1.3.	Thawing frozen cells.....	34
3.2.1.4.	MTT cell viability assay.....	35
3.2.1.5.	Liposome based cell transfection.....	35
3.2.1.6.	Cell culture treatments.....	36
3.2.1.7.	Preparation of cells for morphology analysis.....	37
3.2.2.	3D cell culture models	
3.2.2.1.	Preparation of collagen matrix.....	37
3.2.2.2.	3D collagen-based invasion assay.....	37
3.2.3.	Animal experiments	
3.2.3.1.	Isolation of murine fibroblasts.....	38
3.2.3.2.	Bleomycin instillation in mice.....	39
3.2.3.3.	Tissue homogenization.....	39
3.2.3.4.	Preparation of mouse Precision Cut Lung Slices.....	40
3.2.3.5.	Preparation of human Precision Cut Lung Slices.....	40
3.2.4.	Cultivation of 3D <i>ex vivo</i> mPCLS.....	40
3.2.5.	Decellularization of mPCLS.....	40
3.2.6.	Recellularization of mPCLS.....	41
3.2.7.	<i>Ex vivo</i> fibrosis-mimicking mPCLS models.....	41

---

3.2.8. Protein analysis	
3.2.8.1. Protein isolation from fibroblasts in 2D cell culture.....	41
3.2.8.2. Concentration of protein from cell supernatants.....	42
3.2.8.3. Protein isolation from fibroblasts in 3D cell culture.....	42
3.2.8.4. Protein extraction from PCLS.....	42
3.2.8.5. Protein isolation from lung tissues.....	43
3.2.8.6. Bicinchoninic acid (BCA) assay.....	43
3.2.8.7. SDS-PAGE and immunoblotting.....	43
3.2.8.8. RhoA G-LISA assay.....	44
3.2.8.9. Proteomic screening.....	44
3.2.8.10. Immunofluorescence staining in primary human lung fibroblast.....	44
3.2.8.11. Immunofluorescence staining of paraffin-embedded tissue sections.....	45
3.2.8.12. Immunofluorescence staining of PCLS.....	45
3.2.9. RNA analysis	
3.2.9.1. mRNA isolation from primary fibroblasts.....	46
3.2.9.2. mRNA isolation from 3D cell culture.....	46
3.2.9.3. mRNA isolation from PCLS.....	46
3.2.9.4. cDNA synthesis by Reverse Transcription.....	47
3.2.9.5. Quantitative Real Time Polymerase Chain Reaction (qRT-PCR).....	47
3.2.9.6. Microarray.....	48
3.2.10. In silico analysis	
3.2.10.1. Analysis of cell morphology.....	48
3.2.10.2. Quantification of 3D cellular invasion.....	48
3.2.10.3. Bioinformatical analysis.....	49
3.2.10.4. Statistical analysis.....	49
<b>4. Chapter A: Characterization of SFRP1 as a novel regulator of lung fibrosis</b>	
<b>4.1. Introduction.....</b>	<b>50</b>
<b>4.2. Results.....</b>	<b>51</b>
4.2.1. <u>Part I: Role of SFRP1 in lung fibrosis</u>	

4.2.1.1.	Upregulation of SFRP1 in a mouse fibrosis model.....	51
4.2.1.2.	SFRP1 is heterogeneously expressed in IPF patients.....	53
4.2.1.3.	<i>Ex vivo</i> lung injury models demonstrate an enhanced SFRP1 expression.....	56
4.2.2.	<u>Part II: Functional characterization of SFRP1 in lung fibroblasts</u>	
4.2.2.1.	Molecular signature of the invasome in lung fibroblasts.....	58
4.2.2.2.	Invading fibroblasts show reduced SFRP1 expression in primary human fibroblasts.....	61
4.2.2.3.	TGF $\beta$ 1 downregulates SFRP1 expression in fibroblasts.....	62
4.2.2.4.	SFRP1 expression in lung fibroblast is not regulated epigenetically.....	65
4.2.2.5.	SFRP1 is a negative regulator of fibroblast invasion.....	69
4.2.2.6.	SFRP1 regulates distinct genes and proteins related to the actin cytoskeleton.....	72
4.2.2.7.	Lack of SFRP1 alters RhoA expression and activity in fibroblasts.....	76
4.2.2.8.	SFRP1 depleted human lung fibroblasts display morphological changes <i>in vitro</i> .....	77
4.2.3.	<u>Part III: SFRP1 expression in distinct fibroblast sub-populations</u>	
4.2.3.1.	In the lung mostly fibroblasts exclusively express SFRP1.....	79
4.2.3.2.	Single cell clones derived from healthy primary human fibroblasts can be classified according to their SFRP1 expression.....	82
4.2.3.3.	Single cell RNA sequencing validates SFRP1 expression in $\alpha$ SMA negative fibroblast subtypes in the diseased lung.....	83
<b>4.3.</b>	<b>Discussion</b>	
4.3.1.	Regulation of SFRP1 in fibrosis models.....	87
4.3.2.	SFRP1 as a modulator of fibroblast invasion.....	88
4.3.3.	Epigenetic regulation of SFRP1 expression in lung fibroblasts.....	90
4.3.4.	TGF $\beta$ 1-induced regulation of SFRP1 expression.....	91
4.3.5.	Potential role of RhoA activation in regulation of cellular morphology and invasion of SFRP1 depleted fibroblasts.....	94
4.3.6.	SFRP1 expression in distinct fibroblast sub-populations.....	96
<b>5.</b>	<b>Chapter B: Validation of a pre-clinical <i>ex vivo</i> tool to confirm novel targets in IPF</b>	
<b>5.1.</b>	<b>Introduction.....</b>	<b>99</b>
<b>5.2.</b>	<b>Results.....</b>	<b>99</b>

---

5.2.1. Enrichment of fibrosis-related markers in mPCLS injury model.....	99
5.2.2. Analysis of an anti-fibrotic drug in the mPCLS injury model model.....	103
<b>5.3. Discussion.....</b>	<b>104</b>
<b>6. Chapter C: Studying instructiveness of ECM in 3D-LTCs</b>	
<b>6.1. Introduction.....</b>	<b>107</b>
<b>6.2. Results.....</b>	<b>108</b>
6.2.1. Validating effective decellularization of <i>ex vivo</i> mouse 3D-Lung tissue cultures (LTCs).....	108
6.2.2. Fibroblasts engrafted into decellularized ECM show a different protein expression profile.....	109
6.2.3. Repopulated fibroblasts adhere to d3D-LTCs by forming focal adhesion contacts.....	111
6.2.4. Specific niches within the microenvironment of 3D-LTCs modulate the morphology of repopulated fibroblasts.....	113
6.2.5. Engrafted fibroblasts demonstrate altered 3D migration in distinct ECM niches.....	114
<b>6.3. Discussion.....</b>	<b>116</b>
<b>7. Conclusion and future direction.....</b>	<b>119</b>
<b>8. References.....</b>	<b>122</b>
<b>9. Abbreviations.....</b>	<b>138</b>
<b>10. Acknowledgement.....</b>	<b>141</b>





## Summary

Idiopathic pulmonary fibrosis (IPF) is a severe and fatal Interstitial Lung disease (ILD) characterized by a progressive scarring of the lung. Many questions regarding the etiology and pathogenesis of this disease still remain unsolved. The current inflammatory theory suggests a deregulated communication between the mesenchymal and epithelial components due to lung injury which finally advances to an irreversible process of fibrosis and tissue remodeling. Inflammatory mediators, such as TGF $\beta$ 1, trigger the activation of fibroblasts which then migrate into the intra-alveolar space, proliferate, and subsequently as myofibroblasts massively deposit extracellular matrix (ECM). Ultimately, this results in impairment of gas exchange and death by asphyxiation. Hence, the dynamic process of tissue remodeling depends on an activated, versatile invasive fibroblast phenotype.

Secreted frizzled-related protein 1 (SFRP1), a Wnt signaling pathway inhibitor was identified as a negative regulator of fibroblast invasion (Oehrle et al., 2015). SFRP1 expression was elevated in the course of fibrosis in the bleomycin-induced (Bleo) mouse model (Schiller et al., 2015). Here, the role of SFRP1 was investigated in the first chapter with particular focus on the regulation and cellular molecular function of SFRP1 in lung fibrosis. First, the expression of SFRP1 was analyzed in fibrotic mouse (Bleomycin-induced fibrosis model) and IPF patient tissue resections. Additionally, *ex vivo* fibrosis-mimicking mouse and human PCLS systems were employed to investigate SFRP1 expression in fibrotic conditions. The data provided in the thesis revealed that SFRP1 was expressed in the early phase of fibrosis and strongly upregulated in the fibrogenesis process. Next, the molecular function of SFRP1 was assessed in specific lung fibroblast populations. The in-depth investigation revealed a cross-talk between SFRP1 and the pro-fibrotic regulator TGF $\beta$ 1, where TGF $\beta$ 1-activated (myo) fibroblasts indicated significantly reduced expression of SFRP1. Moreover, contrary to numerous observations in cancer cells, classical epigenetic mechanisms were demonstrated to be uninvolved in the regulation of SFRP1 in lung fibroblasts. Finally, three subtypes of lung fibroblast population were identified based on their characteristic SFRP1 expression: SFRP1<sup>low</sup>, SFRP1<sup>high</sup> and SFRP1<sup>med</sup> (medium expression). Among them, SFRP1<sup>low</sup> fibroblasts that were shown to be highly invading also demonstrated significant reduction in RhoA expression and activation. Interestingly, SFRP1<sup>high</sup> fibroblasts were indicated to be highly distinct from  $\alpha$ SMA<sup>high</sup> myofibroblasts in fibrotic and healthy mouse and human cells and tissues.

The second topic of the thesis marked the development of an injury and/or early fibrosis-mimicking *ex vivo* tool to pre-clinically test compounds with antifibrotic activity. Precision cut lung slices (PCLS) present a sophisticated system that can bridge the gap between *in vitro* and pre-clinical *in vivo* studies.

Hence, utilizing this ex vivo tool, mouse PCLS were stimulated with a pro-fibrotic cocktail to mimic early fibrosis conditions. After treatment with the pro-fibrotic cocktail, specific fibrosis related biomarkers, including SFRP1, were found upregulated in this 3D model. Finally, by applying the anti-inflammatory and anti-fibrotic drug Tranilast, I could demonstrate that the upregulation of the before mentioned fibrosis related markers was inhibited.





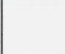

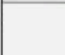



The final topic of my thesis analyzed the functional interplay between the extracellular matrix niche and the embedded cells. A 3D cell culture ECM model was developed using decellularized lung tissue scaffolds from healthy and diseased mouse lungs of 300µm thickness. The engrafted primary human and mouse lung fibroblasts revealed interesting morphological plasticity based on distinct ECM niches. Furthermore, it was demonstrated that attachment of the fibroblasts to decellularized ex vivo lung scaffolds was deployed via focal adhesions. Additionally, the repopulated fibroblasts demonstrated differential migratory behavior based on their surrounding ECM niche along with deregulated expression of certain migration-related markers.

In summary, the results obtained in the thesis revealed SFRP1 as a potential early biomarker for lung fibrosis. SFRP1<sup>low</sup> and SFRP1<sup>high</sup> fibroblast populations regulated by lung injury and/or TGFβ1 stimulation were demonstrated to substantially affect lung fibroblast invasion, RhoA protein expression and activation and extent cell morphology. In fibrotic lung tissues of human and murine origin, an overall increase in SFRP1 expression was observed, which could be attributed to certain fibroblast subpopulations by scRNAseq technology, as well as confirmative stainings. Besides, innovative ex vivo tools were developed that could aid in extending the current knowledge in drug discovery as well as understanding chronic lung disease pathogenesis.

# 1. Introduction

## 1.1. Anatomy and physiology of the lung

The lungs are a pair of elastic, porous organs located on each side of the thorax which is responsible for gaseous exchange between the circulatory system and the environment. The lungs when fully expanded contain approximately 6 L of air [1]. The pleural membrane divides the lungs on the right and left with upper, middle and lower lobes and with upper and lower lobes respectively. When the air is taken in, it passes through the upper airways consisting of nasal cavity, pharynx and larynx and then subsequently passes to the lower airways encompassing the trachea, primary bronchi and the bronchial tree. From there onwards, the air travels into the small bronchioles and alveoli within the lung tissues. The conducting zone comprises of the airway regions that begin with the trachea and do not undergo any gaseous exchange. The trachea bifurcates into the two main bronchi which segregate into an array of bronchial and bronchiolar airways [1]. The peripheral airways are trailed by the respiratory bronchioles which is a transitional region and displays both alveolar and bronchial features (Fig.1.1). The alveoli are the functional units for gas exchange and are present in the terminal parts of the bronchi. The airway wall in the terminal end is comprised of alveoli which are referred to as alveolar ducts. These ducts are lined with alveoli which are called alveolar sacs. There are roughly 300 million alveoli present within the lungs within a total surface area of approximately 90 m<sup>2</sup> [1].

	Anatomy	Structure	Generation (Z)	Cell Types
Conducting zone		Larynx	N/A	<ul style="list-style-type: none"> <li>Ciliated cells</li> <li>Goblet cells</li> <li>Basal cells</li> </ul>
		Trachea	0	<ul style="list-style-type: none"> <li>Ciliated cells</li> <li>Goblet cells</li> <li>Basal cells</li> <li>Serous cells</li> <li>Serous gland cells</li> <li>Mucous gland cell</li> </ul>
		Primary bronchi	1	<ul style="list-style-type: none"> <li>Ciliated cells</li> <li>Goblet cells</li> <li>Basal cells</li> <li>Serous cells</li> </ul>
		Secondary bronchi	2	
		Tertiary bronchi	3	
		Small bronchi	4	
		Bronchioles	5	<ul style="list-style-type: none"> <li>Ciliated cells</li> <li>Clara cells</li> <li>Basal cells</li> </ul>
		Terminal bronchioles	6-16	
Respiratory zone		Respiratory bronchioles	17-19	<ul style="list-style-type: none"> <li>Ciliated cells</li> <li>Clara cells</li> <li>Basal cells</li> <li>Alveolar type I cells</li> <li>Alveolar type II cells</li> </ul>
		Alveolar sacs	23	<ul style="list-style-type: none"> <li>Alveolar type I cells</li> <li>Alveolar type II cells</li> </ul>

**Fig 1.1: Conducting and respiratory zone of the human respiratory system**

The conducting zone is composed of the trachea, bronchi and terminal bronchioles. Gaseous exchange does not take place in this region. The respiratory zone comprises of respiratory bronchioles, the alveolar ducts and alveolar sacs. This is the region for gaseous exchange between the lung and capillaries. Upto 23 generations of airway branching can occur (BéruBé et al., 2010).

The boundary that separates the pulmonary capillaries from air in the alveoli is composed of endothelial cells, a constricted interstitial space and epithelial cells. There are two types of alveolar epithelial cells present in the lung namely alveolar type I (AT I) type II (AT II) cells. The AT I cells are responsible for gas exchange in the alveolus and the AT II cells are the progenitor cells that synthesize and secrete the components required for the pulmonary surfactant [3].

**1.2. Interstitial Lung Diseases (ILD)**

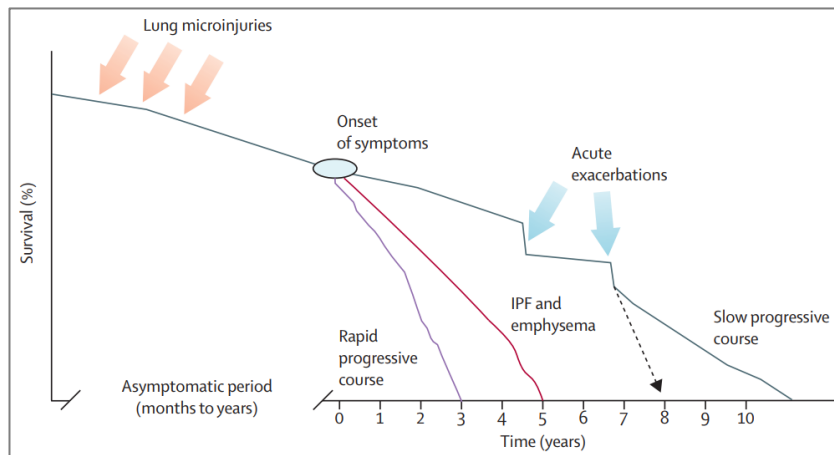
Interstitial lung disease (ILD) is an umbrella term which comprises of chronic pulmonary disorders characterized by diffuse infiltrates, scarring of alveolar structures and finally loss of functional gas exchange units. The term “interstitial” is however a misnomer, as these disorders are not just confined to the alveolar Interstitium [4]. The alveolar region surrounded by the alveolar epithelial cells on one side and endothelial basement membranes on the other is called the interstitium. It is composed of several connective tissue components, mesenchymal cells, inflammatory cells and immune effector cells [5]. The term ILD entails more than 150 different sub-groups having the same pathological, physiological and clinical manifestations but different underlying etiologies. ILDs are classified according to their causes like inhaled inorganic or organic substances, radiation exposure, drug induced, certain connective tissue disorders, certain infections or idiopathic [6].

**1.3. Idiopathic Pulmonary Fibrosis (IPF)**

Idiopathic pulmonary fibrosis (IPF) is a chronic, progressive and devastating lung disease of unknown etiology where patients have a median survival rate of 3-5 years from the time of diagnosis. IPF is the most prevalent form of ILD that affects almost 1.25 – 23.4 people per 100,000 population in Europe with a higher frequency in men than women [7]. The incidence rate rises dramatically with age as evidenced in the United States where surprisingly 0.2% of the population older than 75 years is already affected with IPF [8]. Although the cause of IPF is unknown, a correlation with the environmental triggers like cigarette smoke, exposure to wood or metal dust, radiation exposure has been reported. In addition, several comorbid conditions like obesity, diabetes mellitus, gastroesophageal reflux, pulmonary hypertension, obstructive sleep apnoea, coronary artery disease and emphysema have yet undefined effects on the clinical course of IPF [9].

### 1.3.1. Diagnosis and treatment strategies of IPF

Experts from multiple disciplines like pulmonology, radiology and pathology have to come together for diagnosing IPF. A pattern indicative of any usual or idiopathic interstitial pneumonia with known occupational or environmental triggers or any other systemic disease related needs to be excluded [9]. There currently exists four diagnostic criteria according to the high-resolution tomography (HRCT) studies of the lung: usual interstitial pattern (UIP), intermediate pattern, probable UIP pattern and an alternate diagnosis [10]. However, biomarkers from blood samples or Broncho alveolar lavage (BAL) for efficient diagnosis and outcome prediction are poorly defined. A rapid decline of forced vital capacity (FVC), which is the maximal volume of gas that can be forcefully exhaled after a full inhalation, has been shown to be associated with the poor prognosis in IPF [11]. The origin and progression of the disease varies greatly among the individual patients and cannot be foreseen during diagnosis. Some individuals present a slow progression and manifestation rate where others display chronic exacerbations comparably early from the time of diagnosis (Fig.1.2) [9].



**Figure 1.2: Schematic demonstration of potential progression and clinical development of IPF**

The natural history pattern in IPF patients is very heterogeneous in nature. Majority of the patients experience a relatively slow disease progression along with slow lung function decline after diagnosis. However around 10% of the patients present rapid disease progression and displays acute clinical lung deterioration comparably early from the time of diagnosis [9].

Despite the strong research efforts over the past few decades, no efficient pharmaceutical therapy has been discovered till date. Diagnosis for IPF is generally hard as the symptoms resemble other lung diseases. The treatment for IPF are divided into pharmacological and non-pharmacological strategies. Although the ATS-ERS committee guidelines in the year 2011 accepted oxygen therapy for long-term care and lung transplantation, only a few patients qualify for lung transplantation [12]. The non-pharmacological treatments available for IPF patients are non-invasive ventilation (NIV) along with oxygen therapy where the patients benefit from less breathlessness, fatigue and improved quality of life. Pulmonary rehabilitation and symptom management are undertaken by doctors to improve the overall

quality of life, whereas lung transplantation is a major procedure that will significantly improve the life expectancy of the IPF patients. But due to the shortage of donor lungs and the rigid criteria of the transplant centers, most people living with the disease do not get to receive a transplant [13]. All the important non-pharmacological treatment options for IPF are summarized in Table 1.1.

**Table 1.1: Non-pharmacological treatments for IPF**

<i><b>Treatment</b></i>	<i><b>Description</b></i>
<b>Non-invasive ventilation and Oxygen therapy</b>	IPF causes levels of oxygen to fall in the blood and when they drop below 88%, high-flow oxygen through nasal cannula and noninvasive ventilation (NIV) are potential options then.
<b>ECMO</b>	Patients are supported by extracorporeal membrane oxygenation (ECMO), while waiting for a lung transplant.
<b>Pulmonary rehabilitation</b>	It includes, breathing exercises, managing anxiety, stress and depression along with nutritional counseling.
<b>Symptom management</b>	The patients are treated for specific symptoms like coughing, gastro-esophageal reflux, breathlessness and anxiety.
<b>Lung transplant</b>	The restoration of one or both the lungs from a donor is termed as lung transplantation.

*Modified from [13] and [14].*

Although, anti-inflammatory agents like prednisolone and azathioprine was recommended for standard use by the ATS-ERS guidelines in the year 2020, the side-effects of these compounds could not be pacified. Table 1.2 shows some important medicinal and biological agents currently in use for the treatment of IPF. The efficacy of these established management strategies is largely untested and hence mortality rate continues to be high. Newer strategies which targets inflammatory mediators, pro-fibrogenic mediators, fibroblast proliferation and activation, and autoimmunity needs to be examined and alternative safe approaches has to be established.

Table 1.2: Pharmacological treatments for IPF

<i>Agents</i>	<i>Mode of action</i>
<b>Pirfenidone</b>	Inhibitor of TGF $\beta$ , anti-inflammatory and antioxidant
<b>Nintedanib (BIBF1120)</b>	Multiple tyrosine kinase inhibitor
<b>Corticosteroids (prednisone)</b>	Anti-inflammatory and immunosuppressant
<b>Mycophenolate (mofetil)</b>	Anti-inflammatory and immunosuppressant
<b>Azathioprine</b>	Anti-inflammatory and immunosuppressant
<b>Carlumab</b>	CCL2 inhibitor
<b>Ethanercept</b>	Receptor antagonist of TNF
<b>Imatinib</b>	Tyrosine kinase inhibitor
<b>Pamrevlumab</b>	Monoclonal antibody against CTGF
<b>Thalidomide</b>	Inhibitor of TGF $\beta$ 1 signaling and VEGF expression
<b>GS-6624</b>	Anti-LOXL2 antibody
<b>Doxycycline</b>	MMP inhibitor
<b>GC1008</b>	Anti-TGF $\beta$ 1-3 antibody

*Modified from [13], [15] and [16].*

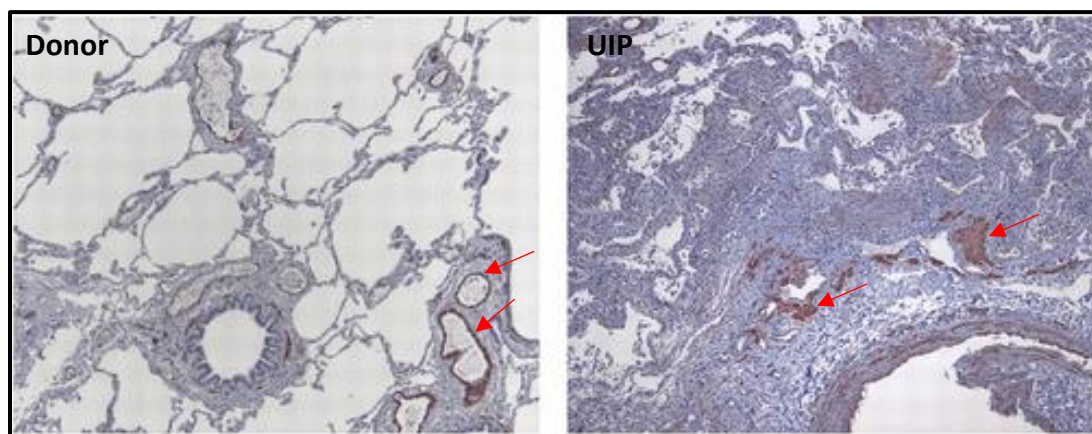
Currently there are two prescribed anti-fibrotic drugs: Pirfenidone and Nintedanib that have been approved by the European Medicines Agency (EMA, 2011/2014) and the US Food and Drug Administration (FDA, 2015/2014). Although they slow down development of scar tissue and IPF progression, however they are not able to halt or reverse the lung damage. Thus, the only successful intervention for IPF until today is lung transplantation [17].

### 1.3.2. Histopathological features of IPF

The ATS consensus report in the year 2011 reported IPF to be associated with the pathological features of UIP [12]. UIP represents a spatial and temporal heterogeneity where the lung upon injury displays a

different pattern in the periphery from that of the center of the pulmonary lobule. The sub-pleural or paraseptal regions are affected by scarring and microscopic honeycombing and they intersect abruptly within normal lung tissue. Honeycombs are huge airspaces that are lined with bronchiolar epithelium that are filled with mucous and inflammatory cells such as macrophages and neutrophils [18]. The glossary from Fleischner society defined honeycombing as fibrotic lung tissues that contained several cystic airspaces along with thick walls and basically represented the end stage of various chronic lung diseases [19].

One of the important hallmarks of UIP are fibroblastic foci characterized by the accumulation of hyper proliferative, activated fibroblasts and myofibroblasts covered by hyperplastic alveolar and bronchial epithelial cells. These fibrotic lesions are histopathologically detected by their expression of alpha smooth muscle actin ( $\alpha$ SMA) (Fig.1.2). These small and distinct fibroblastic foci are located between alveolar and interstitial regions of the lung and their formation is connected to the lung injury sites. The number of fibroblastic foci is associated with increased disease activity and progression.



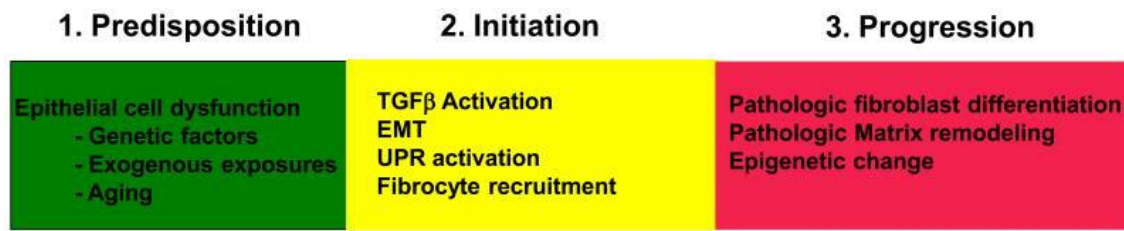
**Figure 1.3: Histopathological appearance of UIP**

Immunohistochemical staining for alpha smooth muscle actin ( $\alpha$ SMA) of tissue sections from a normal donor lung (left panel) and a lung with usual interstitial pneumonia (UIP) pattern (right panel). The  $\alpha$ SMA-staining in brown is indicated with red arrows. Intense signal for  $\alpha$ SMA (red arrow) is seen in the fibroblastic foci of the UIP lung (*modified* from Eickelberg and Laurent 2010).

### 1.3.3. IPF pathogenesis

According to current perception, IPF results from impaired and non-resolved wound healing coupled with excessive extracellular matrix (ECM) deposition and accumulation, decreased (myo) fibroblasts apoptosis and chaotic epithelial cell repair [20]. The main driver for fibrogenesis is inflammation and there is increasing evidence for strong contribution of the inflammatory cells in tissue injury and repair [21]. However, with failures of anti-inflammatory therapeutic approaches, people started to consider IPF more strongly driven by an aberrant wound healing process instead [11]. The pathophysiology of IPF can be subdivided into three stages: predisposition, initiation and progression (Fig 1.4).





**Figure 1.4: Pathophysiological stages of IPF**

IPF pathogenesis can be categorized into three distinct stages. The first pre-disposition stage comprises environmental triggers (normal or occupational), gene mutations and aging which is able to influence a person to develop lung fibrosis. The next initiation phase involves pro-fibrotic events, such as activation of TGF- $\beta$ , resident fibroblast recruitment, epithelial-to-mesenchymal transition (EMT), and initiation of the unfolded protein response (UPR). Finally, the progression phase includes molecular events which leads directly to fibrosis, like fibroblast activation and transdifferentiation, dysregulated matrix deposition and remodeling, increased matrix stiffness, and other pro-fibrotic epigenetic changes. [8]

Despite an extensive understanding of IPF, the exact causative mechanisms of the disease yet remain elusive. According to the current concept, persistent micro-injuries to the lung epithelium along with a combination of environmental stressors, viral or age-related disorders or a genetic predisposition triggers the onset of IPF [22]. In another large genome wide-associated study in 2011, a significant alteration was found with the SNP rs35705950, which is located upstream of the mucin 5B (MUC5B) gene on chromosome 11. This alteration was found in 34% of the IPF patients and led to 37.4 folds higher expression of MUC5B in the IPF lungs. However, the molecular consequences related to dysregulated MUC5B expression is yet to be known [23]. Other common genetic variants are listed in Table 1.3. Additional recent studies have uncovered several rare genetic variants as well in at least 11 loci in IPF which are summarized in Table 1.4.

**Table 1.3: Common gene variants in IPF**

<i>Risk allele(s)</i>	<i>Gene</i>	<i>Gene function</i>	<i>References</i>
rs408392, rs419598, rs2637988	IL1RN	Inhibitor of pro-inflammatory effect of IL-1alpha and IL-1beta	[24]
rs4073, rs2227307	IL8	Pro-inflammatory cytokine	[25] [26]
rs2609255	FAM13A	Signal transduction	[27]
rs2736100	TERT	Maintains telomere length	[24]
rs35705950	MUC5B	Airway defense by mucus production and mucociliary transport	[24]
rs7934606	MUC2	Mucin production	[27]

<b>rs111521887,</b> <b>rs5743894, rs2743890</b>	TOLLIP	Moderator of innate immune responses mediated by toll-like receptor and the transforming growth factor $\beta$ signaling pathway	[26]
<b>rs2076295</b>	DSP	Tightly links adjacent cells	[27]

Modified from [28].

**Table 1.4: Rare gene variants in IPF**

<i>Gene</i>	<i>Gene function</i>	<i>Pathological consequences</i>	<i>References</i>
<b>SFTPC</b>	Component of surfactant fluid	Altered trafficking with disrupted proteostasis and increased ER stress	[24] [29]
<b>SFTPA2</b>	Modulates innate and adaptive immunity	Increased ER stress	[30] [31]
<b>ABCA3</b>	Transport lipids across plasma membrane	Retention of lipids in the ER, ER stress, and apoptotic signaling	[32]
<b>TERT</b>	Enzyme in telomerase complex	Telomere shortening	[24] [33]
<b>TERC</b>	Template in telomerase complex	Telomere shortening	[24] [33]
<b>DKC1</b>	Stabilizes the template in telomerase complex	Telomere shortening	[34] [24]
<b>TINF2</b>	Telomere maintenance	Telomere shortening	[35] [36]
<b>RTEL1</b>	DNA helicase	Telomere shortening	[35] [37]
<b>PARN</b>	mRNA stability	Telomere shortening	[38] [35]

Modified from [28].

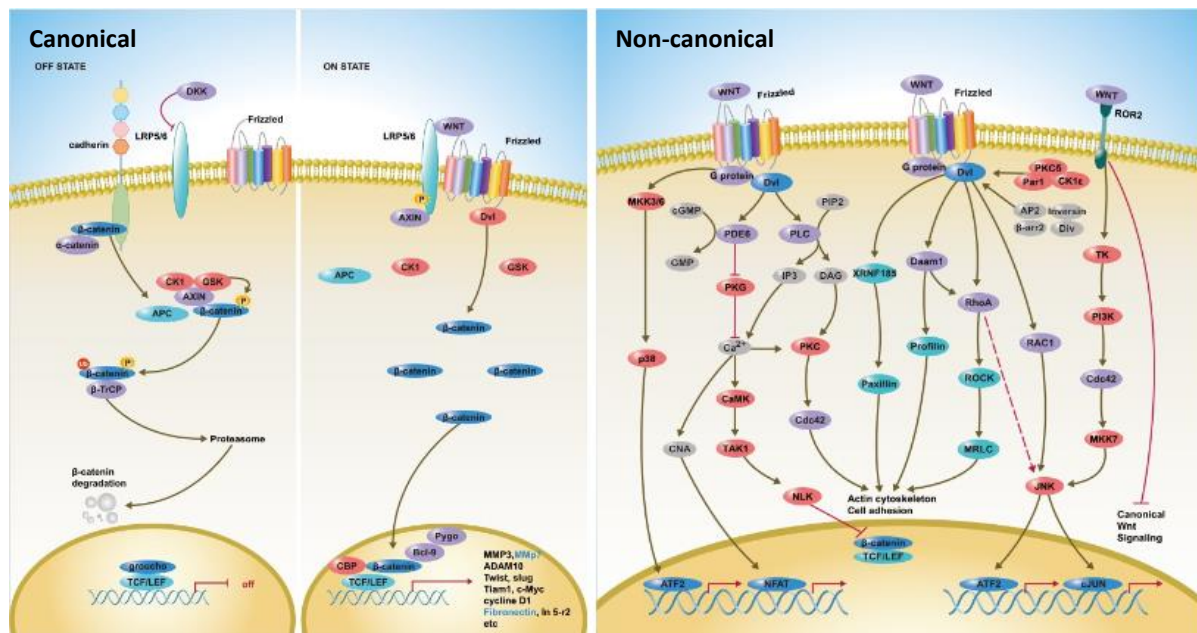
Furthermore, epigenetic changes like DNA methylation [39] and microRNA expression changes are also considered to contribute to disease progression. Several factors that contribute to dysregulated fibrinolysis include matrix metalloproteinases (MMPs), tissue inhibitor of metalloproteinases (TIMPs), oxidative stress and imbalance of different pro-fibrotic cytokines or chemokines along with accumulation of activated fibroblasts, leading to a perpetuating alveolar collapse which contributes significantly to the disease progression [40]. Although a detailed mechanism of the progressive character of IPF is not yet unearthed, the aberrantly remodeled ECM along with excessive fibroblast proliferation, invasion, activation, differentiation and matrix deposition are the most consistent features of IPF [41; 42].

### 1.3.4. Aberrant Wnt signaling in IPF

The classical Wingless/integrase-1 (Wnt) signalling pathway, conserved throughout evolution is responsible for the development of various organs. Wnt ligands are secreted glycoproteins which guide the pulmonary cells to embrace a particular fate all through the lung developmental phase as well as during tissue homeostasis in adults. 19 distinct Wnt ligands are present in humans, which are categorized according to their amino acid sequences. Classically, Wnt signaling is classified into canonical and non-canonical signaling pathways. The canonical Wnt signaling depends on the activation of  $\beta$ -catenin (Fig 1.5) and the Wnt ligand activated pathways independent of the  $\beta$ -catenin are termed as non-canonical Wnt signaling [43].

In the canonical pathway, the Wnt ligands bind with the frizzled (Fz) receptors and co-receptor lipoprotein receptor-related protein (LRP) 5/6 forming a 'signalosome' which results in a build-up of  $\beta$ -catenin.  $\beta$ -catenin is then translocated to the nucleus where it modulates gene transcription. When Wnt ligands are absent,  $\beta$ -catenin gets bound to the destruction complex and finally degraded. Secreted Wnt pathway antagonists like secreted Frizzled related protein (SFRP), Dickkopf (Dkk) and Wnt inhibitory factor (WIF) block the interaction of the Wnt ligands with the Frizzled receptors thereby arresting Wnt signaling. The non-canonical Wnt signaling comprises the planar cell polarity pathway (PCP), which involves Jun N-terminal kinase (JNK) and the Wnt/ $\text{Ca}^{2+}$  pathway [44] (Fig.1.5).

The PCP signaling is transmitted through the Frizzled receptors independent of the co-receptor LRP5/6 and activates Dvl. Dvl subsequently mediates the activation of Rho via Daam1 which thereby activates Rho kinase (ROCK). Dvl also activates JNK via Rac. ROCK and JNK pathway in a unified way regulate cytoskeletal and morphological changes in the cell along with changes in cell migration and polarization. The Wnt- $\text{Ca}^{2+}$  pathway activates the G proteins cascade to mediate activation of Dvl via the Frizzled receptors. Dishevelled then activates the phosphodiesterase (PDE) which in turn inhibits protein kinase G (PKG) and which then inhibits  $\text{Ca}^{2+}$  release. Dvl activates inositol triphosphate (IP3) via phospholipase C (PLC), which leads to release of intracellular  $\text{Ca}^{2+}$ . This  $\text{Ca}^{2+}$  release activates calmodulin kinase (CaMK) and calcineurin. CaMK inhibit  $\beta$ -catenin/TCF function to negatively regulate dorsal axis formation and mediate tissue separation and cell movements (Fig.1.5).



**Figure 1.5: Schematic representation of canonical (left) and non-canonical (right) WNT signaling pathway**

*Modified from (Tw.sinobiological.com, 2019)*

The last decade has witnessed extensive research regarding the role of Wnt signaling pathways in chronic lung diseases. The idea of alterations in developmentally active pathways (like Wnt, Sonic Hedgehog, Notch) have already been established based on the gene expression profiling from IPF lungs of human and other animal models. The appearance of a “Wnt signature” from the gene expression analysis within the IPF lungs implicate that this developmental signaling pathway is reactivated following injury in the adult IPF lungs [45, 46, 47].

The canonical Wnt/β-catenin signalling is found to be active in various cell types in human and experimental IPF animal models [47]. Inhibition of the Wnt/β-catenin pathway also showed an attenuation in an experimental mice fibrosis model [48]. Specifically, the gene expression of Wnt-1, Wnt-10B, Wnt-7B, FZD2, FZD3, CTNNB1 (β-catenin) and LEF1 was found to be increased in the IPF lung tissues compared to healthy donors [46]. The Wnt inhibitor DKK1 was also found to have an increased expression in the hyperplastic alveolar epithelial cells of human IPF lungs compared to the donor lungs [49]. Another clinical study in 2014 revealed elevated expression levels of co-receptors LRP5/6 in peripheral blood mononuclear cells (PBMCs) of IPF patients. The study shows that the LRP5/6 transcript levels were directly correlated with IPF progression and negatively related to clinical parameters such as lung diffusion capacity for carbon monoxide (DLco) and composite physical index (CPI) [50]. Although LRP5 deficiency was shown experimentally to regulate alveolar macrophage differentiation, immune cell-ECM remodeling as well as to inhibit bleomycin-induced fibrosis, LRP5 deficiency in mice failed to protect them from fibrosis induced by TGFβ [50] and asbestos [51]. Increased expression of Wnt target genes

like Wnt-inducible signaling protein-1 (WISP1) has also been demonstrated, which implies an enhanced Wnt/ $\beta$ -catenin signaling in IPF lung tissues [47].

The  $\beta$ -Catenin-independent or non-canonical Wnt signaling pathway in lung fibrosis is much less studied. The Wnt5A is largely known to exert its effect independent of  $\beta$ -Catenin and has been found to be upregulated in IPF fibroblasts [52]. A study in 2018 has shown that increased extracellular vesicles (EVs) especially exosomes in the BAL fluid (BALF) of IPF patients acted as carriers for Wnt5A and thus contributed to disease pathogenesis [53]. A recent study demonstrated that inhibiting the Rho-associated protein kinase (ROCK) signaling which is a known downstream effector of RhoA decreases fibrosis in a mouse model of IPF [54, 55, 56]. Another report states that TGF $\beta$  and mechanical stress in IPF regulate through a RhoA dependent pathway mediated via Rho Family GTPase 3 (Rnd3) and p190RhoGAP (a Rnd3 effector) to promote the fibrotic phenotype in fibroblasts [57]. Thus, reactivation of Wnt signaling in IPF represents an “attempted regeneration” signal and present a promising area to develop therapeutic strategies.

### **1.3.5. Secreted Frizzled Related Proteins (SFRPs) in IPF**

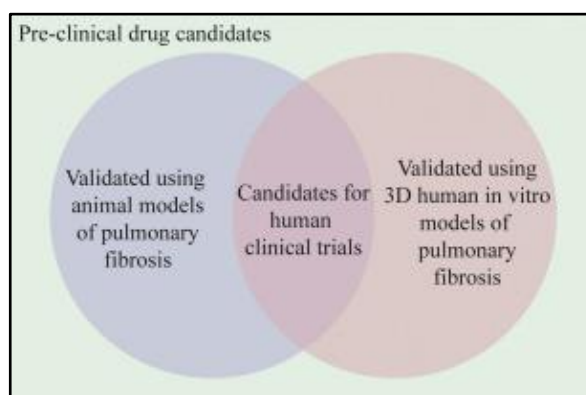
Secreted frizzled related proteins (SFRPs) are secreted Wnt antagonists having eight known family members. The family members are classified according to sequence homology where, SFRP1, SFRP2 and SFRP5 forms one subgroup, SFRP3 and SFRP4 forms another and lastly Sizzled, Sizzled2 and Crescent forms the third subgroup [58]. SFRPs has a cysteine rich domain (CRD) that shares 30-50% homology to the Frizzled receptors and hence can directly bind to the Wnt ligands altering their ability to form the Wnt-receptor complex [59]. Interestingly, CRD of SFRP1 can interact with itself and with that of Frizzled receptors [60]. Gene expression profiling from lung biopsies has shown increased SFRP2 levels in IPF patients compared to donors [61]. Another transcriptional signature study has reported an increase in SFRP1 expression in IPF patient lungs [62]. Another recent study in 2019 has found that changes in promoter hypermethylation downregulates SFRP1 and SFRP4 in different stages of bleomycin induced pulmonary fibrosis in mice [63]. Although SFRP proteins play an important role in modulating IPF, their role in the disease is still not known clearly.

### **1.3.6. IPF disease models**

Experimental models using animals have been widely developed to understand the fibrotic responses and perform initial pre-clinical testing for various anti-fibrotic drugs. Among them, the bleomycin-induced pulmonary fibrosis model in mouse and rat have been most widely used since the 1970's as the most standard animal model. The bleomycin antibiotic was originally isolated from *Streptomyces verticillatus*. A single or booster dose of intratracheal bleomycin instillation causes huge inflammatory and fibrotic

reactions with symptoms peaking at day 14 [64]. However, one major drawback of this transient model is the inability to mimic the chronic nature of the disease as seen in human. Fluorescein isothiocyanate (FITC) model of pulmonary fibrosis was also extensively studied [65]. Although fibrosis in the FITC model is sustained for a period of 6 months compared to 28 days in the bleomycin model, the FITC model is not considered clinically relevant because of the huge variation in fibrotic responses from human [64]. Additional agents that have been used to induce fibrosis in rodents are irradiation [66], chemical Paraquat herbicide [67], minerals like silica [68] and asbestos [69, 70]. In addition, there are established cytokine overexpression animal models using either gene-transfer or transgenic approaches or both which results in lung fibrosis. The cytokines in use are TGF- $\beta$  [71 and 72], TGF- $\alpha$  [73], IL-13 [74], TNF- $\alpha$  [75] and IL-1 $\beta$  [76].

The primary limiting factor for using animal models is the artificially triggered fibrosis along with the physiological and anatomical differences between human and rodent lungs. Although animal models are incapable of mimicking all the features of IPF, they are still widely used to carry out the initial investigation of fibrotic signaling pathways and different lung cell or cell-ECM interactions [77].



**Figure 1.6: Pre-clinical drug target validation prior to human clinical trials.** (Sundarakrishnan et al., 2018)

A wide variety of different compounds showed a different mode of action in the animal models and in pulmonary fibrosis patients. Hence, the compound targets, efficacies or side effects are validated in different established *in vitro* (2D, 2.5D and 3D) and *ex vivo* tissue model systems of IPF before they are used in human pre-clinical trials (Fig.1.6). Two-dimensional (2D) cellular models of fibrosis are critical in understanding the disease mechanism as they enable study of cell responses to soluble cues, matrix mechanics and other secreted extracellular matrix molecules in a controlled environment setting. While the primary lung cells mimic the *in vivo* lung phenotype much better, they are limited by donor or patient-based variabilities and the Hayflick limit, which is the maximum number of times the cells can divide before senescence. On the other hand, immortal cell lines present a much more robust platform to conduct reproducible high throughput studies. Although the 2.5D and 3D *in vitro* culture systems provide a much more complex *in vivo* mimicking environment for the cells, the 2D setup still provides a robust platform for *in vitro* investigation, due to the relative ease of imaging and profiling cells for gene and protein expression [78]. Sandwich culture systems and use of ECM coated plates have both been termed as 2.5D and enable better study of complex cell-cell and cell-ECM interactions. Commercially available Transwell 2.5D systems for lung fibrosis have been used for air-liquid interface (ALI) induced epithelial maturation,

surfactant and mucin production in airway epithelial cells [79]. In addition, airway epithelial and microvascular endothelial cells have been cultured on reconstituted basement membrane called Matrigel producing complex structures showing acini and tubule formation from the respective cells [80, 81]. As, neither Transwell nor basement membrane culture systems are able to support fibroblast integrin adhesions in all 3 dimensions, sandwich cultures have been recently established to study migration and chemotaxis similar to the 3D models. Mostly fibroblasts or other cells are sandwiched between two layers of mechanically tunable materials like polyacrylamide to support integrin adhesion in all planes [82]. Although 2.5D culture systems present better cell-cell and cell-ECM interactions compared to 2D setups, three dimensional (3D) *in vitro* models replicate the native lung tissue microenvironment with a greater accuracy. Since the ECM pivotally influences behavior of the cells residing in a native three-dimensional environment, it has led to the conclusion that mesenchymal cells should be studied in such an environment that closely mimics the structure and dimensionality of the ECM [83, 84]. Collagen type I hydrogels have been extensively used to study fibroblast-mediated collagen contraction due to soluble or matrix cues. A study in 1999 showed that this degree of collagen gel compliance by the fibroblasts had a direct relationship with the level of alpha smooth muscle actin ( $\alpha$ SMA) expression [85]. In addition to collagen, other natural hydrogels include fibrin, laminin and elastin [86, 87]. In comparison to artificially synthesized biopolymers like polyacrylamide [88, 89] and polyethylene glycol [90], natural biopolymers resemble the physiological ECM architecture more closely. Precision cut tissue slices have presented a practical solution to overcome these limitations. Precision-cut lung slices (PCLS) provide a valuable tool for investigating multiple regions of the lung simultaneously. Human PCLS stimulated with a pro-fibrotic cocktail can mimic early fibrosis conditions as in IPF [91]. Additionally, acellular lung scaffolds are used to study cell-ECM interactions and for developing novel cell culture systems [41]. Taken together, 3D cell culture models exhibit both advantages and disadvantages and the choice of use for a study highly depends on the specific research question in context.

## **1.4. Lung fibroblasts**

Fibroblasts are derived from mesenchymal cells and are the “workhorses” of the most abundant tissue type in the body: connective tissues [92]. In general, fibroblasts can be identified by their classical, elongated spindle-shape morphology [93]. As fibroblasts are one of the central mediators of lung fibrosis, a lot of the current IPF treatments now target fibroblast biology [92].

### **1.4.1. Fibroblasts in wound healing**

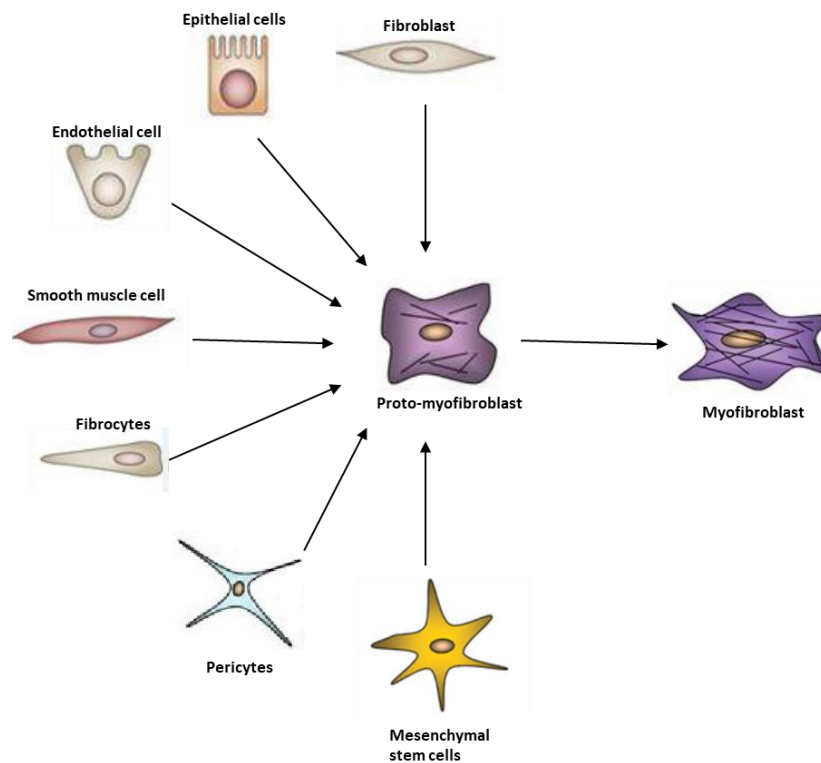
Fibroblasts play a critical role in wound healing processes such as degrading fibrin clots, producing new ECM material and collagen structures [94, 95]. Fibroblasts are known to be chemotactic, which means that they can migrate and accumulate in different tissue areas in response to secreted growth factors and

chemokines. Therefore, in the initial stages of tissue injury, fibroblasts migrate towards the wound and then subsequently transdifferentiate into highly contractile myofibroblasts. The myofibroblasts produce increased amounts of ECM proteins like elastin, fibronectin and collagens. In this process, a temporary ECM scaffold is produced that helps in wound closure and after the wound is sealed, the scaffold dissolves and myofibroblasts undergo apoptosis [96]. Although the precise mechanism for myofibroblast cell death is still unknown, this process is crucial for maintaining normal tissue homeostasis after a wound or injury [97].

#### **1.4.2. Activated fibroblasts in IPF**

Fibroblast are a heterogeneous cell population, as different subtypes display varying capacities of ECM and collagen production. Especially, skin and lung fibroblast populations have been investigated in detail. [98, 99]. As, fibroblasts are not a terminally differentiated cells, they can be activated and transdifferentiate into other cell types. Generally, myofibroblasts are not found in healthy tissue and originate after an injury as a wound-healing response [100]. Various pre-cursor cells such as fibroblasts [101], epithelial cells [102], endothelial cells [103], smooth muscle cells [104], fibrocytes [105], pericytes [106] and mesenchymal cells [107] are said to transform into myofibroblasts under certain stress conditions. The TGF- $\beta$ 1 cytokine is produced from injured lung tissues and is the main inducer for myofibroblast differentiation. Any stress in the ECM leads to the proteolytic cleavage and subsequent release of the TGF- $\beta$ 1 dimer, which then binds to the TGF $\beta$ 1 RI-TGF $\beta$ 1-RII complex inducing myofibroblast maturation [108]. A particular isoform of fibronectin, called the ED-A isoform along with TGF $\beta$ 1 can activate  $\alpha$ -smooth muscle actin ( $\alpha$ SMA) expression and its subsequent incorporation within stress fibers and serves as a hallmark for differentiating myofibroblasts. In contrast, proto-myofibroblasts contain stress fibers composed of  $\beta$ - and  $\gamma$ -actins. Normally, after the tissue repair process, the myofibroblasts undergo apoptosis, but in lung fibrosis they survive, which then subsequently leads to aberrant tissue fibrosis and remodeling processes [109].





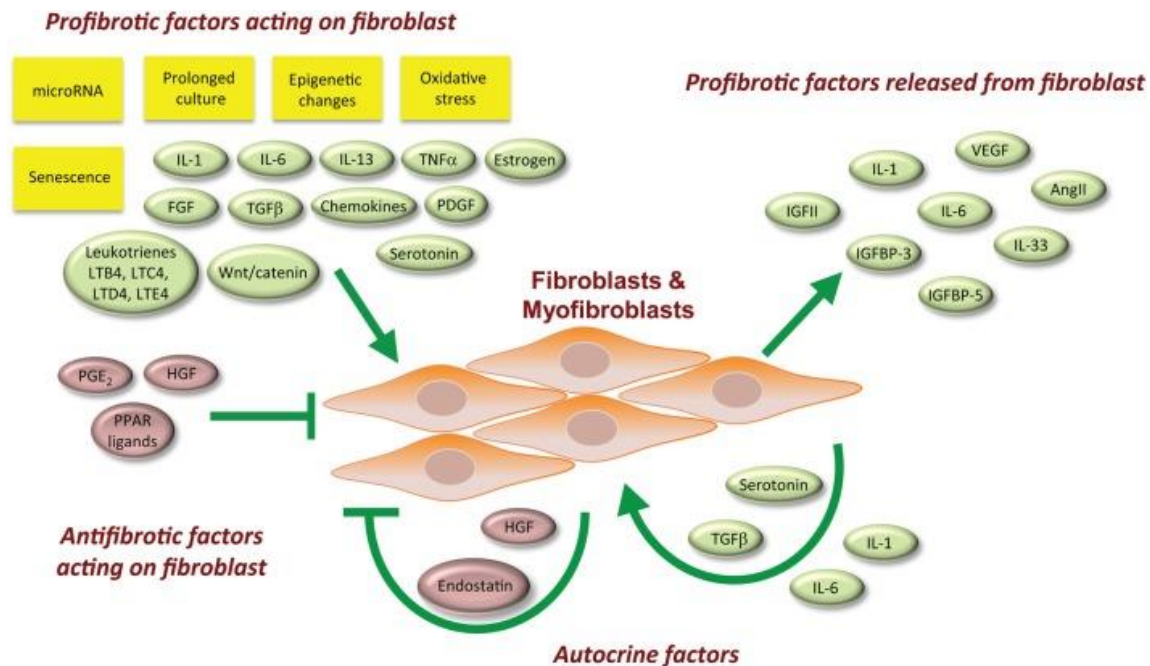
**Figure 1.7: The origin of myofibroblasts**

Pre-cursor cells such as fibroblasts, epithelial cells, endothelial cells, smooth muscle cells, fibrocytes, pericytes and mesenchymal cells give rise to a proto-myofibroblast phenotype that under the effect of growth factors and mechanical stress undergo transformation to myofibroblast phenotype.

A spectrum of pro and anti-fibrotic factors acts upon the fibroblasts either in a paracrine or/and autocrine fashion which drives the activation of these fibroblasts in fibrosis [8, 110]. Platelet-derived growth factor (PDGF) and transforming growth factor-beta ( $TGF\beta$ ) are the most comprehensively studied pro-fibrotic growth factors which are known to regulate fibroblast to myofibroblast transdifferentiation in IPF [108, 111]. On the other hand, fibroblast growth factor 2 (FGF2) secreted by adipose tissue derived stromal cells can act as an anti-fibrotic growth factor that aids de-differentiation of myofibroblasts to fibroblasts [112, 113].

Additionally, Wnt/ $\beta$ -catenin signalling components in epithelial cells were reported to direct pro-fibrotic responses to fibroblasts in IPF [47]. Recently, epithelial cells have been demonstrated to communicate with fibroblasts along the CXCL12-CXCR4 chemokine axis in IPF [114]. Moreover, inflammatory mediators like Prostaglandin E2 (PGE2) were shown to mediate anti-fibrotic signals between epithelial cells and fibroblasts and limit fibroblast migration, proliferation and collagen secretion [115, 116]. Furthermore, a study in 2017 have indicated transformation of the lipofibroblasts to myofibroblasts during fibrogenesis and vice versa during fibrosis resolution [117]. Taken together, the different fibrotic signaling

components acting upon the fibroblasts play a multitude of roles in the transdifferentiation process to myofibroblasts.



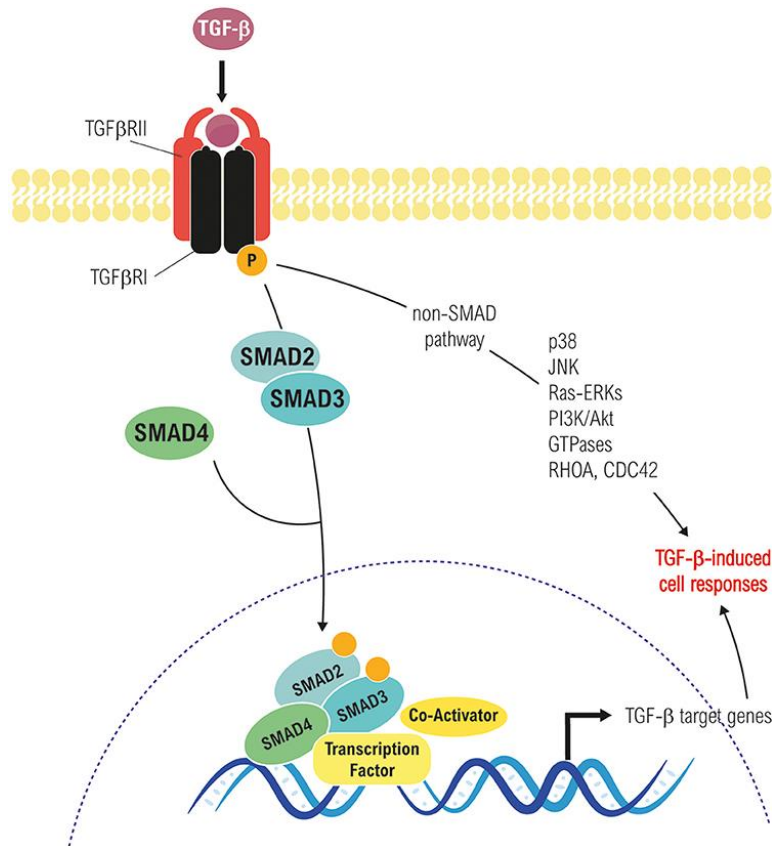
**Figure 1.8: Schematic overview of the pro-fibrotic stimuli directing myofibroblast transformation in IPF**

The pro-fibrotic factors drive transdifferentiation of fibroblasts into myofibroblasts. Activated myofibroblasts can also release pro-fibrotic cytokines in an autocrine manner which contribute to inflammation and ongoing fibrosis. [92]

#### 1.4.3. Transforming Growth Factor-beta (TGFβ) signaling

A large spectrum of pro-fibrotic mediators synthesized by various cell types are known to promote fibroblast proliferation, migration, and transdifferentiation along with increased ECM synthesis. TGFβ1 is the most potent mediator which acts as the central player in several diseases [118]. TGFβ1 is a member of the TGF-β superfamily and of all three mammalian isoforms (TGFβ 1, 2 and 3), TGFβ1 is ubiquitously expressed. The expression of TGFβ1 is highly induced in fibrotic tissues in rodent disease models [119] as well as in IPF patients [120]. Overexpression of active TGFβ1 leads to persistent lung fibrosis whereas blocking TGFβ1 signaling ameliorates pulmonary fibrosis [121]. TGF-β1, synthesized as a small latent complex consists of a non-covalently associated active TGF-β1 with latency associated peptide (LAP). The synthesis of this latent TGFβ1 is increased by inflammatory mediators such as TNF-α. Although, it is secreted as an inactive molecule, it needs to be activated to perform any biological function [122]. Several Proteases [123], integrins [124], pH extremities [125] and reactive oxygen species [126] are some of the well-known factors that activate TGF-β1. Activated TGFβ1 mediates the pro-fibrotic effects of mesenchymal cells, aids in transdifferentiation of fibroblasts into myofibroblasts, causes EMT and excessive ECM generation [127].

TGF $\beta$  downstream signaling is transmitted via Smad-dependent (called canonical) pathway and Smad-independent (called non-canonical) pathway [128] (Fig. 1.9).



**Figure 1.9: Canonical (Smad-dependent) and non-canonical (Smad-independent) TGF- $\beta$  signaling pathways**

TGF $\beta$  binds its receptors and forms an activated-receptor complex. The activated complex mediates the canonical signaling through SMADs via phosphorylation. Finally, the SMADs form a trimeric complex which translocates to the cell nucleus and regulates downstream gene expression. TGF $\beta$  mediates the non-SMAD pathway to regulate biological responses via NF- $\kappa$ B, p13k/Akt, RhoGTPases, JNK and MAPK pathway. [129]

Although there is a lot of uncertainty regarding the precise etiology of IPF, it is generally accepted that aberrant wound healing processes and epithelial-mesenchymal crosstalk are major contributors for pathogenesis in fibrosis. In response to cytokines like TGF $\beta$ 1, the alveolar type II epithelial cells are hyper proliferative and immediate recruitment of fibroblasts advances into the development of fibroblastic foci with disease progression. Given the central role of TGF $\beta$ 1 in fibrosis, anti-fibrotic drugs are being developed which target the TGF $\beta$ 1 signaling pathway components [133]. Hence, it might be of particular interest to identify molecular interactors of the TGF $\beta$ 1 pathway in lung fibrosis to gain further insight into the pathogenesis of the disease.

### 1.5. Extracellular matrix (ECM)

Extracellular matrix (ECM) can broadly be defined as a scaffold supporting all the tissues and organs of the body [130]. The cells residing within the complex environment of the ECM respond to changes in the environment (injury/disease) by secreting growth factors, cytokines and other signaling molecules, which then stimulates cellular processes such as proliferation, migration or apoptosis. In mammals, the extracellular matrix comprises of an interstitial matrix with basement membranes [131]. The basement membranes are sheet-like structures of ECM on which various cells rest. The ECM components are produced intracellularly by resident cells and are then secreted via exocytosis.

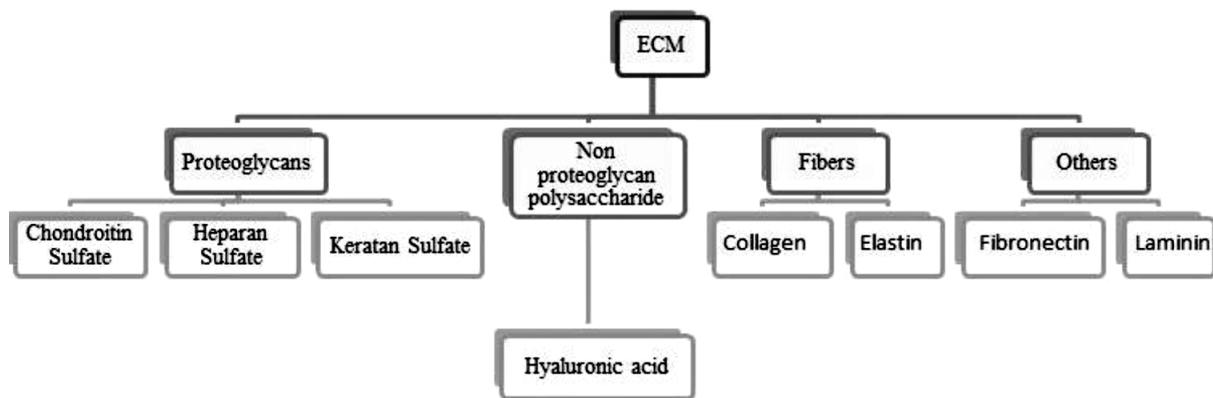


Figure 1.10: Molecular components of ECM

The ECM formation is essential for important physiological processes like growth, wound healing, and maintaining tissue homeostasis [132]. A total understanding of structure and composition of the ECM could help in discerning the complex dynamics of cell invasion. . The ECM stiffness has important implications for cellular migration, gene expression, and further differentiation [134]. Cells are able to sense ECM rigidity and then migrate preferably towards stiffer regions and this phenomenon is called as durotaxis [135]. Cells can adhere to the ECM components either via focal adhesions (connect ECM with actin filaments) or via hemidesmosomes (connect ECM to intermediate filaments). Specific cell adhesion molecules called integrins regulate the attachment of the cells to ECM components like fibronectin and laminin [136]. There is a plethora of cell types that contribute to the development of ECM. Among them, fibroblasts secrete most of the precursor ECM components, resulting in a structural framework for other cell types. Interestingly, fibroblasts have been reported to react to instructive cues from their surrounding ECM microenvironment [137]. Hence, understanding the interplay between cells and the ECM in the context of chronic lung diseases can provide further information regarding disease pathogenesis.

### **1.5.1. Aberrant ECM remodeling in IPF**

The dynamic remodeling of the ECM is part of maintaining normal organ homeostasis and wound healing, but pathological conditions develop when ECM remodeling becomes uncontrolled and aberrant. Therefore, in a diseased condition the dysregulation of this finely balanced process leads to devastating tissue damage along with uncontrolled ECM deposition. Fibroblasts express an array of matrix components which drives matrix deposition and regulate expression of proteases that moderate matrix degradation. The extensive secretion of ECM is one of the major phenotypic response of activated fibroblasts in IPF. One single fibroblast when activated by growth factors or mechanical stimuli produces up to 5,000 molecules of procollagen per minute [138]. Mediators involved in the dynamic process of collagen degradation are usually local polypeptide growth factors like platelet-derived growth factor (PDGF), epidermal growth factor (EGF), fibroblast growth factor (FGF), cytokines such as TGF $\beta$ 1, interleukins and several other cellular enzymes [139].

The extensive amounts of ECM deposition in IPF is not only consequence of aberrantly increased ECM component secretion by the activated fibroblasts, but also might be due to the malfunction of effective degradation of the ECM material especially by the MMPs [45]. Another important aspect of the fibrotic ECM is its significantly altered framework and biochemical and biomechanical composition. A study in an experimental fibrosis model with atomic force microscopy has demonstrated increased ECM stiffness within the lung parenchyma [140]. Therefore, ECM reciprocate information with the fibroblasts influencing a feed forward loop. Taking this inter-dependence of the ECM and the mesenchymal cells, it seems likely that fibroblast behavior studies be performed in 3D matrices or *in vivo* mimicking 3D scaffolds [141].

## 2. Objectives

Idiopathic pulmonary fibrosis remains a challenging and progressive disease with no established effective therapy until today. The lack of proven therapeutic strategies for IPF stems partially from the lack of complete understanding of the underlying pathomechanism and partially from the more or less greater limitations of effective translatable animal models to successfully test potential drug targets and their efficacy [142]. Over time, progressive fibrosis like IPF worsens, destroys the tissue architecture, leads to organ failure and finally to death. The two established drugs Nintedanib and Pirfenidone help to slow down the rate of IPF progression, but cannot reverse or stop the scarring in the lungs [143]. Hence, there is an urgent medical need to identify novel druggable targets acting in the early phase of fibrosis, as well as relevant animal models and tools that can effectively mimic the ongoing fibrosis. The present study aimed to identify and establish SFRP1 as a novel fibrosis associated marker and to develop *ex vivo* tools to help to extend the current knowledge in lung fibrosis. The specific aims were as follows:

1. *Characterization of SFRP1 as a novel regulator and/or biomarker of lung fibrosis.*

Preliminary studies showed that SFRP1, an inhibitor of the Wnt signaling pathway was strongly downregulated on transcript and protein levels in invasive fibroblasts [144]. Contrarily, a time series tissue proteome profiling (Mass spec/Orbitrap) of fibrotic mouse lungs (bleomycin induced lung injury mouse model) demonstrated increased SFRP1 expression in the extracellular matrix fraction [145] at day 14, the peak of fibrosis in the mouse. Additionally, a published whole genome mRNA microarray analysis reported a 2.5-fold upregulation of SFRP1 gene expression in an IPF patient cohort (n=197) when compared to healthy donor controls [39]. However, very little is known about the molecular and tissue-specific function of SFRP1 in healthy and fibrotic lung fibroblasts and tissues. Therefore, the aim of the first study was to decipher the role of SFRP1 in lung fibrosis. In the first part of this project, the expression level of SFRP1 was investigated in fibrotic mouse and IPF tissues as well as in *ex vivo* fibrosis models. Next, I wanted to examine the influence of loss-of-gain functions of SFRP1 on cellular behavior(s) in lung fibroblasts. Moreover, the regulation of SFRP1 expression via pro-fibrotic growth factors and epigenetic mechanisms were further investigated in primary human and mouse lung fibroblasts. The final goals were to identify the cell types (or subtypes) in the lung that express SFRP1 in healthy and fibrotic conditions and further characterize them.

2. *Development and validation of a pre-clinical ex vivo tool for validating novel therapeutics in IPF.* Precision-cut lung slices (PCLS) have presented a potential *ex vivo* solution for bridging the gap between the *in vitro* cell culture experiments and pre-clinical *in vivo* studies [146]. Although a lot of studies have been recently performed with a focus on human PCLS [147, 91], mouse models generally still represent an important tool due to their easy availability and genetic manipulations. Here, the second objective of the study was to develop and further implement an *ex vivo* fibrosis-mimicking model using mouse PCLS. To address this, mouse PCLS were stimulated with a pro-fibrotic cocktail and fibrosis-associated biomarkers, including SFRP1, were verified on transcript and protein levels.
  
3. *Physiological cues from the ECM instruct fibroblast functions in 3D-LTCs.* Bioengineering and regenerative medicine fields have stated an extensive use of acellular biological tissue scaffolds as the key to mitigate the shortage of donor lungs for transplantation in the future [148, 149]. Therefore, it has become crucial to understand the interaction of resident cells with their surrounding ECM niche on cellular and molecular levels. To address this, mouse and human fibroblasts were reseeded on decellularized lung tissue slices (PCLS), as they represent the primary effector cell types in lung fibrosis [150]. Following engraftment of the fibroblasts in various healthy and diseased decellularized lung scaffolds, the altered cellular behavior of these cells due to instructive cues from the ECM were investigated.

### 3. Materials and Methods

#### 3.1. Materials

##### 3.1.1. Antibodies

##### 3.1.1.1. Primary antibodies

<i>Antigen</i>	<i>Product number</i>	<i>Host</i>	<i>Type</i>	<i>Application</i>	<i>Dilution</i>	<i>Manufacturer</i>
CTNND1	610133	mouse	monoclonal	WB	1:1000	BD Sciences
Desmin	sc-271677	mouse	monoclonal	WB	1:500	Santa Cruz
E-cadherin	610181	mouse	monoclonal	WB	1:2500	BD Sciences
Paxillin	610619	mouse	monoclonal	WB	1:500	BD Sciences
Src	2110	mouse	monoclonal	WB	1:1000	CST
Talin	T3287	mouse	monoclonal	WB IF	1:1000 1:100	Sigma
Tropomyosin	T 2780	mouse	monoclonal	WB	1:1000	Sigma
$\alpha$ Actinin1	sc-135819	mouse	monoclonal	WB	1:1000	Santa Cruz
$\alpha$ SMA	A5228	mouse	monoclonal	WB IF	1:2000 1:200	Sigma
$\beta$ -actin-HRP	A3854	mouse	monoclonal	WB	1:40000	Sigma
Caldesmon	ab32330	rabbit	polyclonal	WB	1:1000	Abcam
Calponin h1	NB110-55650	rabbit	monoclonal	WB	1:1000	Novus Biologicals
Caveolin 1	13267	rabbit	monoclonal	WB	1:1000	CST
CDC42	2466	rabbit	monoclonal	WB	1:500	CST
Collagen 1	600-401-103-0.1	rabbit	polyclonal	WB IF	1:1000 1:100	Rockland
Fibronectin	sc.9068	rabbit	polyclonal	IF	1:100	Santa Cruz
GAPDH-HRP	3683	rabbit	monoclonal	WB	1:1000	CST
Ki-67	RBK027	rabbit	monoclonal	IF	1:100	Zytomed
Laminin A/C	2032	rabbit	polyclonal	WB	1:1000	CST
p44/42 Mapk	9101	rabbit	polyclonal	WB	1:1000	CST
pPaxillin	ab32115	rabbit	monoclonal	WB	1:500	Abcam
pSMAD3	ab52903	rabbit	monoclonal	WB	1:2000	Abcam
pZyxin	ab11518	rabbit	polyclonal	WB	1:500	Abcam
Rac	2465	rabbit	polyclonal	WB	1:500	CST



RhoA	2117	rabbit	monoclonal	WB	1:500	CST
Rock1	NB100-624	rabbit	polyclonal	WB	1:1000	Novus Biologicals
SFRP1	ab126613	rabbit	monoclonal	WB	1:500	Abcam
				IF	1:100	
SMAD3	9523	rabbit	monoclonal	WB	1:1000	CST
TenascinC	ab108930	rabbit	monoclonal	WB	1:1000	Abcam
Tensin	sc-28542	rabbit	polyclonal	WB	1:1000	Santa Cruz
TGFβ1	ab9758	rabbit	polyclonal	WB	1:1000	Abcam
Vimentin	sc-7557	rabbit	polyclonal	WB	1:500	Santa Cruz
YAP	4912	rabbit	polyclonal	WB	1:1000	CST
Zyxin	ab11518	rabbit	polyclonal	WB	1:1000	Abcam
β-tubulin	2146	rabbit	polyclonal	WB	1:1000	CST

### 3.1.1.2. Secondary antibodies

<i>Antigen</i>	<i>Product number</i>	<i>Host</i>	<i>Application</i>	<i>Dilution</i>	<i>Manufacturer</i>
Anti-rabbit IgG HRP-linked	NA934V	donkey	WB	1:40000	GE Healthcare
Alexa Fluor 488 donkey anti-mouse IgG	R37114	donkey	IF	1:200	Invitrogen
Alexa Fluor 568 donkey anti-rabbit IgG	A10042	donkey	IF	1:200	Invitrogen
Anti-mouse IgG HRP-linked	NA931V	sheep	WB	1:40000	GE Healthcare

### 3.1.2. Primers

Primers for quantitative real time polymerase chain reaction (qRT-PCR) were purchased from Eurofins, Luxembourg.

<i>Gene</i>	<i>Species</i>		<i>Sequence 5'-3'</i>
ACTA2	human	Fw	CAGGGCTGTTTTCCCATCCATTGT
		Rev	TCAGGGTCAGGATTCCTCTTTTGC
GAPDH	human	Fw	TGACCTCAACTACATGGTTTACATG
		Rev	TTGATTTTGGAGGGATCTCG
HPRT	human	Fw	AAGGACCCACGAAGTGTTG
		Rev	GGCTTTGTATTTTGCTTTTCCA
RHOA	human	Fw	GGAAAGCAGGTAGAGTTGGCT
		Rev	GGCTGTCGATGGAAAAACACA

SFRP1	human	Fw	GGA CCG GCC CAT CTA CCC GT
		Rev	ACA CCG TTG TGC CTT GGG GC
SFRP2	human	Fw	TCTTCCTCTTTGGCCAGCCC
		Rev	TCACATCAATTTGGAGCTTC
SFRP3	human	Fw	TCTGCACCATTGACTTCCAG
		Rev	TTAGAATCTCCTTCACCTCC
SFRP4	human	Fw	TCCTGGCCATCGAGCAGTAC
		Rev	GATGAGGACTTGAAGATCTC
SFRP5	human	Fw	ACTCGGATACGCAGGTCTTC
		Rev	TTCTTGTCCCAGCGGTAGAC
TGF $\beta$ 1	human	Fw	GTGGGTTTCCACCATTAGCAC
		Rev	GGCCAGATCCTGTCCAAGC
ACTA2	mouse	Fw	GCTGGTGATGATGCTCCCA
		Rev	GCCCATTTCCAACCATTACTCC
COL1A1	mouse	Fw	CCAAGAAGACATCCCTGAAGTCA
		Rev	TGCACGTCATCGCACACA
CTGF	mouse	Fw	CTGCACCCGGCCTGCTATGG
		Rev	GAGGCCCTTGTGTGGGTCGC
FN	mouse	Fw	GTGTAGCACAACTTCCAATTACGAA
		Rev	GGAATTTCCGCCTCGAGTCT
GAPDH	mouse	Fw	TGTGTCCGTCGTGGATCTGA
		Rev	CCTGCTTCACCACCTTCTTGA
HPRT	mouse	Fw	ATAGTGATAGATCCATTCTATGACTG
		Rev	TTCAACAATCAAGACATTCTTTCCA
PAI1	mouse	Fw	AAGACTC CCTTCCCCGACTC
		Rev	GGGCGTGGTGAAGTCAAGTATAG
SFRP1	mouse	Fw	GTGCGAGCCGGTCATGCAGT
		Rev	CACACGGTTGTACCTTGGGGC
TGF $\beta$ 1	mouse	Fw	GTGGACCGCAACAACGCC
		Rev	TGGGGGTCAGCAGCCGGT

### 3.1.3. Small interfering RNA (siRNA)

<i>siRNA</i>	<i>Manufacturer</i>	<i>Product Number</i>
Scrambled Silencer® Negative control No. 1	Ambion, Life Technologies; USA	AM4611
Scrambled Silencer® Negative control No. 5	Ambion, Life Technologies; USA	AM4642

Silencer™ Select Negative Control No. 1 siRNA	Ambion, Life Technologies; USA	4390843
Silencer® Select SFRP1 siRNA 1	Ambion, Life Technologies; USA	s12713
Silencer® Select SFRP1 siRNA 2	Ambion, Life Technologies; USA	s12714
Silencer® Select SFRP1 siRNA 3	Ambion, Life Technologies; USA	s12715

### 3.1.4. Cell lines

<i>Cell line</i>	<i>Origin</i>	<i>Manufacturer</i>
CCL206 (MLFb)	Murine newborn lung fibroblasts	ATCC-Nr. CCL-206

### 3.1.5. Human cells and tissues

Lung tissues from healthy and IPF tissue resections were kindly provided by Universities of Giessen and Marburg Lung Center (UGMLC), Gießen, Germany and from the Asklepios Clinic, Gauting, Germany. All tissue samples were approved with ethical consent according to national and international guidelines.

<i>Primary human fibroblasts</i>	<i>Origin</i>	<i>Manufacturer</i>
P1-P4	Non-carcinogenic lung tissue resection from patient with lung metastasis	Asklepios Clinic; Munich, Germany

### 3.1.6. Cell culture media

<i>Cell type</i>	<i>Cell culture medium</i>	<i>Product Number</i>	<i>Manufacturer</i>
MLFbs	DMEM F-12	11320033	ThermoFischer Scientific
	10 % FBS	P30-3702	Pan Biotech
	100 U/mL Penicillin/Streptomycin	15140122	Gibco, Life Technologies
phFbs	DMEM F-12	11320033	ThermoFischer Scientific
	20 % FBS	P30-3702	Pan Biotech
	100 U/mL Penicillin/Streptomycin	15140122	Gibco, Life Technologies
pmFbs	DMEM F-12	11320033	ThermoFischer Scientific
	20 % FBS	P30-3702	Pan Biotech
	100 U/mL Penicillin/Streptomycin	15140122	Gibco, Life Technologies

### 3.1.7. Reagents and chemicals

<i>Product</i>	<i>Manufacturer</i>
Nintedanib	(BIBF 1120), Selleckchem, Munich, Germany
Sfrp1-inhibitor sc-222310	(CHEMBL473916) Santa Cruz, Dallas, USA
Recombinant human SFRP1	5396-SF, R&D Systems, Minneapolis, USA
Low gelling point agarose	A9414, Sigma, Germany
Bleomycin sulfate	Almirall, Barcelona, Spain
Ammonium peroxodisulfate	AppliChem Darmstadt, Germany
Chloroform AppliChem	AppliChem, Darmstadt, Germany
Dithiothreitol (DTT)	AppliChem, Darmstadt, Germany
DNase I AppliChem	AppliChem, Darmstadt, Germany
Ethanol	AppliChem, Darmstadt, Germany
Isopropanol	AppliChem, Darmstadt, Germany
Methanol	AppliChem, Darmstadt, Germany
Non-fat dried milk powder	AppliChem, Darmstadt, Germany
Nonidet P-40	AppliChem, Darmstadt, Germany
Random hexamers	Applied Biosystems, Life Technologies, Carlsbad, USA
Ketamine	Beta Pharma, Princeton, USA
Collagenase I	Biochrom, Berlin, Germany
Coomassie Brilliant Blue R-250	BioRad, Hercules, USA
Dimethyl sulfoxide (DMSO)	Carl Roth, Karlsruhe, Germany
Xylazinehydrochloride	Cp Pharma, Burgdorf, Germany
Fluorescence mounting medium	Dako, Hamburg, Deutschland
Desoxyribonucleotides mix (dNTPs)	Fermentas, Thermo Fisher Scientific, Germany
DMEM (high glucose, 4.5g/l) PAA	GE Healthcare, Cölbe, Germany
DMEM/HAM's F12 PAA,	GE Healthcare, Cölbe, Germany
Penicillin-Streptomycin (10,000 U/ml)	Gibco, Life Technologies, Carlsbad, USA
HEPES solution	H0887, Sigma-Aldrich, Taufkirchen, Germany
Masson-Trichrome	HT15-1KT, Sigma, Germany
Lipofectamine 2000	Invitrogen, Life Technologies, Carlsbad, USA
Lipofectamine RnaiMax	Invitrogen, Life Technologies, Carlsbad, USA
Lipofectamine2000	Invitrogen, Life Technologies, Carlsbad, USA
Phalloidin	Invitrogen, Life Technologies, Carlsbad, USA
RNase inhibitor 20U/μl	Invitrogen, Life Technologies, Carlsbad, USA
Trichostatin A	Med-ChemExpress, NJ, USA
Collagen G from bovine calf skin	Merck Millipore, Berlin, Germany
Fetal bovine serum (FBS, Sera Plus)	PAA, GE Healthcare

ECL Plus Western Blotting Substrate	Pierce, Thermo Fisher Scientific, Schwerte, Germany
Hoechst 33342	Pierce, Thermo Fisher Scientific, Schwerte, Germany
QIAzol Lysis Reagent (79306)	Qiagen, Hilden, Germany
Recombinant human TGFβ1	R&D Systems, Minneapolis, USA
Complete® Mini without EDTA (Protease-inhibitor)	Roche Diagnostics, Mannheim, Germany
Light Cycler 480 SybrGreen I Master Mix	Roche Diagnostics, Mannheim, Germany
Elastase	Sigma, Taufkirchen, Germany
0.2% Trypsin - EDTA solution	Sigma-Aldrich, Taufkirchen, Germany
Bovine serum albumin (BSA)	Sigma-Aldrich, Taufkirchen, Germany
DAPI (4',6-diamidino-2-phenylindole)	Sigma-Aldrich, Taufkirchen, Germany
Decitabine (A3656)	Sigma-Aldrich, Taufkirchen, Germany
Ponceau S solution	Sigma-Aldrich, Taufkirchen, Germany
Restore Plus Western Blot Stripping	Thermo Fisher Scientific, Schwerte, Germany
SB431542	Tocris Bioscience, Bristol, U.K.
Sis3	Tocris Bioscience, Bristol, U.K.
UO126	Tocris Bioscience, Bristol, U.K.
Eosin Y solution	X883, Roth, Karlsruhe, Germany

### 3.1.8. Buffer formulations

<i>Buffer</i>	<i>Reagents</i>
Laemmli loading buffer (6x)	SDS 12% (w/v) Glycerol (87%) 60% (v/v) Bromophenol blue 0.06% (w/v) Tris/HCl, pH 6.8 375 mM DTT 600 mM
RIPA (radio-immunoprecipitation assay) buffer	Tris-Cl pH 7.4 50 mM NaCl 150 mM NP40 1% (v/v) Na-deoxycholate 0.25% (v/v)
Transfer buffer (10x)	Tris/HCl 250 mM Glycine 1.92 M
TBS (Tris-buffered saline) (10x)	Tris/HCl pH 7.4 10 mM NaCl 150 mM
TBS-T (TBS with TWEEN®20)	TBS (10x) 10% (v/v) Tween®20 0.1% (v/v) Millipore-H <sub>2</sub> O 89.99% (v/v)

SDS-PAGE Separation Gel (10%)	Millipore-H <sub>2</sub> O-3.7 ml 1.5 M Tris/HCl pH 8.8-2.25 ml SDS 20%-45 µl Acrylamide-3 ml APS 10%-30 µl TEMED-6 µl
SDS-PAGE Stacking Gel (4%)	Millipore-H <sub>2</sub> O 1.8 ml 0.5 M Tris/HCl pH 6.8 750 µl SDS 20% 15 µl Acrylamide 400 µl APS 10% 15 µl TEMED 3 µl
PBST washing buffer	NaCl 137 mM KCl 2.7 mM Na <sub>2</sub> HPO <sub>4</sub> 10 mM KH <sub>2</sub> PO <sub>4</sub> 2 mM Tween-20 1 % (v/v)
1X BSA (Bovine Serum Albumin)	Bovine serum albumin-5g 20% Triton X-100-2.5ml 10X PBS-50ml
5% Milk Blocking Solution	5 gm Skim Milk powder/100ml 1X TBS-T
SDS (sodium dodecyl sulphate) solution (20%) (w/v)	SDS 200 g Millipore-H <sub>2</sub> O 1 L
PBS (Phosphate buffered saline) pH 7.4	NaCl 1.37 M KCl 27 mM Na <sub>2</sub> HPO <sub>4</sub> 100 mM KH <sub>2</sub> PO <sub>4</sub> 20 mM NaCl 1.37 M

### 3.1.9. Consumables

<i>Consumable</i>	<i>Manufacturer</i>
35-mm Cell-View cell culture dish	Greiner Bio-One, Kremsmünster, Austria
96-well imaging plates, Falcon®	Corning, Thermo Fisher Scientific, Schwerte, Germany
96-well imaging plates, Falcon®	Corning, Thermo Fisher Scientific, Schwerte, Germany

Amicon Ultra 3K-0.5 mL centrifugal filters	Merck Millipore, Darmstadt, Germany
Amicon Ultra 3K-0.5 mL centrifugal filters	Merck Millipore, Darmstadt, Germany
Cell culture dishes	Corning, Thermo Fisher Scientific, Schwerte, Germany
Cell culture dishes	Corning, Thermo Fisher Scientific, Schwerte, Germany
Cell culture multi-well plates	TPP Techno Plastic Producers, Trasadingen, Switzerland
Cell culture multi-well plates	TPP Techno Plastic Producers, Trasadingen, Switzerland
Combitips advanced®	Eppendorf, Hamburg, Germany
Cryovials 1.5 ml	Greiner Bio- One, Frickenhausen, Germany
Falcon Tube (15 ml, 50 ml)	BD Bioscience, Heidelberg, Germany
Filter Tips	Biozym Scientific, Hessisch Oldendorf, Germany
Glas Pasteur pipettes	VWR International, Darmstadt, Germany
Hyperfilm ECL Film	Amersham, GE Healthcare, Freiburg, Germany
Measuring pipettes, sterile, single use (5 ml, 10 ml, 25 ml, 50 ml)	VWR International, Darmstadt, Germany
Microscope slides	Thermo Fisher Scientific, Darmstadt, Germany
Nalgene cryogenic tubes	Thermo Fischer Scientific, Waltham, MA
Nylon filters, pore size 70 µm	BD Bioscience, Heidelberg, Germany
PCR plates, 96-well plate	Kisker Biotech, Steinfurt, Germany
Protein LoBind Tubes (1.5 ml)	Eppendorf, Hamburg, Germany
PVDF membrane	Merck Millipore, Darmstadt, Germany
Reaction tubes (0.5 ml, 1.5 ml, 2 ml)	Eppendorf, Hamburg, Germany
Reagent reservoirs, 50 mL	Corning, New York, USA
Sealing foils for PCR plates	Kisker Biotech, Steinfurt, Germany
Sterican cannulas	BD Biosciences, Heidelberg, Germany
Syringes	Neolab, Heidelberg, Germany
Thincert™ 6-well cell culture inserts (pore Ø 8µm)	Greiner Bio- One, Frickenhausen, Germany
Tips	Eppendorf, Hamburg, Germany
white 96-well microplates	Berthold Technologies, Bad Wildbad, Germany
white 96-well microplates	Berthold Technologies, Bad Wildbad, Germany
µ-Plate 24 Well	Ibidi, Planegg/Martinsried, Germany

### 3.1.10. Laboratory equipment and software

<i>Laboratory equipment</i>	<i>Manufacturer</i>
-20°C freezer MediLine LGex 410	Liebherr, Biberach, Germany
2100 Antigen Retriever	Aptum Biologics, Southampton, U.K.
-80°C freezer U570 HEF	New Brunswick, Hamburg, Germany
Aerosolizer, micro sprayer	IA-1C, Penn-Century, Wyndmoor, PA
Analytical scale XS20S Dual Range	Mettler Toledo, Gießen, Germany
Autoclave DX-45	Systec, Wettenberg, Germany
Autoclave VX-120	Systec, Wettenberg, Germany
Axiovert 40C microscope	Zeiss, Jena, Germany
Cell culture work bench Herasafe KS180	Thermo Fisher Scientific, Darmstadt, Germany
Centrifuge MiniSpin plus	Eppendorf, Hamburg, Germany
Centrifuge Rotina 420R	Hettich, Tuttlingen, Germany
Centrifuge with cooling, Micro200R	Hettich, Tuttlingen, Germany
CO2 cell Incubator BBD6620	Thermo Fisher Scientific, Darmstadt, Germany
Confocal microscope LSM 710	Zeiss, Jena, Germany
Corning® LSE™ Mini Microcentrifuge, 120V	Corning, Wiesbaden, Germany
Demineralized water	Thermo Fisher Scientific, Darmstadt, Germany
Dry ice container Forma 8600 Series, 8701	Thermo Fisher Scientific, Darmstadt, Germany
Electronic pipet filler	Eppendorf, Hamburg, Germany
Film developer Curix 60	AGFA, Morsel, Belgium
Fisher Science Education™ 4-Way Microtube Racks	Thermo Fisher Scientific, Darmstadt, Germany
Fridge MediLine LKv 3912	Liebherr, Biberach, Germany
Gel image system ChemiDoc XRS+	Biorad, Hercules, USA
Ice machine ZBE 110-35	Ziegra, Hannover, Germany
Light Cycler LC480II	Roche Diagnostic, Mannheim, Germany
Liquid nitrogen cell tank BioSafe 420SC	Cryotherm, Kirchen/Sieg, Germany
LSM 710	Zeiss, Jena, Germany
Magnetic stirrer KMO 2 basic	IKA, Staufen, Germany
Mastercycler Nexus	Eppendorf, Hamburg, Germany
Microdismembrator	Sartorius, Göttingen, Germany
Microm HMS740 Robot-Stainer	Thermo Fisher Scientific, Darmstadt, Germany
Multipette stream	Eppendorf, Hamburg, Germany
Nalgene® Freezing Container (Mr. Frosty)	Omnilab, Munich, Germany
NanoDrop 1000	PeqLab, Erlangen, Germany
pH meter InoLab pH 720	WTW, Weilheim, Germany
Pipettes Research Plus	Eppendorf, Hamburg, Germany
Plate centrifuge 5430	Eppendorf, Hamburg, Germany



Plate reader Sunrise	Tecan, Crailsheim, Germany
Plate reader TriStar LB941	Berthold Technologies, Bad Wildbach, Germany
Power Supply Power Pac HC	Biorad, Hercules, USA
Roll mixer	VWR International, Darmstadt, Germany
Scale XS400 2S	Mettler Toledo, Gießen, Germany
Shaker Duomax 1030	Heidolph, Schwabach, Germany
Syringe pump	AL-1000, World precision instruments, USA
Thermomixer compact	Eppendorf, Hamburg, Germany
Ultra-pure water supply MilliQ Advantage A10	Merck Millipore, Darmstadt, Germany
Vibratome	Hyrax V55, Zeiss, Jena, Germany
Vortex Mixer	IKA, Staufen, Germany
VWR® Tube Rotator and Rotisseries	VWR International, Darmstadt, Germany
Water bath Aqua Line AL 12	Lauda, Lauda-Königshofen, Germany

<i>Software</i>	<i>Manufacturer</i>
Adobe Illustrator	Adobe Systems, San Jose, USA
Axio Vision	Zeiss, Jena, Germany
GraphPad Prism 5	GraphPad Software, La Jolla, USA
Image J	NIH, Wisconsin, USA
Image Lab Software, Version 5.2.1	Biorad, Hercules, USA
Imaris 9.0 software	Bitplane, Zurich, Switzerland
LightCycler® 480 SW 1.5	Roche Diagnostics, Mannheim, Germany
Magelan Software	Tecan, Crailsheim, Germany
Microsoft Office Professional Plus 2016	Microsoft, Redmond, USA
Tristar MicroWin 2000	Berthold Technologies, Bad Wildbach, Germany
Zen digital Imaging for Light microscopy Software	Zeiss, Oberkochen, German

### 3.1.11. Standards and kits

<i>Standards</i>	<i>Manufacturer</i>
1 kb DNA ladder	Peqlab, Erlangen, Germany
100 bp DNA ladder	Peqlab, Erlangen, Germany
Protein marker V	Peqlab, Erlangen, Germany
Ultra low range DNA ladder I	Peqlab, Erlangen, Germany

<i>Kits</i>	<i>Manufacturer</i>
BCA Protein Assay kit	Biochrom, Berlin, Germany
LightCycler 480 SYBR Green I Master	Roche Diagnostics, Mannheim, Germany
PeqGold RNA kit	Peqlab, Erlangen, Germany
RhoA G-LISA kit	Cytoskeleton Inc., Denver, USA
Roti Quick Kit	Carl Roth, Karlsruhe, Germany

## 3.2. Methods

### 3.2.1. Cell biological methods

#### 3.2.1.1. Isolation and culture of primary human lung fibroblast

Primary human lung fibroblasts (phFbs) were harvested from the lung tissues derived from tumor-free area of lung resections or lung explants provided by the CPC-M Bio archive, Munich, Germany. For this, the lung tissue explants were taken in a 10cm cell culture dish with pre-warmed DMEM F-12 supplemented with 20% FBS and 100 U/ml of penicillin and streptomycin. The tissues were then minced into 1-2 mm<sup>2</sup> pieces via sterile scissors or scalpel and thereafter transferred to a 50ml falcon tube. 5 mg of Collagenase I (Biochrom) was added into the falcon with diced lung tissue pieces in medium and digested at 37°C for 1 hour. Thereafter the filtrates containing the cells were passed through 70 µm nylon filters (BD Falcon) and washed twice with sterile 1X PBS for 5 mins each at 450g at 4°C. The supernatant was carefully discarded and the pellet resuspended in supplemented DMEM F-12 medium and subsequently cultured in 10 cm cell culture dishes under standard conditions at 37°C and 5% CO<sub>2</sub>. Medium was changed 3 times a week and cells were grown until 80-90% confluency and then split. Cells were washed once with 1X PBS and 0.25% of Trypsin-EDTA (Sigma) were then added and the plate kept for 5 mins at 37°C. Cell suspension was then transferred to a 50 ml falcon and centrifuged for 5 mins at 500g. Next, media containing trypsin was aspirated out and the cell pellet was immediately suspended in fresh FBS and antibiotic supplemented DMEM F-12 media. All experiments were performed with phFbs from passage 3-8.

#### 3.2.1.2. Cryopreservation of mammalian cells

Cryopreservation was achieved by freezing cells in liquid nitrogen. First the cells were washed with 1X PBS, trypsinized with pre-warmed trypsin-EDTA solution for 5 mins at 37°C in complete medium. Cell

suspension was then transferred to a 50ml falcon and rotated for 5 mins at 500g. Next, the trypsin containing media was aspirated out and the pellet suspended in freezing medium (90% FBS supplemented with 10% DMSO). Subsequently the cell suspensions (in approx.  $1-2 \times 10^6$  cells/ml concentration) were transferred to cryovials and frozen in a Mister Frosty (Omnilab) overnight at  $-80^{\circ}\text{C}$  and then kept in liquid nitrogen at  $-195^{\circ}\text{C}$  for long-term storage.

#### **3.2.1.3. Thawing frozen cells**

The frozen cell suspension in cryovials were placed in the water bath at  $37^{\circ}\text{C}$  for approximately 2-3 mins or until the suspension was defrosted. Next, the cell suspension was immediately diluted with 1 ml pre-warmed DMEM F-12 media supplemented with 20% FBS and 100 U/ml of penicillin/streptomycin and promptly transferred to a 50 ml falcon with an additional 8 ml of the FBS supplemented DMEM media. Cells were then centrifuged at 500g for 5 mins and the supernatant was carefully discarded. The cell pellet was resuspended in fresh 20%FBS and antibiotic containing DMEM F12 media and subsequently transferred to a 10 cm sterile cell culture dish and cultured under standard cell culture conditions at  $37^{\circ}\text{C}$  and 5%  $\text{CO}_2$ .

#### **3.2.1.4. MTT cell viability assay**

Metabolic activity of the cells was determined by the MTT assay which measured the reduction of the soluble MTT (3-(4,5-dimethylthiazol-2-yl)-2,5-diphenyltetrazolium bromide) to the insoluble purple colored formazan via NAD(P)H dependent process [151]. Firstly, 5 mg/ml of MTT solution was prepared by dissolving the soluble MTT (Sigma) in 1X PBS, then vortexed, filter sterilized and stored in  $-20^{\circ}\text{C}$  in the dark. Then the MTT solvent was prepared mixing 0.1% Triton-X-100 (Aplichem) in isopropanol. Cells were cultured in 96 well plates. Next, 20 $\mu\text{l}$  of MTT solution was added per well of the plate and incubated at  $37^{\circ}\text{C}$  for 1 hr. Wells containing 0.1% DMSO along with medium served as negative control and well containing only media served as a blank control. Medium was then aspirated out gently and the formazan crystals formed were dissolved in 100  $\mu\text{l}$  of the MTT solvent prepared earlier. The absorbance of the plate was then measured at 570 nm using a Sunrise TM plate (Tecan).

#### **3.2.1.5. Liposome based cell transfection**

Human siRNAs used in all the studies here were purchased from Thermo Fischer Scientific (Table 3.1.2) as lyophilized products and were diluted in Nuclease free water. Briefly, the lyophilized vial was centrifuged and the siRNA was suspended in nuclease free water at a final concentration of 100  $\mu\text{M}$ . The siRNA stock solutions were further diluted in nuclease-free water in order to obtain a working concentration of 2  $\mu\text{M}$  which can be stored at  $-80^{\circ}\text{C}$  for long term without degradation. The transfection mix was prepared by formulation of solution A and B as follows:

**Table 3.2.1: Transfection-mix for 1 well (6-well format):**

<i>Solution</i>	<i>Reagent</i>	<i>Volume (<math>\mu</math>l)</i>
<b>Solution A</b>	OptiMem Media	114
	siRNA	15
<b>Solution B</b>	OptiMem Media	114
	Lipofectamine RNai Max <sup>®</sup>	7

At first, solutions A and B were prepared separately and incubated for 5 mins at room temperature inside the cell culture hood. Then, both solutions were pooled together in one eppendorf and incubated for 20 mins at room temperature in order to form the siRNA-lipofectamine complexes. In parallel,  $2.5 \times 10^4$  cells were seeded in 2 ml media (DMEM, 20% FBS without penicillin/streptomycin) per well of a 6-well plate. Subsequently, 250  $\mu$ l of the transfection mix was added to each well along with antibiotics-free cell culture medium and mixed with the 2ml of cell suspension. For untreated condition, 250  $\mu$ l of the Opti-Mem media was added in the cell suspension. For the experiment testing siRNA efficiency and stability across 6 days, pHFs were transfected for 48 hrs and then replenished with fresh media without siRNA and kept for additional 24, 48 and 96 hrs. Protein isolations (3.2.8.1) were carried out from each time-points.

To assess the stability of the knockdown, a time-resolved study for the siRNA treatment was performed with a pHFb cell line. After 48 hrs of siRNA incubation with the cells, the siRNA containing medium was aspirated out and the cells were washed with sterile 1X PBS. Subsequently, the cells were further cultured in fresh medium with antibiotics for additional 96 hours. Protein extraction for immunoblotting was performed every 2 days.

### **3.2.1.6. Cell culture treatments**

Primary human fibroblasts (pHFs) and mouse lung fibroblasts (CCL206; mLFbs) were seeded in a 24-well ( $1.0 \times 10^5$  cells/ well) or 6-well ( $2.5 \times 10^5$  cells/ well) plates in 20 % FBS and 100 U/ml of penicillin/streptomycin supplemented DMEM-F12 media. Cells were synchronized in serum starved media (DMEM-F12, 1% FBS and 100 U/ml penicillin/streptomycin) next day for 24 hrs prior to treatment with growth factors and inhibitors. Subsequently, the cells were stimulated with 1 ng/ml of human recombinant TGF $\beta$ 1 in starvation media for 48 hrs. Additionally, pHFs and mLFbs were also stimulated with 10 ng/ml of EGF, 10 ng/ml of FGF2, 10 ng/ml of PDGF BB, 10 ng/ml of TNF $\alpha$ , 1  $\mu$ g/ml of LPS, 100ng/ml of Wnt3A and 10ng/ml of Wnt5A.

For inhibitor treatments, cells were serum starved for 24 hrs as described above prior to treatments and then subsequently stimulated with individual inhibitors for 24 to 48 hrs. phFbs were stimulated with 10  $\mu$ M of SB431542, 6  $\mu$ M of Sis3, 10  $\mu$ M of U0126, 2  $\mu$ M of BIBF-1120 (Nintedanib), 10  $\mu$ M of SP600125, 150  $\mu$ M of Tranilast, 10-30  $\mu$ M of commercially available SFRP1 Inhibitor (Sigma, CAS915754-88-0) and 0.5-1  $\mu$ g/ml of Rho inhibitor (CT04).

Relating to epigenetic regulation studies, phFbs were seeded in 6-well ( $2.5 \times 10^5$  cells/ well) culture dishes in 20 % FBS and 100 U/ml of penicillin/streptomycin supplemented DMEM-F12 media. Subsequently, the cells were stimulated with 0.05-5  $\mu$ M of 5-aza-2'-deoxycytidine (DAC), 30-3000 nM of Trichostatin A (TSA) for 48 and 72 hrs. DMSO as a vehicle control was directly added to the unstimulated cells.

### 3.2.1.7. Preparation of cells for morphology analysis

Cells were plated in a density of  $5 \times 10^2$  cells/well in 96-well plates in DMEM-F12 media supplemented with 20%FBS and 100 U/ml penicillin-streptomycin. The cells were kept in the incubator for 24 hrs to allow cell attachment and growth under standard cell culture conditions of 37°C and 5% CO<sub>2</sub>. Subsequently, the cells were fixed next day with 4% PFA for 30 minutes at RT. The fixed cells were next stained with DAPI (nuclear dye) and Phalloidin (label F-actin) diluted in 1X PBS and incubated overnight at 4°C. The next day, cells were washed twice with 1X PBS and stored in fresh PBS until imaging.

## 3.2.2. 3D cell culture models

### 3.2.2.1. Preparation of collagen matrix

Matrices from Collagen G gel (Biochrom AG, produced from calf skin) was first prepared. Briefly, solution A containing 1:1 0.7(M) NaOH and sterile filtered 1(M) HEPES was mixed 1:1 with 20% FBS in 10X PBS resulting in solution B. Next, a third solution C was prepared by gently mixing solution B and Collagen G in 1:4 ratio (Table 3.2). All reactions were kept on ice, as Collagen G solidifies at RT.

**Table 3.2.2: Preparation of collagen matrices**

	<i>Ratio</i>	<i>Ingredients</i>
<b>Solution A</b>	1:1	0.7(M) NaOH + 1(M) HEPES
<b>Solution B</b>	1:1	Solution A + 20% FBS in 10X PBS
<b>Solution C</b>	1:4	Solution B + Collagen G

For the invasion assay in a 96-well plate, 50 $\mu$ l of the collagen solution was pipetted per well and 500 $\mu$ l per ThinCert cell culture insert for the 6-well plate. An electronic Multipipette (Eppendorf) was used to

carefully dispense the viscous collagen solution in the cell culture dishes to avoid bubbles and to have reproducible results. The final collagen G solution was incubated at 37°C for 4-6 hrs to allow polymerization of the gel.

### 3.2.2.2. 3D collagen-based invasion assays

For the invasion assay using Thin-Certs in a 6-well plate,  $2.5 \times 10^5$  cells were seeded on top of the polyethylene terephthalate (PET) capillary 8  $\mu$ m pore membrane after gelation of the collagen matrix. DMEM-F12, 20% FBS and 100 U/ml penicillin-streptomycin media was used to culture these pHFBs in the Thin-Certs. The cells were left to invade the collagen matrix for 96 hrs under standard cell culture conditions of 37°C and 5% CO<sub>2</sub>. The collagen matrix on the bottom of the Thin-Certs have the invaded fibroblast population and the PET capillary membrane contained the non-invading fibroblasts attached. After 4 days, the culture insert was washed twice with ice cold PBS and the collagen matrix was separated from the membrane gently using a pair of tweezers. Protein and RNA were subsequently isolated from the two fractions as described in sections 3.2.8.3 and 3.2.9.2 respectively.

After gelation in the 96-well plate,  $2 \times 10^4$  cells/well were seeded on top of the polymerized collagen matrix. Cells were again similarly left to invade the collagen matrix for 96 hrs under standard cell culture conditions of 37°C and 5% CO<sub>2</sub>. Thereafter, the wells were washed with 1X PBS and fixed with 4% PFA for 30mins at RT and then subsequently stained with DAPI (1:1000) overnight at 4°C. For a separate study, cells were permeabilized with Triton-X-100 after fixation for 15 mins at RT and stained with DAPI (1:1000), phalloidin (1:300) and anti- $\alpha$ SMA antibody (1:2000) overnight at 4°C. Staining with phalloidin was carried out to visually assess the integrity of single cells and  $\alpha$ SMA staining to identify myofibroblasts. Each well containing the 3D collagen matrix embedded cells were imaged using a LSM 710 confocal microscope. Quantification of invasion capacity was accomplished according to 3.2.10.2.

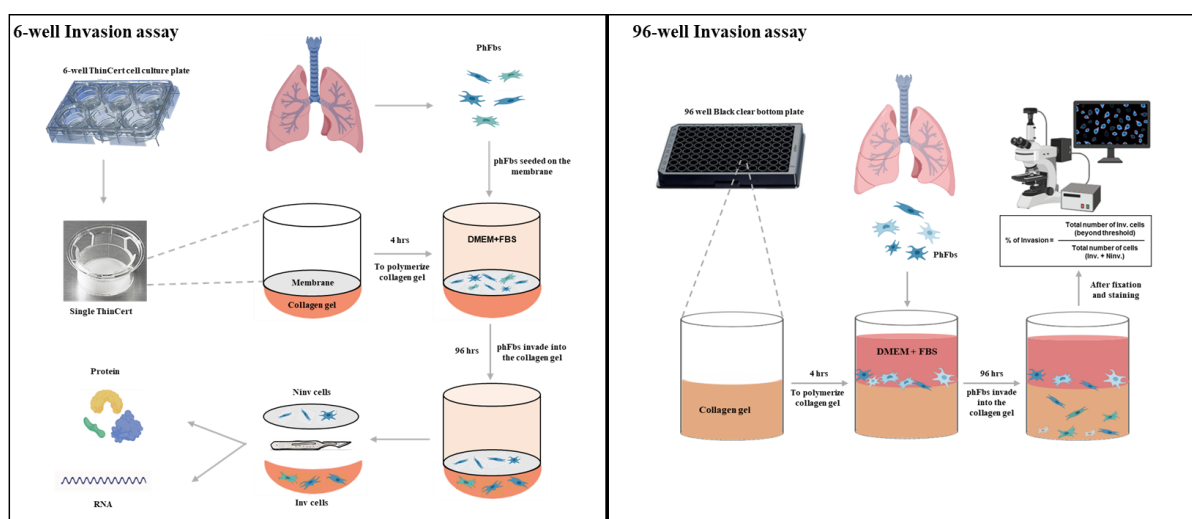


Figure 3.1: Schematic representation of 6-well and 96-well invasion assays

### 3.2.3. Animal experiments

Animal experiments were carried out according to the German protection law and were then approved by an external review committee for animal care. C57BL/6 mice were obtained from Charles River Laboratories and kept in Helmholtz Zentrum München. The mice were kept in rooms maintained at constant temperature and humidity and provided with food and water *ad libitum*. All animal experiments were carried out with 8-12 weeks old C57BL/6 mice.

#### 3.2.3.1. Isolation of murine fibroblasts

Experimental mice were weighed first and the amount of ketamine/Xylazine were calculated accordingly (100 µl/10 g weight). The mice were anesthetized using injections with 1:1 ratio of the ketamine/Xylazine and waited until they were sleeping. After flushing the lungs (until almost white) with 1X PBS via the right ventricle, the thorax was cleaned and the lungs were removed. The lung lobes were dissected and placed in a 6-well plate in ice cold 1X PBS. The whole lung was cut into 1-2 mm pieces using a scalpel. Afterwards the lung pieces along with the medium was transferred to a 50 ml falcon and collagenase I (5 mg/50 µl) was added to it. Subsequently the solution was digested with collagenase I for 37°C at 400 rpm for 1 hour and then transferred into a filter on a fresh falcon tube. A syringe piston was used to scratch the digested lung solution and then rinsed with sterile 1X PBS. The solution obtained was centrifuged for 5 mins at 400 rpm at 4°C. Finally, after the supernatant was discarded, the pellet was resuspended in fresh medium and cultured under standard cell culture conditions.

#### 3.2.3.2. Bleomycin instillation in mice

Bleomycin treatment in mice were performed by Maximillian Strunz (Helmholtz Zentrum Munich). Briefly, pathogen-free female C57BL/6J mice were acquired from Charles River (Germany) and kept at suitable humidity and temperature and in a biosafety lab. Lung fibrosis was induced by a single dose of Bleomycin (Sigma, Germany). Bleomycin was dissolved in sterile 1X PBS and 2units/kg (For oropharyngeal instillation) and 3units/kg (for intratracheal instillation) of their respective body weight were given. For the control group, 1X sterile PBS was instilled in a similar process as the test group. Meanwhile the test animals were kept under strict inspection for any weight loss or other phenotypic changes. Afterwards, the mice were sacrificed at the respective time-points after Bleomycin instillation.

#### 3.2.3.3. Tissue homogenization

Bead beating was used for tissue homogenization. It was accomplished by rapidly agitating the pre-snap frozen tissue samples with beads or metal balls in a tissue homogenizer (a device that shakes the

homogenization vessel). The beads are either made of glass (silica), steel or ceramic. Samples were then prepared with buffer at either cryogenic temperatures. Samples were kept in liquid nitrogen in small cryotubes with a metal ball inside. Then the tubes were inserted in the homogenisator and operated at 3000 RPM for 30-60 seconds until the tissue was successfully ground to a powder consistency. Care was taken that the cryotubes were properly sealed during the homogenization process. The powdered samples were finally stored at -80°C.

#### **3.2.3.4. Preparation of mouse Precision Cut Lung Slices**

Mouse precision cut lung slices were generated as previously described [152]. Mouse lungs were first filled with pre-warmed 2% (w/v) low-melting point agarose (Sigma Aldrich, A9414) via tracheal cannula utilizing a syringe pump to control the flow rate. The agarose was diluted with DMEM F-12 medium including 100 U/ml penicillin-streptomycin, and 2.5 µg/ml of amphotericin B (Sigma Aldrich, A2942). Subsequently, the lungs were carefully taken out and immediately put in culture medium and transferred on ice. Approximately, 10-15 mins are given for the gelling of agarose in ice. Afterwards, each mouse lung lobes were dissected and sliced in a Vibratome (Hyrax V55; Zeiss, Jena, Germany) to obtain 300 µm thick sections. For immunofluorescence, the PCLS were immediately fixed using ice-cold methanol for 5-10 mins and for RNA or protein isolation, the slices were snap frozen.

#### **3.2.3.5. Preparation of human Precision Cut Lung Slices**

Human precision cut lung slices were generated as previously described [147]. Briefly, the resected tissue was inspected and selected for slicing when the tissue score index was above 72. Any ventilating bronchus of 0.5-3 mm in diameter was closed by clamping a cannula. Afterwards, a peripheral venous catheter was prepared by removing the obturator and attached with a syringe containing low melting point agarose. The ventilating end of the bronchus or any other large airways were sealed with a surgical clamp. Then the agarose was poured via the syringe at a rate of 0.3 mL/sec. Then the tissue was incubated at 4 °C for 30 min to assure agarose solidification. Block tissue regions of 1-1.5 cm<sup>3</sup> were excised, where one side was covered with pleura. Finally, the lung tissue block was sliced using the Vibratome with the settings: thickness of 500 µm, frequency of 100 Hz, amplitude of 1.2 mm, forward speed (of the blade) at 3-12 µm/s. The resulting human PCLS were stored in a 12-well plate with cultivation medium.

#### **3.2.4. Cultivation of 3D *ex vivo* PCLS**

The mouse and human PCLS obtained were cultured in 12- well culture dishes with DMEM F-12 medium supplemented with 0.1 % FBS and 100 U/ml of penicillin and streptomycin and 2.5 µg/ml of Amphotericin B under standard conditions at 37°C and 5% CO<sub>2</sub>.



### 3.2.5. Decellularization of mPCLS

The mPCLS were decellularized according to the protocol established in Burgstaller et al., 2018. Briefly, the 300µm thick mPCLS were washed thrice with sterile deionized water for 5mins and subsequent incubation in 50ml deionized water in a falcon tube on a roller at 4°C for 16 hours. Afterwards, the slices were kept in a 50ml falcon containing 0.1% SDS for 4 hours at room temperature. Following it, the slices were washed twice with deionized water for 10 mins each. Subsequently, the slices were kept in 1 (M) NaCl for 16-18 hours on a roller at 4°C. The LTCs were again washed two times with deionized water for 10 mins each and the incubated in 1X PBS containing 5mM of MgCl<sub>2</sub> and 30 g/ml DNase for 3 hrs at 37°C. At last, the slices after washing for another 3 times were stored in cell culture plates in sterile 1X PBS with penicillin-streptomycin (Sigma).

### 3.2.6. Recellularization of mPCLS

The recellularization protocol followed was according to Burgstaller et al., 2018. Briefly, the decellularized lung slices were repopulated with a suspension of (3 x 10<sup>6</sup> cells/ml) primary mouse or human fibroblasts. The decellularized lung slices along with the cells were put in 15 ml falcons together in DMEM F-12 medium containing 10% FBS. The tubes were sealed with parafilm to allow gas exchange and placed on a tube roller (10-15 rpm) at standard cell culture conditions of 5% CO<sub>2</sub> and 37°C. Followed by 16 hours of incubation, the decellularized lung slices with the engrafted fibroblasts were cultured in 24 well plates in DMEM F-12 with 10%FBS for 2-9 days under standard cell culture conditions.

### 3.2.7. *Ex vivo* fibrosis-mimicking PCLS models

The mouse and human PCLS obtained were cultivated in 12 well culture dishes. Freshly cut slices were treated with the fibrotic cocktail (FC) and control cocktail (CC) for 5 days. The FC was prepared in medium supplemented with 5 ng/ml recombinant human transforming growth factor-β (TGF-β) (R&D Systems), 5 µM of platelet-derived growth factor-AB (PDGF-AB) (GIBCO), 10 ng/ml tumor necrosis factor-α (TNF-α) (R&D Systems), and with 5 µM lysophosphatidic acid (LPA) (Cayman Chemical). The CC was prepared in parallel with all the diluents of the factors used in the FC.

### 3.2.8. Protein analysis

#### 3.2.8.1. Protein isolation from fibroblasts in 2D cell culture

Cells cultured in standard cell culture dishes were washed twice with sterile 1X PBS and then scraped with a cell scratcher in 200 µl of lysis buffer containing RIPA buffer enriched with 1x Roche complete mini protease inhibitor cocktail and Phospho-Stop phosphatase inhibitor (per well in a 6-well dish). The

collected cell lysates were then transferred to an eppendorf placed on ice and subsequently mixed in a rotor at 4°C for about 1 hour. Following the incubation, the lysates were centrifuged at 15,000 RPM for 15 min at 4°C to separate the supernatant (total protein) and the pellet (cell debris). Lastly, cell supernatants and pellets were stored at -80°C for long term storage.

### **3.2.8.2. Concentration of protein from cell supernatants**

Supernatants collected from cells in culture conditions were at first thawed in room temperature. Centrifugal Filter tubes (Amicon Ultra-0.5, Millipore) were used to concentrate the cell supernatants and was performed according to the manufacturer's instruction. Shortly, 500 µl per sample was added into a filter tube inserted into a second microcentrifuge tube. Samples were subsequently centrifuged for 20-30 min at 14,000 RPM at 4°C. To retrieve the concentrated proteins, the filter tubes were inverted and placed in a fresh microcentrifuge tube and centrifuged for 2 min at 1000 RPM at 4°C. Lastly, the concentrated filtrate was stored at -80°C for further analysis.

### **3.2.8.3. Protein isolation from fibroblasts in 3D cell culture**

For protein isolation from 3D cell cultures, collagen gel and membrane were separated as mentioned in section 3.2.2.2. Two gels were pooled into one 2 ml Eppendorf tube and 80 µl (2120 U) of collagenase type1 (Biochrom) was added to it. The tube was incubated in a thermal shaker at 37°C for around 1 hour until the collagen gel is completely degraded, followed by centrifugation for 2 minutes at 500 RPM at 4°C. The resulting pellet was washed two times with sterile cold 1X PBS and lysed with 50 µl of lysis buffer containing RIPA buffer with 1x Roche complete mini protease inhibitor cocktail and Phospho-Stop phosphatase inhibitor. For the non-invading cells, the membranes from the transwell inserts were cut out using a scalpel. Cells were scratched off from two membranes into 1 vial of 200 µl ice cold RIPA buffer with 1x Roche complete mini protease inhibitor cocktail and Phospho-Stop phosphatase inhibitor. The samples were then incubated in ice for around 30 mins followed by centrifugation at 14,000 RPM at 4°C for 15 minutes. The cell debris was discarded and the supernatant was stored at -80°C for further analysis.

### **3.2.8.4. Protein isolation from PCLS**

For protein isolation from the mouse and human PCLS, 500 µl of lysis buffer containing RIPA buffer enriched with 1x Roche complete mini protease inhibitor cocktail and Phospho-Stop phosphatase inhibitor were added to each vial (4 mPCLS pooled per vial, 2 huPCLS pooled per vial). The eppendorfs with the tissue lysates were placed in a rotor at 4°C for 5-6 hours and subsequently centrifuged for 15 min

at 15,000 RPM at 4°C. Tissue lysates were then stored at -80°C and protein concentration was later determined using the Pierce BCA Protein Assay Kit.

#### **3.2.8.5. Protein isolation from lung tissues**

The efficient disruption and homogenization of tissues as described in section 3.2.3.3 ensures a high yield of proteins. 500 µl of a lysis buffer containing RIPA buffer supplemented with 1x Roche complete mini protease inhibitor cocktail and Phospho-Stop phosphatase inhibitor were added per cryo-vial of lung tissue homogenate. The eppendorfs with the cell lysates were placed in a rotor at 4°C for 1 hour and afterwards transferred to a new microcentrifuge tube without the metal ball and subsequently, the tissue lysates were centrifuged for 15 min at 15,000 RPM at 4°C. Tissue lysates were then stored at -80°C and protein concentration was later determined using the Pierce BCA Protein Assay Kit.

#### **3.2.8.6. Bicinchoninic acid (BCA) assay**

Protein abundance of cell lysates from cells and tissues were assessed via the bicinchoninic acid assay (BCA assay). A bovine serum albumin (BSA) titration curve with a concentration range of 0-2 µg/µl diluted in PBS served as a standard to determine protein concentrations. At first, cell lysates were mixed with nuclease-free water in a 1:10 ratio in a 96-well plate. Wells containing only lysis buffer with no cells served as controls. 10 µl of BSA standards were pipetted in the same plate. 200 µl of the BCA reagent according to the manufacturer's protocol (Thermo Fisher Scientific) was added per well. Following incubation at 37 °C for 30 min, the absorbance recorded at 562 nm using a Sunrise TM plate reader (TECAN) for estimation of protein concentrations.

#### **3.2.8.7. SDS-PAGE and immunoblotting**

Protein samples were mixed with 6x lämli loading buffer (final concentration 1x) and proteins were separated using standard SDS (10%) PAGE (20 - 30 mA per gel). For immunoblotting, proteins were transferred to methanol activated PVDF (Millipore) membranes (350 mA for 60 minutes). Subsequently, membranes were then blocked with 5% milk in 1xTBST (0.1% Tween®20 in TBS) and incubated with primary, followed by HRP-conjugated secondary antibodies at 4°C overnight and at room temperature for 2 hours, respectively. Upon antibody incubation, the PVDF membranes were washed thrice with 1X TBST for 10 min each and proteins were finally visualized by using western blot chemiluminescent substrates (SuperSignal®, Thermo Fisher). The membranes were either visualized by developing an X-Ray film using a Western Blot developer machine (AGFA) or the protein signal was detected with the Chemidoc XRS+ system (Bio-Rad).

### 3.2.8.8. RhoA G-LISA assay

The RhoA G-LISA assay (Cytoskeleton Inc.) was performed according to the manufacturer's protocol. Briefly, at first the cell lysates were prepared for the assay. Then the lysates were snap frozen in liquid nitrogen and thawed on the day of the activation assay. As, equal protein concentrations were required for the assay, concentration of the lysates were quantified using 10 $\mu$ l of the lysate with 290 $\mu$ l of Precision Red™ Advanced Protein Assay Reagent. The absorbance was subsequently assessed by a plate reader at 600 nm. Lysate concentration between 0.4-2.0 mg/ml was used. The lysates having the same concentration were then transferred to the coated wells and bound to the wells by the binding buffer. After a series of washing steps, anti-RhoA and subsequently secondary HRP labelled antibody were used to detect the bound active RhoA-GTP cell lysates. The degree of RhoA activation was finally quantified by measuring absorbance at 490 nm using a microplate spectrophotometer.

### 3.2.8.9. Proteomic screening

Proteomic analysis by LC-MS/MS as described was performed by Dr. J. Merl-Pham (HMGU). Briefly, 10  $\mu$ g concentration of protein from whole cell lysate were subjected to tryptic digest using a modified FASP procedure [153]. Following subsequent proteolyzing steps, LC-MS/MS was performed with the peptides collected on a Q-Exactive HF mass spectrometer (Thermo Scientific). Quantification of the acquired spectra was done with the Proteome discoverer 2.2.

### 3.2.8.10. Immunofluorescence staining of primary human lung fibroblast

phFbs were seeded in black 96 well imaging plates (Corning) in a density of 5x10<sup>2</sup> cells/ well. Cells were cultured in DMEM F-12 medium supplemented with 1% FBS and Pen-Strep overnight. Subsequently, the next day the cells were fixed in 4% PFA in PBS at 37°C for 30 minutes at room temperature and then permeabilized with 0.5% Triton-X in 4% PFA for 15 minutes. Phalloidin (Thermo Fischer) (1:300) and DAPI (1:1000) were mixed in 1% bovine serum albumin (BSA, Sigma) in PBS and added to the samples and incubated at 4°C for 18 hours. Afterwards, samples were washed three times with PBS for 10 minutes each. Images were acquired with a LSM 710 as z-stacks and a LD C-Apochomat 406/1.1 NA water objective lens (Carl Zeiss).

For the phFbs seeded on a collagen gel, the cells were fixed with 4% paraformaldehyde (PFA) diluted in 1X PBS at room temperature for 30 mins after the invasion period (as discussed in section 3.2.2.2). Hoechst (Pierce) was diluted in 1% BSA in PBS and incubated at 4°C overnight. The next day cells were subsequently washed off by rinsing three times with 1X PBS. Cells were finally imaged in PBS with a LSM 710 as z-stacks.

### 3.2.8.11. Immunofluorescence staining of paraffin-embedded tissue sections

Formalin-fixed paraffin-embedded (FFPE) lung tissue sections from PBS and Bleo mouse lungs and from healthy donors and IPF patients were first placed in an incubator at 60°C for an hour followed by tissue deparaffinization process. Using a Microm HMS 740 Robot-Stainer (Thermo Fisher Scientific), the slides containing the tissue sections were automatically incubated with several chemicals as described here:

**Table 3.2.3: Deparaffinization protocol**

<i>Description</i>	<i>Reagents</i>	<i>Cycles</i>	<i>Time</i>
<b>Deparaffinization step</b>	Xylene	2x	5 min
	100% ethanol	2x	2 min
	90% ethanol	1x	1 min
<b>Hydration step</b>	80% ethanol	1x	1 min
	70% ethanol	1x	1 min
	dH <sub>2</sub> O	1x	30 sec

Next, the tissue section containing slides were placed in R-Universal buffer (Aptum Biologics) followed by transfer to an antigen retrieval buffer containing pressure chamber (2100 Retrieval, Aptum Biologics). After 30 mins inside the pressure chamber, the slides were washed once in 1X Tris buffer for 10 min and then incubated in 5% BSA in PBS for 40 mins at room temperature. Subsequently the tissues sections were stained with primary antibodies overnight at 4°C under humid conditions. Next day, the slides were washed twice in 1X PBS for 10 min, and further incubated with fluorescently-labeled secondary antibodies for 2 hours at room temperature under humid conditions. Following two additional washes, slides were then counterstained with DAPI for 1 hour at room temperature, washed again two times with 1X PBS for 10 min and subsequently dried at room temperature. Finally, using fluorescent mounting medium (Dako), the tissue slides were mounted and kept in the dark at 4°C until further analysis.

### 3.2.8.12. Immunofluorescence staining of PCLS

The mouse and human PCLS were cultivated in 12-well plates in DMEM F-12 supplemented with 0.1% FBS and Pen-strep as discussed in section 3.2.4. Subsequently, the slices were fixed with ice cold methanol for 5 mins at -20°C. Afterwards the slices were permeabilized using 0.25% Triton-X-100 at room temperature for 15 mins. Subsequently, the slices were washed twice with 1X PBS for 10 mins each and then incubated with the primary antibodies diluted in 1% BSA in PBS and incubated overnight at 4°C. Next day, the slices were washed twice in 1X PBS for 10 min, and further incubated with

fluorescently-labeled secondary antibodies for 2 hours at room temperature. Following two additional washes, the PCLS were taken individually in 35 mm dishes and visualized using LSM 710 microscope.

### **3.2.9. RNA analysis**

#### **3.2.9.1. mRNA isolation from primary fibroblasts**

From standard 2D cell culture, mRNA isolation was accomplished using the PeqGold RNA kit (Peqlab) according to the manufacturer's instruction. Subsequently, the concentration of the harvested mRNA was determined spectrophotometrically at a wavelength of 260 nm using the Nano Drop 1000.

#### **3.2.9.2. mRNA isolation from 3D cell culture**

For mRNA isolation, the gel and membrane were separated as discussed in section 3.2.2.2. Two gels were pooled and 1 ml of QIAzol Lysis Reagent (Qiagen) was added and incubated at room temperature for 10-15 minutes. The solution was gently mixed until complete disintegration. For membrane samples, a minimum of two membranes were pooled into one well of a 6-well plate and then incubated in 1 ml of QIAzol Lysis Reagent for 10 minutes. The samples were subsequently transferred to fresh 1.5 ml Eppendorf tubes and 200 µl chloroform was added to them. After vortex, the samples were centrifuged at 12000 g at 4°C for 15 minutes to separate the phases. The upper aqueous phase was then transferred into a fresh tube and RNA was further purified using the RNeasy Mini Kit (Qiagen) according to the manufacturer's protocol. The concentration of the isolated RNA was noted spectrophotometrically at a wavelength of 260 nm with the Nano-Drop 1000.

#### **3.2.9.3. mRNA isolation from PCLS**

At first, the mouse or human PCLS were washed twice with sterile 1X PBS and then immediately snap-frozen using liquid nitrogen. The frozen slices were then powdered in a microdismembrator S (Thermo Fisher Scientific, Germany). Subsequently, 3-4 mPCLS or 1-2 huPCLS were randomly pooled per vial and mRNA was isolated according the manufacturer instructions for the PeqGold RNA kit (Peqlab). Lastly, the RNA concentration was assessed using a Nano-drop spectrophotometer (Thermo Fisher Scientific).

### 3.2.9.4. cDNA synthesis by Reverse Transcription

To perform cDNA synthesis, 1 µg of the isolated mRNA was calculated and diluted with sterile nuclease-free water to a total volume of 20 µl. Subsequently, this mixture was denatured in a Master cycler, using the following settings:

Lid: 45°C

70°C for 10 mins

Hold: at 4°C

Next, a master-mix was prepared using the following reagents at the indicated concentrations (Table 3.2.4)

**Table 3.2.4: Master Mix for cDNA synthesis**

<i>Reagent</i>	<i>Stock concentration</i>	<i>Final concentration</i>	<i>Final volume (µl)</i>
<b>10x PCR Buffer II</b>	10x	1x	4
<b>MgCl<sub>2</sub> solution</b>	25 mM	5 mM	8
<b>PCR Nucleotide Mix (dNTP)</b>	10 mM	1 mM	4
<b>Random Hexamers</b>	50 µM	2.5 µM	2
<b>RNase Inhibitor</b>	20 u/µl	1 u/µl	2
<b>MuLV Reverse Transcriptase</b>	50 u/µl	2.5 u/µl	2
<b>Denatured RNA</b>	-	-	18
<b>Total volume of the master mix</b>			40

Lastly, an ependorf Master-cycler was used to carry out the reverse transcription process. The following settings were used:

Lid: 105°C,

20°C for 10 min

42°C for 60 min

99°C for 5 min.

At last, the cDNA was diluted to a total volume of 200 µl with nuclease-free water and stored at – 80°C for further analysis.

### 3.2.9.5. Quantitative Real Time Polymerase Chain Reaction (qRT-PCR)

Quantitative real-time RT-PCR was performed using a SYBR Green LC480 system (Roche). The master mix was prepared according to:

**Table 3.2.5: qPCR reaction mix per one assay**

<i>Reagent</i>	<i>Stock concentration</i>	<i>Final concentration</i>	<i>Final volume (μl)</i>
<b>DNase/RNase-free H2O</b>	-	-	1
<b>SYBR green I Master Mix</b>	2x	1x	5
<b>Forward/Reverse Primer Mix</b>	10 μM each	0.5 μM each	2
<b>cDNA</b>	6.25 ng/μl	12.5 ng/μl	2
<b>Total</b>			10

The master mix (Roche) was pipetted per well in a 96-well plate. Samples were always added in duplicates and then the plates were centrifuged for 2 min at 1000 rpm prior to starting measurement. The standard program of the Light Cycler 480II (Roche): 95°C for 5 mins followed by 45 cycles of 95°C for 5 sec (denaturation), 59°C for 5 sec (annealing), 72°C for 20 sec (elongation), 60 – 95°C for 1 min with continuous acquisition (melting curve). Gene expression of the different samples was normalized to housekeeping genes Glyceraldehyde 3-phosphate dehydrogenase (GAPDH) and hypoxanthine guanine phosphoribosyl transferase (HPRT). Relative gene expression was determined using the  $\Delta\Delta CT$  method.

### 3.2.9.6. Microarray

Microarray analysis was performed by Dr. Martin Irmeler (HMGU). Briefly, total RNA harvested as described earlier (3.2.9.1) were checked for their purity using the Agilent 2100 Bioanalyzer system. Pure high-quality RNA having RNA integrity number at least more than 8 was utilized for further analysis. Then, 150 ng of the total RNA was amplified using the Affymetrix® GeneChip® WT Terminal Labeling Kit and Ambion® WT Expression Kit. The resulting amplified cDNA was hybridized on Affymetrix Mouse Gene 1.0 ST arrays. For human fibroblasts, the amplified cDNA was hybridized on Human Clariom S arrays. Subsequent staining and scanning was done according to the Affymetrix protocol.

## 3.2.10. In silico analysis

### 3.2.10.1. Analysis of cell morphology

For analysis of cell morphology, phFbs were cultured as described in section 3.2.1.8 and imaged according to section 2.3.2.7. Confocal fluorescent z-stacks were volume rendered with Imaris 7.4.0 software (Bitplane). Subsequently, the cell shape parameters were further quantified using Cell Profiler.



### 3.2.10.2. Quantification of 3D cellular invasion

The acquired imaging data sets, as described in section 3.2.2.2, were imported into Imaris 8.4.0 software (Bitplane) and cropped in 3D. Using their spot-detection algorithm, one spot was assigned for each fluorescent nucleus. Then, the total number of spots was filtered based on their z-position, where a threshold was fixed at the lowest point of the collagen gel. Next from the statistics tool, the number of spots or cells invading into the collagen gel can be obtained along with the total number of spots. Thus, from there the number of non-invading cells and thereby the percentage of invasion can be calculated. The percentage for relative invading fraction (Rel.Inv.fraction) was calculated as:

$$\% \text{Rel.Inv.fraction} = \frac{\text{Total number of invading cells (Beyond threshold)}}{\text{Total number of cells (Invading + Non-invading)}}$$

### 3.2.10.3. Bioinformatical analysis

For the statistical transcriptome analysis, expression console (Affymetrix) was used for quality control and to obtain annotated normalized robust multiarray average approach (RMA) gene-level data (standard settings including sketch-quantile normalization). Heatmaps were generated with CARMAweb (Rainer, Sanchez-Cabo et al. 2006) and cluster dendrograms with the R script hclust. Analysis of single cell data obtained from Droplet based sequencing was kindly performed by Maximilian Strunz and Christoph Mayr. To lessen the technical bias introduced by ambient RNA, SoupX (Young, & Behjati, 2018) was applied and the pCut parameter was set to 0.3. Data analysis of the cells that passed the quality controls were represented in a t-distributed Stochastic Neighbor Embedding (t-SNE) plot or Uniform Manifold Approximation and Projection (UMAP) plot showing distinct gene expression profiles.

### 3.2.10.4. Statistical analysis

Statistical analysis was performed using GraphPad Prism v8.0 (GraphPad Software). Data were presented as mean  $\pm$  standard deviation (SD). Statistical analysis was performed using unpaired and paired t-tests (two-tailed) or One-way ANOVA with Dunnett's multiple comparison test. For microarray experiments statistical analyses were performed by utilizing the statistical programming environment R (R Development Core Team Ref1). Genewise testing for differential expression was done employing limma t-test and Benjamini.

## **4. Chapter A: Characterization of SFRP1 as a novel regulator of lung fibrosis**

### **4.1. Introduction**

The remodeling of extracellular matrix (ECM) during tissue repair in lung fibrosis is a complex and dynamic process. The lung is constantly being exposed to harmful environmental substances, viral or bacterial infections and even autoimmune reactions. Subsequent lung regeneration is intervened by reactivated developmental pathways and programs [137]. This eventually leads to an altered ECM secreted by the mesenchymal cells. To comprehensively characterize aberrant ECM deposition in fibrosis and discover potential regulators for remodeling mechanisms, a quantitative detergent solubility profiling (QDSP) along with a systematic comparative analysis of the transcriptomic profiles were performed with unbiased measurement of the interactions between the mediators and the ECM. In this study [145] the authors identified and validated novel constituents of the provisional extracellular repair matrix, like Emilin-2 and Collagen-28, in the bleomycin-induced fibrotic mouse model. Data mining in this proteomics dataset revealed Secreted frizzled related protein1 (SFRP1) amongst the highest upregulated proteins in the insoluble ECM fraction at day 14 after bleomycin treatment. Reportedly, SFRP1 binds to the soluble Wnt ligands and thereby antagonizes their interaction with the frizzled receptors. A dysregulated activation of the Wnt signaling plays a key role in the pathogenesis of various diseases [43]. Several transcriptomic analyses have confirmed enrichment of various Wnt-related genes specifically SFRP1 in the IPF lungs [45, 154]. Moreover, several studies have reported epigenetic regulation of SFRP1 in various types of metastatic cancers. A pan-cancer analysis has shown that SFRP1 was the only one among its isoforms to associate persistently with tumor suppressive functions [155]. Given the importance of active Wnt signaling in lung regeneration, it is conceivable that SFRP1 as one of the major antagonists of this pathway plays an important role in lung diseases and repair. However, surprisingly very little is known about the role of SFRP1 in non-cancer diseases relating to the adult lung.

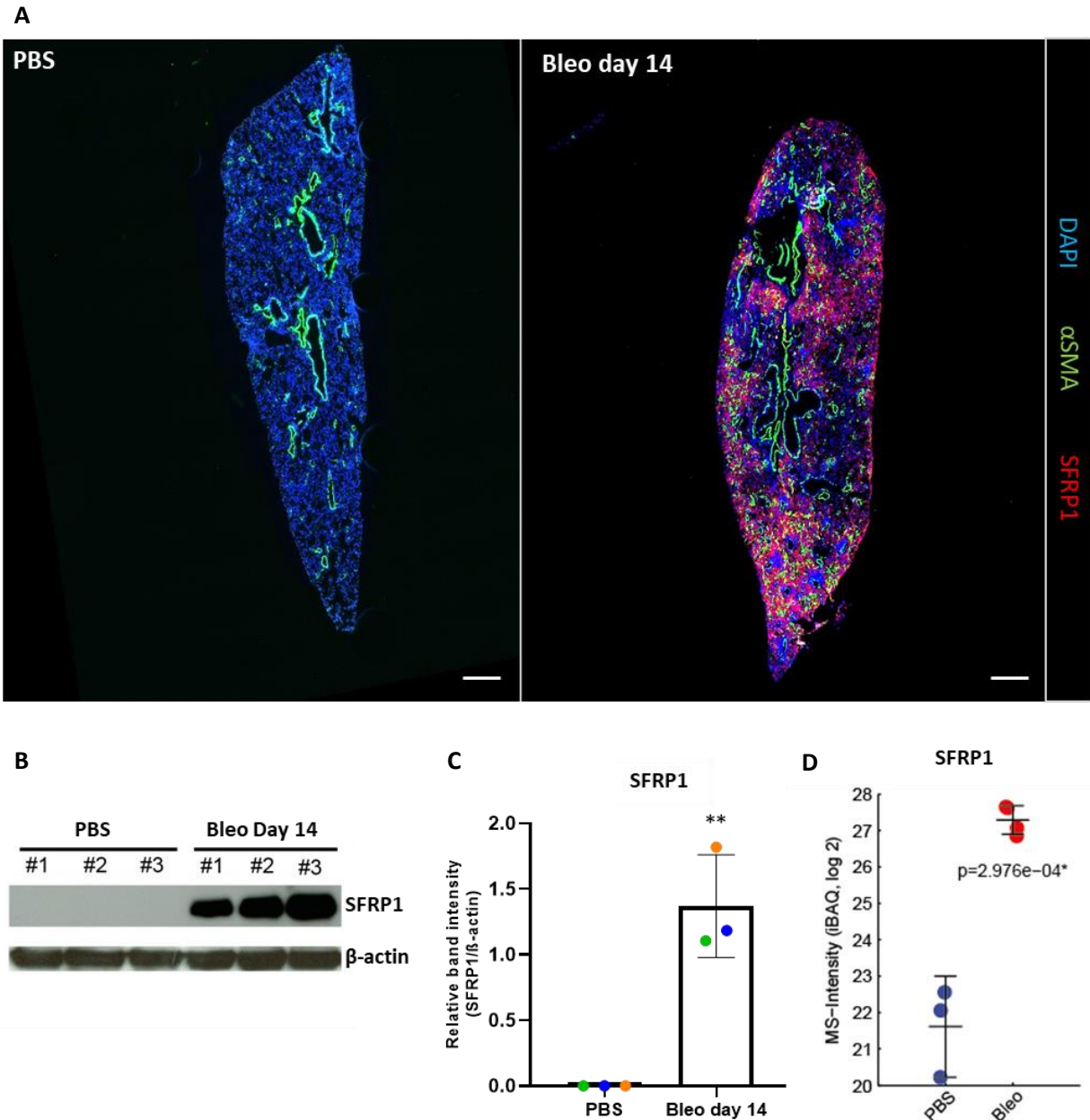
To understand the role of SFRP1 with regards to lung fibrosis, lung tissues from IPF patients and bleomycin-induced mice were analyzed together with various *ex vivo* models. Additionally, the modulatory function of SFRP1 in general was assessed in specific healthy and fibrotic lung fibroblast populations.

## 4.2. Results

### 4.2.1. Part I: Role of SFRP1 in lung fibrosis

#### 4.2.1.1. Upregulation of SFRP1 in a mouse fibrosis model

The use of animal models reproducing key features of IPF has become indispensable in investigating the underlying pathologies of fibrosis. The bleomycin model is the most extensively used and best characterized among different animal models of pulmonary fibrosis [156]. The intratracheal instillation of bleomycin (Bleo) results in bronchiocentric accentuated fibrosis and scarring which is very similar to human pulmonary fibrotic diseases. The “switch” between the inflammatory phase and fibrotic stage occur around day 9 after Bleo treatment and the fibrosis symptoms peak at around day 14 [157]. IPF is characterized by scarring of pulmonary parenchyma due to the accumulation of  $\alpha$ - smooth muscle actin ( $\alpha$ SMA) positive myofibroblasts in the fibrotic foci sites [158]. Therefore, SFRP1 expression in fibrotic areas of the mouse lungs were visualized with immunofluorescence co-staining of SFRP1 and  $\alpha$ SMA on 3-5  $\mu$ m thick FFPE sections of Bleo day 14 and healthy PBS mouse lungs. As depicted, SFRP1 expression was found to be increased in fibrotic lung sections at day 14 compared to PBS lung sections (Fig. 4.1 A). To evaluate the expression of SFRP1 in the fibrotic Bleo mouse model, total lungs from 3 healthy (PBS instilled) and 3 Bleo induced (day 14) mice were harvested and homogenized to assess protein levels. SFRP1 protein expression normalized with  $\beta$ -actin levels confirmed a 1.37-fold increase in bulk SFRP1 expression in the Bleo day 14 mouse lungs compared to healthy PBS instilled control lungs (Fig. 4.1 B-C). Furthermore, by using a quantitative detergent solubility protein profiling method, specific fractions from the total mouse lung homogenates were extracted. Total protein abundance study from all the fractions revealed increased SFRP1 expression (p-value: 2.976e-04) in the Bleo-induced mouse lungs compared to PBS-instilled control mouse lungs [145] (Fig. 4.1 D).

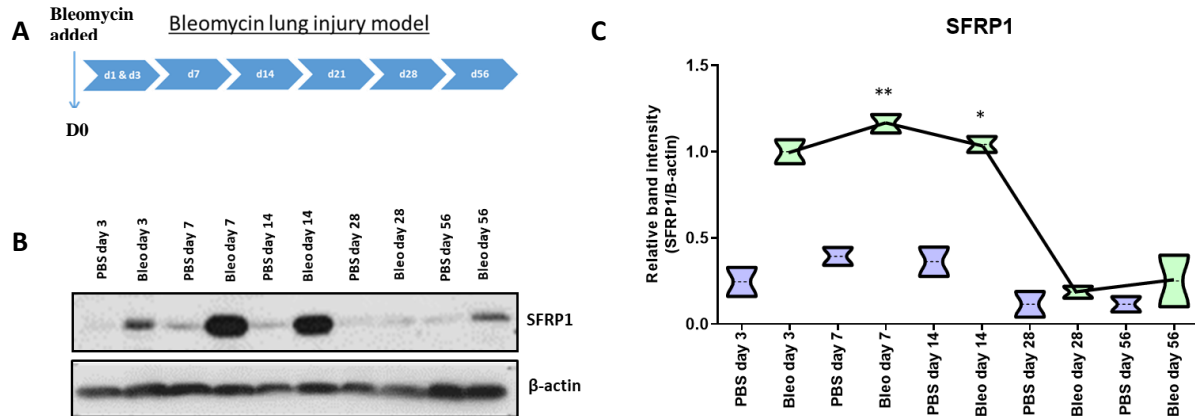


**Figure 4.1: Increased SFRP1 expression in fibrotic mouse lungs**

Immunofluorescence co-staining of FFPE sections of control and fibrotic mouse lungs immunofluorescently stained for DAPI (blue), SFRP1 (red) and  $\alpha$ SMA (green) Scale bar: 150  $\mu$ m(A). SFRP1 expression is significantly increased in fibrotic mouse lungs at day 14 as revealed by immunoblot analysis of whole lung lysates from PBS and Bleo day 14 (B) and quantitative densitometry graph normalized with  $\beta$ -actin values. Data are shown as mean  $\pm$  SEM. Statistical analysis: Paired two-tailed t-test. \*\*\*p-value < 0.001, \*p-value < 0.05 (C). The total protein abundance of SFRP1 from MS analysis shown here (PBS n=3 and Bleo n=3). Data are shown as mean  $\pm$  SEM. Statistical analysis: One-way ANNOVA (D).

Next, SFRP1 protein expression changes in fibrotic mouse lungs after Bleo induced injury were investigated in a time series. Classical hallmark time-points in Bleo-mediated lung injury were associated with inflammation ( $\sim$  day 3), fibrogenesis ( $\sim$  day 14), remodeling ( $\sim$  day 28) and finally resolution ( $\sim$  day 54) (Schiller et al., 2015). Here, total lungs from 2-3 mice at different time-points throughout the Bleo

treatment were homogenized (Fig. 4.2 A). Early expression of SFRP1 was observed from day 3 onwards in the fibrotic mouse lungs followed by a progressive increase in expression with peaks at day 7 and day 14 during the fibrogenic phase. SFRP1 expression was found to decline rapidly with the onset of the resolution stage from day 28 on (Fig.4.2 B- C).



**Figure 4.2: Dynamics of SFRP1 expression in the fibrotic mouse model**

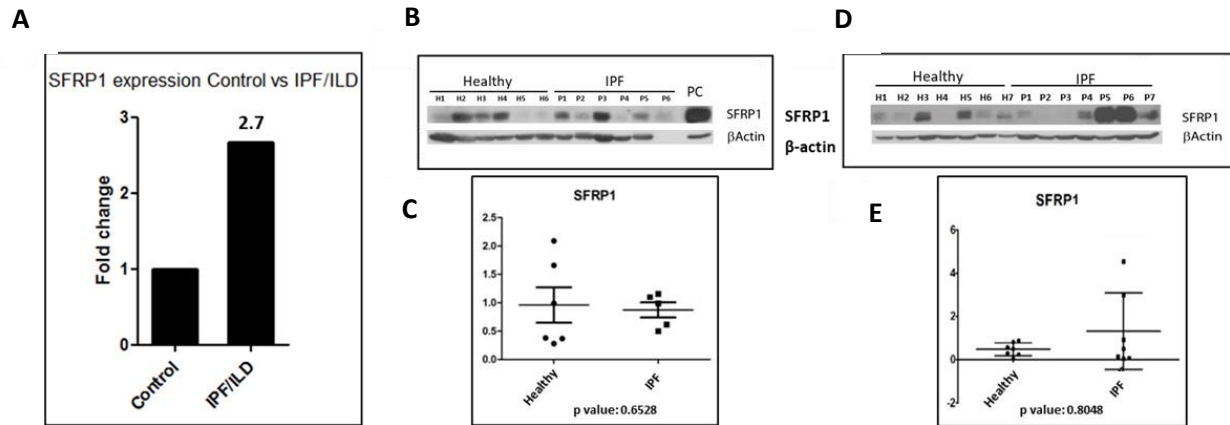
Time-resolved fibrogenesis in the IPF mouse model after bleomycin injury (A). Representative western blots (n=2, 3) for SFRP1 protein expression at different time-points during fibrogenesis (B). Quantification of SFRP1 expression by densitometric analysis demonstrating significant alterations of SFRP1 expression levels during the time-course. Data are shown as mean ± SEM. Statistical analysis: Paired two-tailed t-test. \*\*\*p-value < 0.001, \*p-value < 0.05 (C).

#### 4.2.1.2. SFRP1 is heterogeneously expressed in IPF patients

Prominent features of IPF include its irreversible and progressive nature which are not fully recapitulated by the available murine models [159]. There has been significant progress in the recent years to understand the abnormal molecular mechanisms causing the IPF. The data revealed SFRP1 among the upregulated genes with a 1.127-fold upregulation in IPF patients related to healthy controls or other interstitial diseases. A more recent study performed an unbiased mRNA profiling on 194 human tissue samples including 84 healthy control and 110 IPF patient lung samples [39]. The study found a significant 2.7-fold upregulation of SFRP1 in the IPF cohort compared with the healthy human lung tissues (Fig. 4.3 A). Another study in 2012 reanalyzed previously published microarray datasets on chronic interstitial lung disorders and performed global mappings of the functional motifs to differentiate IPF from other interstitial lung diseases [45].

We obtained samples from two separate patient cohorts which contained lung resections from healthy donors and IPF patients. One cohort belonged to the Munich Lung Tissue (MLT) bio-archive obtained from the Asklepios Clinic and another to Gießen, Germany. The lung tissues obtained from MLT comprised of 6 healthy (H) and 6 IPF (P) (Fig. 4.3 B) and the Gießen cohort encompassed 7 healthy and

7 IPF tissue samples (Fig. 4.3 D). The human tissue samples were found to be very heterogeneous with respect to SFRP1 expression. SFRP1 protein expression as calculated by densitometric analyses from both MLT (Fig. 4.3 B-C) and Gießen (Fig. 4.3 B-C) cohort demonstrated insignificant changes between healthy and IPF tissues.

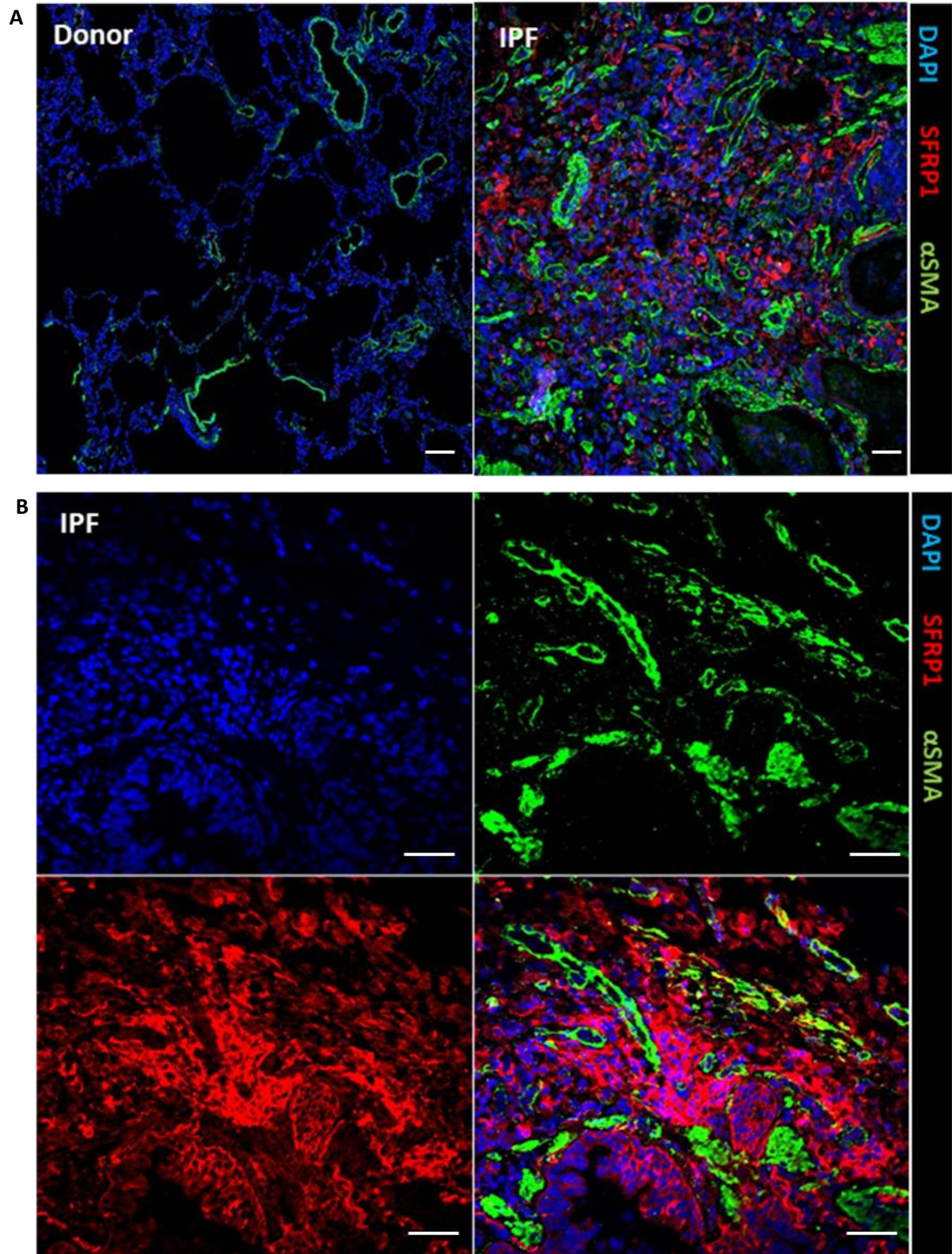


**Figure 4.3: Expression of SFRP1 in healthy human controls and IPF patients**

Transcriptomic profile of 84 healthy controls and 110 IPF patient lung samples display increased SFRP1 expression within the IPF cohort (data taken from [39]) (A). SFRP1 protein expression in healthy (H) and IPF (P) samples from an MLT cohort observed by immunoblotting (B) with non-significant changes between the two conditions (p value of 0.6528 as calculated by densitometric analysis (C)). A similar SFRP1 expression pattern was found in healthy (H) and IPF (P) samples from a Gießen cohort by immunoblotting (D) demonstrating non-significant changes between controls and disease states (p value of 0.8048 as calculated using densitometric analysis) (E).

Next, localization of SFRP1 protein expression in the IPF lung tissue sections were investigated. For that, FFPE lung sections from healthy controls and IPF patients were obtained and co-stained with  $\alpha$ SMA to locate fibrotic foci regions. Increased SFRP1 expression in the IPF fixed tissue sections compared to healthy controls were noted. Moreover, as expected increased fibrotic lesions marked with increased  $\alpha$ SMA staining were found in the IPF FFPE sections. Interestingly,  $\alpha$ SMA-positive myofibroblasts located within fibroblastic foci (shown in white arrows) showed mostly a mutual exclusion with SFRP1 (shown in yellow arrows) positively stained cells.





**Figure 4.4: In IPF tissue sections SFRP1 and  $\alpha$ SMA expression are mostly mutual exclusive**

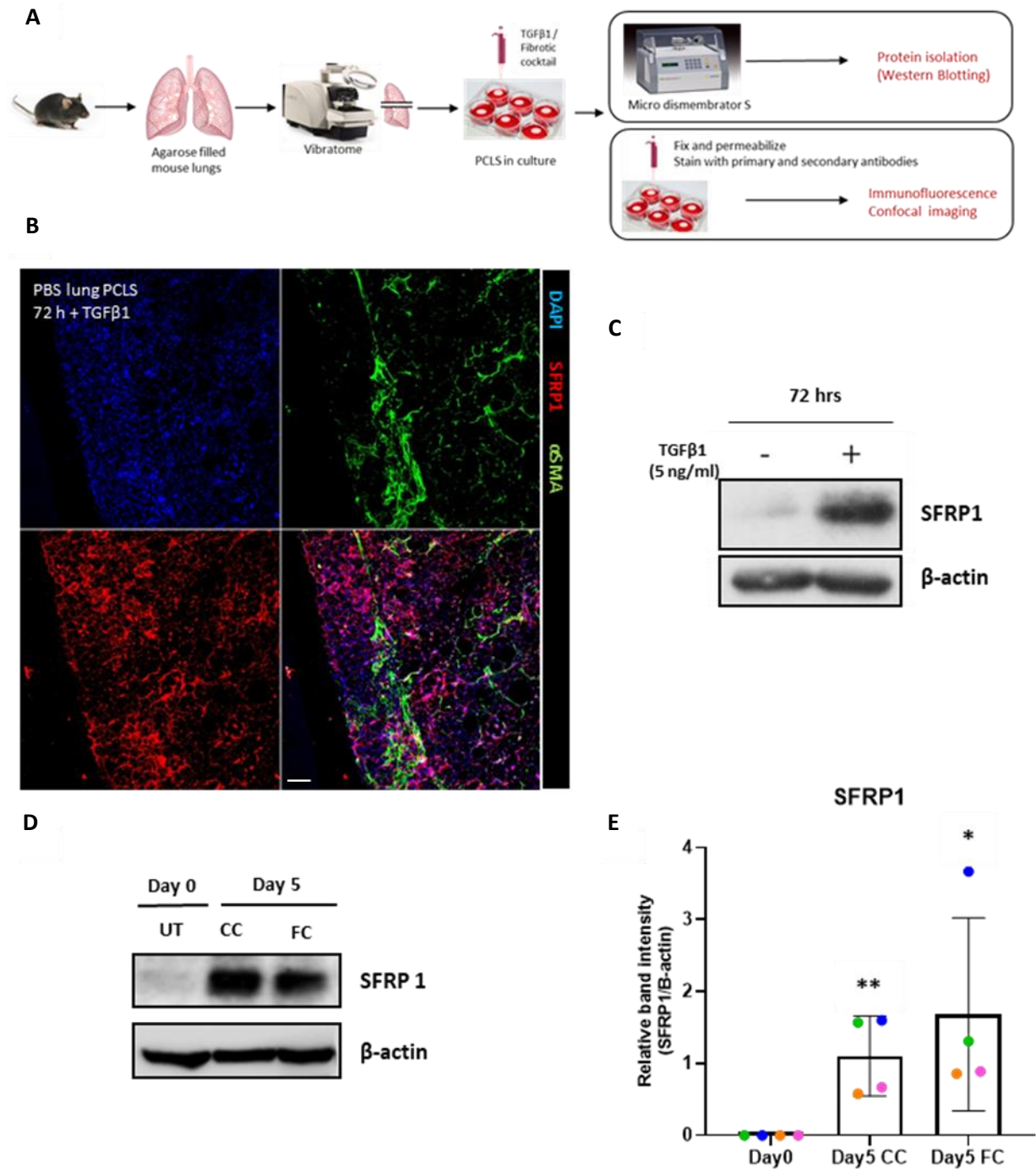
Representative immunofluorescence staining of healthy control and IPF lung FFPE sections co-stained for DAPI (in blue), SFRP1 (in red) and  $\alpha$ SMA (in green). Images were acquired by confocal microscopy (A). The lower panel shows a different IPF patient sample immunofluorescently stained for SFRP,  $\alpha$ SMA and DAPI. SFRP1 positive cells were indicated by yellow arrows and  $\alpha$ SMA positive cells were indicated with white arrows (B). Scale bar. 50  $\mu$ m.

#### **4.2.1.3. *Ex vivo* lung injury models demonstrate an enhanced SFRP1 expression**

To further investigate our findings in a complex 3D cell culture system that mimics fibrosis *ex vivo*, a murine precision-cut lung slice (PCLS) injury system was utilized. PCLS spatially retain much of the cellular diversity as found in the *in vivo* native lung and overcome the limitations associated with 2D and 3D cellular models. A recent study in 2017 showed that early fibrosis symptoms could be mimicked in human PCLS treated with pro-fibrotic growth factors [91]. In line with this study, SFRP1 expression was investigated in healthy and “fibrotic” PCLS conditions. First, 300  $\mu$ m thick PCLS from wild type C5BL6/7 mice were tested. A study by Hesse and colleagues demonstrated earlier that genes related to ECM remodeling pathways were upregulated in the bleomycin induced rat PCLS and human PCLS when treated with TGF $\beta$ 1 [160]. Hence, we treated healthy mouse PCLS (mPCLS) with TGF $\beta$ 1 (5 ng/ml) for 3 days (72 hrs). Following treatment, the slices were harvested for protein and immunoblotting was performed. Increased SFRP1 expression in the TGF $\beta$ 1 treated mPCLS compared to untreated PCLS were observed (Fig. 4.5 C). Moreover, immunofluorescence co-stainings of TGF $\beta$ 1 treated slices demonstrated elevated SFRP1 expression, similar to FFPE sections from fibrotic mouse lungs in the bleomycin model. Additionally, we observed an increased  $\alpha$ SMA staining of cells similar to myofibroblast in the TGF $\beta$ 1 treated PCLS. Again,  $\alpha$ SMA and SFRP1 expressing cells appeared to be mutually exclusive (Fig. 4.5 B). These findings underline that PCLS treated with TGF can mimic as a 3D tissue culture model *ex vivo* fibrosis related observations similar to the mouse bleomycin fibrosis model.

Next, healthy mouse slices were treated with a fibrotic cocktail (FC) containing pro-fibrotic growth factors (TGF $\beta$ 1, TNF $\alpha$ , PDGF AB and LPA) for 5 days (120 hrs). For vehicle control, control cocktail (CC) were used to treat the slices for the same duration (5 days). Furthermore, to investigate the effects of culturing conditions, controls from day 0 (= uncultured samples directly taken after slicing) were used. Immunoblotting from samples taken from four independent mouse experiments (n=4) exhibited a clear increase in SFRP1 protein expression in the FC treated mPCLS compared to day 0 controls. Surprisingly, at CC treated mPCLS demonstrated an increase of SFRP1 protein expression after 5 days in culture which was similar to that observed with the FC treatment in comparison to day 0 untreated samples (Fig. 4.5 D). Densitometric quantification was used for the four biological replicates and a paired two-tailed t-test was performed to analyze statistical significance (Fig. 4.5 E).

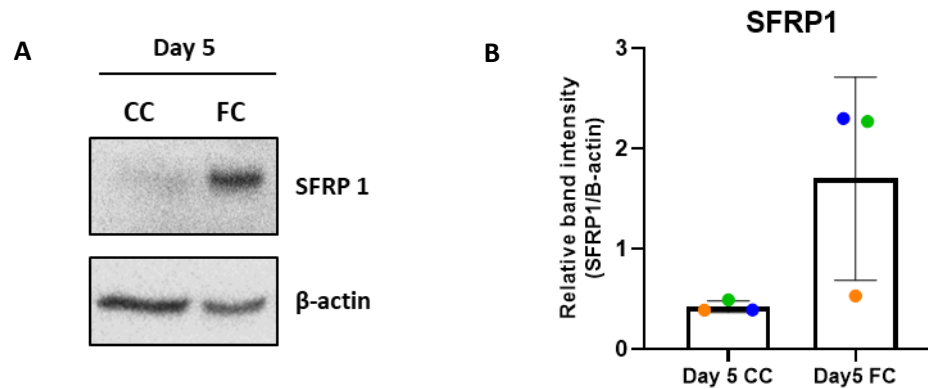




**Figure 4.5: *Ex vivo* mouse lung injury model displays an increase in SFRP1 expression**

Schematic representation of the workflow to obtain lung slices from mice and treating them with growth factors like TGFβ1 or fibrotic cocktail and downstream analyses (A). Immunofluorescent staining of the nuclei (with DAPI, in blue), SFRP1 (in red) and αSMA (in green) of PBS lung slice treated with 5 ng/ml of TGFβ1 for 72 hrs. Scale bar 50 μm (B). The mPCLS obtained from healthy PBS instilled mouse were treated with TGFβ1 (5 ng/ml) for 72 hrs and the total protein lysates harvested from the slices were used for immunoblotting (C). Mouse lung slices untreated at day 0, or treated with control cocktail (CC) and fibrotic cocktail (FC) for 5 days were lysed for protein samples. One representative western blot out of four independent biological experiments (n=4) is shown (D) and densitometric quantifications are shown as mean ± SEM (E) Statistical analysis: Paired two-tailed t-test. \*\*\*p-value < 0.001, \*p-value < 0.05.

Furthermore, to validate results in a human *ex vivo* fibrosis model, human PCLS (huPCLS) were used. Healthy lung tissue from tumor resections were filled with low melting agarose and precisely cut to obtain 500  $\mu\text{m}$  thick slices. The huPCLS were treated with FC and CC for 5 days (120 hrs) and proteins were extracted. Increased SFRP1 expression was depicted from three patient samples treated with FC (Fig. 4.6 A). Densitometric analysis was performed with SFRP1 protein expression normalized with  $\beta$ -actin levels (Fig. 4.6 B). SFRP1 protein expression was found to be strongly upregulated in the huPCLS treated with FC for 5 days in culture compared to the slices treated with CC (p-value: 0.094).



**Figure 4.6: *Ex vivo* human lung injury model shows an increase in SFRP1 expression**

Immunoblotting performed with proteins harvested from huPCLS treated with CC and FC for 5 days. Representative western blot from human lung tissue is shown to show increase in SFRP1 expression in FC treated huPCLS compared to CC treated slices (A) and densitometric quantification ( $n=3$ ; p value: 0.0948) thereof (B). Data are shown as mean  $\pm$  SEM.

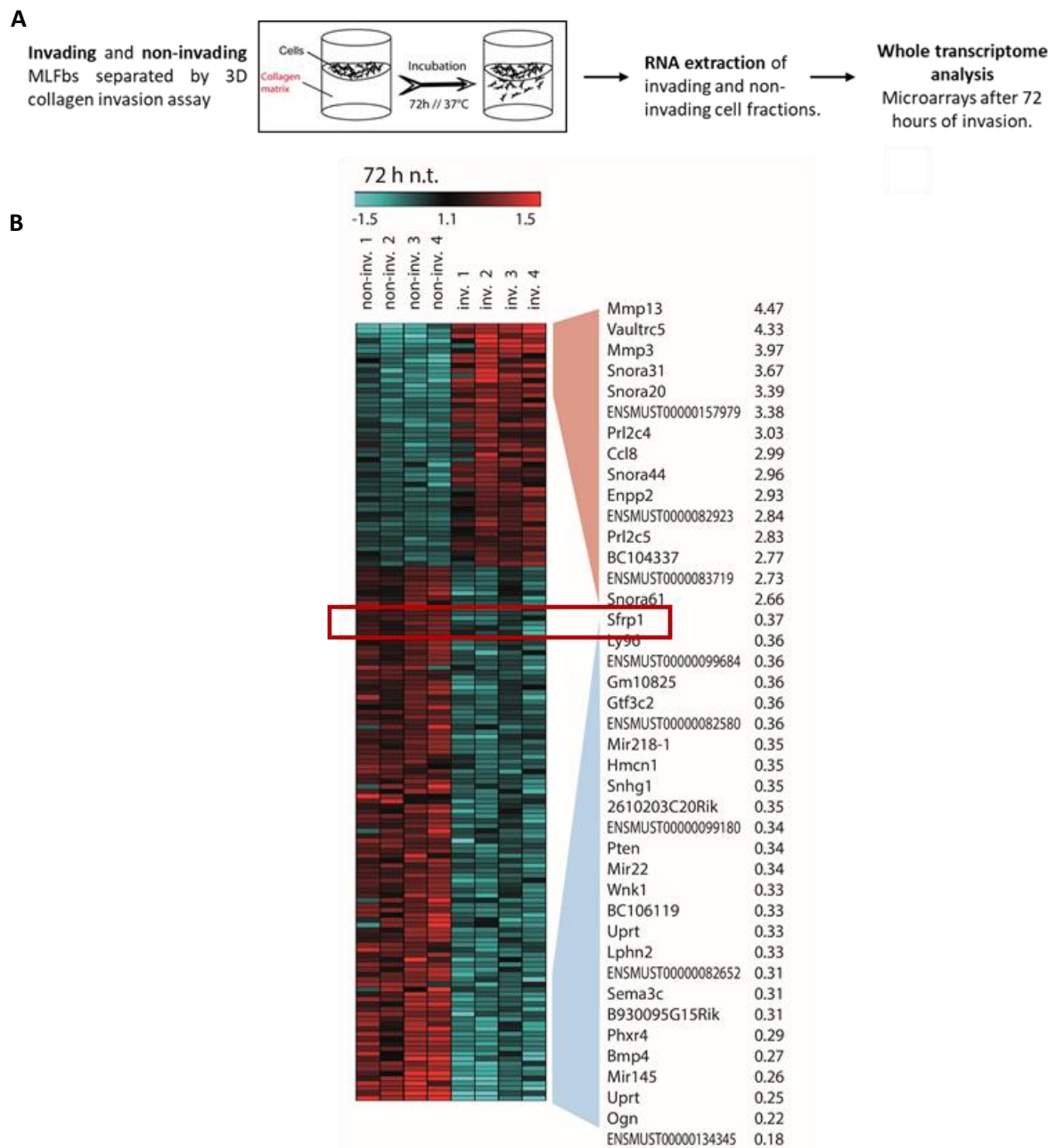
Taken together, my data strongly indicate a pivotal role of SFRP1 in fibrogenesis as exhibited in the mouse lung fibrosis model, in IPF patient samples as well as in *ex vivo* injury models using various mouse and human lung tissues.

## 4.2.2. Part II: Functional characterization of SFRP1 in lung fibroblasts

### 4.2.2.1. Molecular signature of the invasome in lung fibroblasts

Fibroblast invasion represents one key pathomechanism in lung fibrosis and invading fibroblasts have been demonstrated as the effector cells that massively contribute to fibrogenesis. Hence, it was crucial to understand the invading fibroblast phenotype which plays a pivotal role in tissue repair and regeneration in fibrogenesis [144]. To comprehensively characterize the invading fibroblast population on a molecular level, a 3D collagen-based invasion assay was utilized (as described in section 3.2.2.2). Invading (inv.) and non-invading (non-inv.) mouse lung fibroblast populations were obtained after 72 hrs and 96 hrs of invasion from the assay. In this signature 1086 genes had  $>1.5$  times fold change after 72 hrs of invasion and 163 genes had an expression ratio more than 2-fold. The 2 main clusters were separated as invading

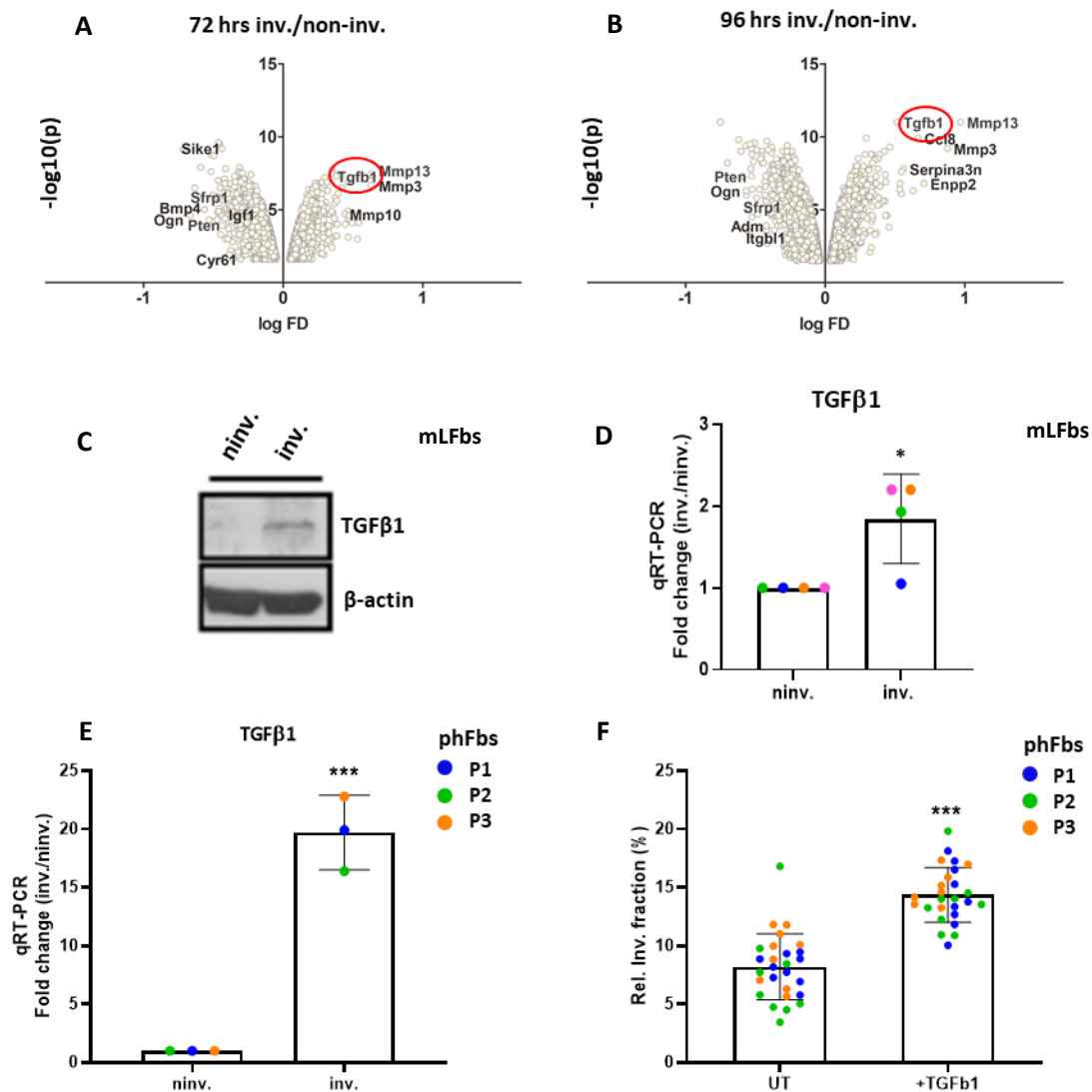
and non-invading fibroblasts [144]. SFRP1 was found in this study as a significantly downregulated gene (fold change: 2.7) in the invading fibroblasts at 72 hrs (as marked with a red square) (Fig. 4.7 B).



**Figure 4.7: Heatmap displaying the invasome of fibroblasts**

Schematic representation of the assay workflow (Invading and non-invading fibroblasts were separated after 72 hrs of invasion). The following heatmaps reveal the top >2 fold differentially regulated genes found from the microarray analysis (Affymetrix Mouse Gene 1.0 ST array). The targets that are highly expressed in the invading fibroblasts compared with the non-invading fractions were illustrated in red and the low expressed genes in blue. Each column represented one independent experiment. P-values were plotted against fold change values in a log-scale (B). (Published in [144]). **Note:** Transcriptomic analysis performed by Dr. Martin Irmeler and Bettina Oehrle (Helmholtz Zentrum Munchen).

Interestingly, TGF $\beta$ 1 was also found to be upregulated in the invading fibroblasts with 2.4-fold after 72 hrs (Fig.4.8 A) and 3.3-fold after 96 hrs (Fig. 4.8 B) of invasion [144]. To validate this finding further, protein and RNA from invading (inv.) and non-invading (ninv.) mouse fibroblasts were harvested (as discussed in sections 3.2.8.3 and 3.2.9.2 respectively). As expected, TGF $\beta$ 1 protein expression was significantly elevated in invading mouse fibroblasts (Fig 4.8 C). Consistent with the transcriptomic data, validating qPCR results displayed a significant upregulation of TGF $\beta$ 1 (fold change: 1.8-fold) in the invading mouse fibroblasts (Bettina Oehrle, Ph.D. thesis, 2015) (Fig. 4.8D). Moreover, significant upregulation of TGF $\beta$ 1 transcript levels by 19.6-fold were observed with c and verified in three different primary human fibroblast lines from different patients (P1, P2 and P3) (Fig. 4.8 E). To investigate whether TGF $\beta$ 1 stimulation in the human fibroblasts increased their invasive capacity, invasion assay with primary human fibroblasts in a 96- well format (as discussed in section 3.2.2.2.) were performed. Indeed, TGF $\beta$ 1-stimulated (1 ng/ml) phFbs displayed a significant increase in their invasive capacity compared to untreated controls. (Fig. 4.8 F).

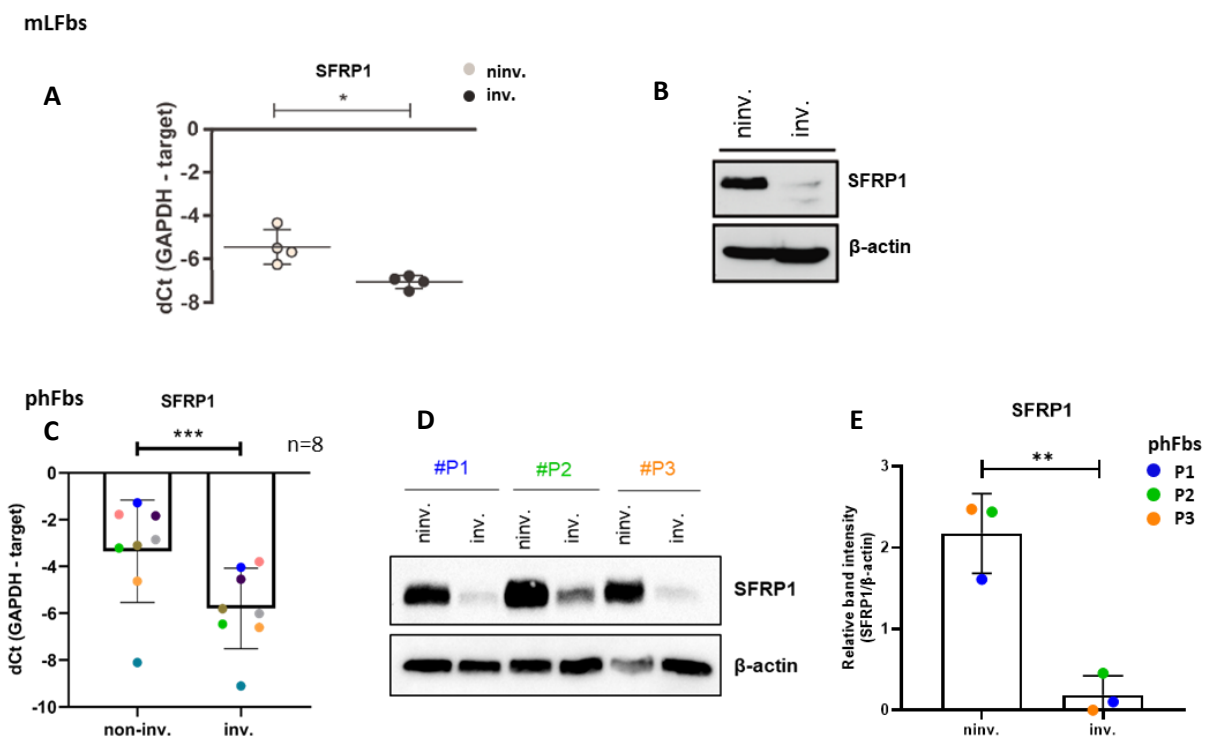


**Figure 4.8: TGFβ1 increases fibroblast invasion**

Volcano plot depict >1.5-fold gene expression of invasion signatures after 72 hrs (A) and 96 hrs (B). TGFβ1 upregulated in invading fibroblasts is marked in red. Mouse invading and non-invading fibroblast lysates were probed for TGFβ1 (C) (A-C; Oehrle, Burgstaller et al., 2015). QRT-PCR analysis revealed a significant increase of TGFβ1 mRNA expression in invading mouse lung fibroblasts (mLFbs) (n=4). GAPDH was used as a housekeeper gene (D). QRT-PCR analysis of normalized TGFβ1 gene expression from 3 different phFb patient lines. GAPDH was used as a housekeeper gene. Data are depicted as mean ± SEM from three independent experiments (n=3) (E). 96-well plate invasion assay from 3 different fibroblast patient lines (P1, P2 and P3) and percentage of invasion quantified from 10 technical replicate wells for each condition. Statistical analysis: Paired two-tailed t-test. \*\*\*p-value < 0.001, \*p-value < 0.05. **Note:** Sections A-C has been published in Oehrle, Burgstaller et al., 2015.

#### 4.2.2.2. Invading fibroblasts show reduced SFRP1 expression in primary human fibroblasts

SFRP1 was identified by microarray analysis as consistently down-regulated in both 72 and 96 hrs invading mouse fibroblast populations [144]. Reduced SFRP1 expression was at first verified in invading mLFbs on protein and mRNA level. SFRP1 mRNA expression showed significant reduction (2.35 folds) in invading mouse fibroblasts (Fig. 4.9 A; Bettina Oehrle, Ph.D. thesis, 2015). On protein level, immunoblot analysis demonstrated a strong decrease in SFRP1 expression upon mouse fibroblast invasion (Fig. 4.9 B; Bettina Oehrle, Ph.D. thesis, 2015). Next, to investigate whether a similar regulation exists in primary human lung fibroblasts, SFRP1 protein and mRNA expression were analyzed in invading and non-invading human fibroblasts in different patient fibroblast cell lines. Indeed, SFRP1 mRNA expression was found to be significantly reduced (2.7 folds) in the invading fibroblast fraction, as quantified from eight different patient cell lines (Fig. 4.9 C; Bettina Oehrle, Ph.D. thesis, 2015). Additionally, protein expression of SFRP1 was verified in three different patient fibroblast cell lines (P1, P2 and P3) and was noted to be significantly increased in invading fibroblasts (Fig 4.9 D-E).



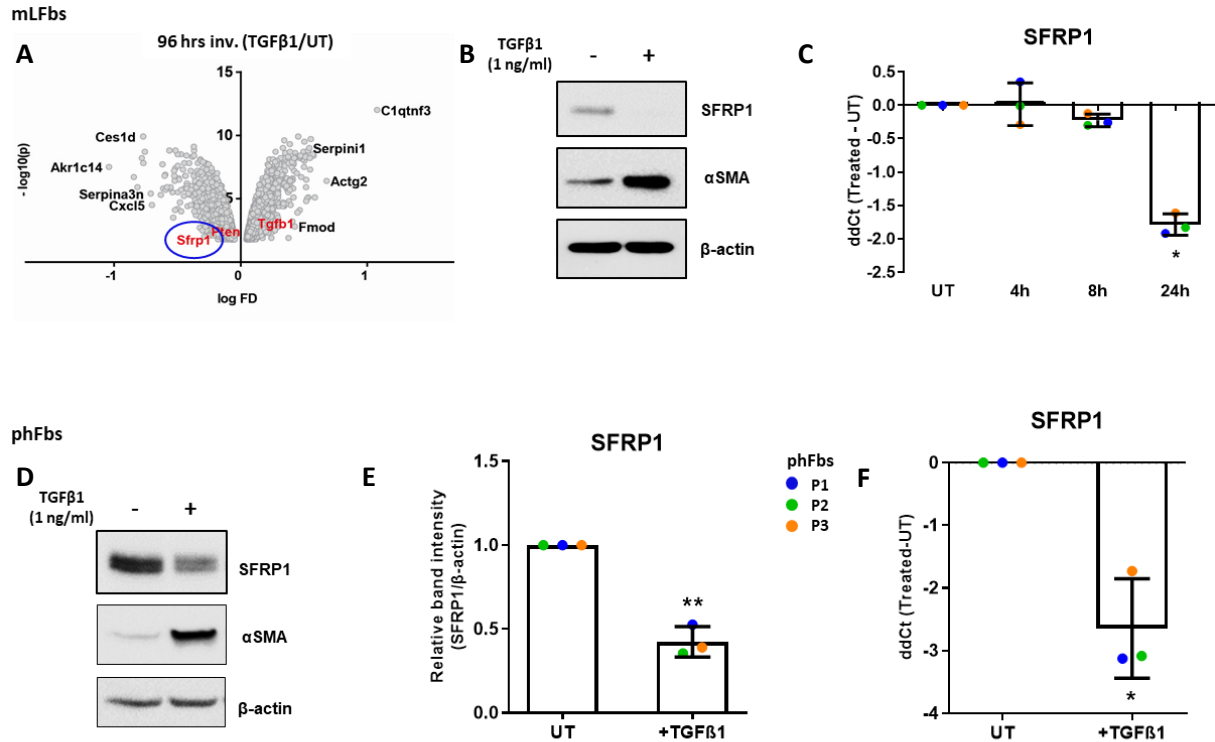
**Figure 4.9: SFRP1 expression is increased in invading mouse and primary human lung fibroblasts**

qRT-PCR analysis in four independent experiments from mLFbs showed a decreased SFRP1 gene expression in invading compared to non-invading fibroblasts. GAPDH was used as the normalizing housekeeping gene (A). Protein isolated from invading and non-invading mLFbs was used in western blotting and probed for SFRP1 and  $\beta$ -actin as loading control (B). qRT-PCR analysis in eight different patient cell lines showed increased SFRP1 mRNA expression and GAPDH was used as a housekeeper gene (C). Western blots from three different pHFs probed for SFRP1 and  $\beta$ -actin as loading control (D). Densitometric quantification of SFRP1 expression normalized with  $\beta$ -actin expression from the three patient pHFs were shown (E). Statistical analysis: Paired two-tailed t-test. \*\*\*p-value < 0.001, \*\*p-value < 0.01 and \*p-value < 0.05. **Note:** Sections A and B taken from Bettina Oehrle, Ph.D. thesis, 2014.

**4.2.2.3. TGF $\beta$ 1 downregulates SFRP1 expression in fibroblasts**

SFRP1 transcripts were strongly reduced in TGF $\beta$ 1-mediated fibroblast invasion signature (Fig 4.10 A, gene expression data not shown here; published in Oehrle, Burgstaller et al., 2015), hence this could suggest that TGF $\beta$ 1 potentially influenced SFRP1 expression which might be critical for aberrant fibroblast invasion. Therefore, the authors investigated further the kinetics of SFRP1 regulation in response to TGF $\beta$ 1. In that respect, TGF $\beta$ 1 (1 ng/ml; 48 hrs) stimulated mouse fibroblasts displayed reduced SFRP1 protein expression compared to untreated controls. Moreover, TGF $\beta$ 1 activated cultured fibroblasts displayed elevated  $\alpha$ SMA protein expression, which served as a positive control for the TGF $\beta$ 1 treatment [161] (Fig. 4.10 B). Next, the dynamics of TGF $\beta$ 1 stimulated mouse lung fibroblasts on 2D culture dishes were observed over a period of 24 hrs starting at 4 hrs. A gradual downregulation of SFRP1 mRNA expression were observed upon TGF $\beta$ 1 stimulation from over the period of 24 hrs (ddCt value of -1.8) (Fig. 4.10 C; Bettina Oehrle, Ph.D. Thesis, 2015). To find a similar regulation in primary human fibroblasts, dynamics of SFRP1 protein and mRNA expression were studied in these cells following TGF $\beta$ 1 stimulation. With that, I observed a similar strong repression of SFRP1 protein expression in TGF $\beta$ 1 (1 ng/ml; 48 hrs) activated primary human fibroblasts along with an increased  $\alpha$ SMA expression confirming a proper TGF $\beta$ 1 activation in the experiments (Fig. 4.10 D). Densitometric analysis was used to quantify the western blot data from three different independent experiments using patient cell lines (P1, P2 and P3) (Fig. 4.10 E). In line with the mouse studies, SFRP1 mRNA expression was substantially diminished in TGF $\beta$ 1 (1 ng/ml; 48 hrs) stimulated primary human fibroblasts (ddCt value of -2.6) (Fig. 4.10 F).

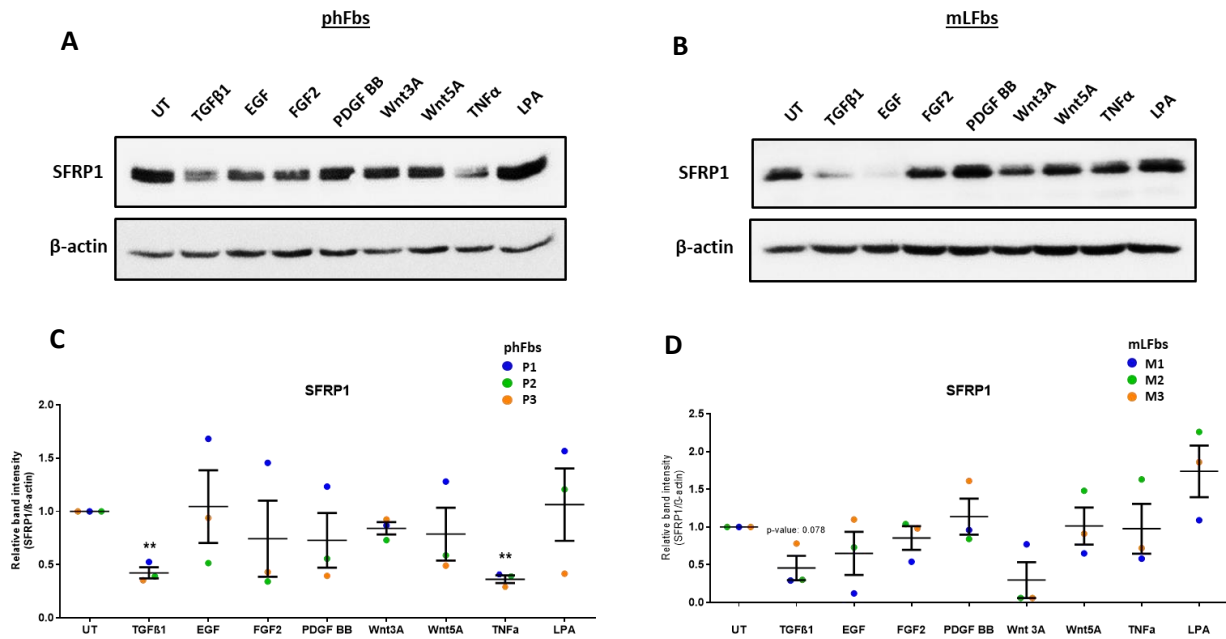




**Figure 4.10: SFRP1 expression is decreased in TGFβ1 treated mouse and human fibroblasts**

Volcano plot showing >1.5-fold gene expression of TGFβ1 treated fibroblast invasion signature, SFRP1 expression marked in blue (**published in Oehrle, Burgstaller et al., 2015**) (A). Cell lysates from mLFbs treated with TGFβ1 for 48 hrs and untreated controls were used for immunoblotting and probed for SFRP1 and β-actin (B). mRNA isolated from mLFbs treated with TGFβ1 over a period of 24 hrs were used for qRT-PCR analysis and SFRP1 transcript expression was normalized with GAPDH expression values (C). Cell lysates from patient derived primary human lung fibroblasts treated with TGFβ1 and untreated controls were used for immunoblotting and probed for SFRP1 and β-actin loading control. One of the representative blots out of three independent experiments (n=3) are shown here (D). Densitometric analysis graph showing quantitative data (n=3) from three different patient lines (P1-P3) (E). qRT-PCR analysis of SFRP1 transcript expression normalized with GAPDH values from (n=3) patient fibroblasts (F). Statistical analysis: Paired two-tailed t-test. \*\*p-value < 0.01, \*p-value < 0.05.

To identify other pro-fibrotic factors that affect SFRP1 expression, pHFbs and mLFbs were stimulated with EGF, FGF2, PDGF BB, Wnt3A, Wnt5A and LPA along with TGFβ1 for 48 hrs (as discussed in section 3.2.1.7). The protein harvested from the total cell lysates were subjected to Western blotting and subsequent densitometric analyses (n=3). The results demonstrated significantly reduced expression of SFRP1 in pHFbs stimulated with TGFβ1 and TNFα (Fig. 4.11 A-B). In the mLFbs, SFRP1 expression was observed to be strongly decreased in TGFβ1-treated fibroblasts (p-value: 0.078), but TNFα treatment in mLFbs did not show any effect unlike in pHFbs (Fig. 4.11 C-D). Hence apart from TGFβ1, none of the other treatments had a consistent effect on SFRP1 expression in both mouse and human fibroblasts.

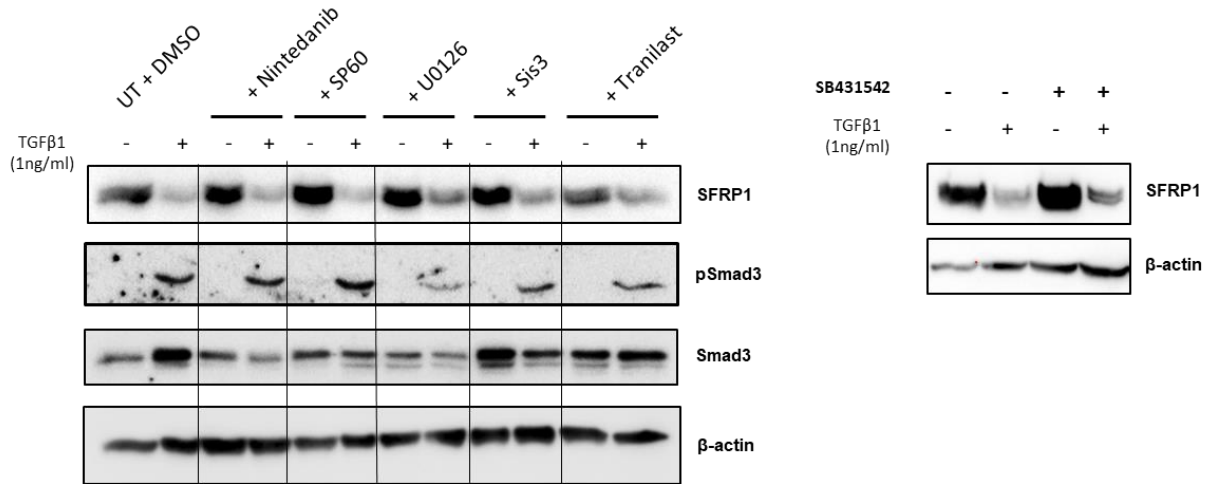


**Figure 4.11: SFRP1 protein expression in fibroblasts stimulated with various growth factors**

Representative western blot (n=3) for SFRP1 protein expression in phFbs (A) and mLFbs (C) stimulated with TGFβ1, EGF, FGF2, PDGF BB, Wnt3A, Wnt5A and LPA(B). Quantification of SFRP1 expression by densitometric analysis demonstrate significant reduction of SFRP1 expression level in phFbs treated with TGFβ1 and TNFα (B) and strong decrease in SFRP1 expression in TGFβ1 treated mLFbs (D). Data are shown as mean ± SEM. Statistical analysis: One-way ANOVA with Dunnett's multiple comparison test. \*\*p-value < 0.01.

Subsequently, in order to get a first mechanistic insight into the regulation of SFRP1 expression in connection with TGFβ1 signaling in phFbs, I tested various known inhibitors of TGFβ1 signaling. Firstly, phFbs were tested with inhibitors of the canonical TGFβ pathway. Inhibitors considered for this study were SB431542, which is a specific inhibitor targeting TGF-β type I receptor/Alk5 receptor and Sis3, which is a specific inhibitor of Smad3 phosphorylation. The inhibitors were applied alone and together with TGFβ1 (1 ng/ml) for 48 hrs in phFbs. SFRP1 protein expression changes along with possible alterations in Smad3 phosphorylation levels were monitored by immunoblotting. Next, phFbs were treated with the non-canonical TGFβ pathway inhibitors like U0126, an inhibitor targeting pErk1/2 and SP60 (SP600125), an inhibitor of JNK1/2/3 in parallel with TGFβ1 stimulation for 48 hrs. In addition, two most commonly used TGFβ function inhibiting anti-fibrotic drugs namely Nintedanib and Tranilast were included in this study. Conclusively, the inhibitors and drugs along with TGFβ1 stimulation failed influence SFRP1 protein expression (n=1) (Fig. 4.12). This might indicate that TGFβ1 regulates SFRP1 expression via unknown different mechanism.

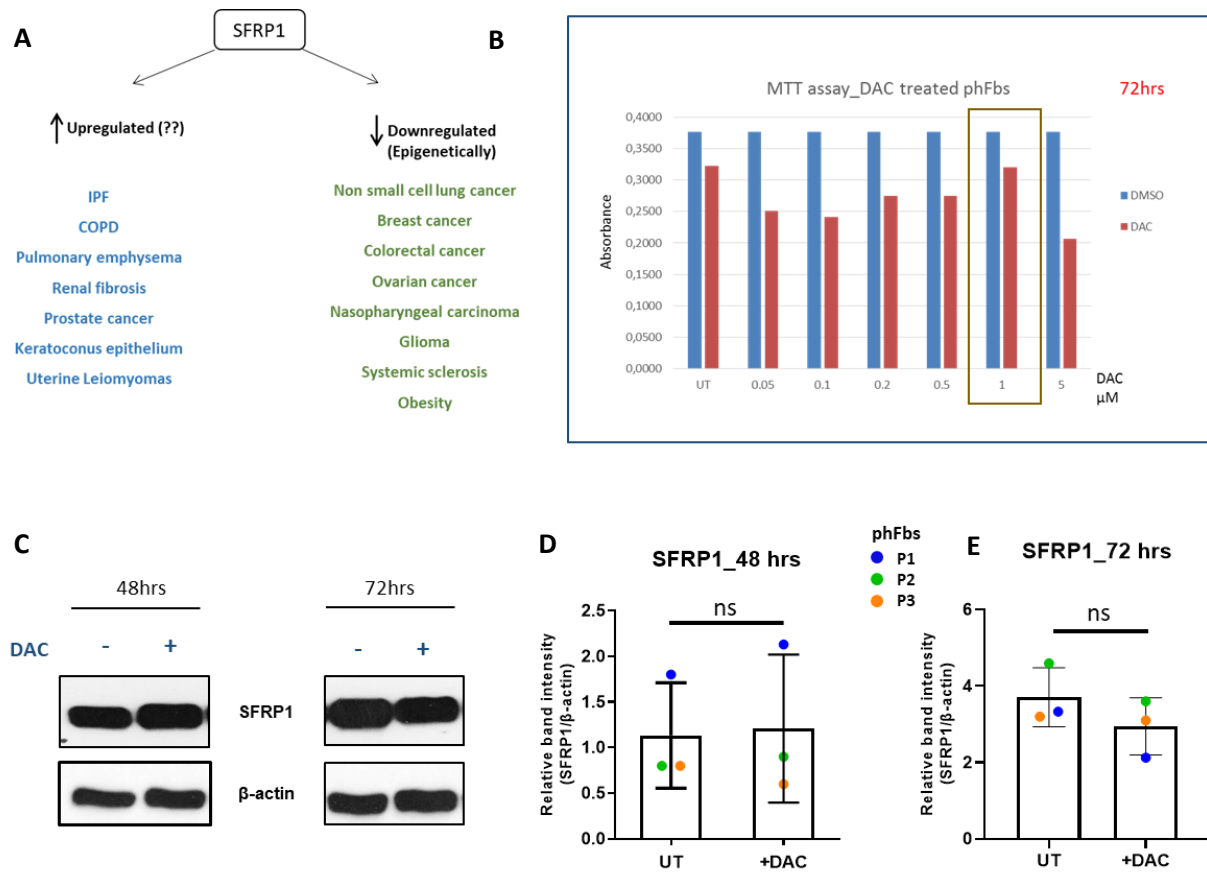




**Figure 4.12: TGFβ1 downregulates SFRP1 expression via a yet unknown mechanism.** A pHb cell line (n=1) was incubated with 1 ng/ml of TGFβ1 along with specific inhibitors targeting canonical or non-canonical TGFβ signaling pathway reactions. The whole protein lysates were used for immunoblotting for SFRP1, pSmad3, (total) Smad3 and β-actin for loading control. Untreated cells were treated with DMSO as vehicle control.

#### 4.2.2.4. SFRP1 expression in lung fibroblast is not regulated epigenetically

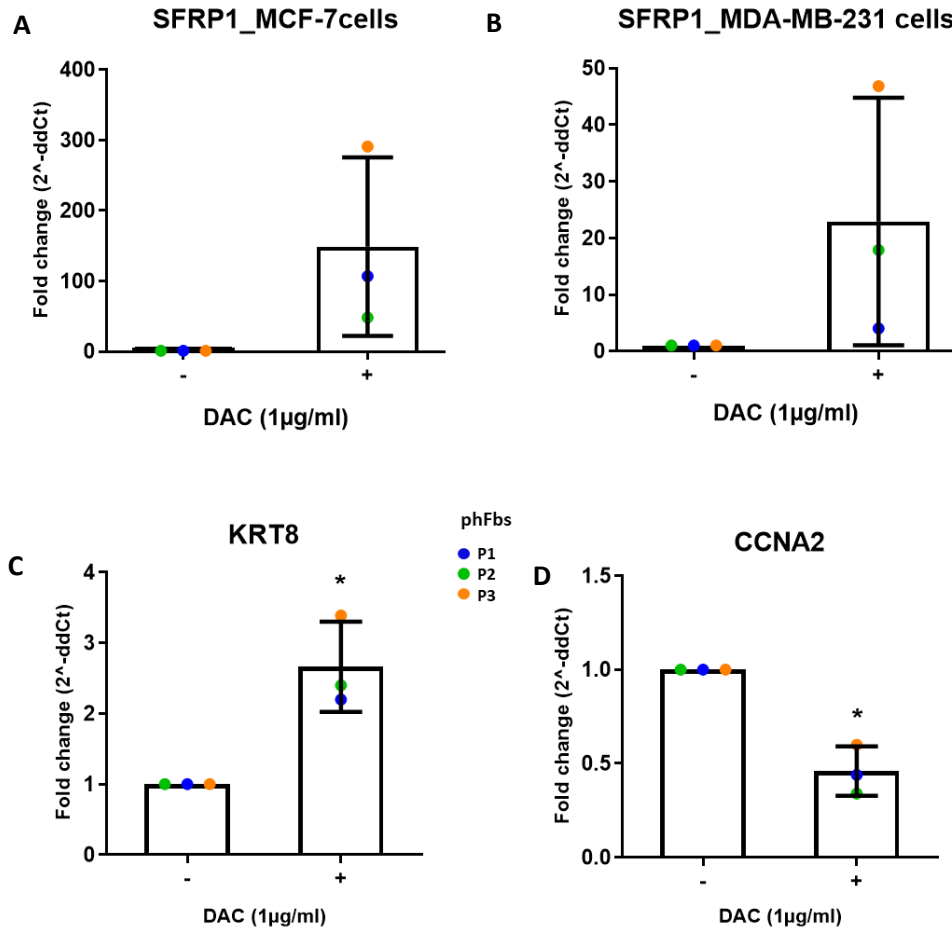
Accumulating evidence from a pan-cancer study with 8000 tumor and healthy samples noted that the consistent loss of SFRP1 in 29 different types of cancer resulted by gene promoter methylation [155]. Apart from cancer, other diseases like systemic sclerosis [162], and keloids [163] also reported that loss of SFRP1 expression was due to promoter hypermethylation in the diseased condition. Here, I wanted to find evidence whether the regulation of SFRP1's expression in fibroblasts in connection with IPF is also due to epigenetic mechanisms (Fig. 4.13 A). To investigate this, patient-derived primary lung fibroblasts were treated with different concentrations of 5-aza-2'-deoxycytidine or Decitabine (DAC) which is an analogue of cytosine and is known to inhibit DNA methyltransferases. Cellular metabolic activity of the fibroblasts after 72 hrs was determined by MTT assay. The concentration of 1 μM of DAC was noted as the effective concentration causing no toxicity in the probed pHbFs (Fig 4.13 B). DAC treated and untreated control pHbFs displayed similar protein expression levels of SFRP1 (Fig. 4.13 C). Densitometric quantification showed that SFRP1 protein levels were not affected by DAC treatment in pHbFs at 48 and 72 hrs (Fig. 4.13 D-E). Likewise, SFRP1 mRNA expression did not display any significant changes compared to untreated fibroblasts (Fig. 4.14 A).



**Figure 4.13: Decitabine treatment in human fibroblasts does not affect SFRP1 expression**

Deduction of a common theme for epigenetic regulation of SFRP1 in diseases as collected from different published datasets (A). PhFbs viability after 72 hrs of DAC treatment (0-5  $\mu$ M; in red) normalized to DMSO controls (in blue) assessed by MTT assay. Optimal concentration is highlighted in orange (B). Representative immunoblot of one patient cell line (out of 3; n=3) treated with DAC (1  $\mu$ M) for 48 and 72 hrs and probed for SFRP1 and  $\beta$ -actin as loading control is shown here (C). Densitometric analysis for 48 hrs (D) and 72 hrs (E). DAC (1  $\mu$ M) treatments were performed with three different phFb cell lines (n=3; P1-P3) for the aforementioned time-points. Statistical analysis: Paired two-tailed t-test. \*\*\*p-value < 0.001, \*p-value < 0.05, ns = not significant.

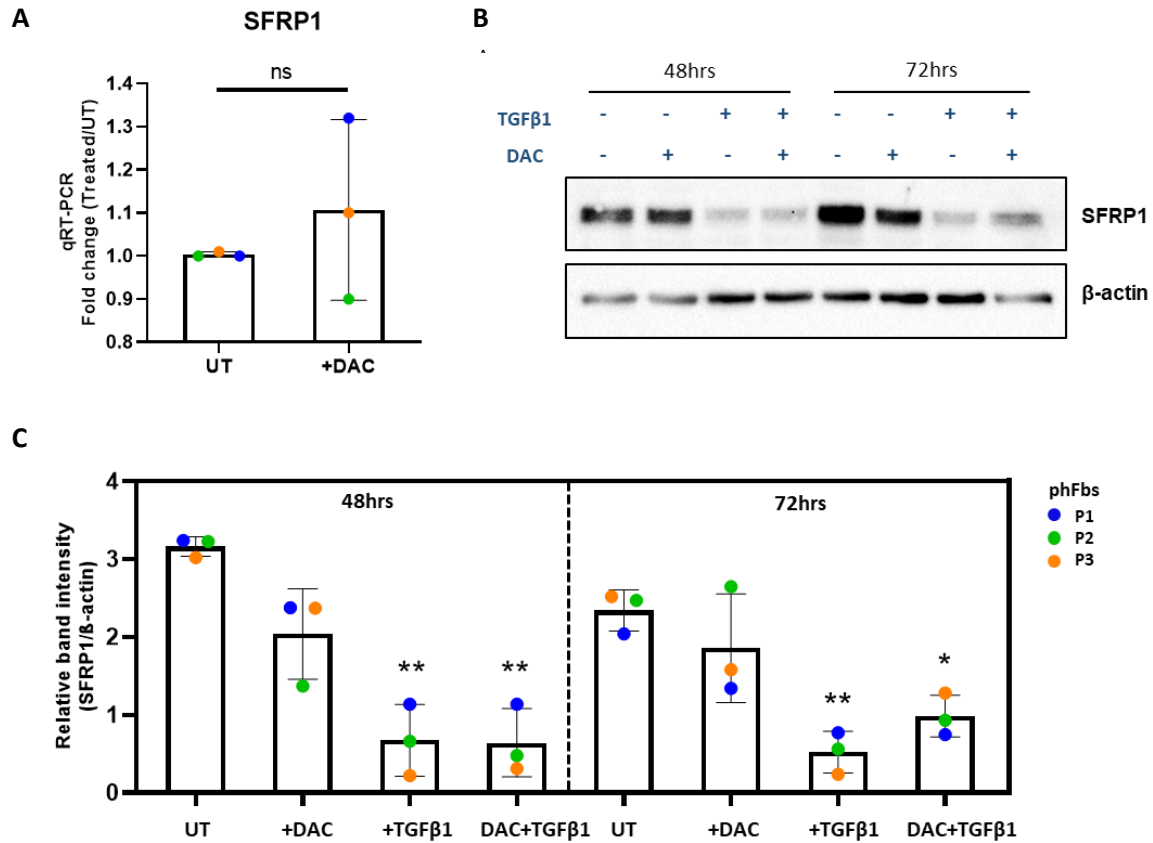
To ensure proper functioning of DAC at the used concentration and time-points, further positive control experiments were performed. The restoration of SFRP1 gene expression in breast cancer cell lines like MCF-7 and MDA-MB-231 were reported on treatment with 1-2  $\mu$ M of DAC for 72 hrs [164]. Hence to correlate, MCF-7 and MDA-MB-231 cells were treated with 1  $\mu$ M of DAC for 72 hrs and SFRP1 gene expression was quantified by qPCR. SFRP1 was found to be upregulated by 148.75 folds in the MCF-7 cells and by 22.91 folds in the MDA-MB-231 cells (Fig. 4.14 A-B). In addition, Keratin 8 (KRT8) was noted to be upregulated and Cyclin A (CCNA2) was found to be downregulated in a LD419 fibroblast cell line treated with 1  $\mu$ M of DAC for 72 hrs [165]. Therefore, I treated phFbs with 1  $\mu$ M of DAC for 3 days and subsequent qRT-PCR analysis revealed significant increase in KRT8 gene expression (p-value: 0.045) and significant decrease of CCNA2 levels (0.019) in the DAC treated phFbs (Fig. 4.14 C-D).



**Figure 4.14: Positive control for DAC treatment**

QRT-PCR analyses show fold change of SFRP1 gene expression in DAC (1 μM) treated MCF-7 (p-value: 0.1807) (A) and MDA-MB-231 (p-value: 0.224) (B) cells (n=3 ; ) normalized to untreated vehicle controls. GAPDH was used as a housekeeper gene. KRT8 (fold change: 2.6; p-value: 0.045) and CCNA2 (fold change: 0.46; p-value: 0.019) gene expression was quantitatively assessed via qRT-PCR from three independent phFb cell lines (P1-P3). Data are shown as mean ± SEM. Statistical analysis: Paired two-tailed t-test: \*p-value < 0.05.

Next, we combined DAC and TGFβ1 stimulation in phFbs. Western blot analysis at two different time-points (48 and 72 hrs) displayed a significant TGFβ1 mediated downregulation of SFRP1 expression, as shown before (compare also section 4.2.2.3). However, no alterations in SFRP1 protein expression by simultaneous stimulation with DAC and TGFβ1 were observed (Fig- 4.15 B-C). From these data I conclude that hypermethylation and thus epigenetics might not play a role in the expression regulation of SFRP1 in human lung fibroblasts.

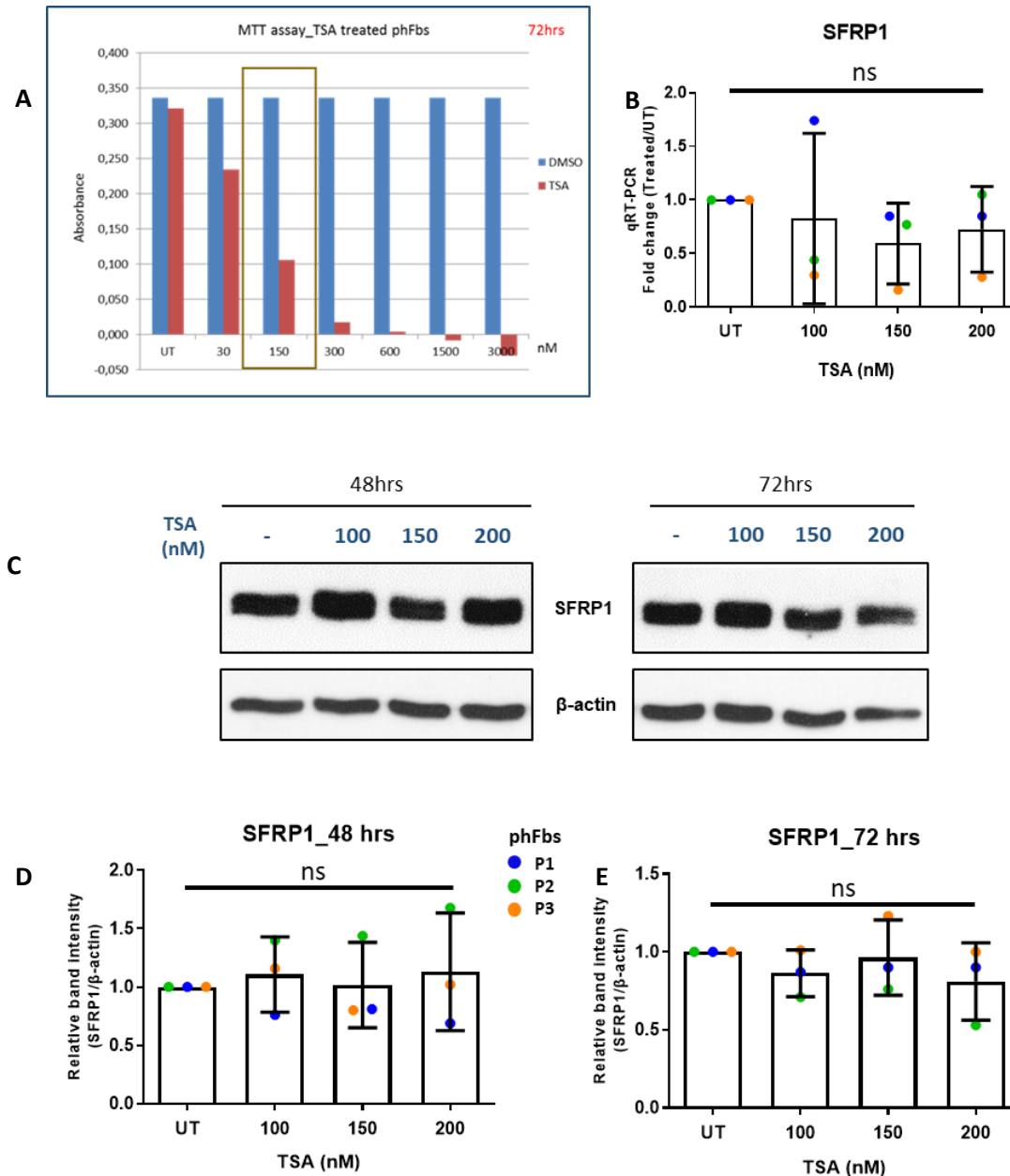


**Figure 4.15: Combined Decitabine and TGFβ1 treatment in human fibroblasts does not affect SFRP1 expression**

QRT-PCR analysis showing fold change of SFRP1 gene expression in DAC (1  $\mu$ M) treated phFbs (n=3; P1-P3) normalized to untreated vehicle controls. GAPDH was used as a housekeeper gene (A). Representative western blot displaying SFRP1 and  $\beta$ -actin protein expression in patient fibroblasts (for n=3; P1-P3) treated with DAC (1  $\mu$ M) along with TGFβ1 (1 ng/ml) for 48 and 72 hrs (B). Quantitative densitometric analysis (n=3; P1-P3) exhibiting normalized band intensity of SFRP1/ $\beta$ -actin in untreated (UT) vehicle control, TGFβ1 treated (+TGFβ1), DAC alone treated (+DAC) and DAC and TGFβ1 combined treated (DAC+TGFβ1) phFbs (C). Statistical analysis: One-way ANOVA with Dunnett's multiple comparison test \* $p$ <0.05, \*\* $p$ <0.01, \*\*\* $p$ <0.001, ns = not significant.

Apart from methylation, acetylation or deacetylation of nonhistone proteins has been demonstrated as another major regulatory event in epigenetics. To check acetylation related regulatory mechanisms, phFbs were treated with Trichostatin A (TSA) which modifies the balance between histone acetyltransferase and histone deacetylase activities. Cellular metabolic activity via MTT assay was reported in the range of 100-200 nM TSA for fibroblasts treated for 72 hrs (Fig. 4.16 A). Fold change values of SFRP1 mRNA expression after 72 hrs did not display any significant changes following TSA (100-200 nM) treatment (Fig. 4.16 B). Also, SFRP1 protein levels assessed by western blotting and quantified with densitometric analysis at 48 and 72 hrs after TSA treatment failed to depict any significant differences compared to untreated vehicle controls (Fig. 4.16C-E).

Overall and in conclusion, regulation of SFRP1's expression in phFbs might not be moderated neither by acetylation, nor by promoter hypermethylation processes, and epigenetics in general.



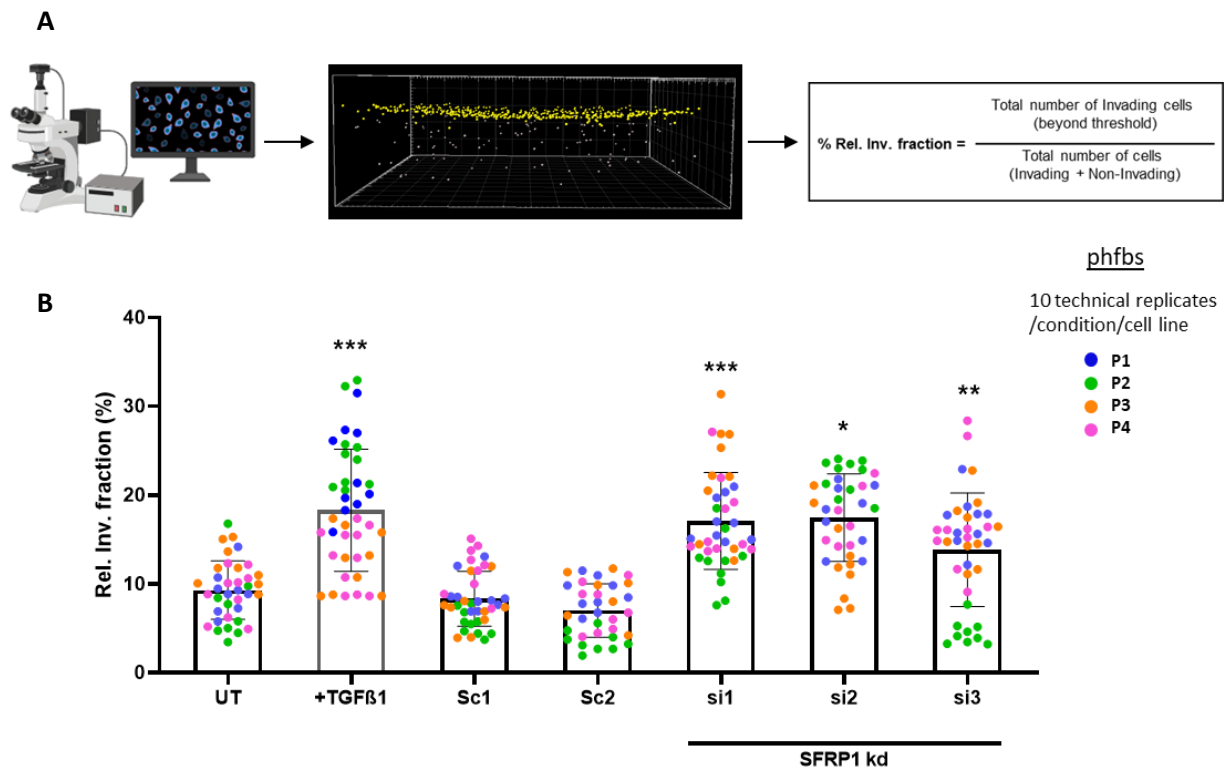
**Figure 4.16: Trichostatin A treatment in human fibroblasts does not affect SFRP1 expression**

Cell viability of pHFs treated with TSA (0-3000 nM; in red) for 72 hrs was checked with an MTT assay normalized to DMSO controls (in blue). Optimal viability concentration is indicated by a box (A). qRT-PCR analysis displaying normalized SFRP1 mRNA expression in untreated vehicle control and TSA (100-200 nM) treated pHFs (n=3; P1-P3). GAPDH was used as a housekeeper gene (B). Protein lysates from pHFs treated with TSA (0-200 nM) were used for immunoblotting at two time-points (48 and 72 hrs) and probed for SFRP1 and β-actin expression (C). Densitometric quantification of SFRP1/β-actin ratios for 48 hrs (D) and 72 hrs (E) TSA treatments are recorded as mean ± SEM. Statistical analysis: One-way ANOVA with Dunnett's multiple comparison test \*p<0.05, \*\*p<0.01, \*\*\*p<0.001, ns = not significant.

#### 4.2.2.5. SFRP1 is a negative regulator of fibroblast invasion

Microarray analysis of invading mouse lung fibroblasts versus non-invading fibroblasts (as discussed in section 4.2.2.1) identified SFRP1 to be one of the most significantly deregulated genes. Therefore, it was of interest if SFRP1 also plays a crucial functional role the invasion of primary human lung fibroblasts.

siRNA knockdown of SFRP1 human fibroblasts was utilized in the invasion assay setting. TGFβ1 activated fibroblasts were used as a positive control for invasion, as TGFβ1 treatment augmented fibroblast invasion (as discussed in section 4.2.2.1). Three different siRNAs targeting different exon parts of SFRP1 were used (si1-3) along with two negative scrambled control (Sc1-2) as well as untreated transfection buffer controls (UT). Strikingly, SFRP1 depleted phFbs displayed a significant increase in their invasive potential similar to TGFβ1 treatment (Fig. 4.17 A-B).

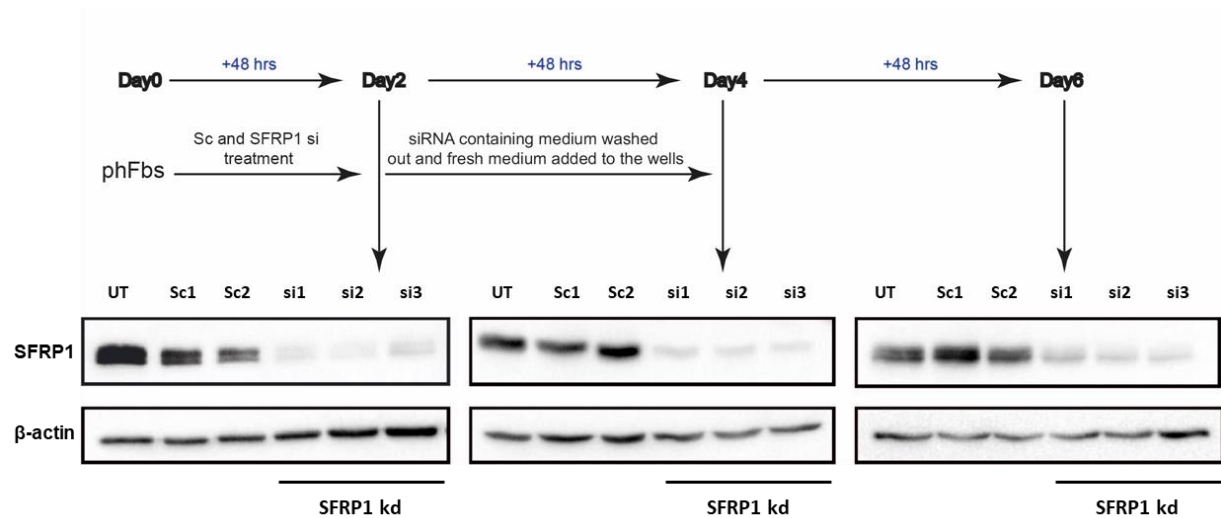


**Figure 4.17: SFRP1 depleted phFbs have increased invasion capacity**

Schematic representation of the analysis of fibroblast invasion by Imaris software (Bitplane AG). Relative invading fraction percentage (Rel. Inv. fraction %) was quantified from the formula shown in (A). The percentage of Rel. Inv. fraction were calculated as mean  $\pm$  SEM from four independent experiments (n=4; P1-P4). The conditions used in the 96- well invasion assay, were untreated phFbs with transfection buffer only (UT), phFbs treated with TGFβ1 (1ng/ml; +TGFβ1), scramble negative control 1 (Sc1), scramble negative control 2 (Sc2), SFRP1 specific siRNA 1 (si1), SFRP1 specific siRNA 2 (si2) and SFRP1 specific siRNA 3 (si3). Statistical analysis: One-way ANOVA with Dunnett's multiple comparison test \*p<0.05, \*\*p<0.01, \*\*\*p<0.001, ns = not significant.

The stability of the siRNA knockdown was assessed by using a time-course of SFRP1 silencing during the invasion assay period. The siRNA treatment of the phFbs was carried out for 48 hrs on 2D plastic dishes and then the cells were transferred onto the collagen gel for an additional 96 hrs (similar as discussed in methods section 3.2.2.2). Additionally, the SFRP1 knockdown efficiency was checked on culture dishes during the same time-period. Proteins were harvested from phFbs as indicated in Fig.4.16 after every 48 hrs and subsequently western blots were performed (as discussed in section 3.2.1.6). The

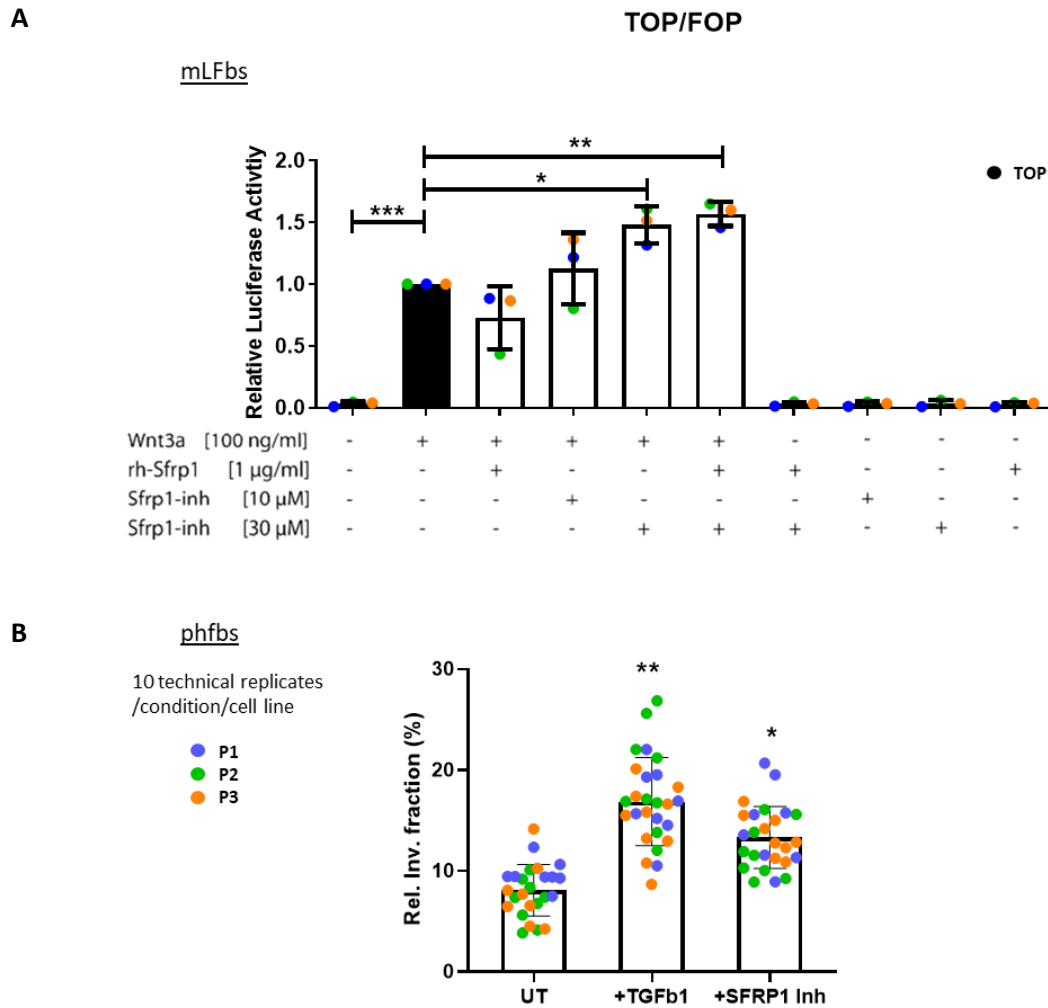
immunoblotting results confirmed a robust and stable knockdown of SFRP1 throughout the invasion assay period (Fig. 4.18).



**Figure 4.18: Stability of SFRP1 knockdown (kd) during invasion**

Protein levels of SFRP1 was analyzed after every 48 hrs of siRNA treatment until day 6 via western blotting. β-actin was used as loading control. Various conditions were tested in this experiment: untreated phFbs with transfection buffer only (UT), scramble negative control 1 (Sc1), scramble negative control 2 (Sc2), SFRP1 specific siRNA 1 (si1), SFRP1 specific siRNA 2 (si2) and SFRP1 specific siRNA 3 (si3) treated phFbs.

SFRP1 knockdown phFbs demonstrated increased invasion (Fig.4.17). To confirm this observation further, a different experiment using a commercial SFRP1 inhibitor (Santa Cruz, CAS915754) was performed. The SFRP1 Inhibitor (Inh) is a diphenylsulfone-sulfonamide compound that antagonize SFRP1 function by a yet unknown mechanism [167]. First, the activity of the inhibitor was checked by a TOP/FOP assay. TOP FLASH or FOP FLASH reporter plasmid transfected mLFbs were treated with recombinant Wnt3A (100 ng/ml), a recombinant SFRP1 (R&D) and the SFRP1 inhibitor (10 μM and 30 μM). Then, luciferase activity was measured from the luminescence read-out. SFRP1inhibitor co-stimulation counteracted the Wnt3A activity and the highest inhibitory effects were seen at a concentration of 30μM (Fig. 4.19 A; Bettina Oehrle, Ph.D. thesis, 2015). Consequently, the SFRP1 inhibitor was used in a concentration of 30 μM for the following experiments. In the invasion assay, the SFRP1 inhibitor-treated phFbs exhibited a significant increase in their invasion capacity compared to vehicle control cells (UT) (Fig. 4.19 B). From this finding, I conclude that SFRP1 depleted phFbs are highly invasive cells.



**Figure 4.19: SFRP1 Inhibitor (Inh) treated phFBs showed an increased invasion capacity**

MLFbs transfected with the TOP/FOP FLASH reporter constructs were treated with Wnt3a (100 ng/ml) as a positive control, rh-Sfrp1 (1 µg/ml) and/or Sfrp1 Inh (10 µM, 30 µM). The Luminescence was measured by a plate reader and the relative luciferase activity was subsequently determined by the ratio of the luminescence in the TOP reporter transfected cells and the FOP-transfected cells from the respective conditions. Statistical analysis used: One-way ANOVA with Dunnett's multiple comparison test. \* $p < 0.05$ , \*\* $p < 0.01$ , \*\*\* $p < 0.001$  (Bettina Oehrle, Ph.D. thesis, 2015) (A). Untreated cells along with TGFβ1 (1 ng/ml) treated and SFRP1 inhibitor (CAS 915754; 30µM) treated phFBs ( $n=3$ ; P1-P3) were used in the invasion assay. The Rel. Inv. fraction % was calculated as mean  $\pm$  SEM from the three independent experiments. Statistical analysis: Paired two-tailed t-test. \*\*\* $p$ -value  $< 0.001$ , \*\* $p < 0.01$ , \* $p$ -value  $< 0.05$  (B).

#### 4.2.2.6. SFRP1 regulates distinct genes and proteins related to the actin cytoskeleton

Given our findings on the role of SFRP1 in fibroblast invasion, it seemed likely that low levels of SFRP1 in fibroblasts are indicative for a special subpopulation or for a special mechanistic regulation of specific cellular functions and/or biological processes. To investigate this further, I applied multi-omics in siRNA depleted phFBs.



Knockdown of SFRP1 efficiently reduced its mRNA levels (fold change: 0.03 and p-value: 0.0003 compared to untreated transfection controls) as shown in Fig. 4.22 A. Regulation of gene expression after 48 hrs of siRNA-mediated transient silencing of SFRP1 was determined by microarray analysis kindly provided by Dr. Martin Irmeler (from Institute of Experimental Genetics, HMGU). Genes that were regulated with a fold change  $>1.5$  and FDR  $<10\%$  compared to controls were taken into consideration. Detection of p-values were used to exclude background signals and significant genes were filtered with  $p < 0.05$ . 119 overlapping genes were found to be deregulated in both siSFRP1 v/s UT and siSFRP1 v/s Sc having  $p < 0.05$  (paired t-test) and fold change (Fc) $>1.5\times$  (Fig. 4.20 A). Of interest, RhoA, is a member of the non-canonical Wnt pathway which is involved actively in the actin cytoskeleton reorganization along with regulation of cell morphology, attachment, and migration. RhoA here was found to be significantly downregulated (Fc: 1.5x) in the SFRP1<sup>low</sup> fibroblasts (Fig. 4.20 B-C).

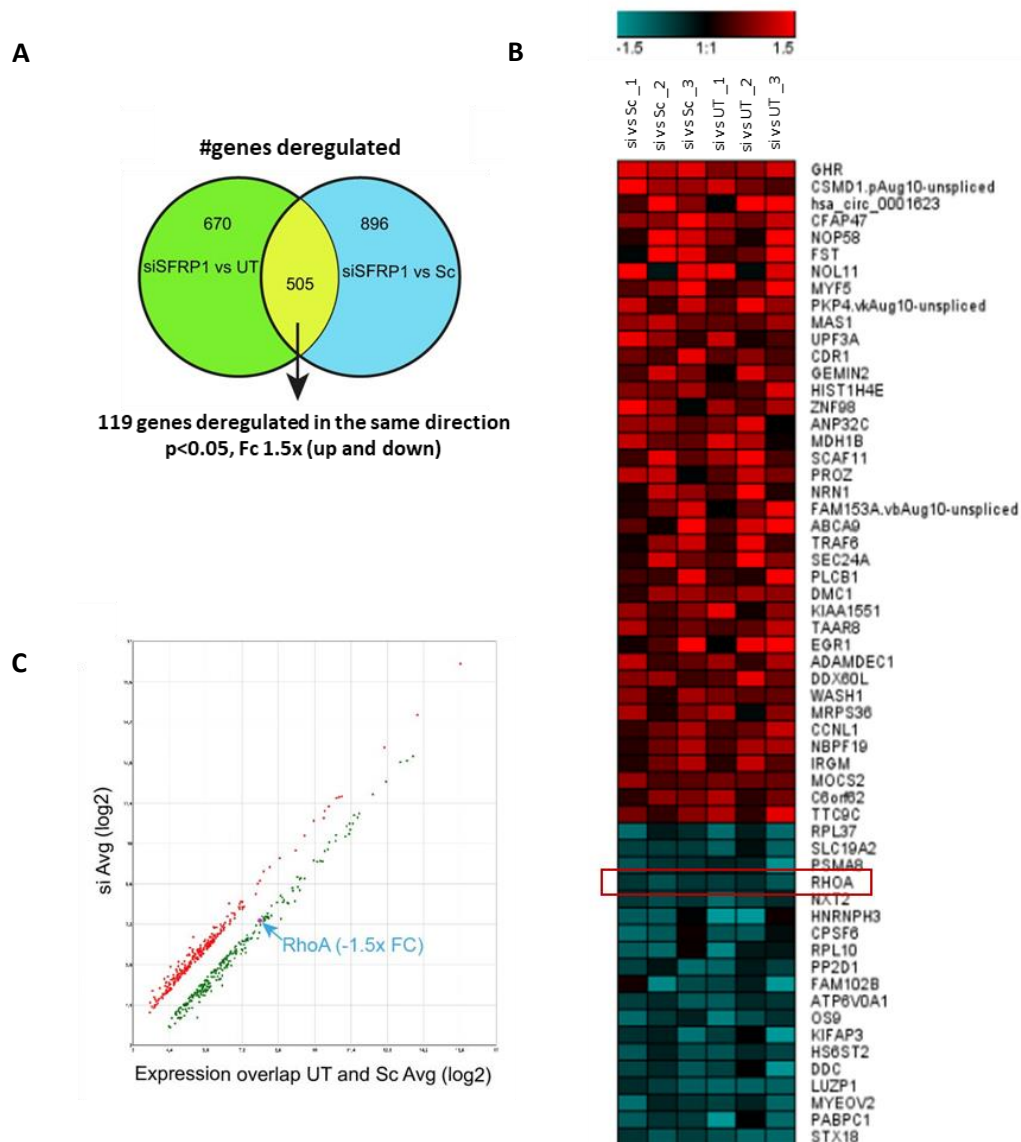
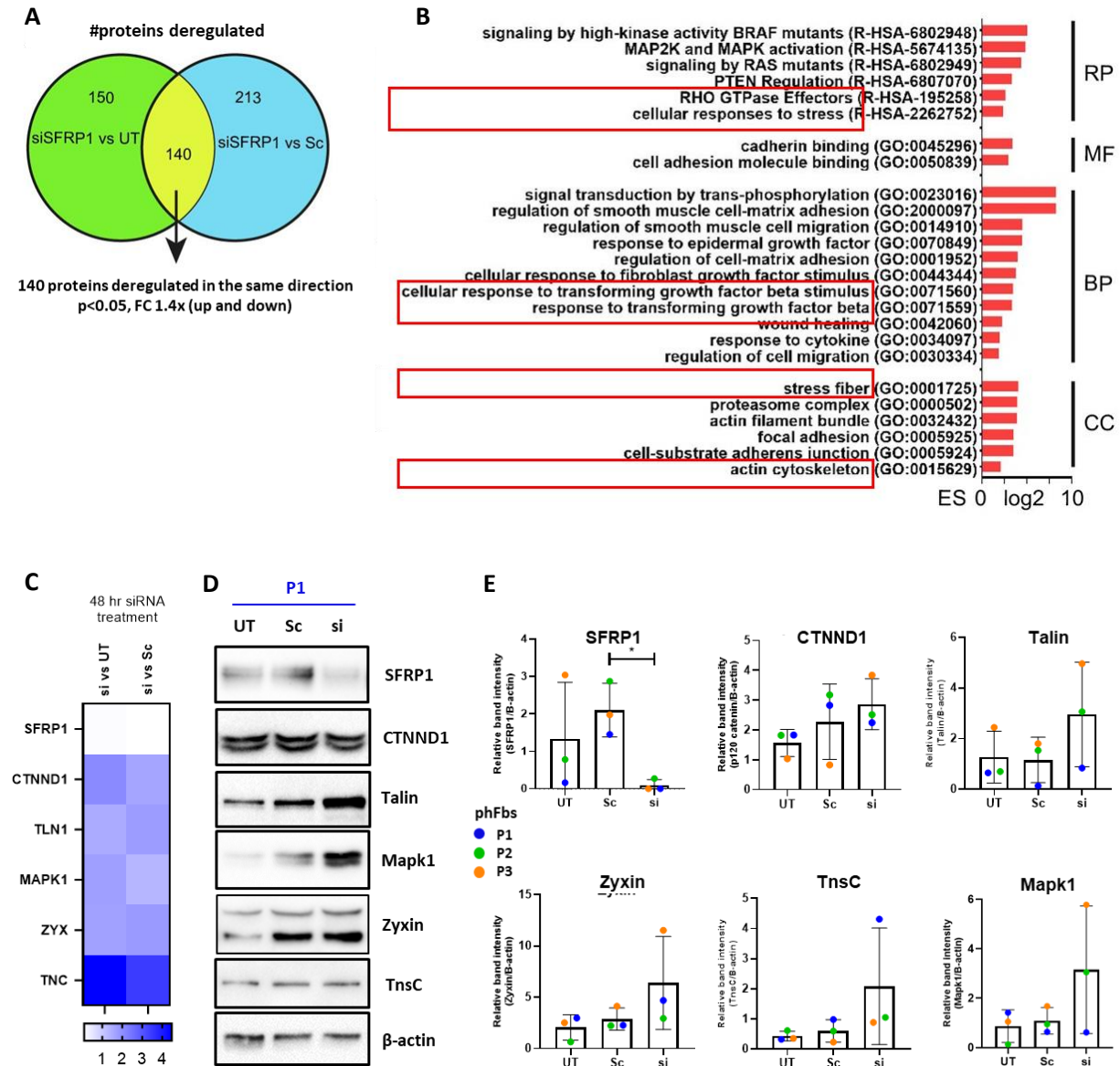


Figure 4.20: Transcriptomic signature of SFRP1<sup>-ve</sup> human lung fibroblasts

Venn diagram showing the number of deregulated genes identified with  $Fc > 1.5x$  and  $p\text{-value} < 0.05$  in siSFRP1 vs UT and siSFRP1 vs Sc analysis and 119 genes were found to overlap in both conditions (A). Genewise testing for differential expression was performed by the paired limma t-test and Benjamini-Hochberg multiple testing correction ( $FDR < 10\%$ ). RhoA expression pattern is highlighted in red (B). Scatter plot of global gene expression overlap between UT and Sc vs siSFRP1 is shown, where upregulated genes are shown in red dots and downregulated genes indicated by green dots. RhoA expression in the plot is indicated in blue text and arrow (C). **Note:** Transcriptomic analysis performed by Dr. Martin Irmeler, Helmholtz Zentrum Munich.

Next, proteomic analyses of SFRP1 depleted phFbs were performed. Alterations in protein expression patterns after 48 hrs of siRNA-mediated transient silencing of SFRP1 were determined by the Q Exactive<sup>TM</sup> RF Hybrid Quadrupole Orbitrap<sup>TM</sup> Mass Spectrometer kindly performed by Dr. Juliane Merl-Pham (Helmholtz Zentrum Munich). After applying 1% protein FDR filtering, 2400 proteins were quantified within the samples. Among them, 140 proteins were differentially abundant in both siSFRP1 v/s UT and siSFRP1 v/s Sc having  $p < 0.05$  (paired t-test) and fold change ( $Fc$ )  $> 1.4x$  (Fig 4.21 A). Using the PSEA-Quant tool (Pseaquant.scripps.edu, 2019), several GO (Gene Ontology) protein sets were identified that were differentially expressed between the two data sets. This enrichment analysis tool identified the GO terms that were over-represented using annotations for that particular gene set. Different GO aspects like Molecular Function (MF), Biological Process (BP), Cellular Component (CC) and Reactome Pathways (RP) were chosen for this analysis. These data indicated an enrichment in the TGF $\beta$  regulated pathways in the SFRP1<sup>low</sup> phFbs (as discussed in section 4.2.2.3). Although the SFRP1<sup>low</sup> fibroblasts did not demonstrate a significant deregulation of RhoA protein expression, they did display an interesting over-representation of the Rho GTPase effector proteins which is confirmative to our findings from the transcriptomic screen. Additionally, some components of the actin cytoskeleton as well displayed an interesting enrichment in SFRP1<sup>neg</sup> phFbs (Fig. 4.21 B).

Subsequently, I wanted to validate some of the interesting proteins found amongst the 140 differentially regulated ones identified in the proteomic analysis. Decreased SFRP1 protein expression levels by siRNA mediated silencing in the phFbs acted as a positive control for the experiment. The same samples that were used for the proteomics study, were used to validate the targets by Western blotting. The abundance ratios of these selected proteins are displayed as a heatmap in Fig 4.21 C. Immunoblotting and further densitometric quantifications thereof demonstrated substantial upregulation for the proteins Catenin Delta 1 (CTNND1), Talin1 (TLN), Mapk1, Zyxin (ZYG) and Tenascin C (TNS), all of which were not statistically significant in my experiments.

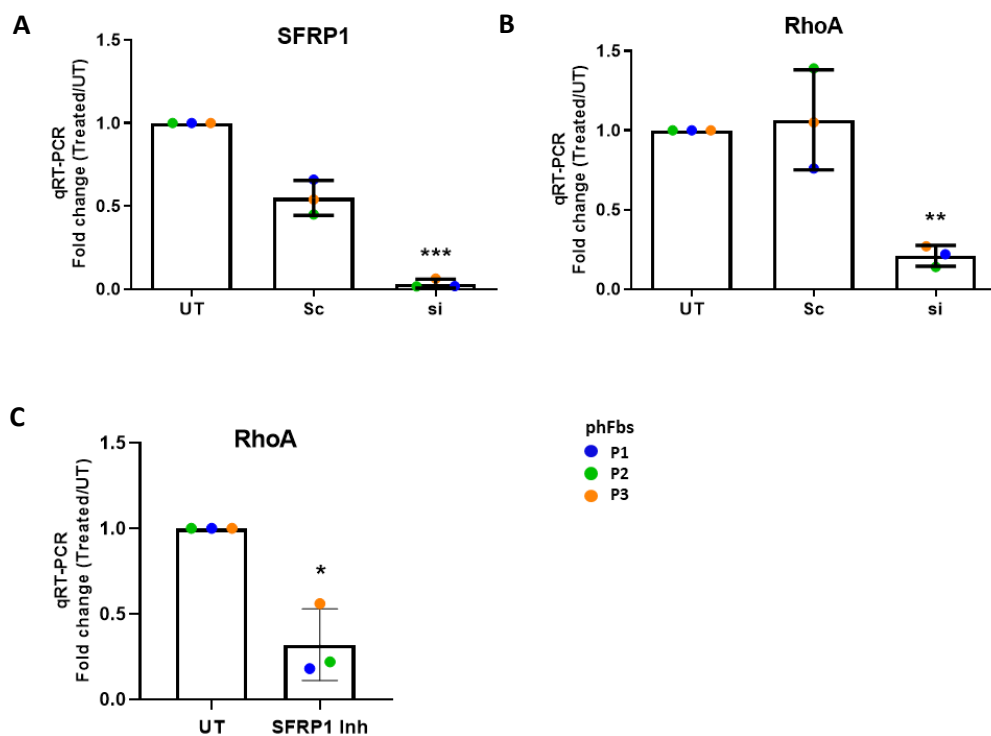


**Figure 4.21: Proteomic signature of SFRP1<sup>low</sup> human lung fibroblasts**

Venn diagram show here the number of deregulated proteins identified with  $F_c > 1.4x$  and  $p\text{-value} < 0.05$  in siSFRP1 vs UT and siSFRP1 vs Sc analysis and 140 proteins were found to overlap in both conditions (A). Statistical testing for differential expression were performed by employing a paired t-test and Benjamini-Hochberg multiple testing correction ( $FDR < 10\%$ ). Normalized enrichment scores (ES) indicate the distribution of Gene Ontology categories. A selection of the top enriched GO pathways is displayed in the graph and RhoA related components are highlighted by red squares (B). Heatmap depicting the chosen proteins found in the proteomic analyzes for validation. High and low abundant proteins are illustrated in the heatmap in blue and white, respectively. Each column represents the average of the abundance ratios from three different biological experiments ( $n=3$ ). (C). Alterations in protein expression of SFRP1, CTNND1, Talin, Mapk1, Zyxin and TnsC in total cell lysates were validated via immunoblot. Shown is one representative immunoblot from three independent biological experiments in phFbs ( $n=3$ ; P1-P3) (D). Densitometric quantifications from (C) are presented as mean  $\pm$  SEM. Statistical analysis: paired t-tests (E). **Note:** Mass spectrometry performed by Dr. Juliane Merl-Pham, Helmholtz Zentrum Munich.

#### 4.2.2.7. Lack of SFRP1 alters RhoA expression and activity in fibroblasts

Data from the microarray and proteomic analysis both hinted at a deregulation of the RhoA/Rock1 signaling pathway, therefore the RhoA expression was further validated in SFRP1 depleted phFbs. As a control, depletion of SFRP1 in phFbs displayed a significant downregulation of SFRP1 transcript levels (fold change: 0.03) demonstrating knockdown efficiency (Fig. 4.22 A). Strikingly, RhoA mRNA expression in SFRP1<sup>low</sup> phFbs was significantly reduced (fold change: 0.24) compared to untreated controls (Fig. 4.22 B) which is in also in line with the microarray data. Moreover, and quite surprising, treatment of phFbs with the specific SFRP1 inhibitor at 30  $\mu$ M produced also a down-regulation in RhoA expression (Fig. 4.22 C).

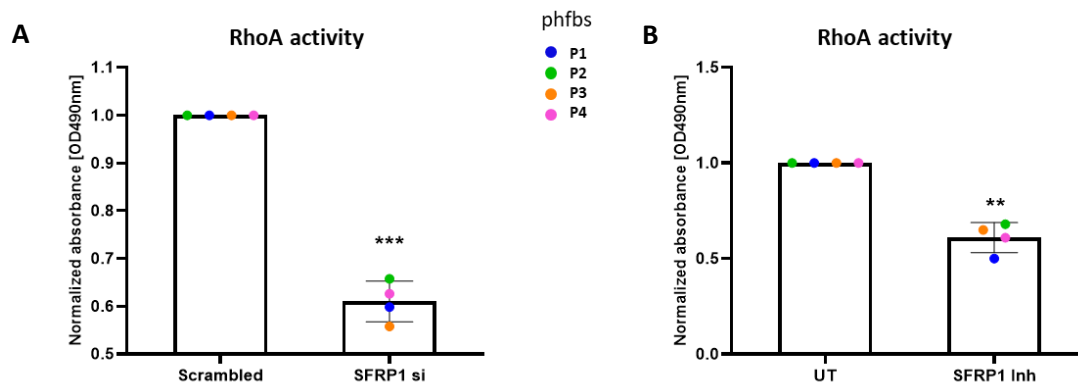


**Figure 4.22: SFRP1 depletion and inhibition in phFbs downregulates RhoA mRNA expression**

mRNA expression of SFRP1 (A) and RhoA (B) was measured in SFRP1 siRNA transfected (si), negative siRNA control (Sc) and transfection buffer control (UT) phFbs (P1-P3). mRNA expression of RhoA was further measured in SFRP1 inhibitor (CAS 915754; 30 $\mu$ M) treated phFbs (C). GAPDH served as a housekeeping gene. Bars indicate the mRNA levels normalized to control cells (UT) and represented as mean  $\pm$  SEM from the three independent experiments (P1-P3). Statistical analysis: Paired two-tailed t-test. \*\*\*p-value < 0.001, \*\*p < 0.01, \*p-value < 0.05.

RhoA, as a member of the non-canonical Wnt pathway, is primarily involved in signaling of the actin reorganization, actomyosin contractility, cell adhesion and cellular morphological polarization. Activation of RhoA is majorly regulated via phosphorylation by guanine nucleotide exchange factors (GEFs). Hence, RhoA shuttles between the alternate active GTP-bound state and inactive GDP-bound state, which is conducted simultaneously via GEFs and GTPase activating factors (GAPs) [168]. To

investigate how SFRP1 depletion could affect the activated RhoA pool within phFbs, a G-LISA RhoA activation assays (Cytoskeleton, Inc.) was utilized. RhoA activity was measured in SFRP1 siRNA (siSFRP1) treated phFbs and normalized to control scramble (Sc) treated cells. The activity of RhoA was found to be significantly diminished (almost 40% downregulation; p-value- 0.0003) in the SFRP1 silenced phFbs (Fig. 4.23 A). To confirm this finding further, RhoA activity in the SFRP1 inhibitor treated (30  $\mu$ M) phFbs was measured. Likewise, RhoA activity was significantly reduced (almost 37% downregulation; p-value- 0.0022) in the SFRP1 inhibitor (30  $\mu$ M) treated cells (Fig. 4.23 B). In summary, significant reduction of RhoA gene expression and activity was demonstrated in the SFRP1<sup>low</sup> phFbs (both by knockdown and using SFRP1 inhibitor).



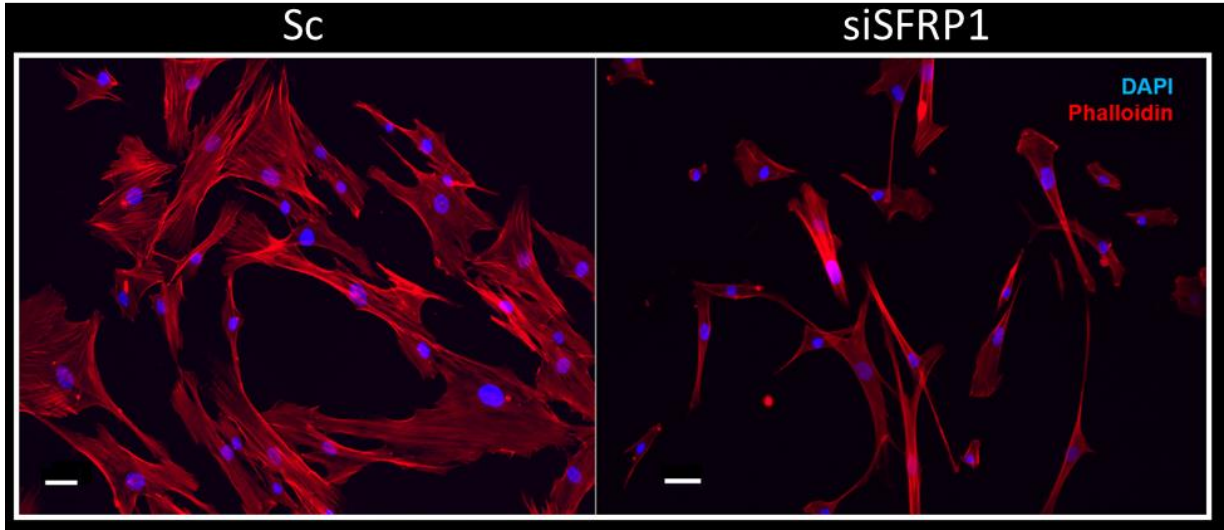
**Figure 4.23: Diminished RhoA activity is found in SFRP1<sup>low</sup> phFbs**

The active form of RhoA was luminometrically detected using a G-LISA RhoA activation assay. RhoA activity was measured in siSFRP1 treated phFbs, normalized to Sc treated cells (A) and in SFRP1 inhibitor (30 $\mu$ M) treated phFbs normalized to untreated vehicle control cells (B). Absorbance was measured at 490 nm and the medium for the cells was taken as a blank control. Data are represented as mean  $\pm$  SEM from four patient cell lines (P1-P4). Statistical analysis: Paired two-tailed t-test. \*\*\*p-value < 0.001, \*\*p<0.01.

#### 4.2.2.8. SFRP1 depleted human lung fibroblasts display morphological changes in vitro

Proteomics of SFRP1 silenced phFbs displayed an enrichment of proteins relating to the GO term cellular components (CC) of stress fibers and actin cytoskeleton and an overall enrichment in cell adhesion proteins (as discussed in section 4.2.2.6). In addition, a significant reduction in RhoA activity and expression was observed in SFRP1 depleted phFbs. RhoA reportedly is a key player for stress fiber formation as well as for cell morphology changes. Given all the data collected before, I next intended to investigate the morphology of phFbs following depletion of SFRP1 after siRNA knock-down. For this experiment, phFbs were grown on standard 2D plastic culture dishes and stained for DAPI (a nuclear dye) and Phalloidin (ThermoFischer, stains F-actin). Surprisingly, from the pilot study with 3 phFbs (2 technical replicates per condition) prominent alterations in cell shape were observed in the siSFRP1

treated pHFs compared with the Sc treated cells. The SFRP1<sup>low</sup> pHFs, as observed were somewhat smaller than the untreated and scramble control treated cells and displayed elongated body shape with reduced cytoplasmic branching. (Fig. 4.24).



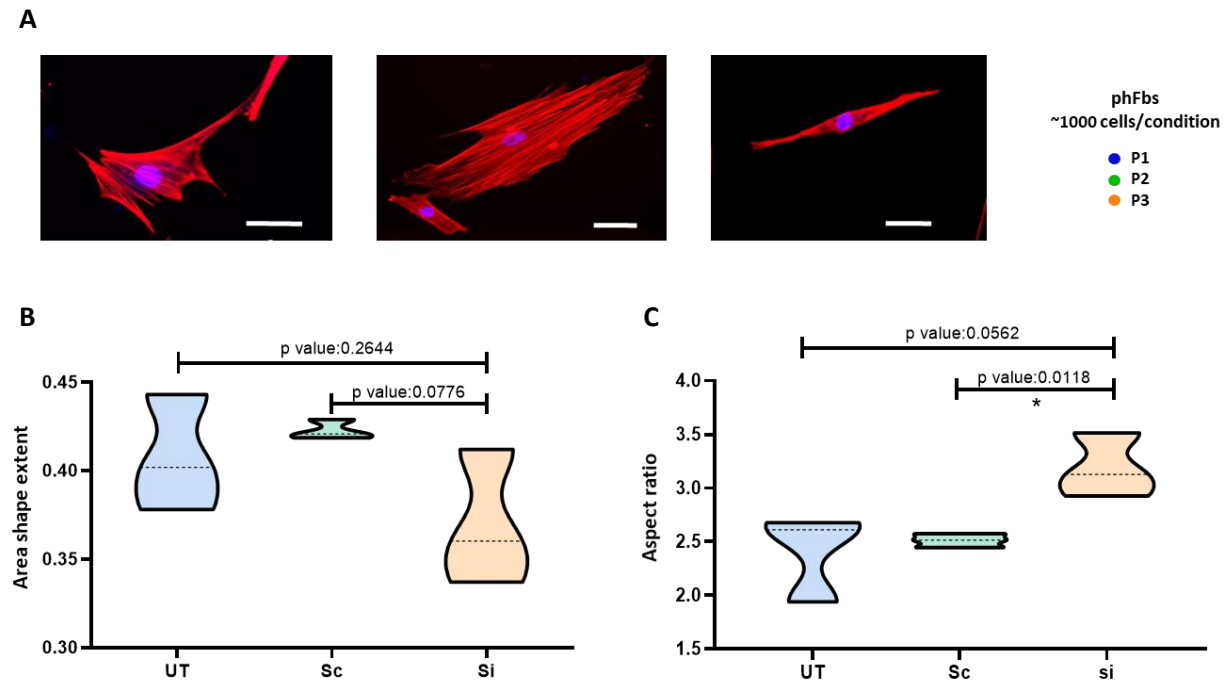
**Figure 4.24: SFRP1 silenced pHFs display differences in cell shape and stress fibers**

Control scramble treated (Sc) and SFRP1 siRNA (siSFRP1) treated pHFs were grown in standard cell culture dishes. The cells are stained with DAPI in blue and Phalloidin in red. One of the representative images out of three independent experiments with patient cells (n=3) are shown. Scale bar is 50  $\mu$ m.

To verify the changes in cell shape parameters, a large-scale experiment with the same three pHF cell lines was performed. Approximately 1000 cells per condition per cell line were analyzed. The morphology of the different fibroblast cell lines was quantified by means of surface rendering of acquired confocal fluorescent z-stacks. Next, *in silico* analysis of the microscopy data using Cell Profiler (Broad Institute) software was performed. Morphological parameters like cell aspect ratio and area shape extent were independently assessed. The area shape extent indicates the extent to which the cell shape can change and is computed by dividing the area of a cell by the area of the smallest hypothetical bounding box possible for that particular cell. A high area extent will therefore represent circular or elliptical cells. Utilizing a cell masking algorithm, the cell nuclei and the cell body were differentially identified by a python-based script. The area shape extent was calculated from the area/volume of the cell body divided by the area/volume of the hypothetical bounding box around it. Additionally, cell aspect ratios were obtained by the ratio of the minimum and maximum feret diameter. The feret diameter is defined as “distance between two parallel lines tangent on either side of the object” (Cell Profiler, manual, v3.0.0) [169], hence the maximum and minimum feret diameters represent the largest and smallest diameter possible respectively. Thus, I could quantitatively show that SFRP1 silenced pHFs (si) had a reduced area shape extent compared to untreated and scramble control cells (Fig. 4.25 B). Moreover, the SFRP1



depleted pHFs presented an increased aspect ratio (Fig. 4.25 C) compared to the untreated and negative siRNA controls. These data highlight that SFRP1 depleted fibroblasts display a switch towards slender and more spindle-shaped cell morphologies.



**Figure 4.25: SFRP1 depleted fibroblasts showed significant morphological changes**

Representative confocal images of human lung fibroblasts cultured in 2D (top). Morphological evaluation of approximately 1000 cells per condition. Data shown represent mean values ( $\pm$ SD) of randomly selected fibroblasts ( $n = 100$ ). Scale bar, 50  $\mu\text{m}$ , a.u. = arbitrary units (A). Geometric parameters of area shape extent (B) and aspect ratio (C) were assessed from surface rendering of acquired confocal fluorescent z-stacks in Cell Profiler. Statistical analysis: unpaired t-test. \* $p < 0.05$ .

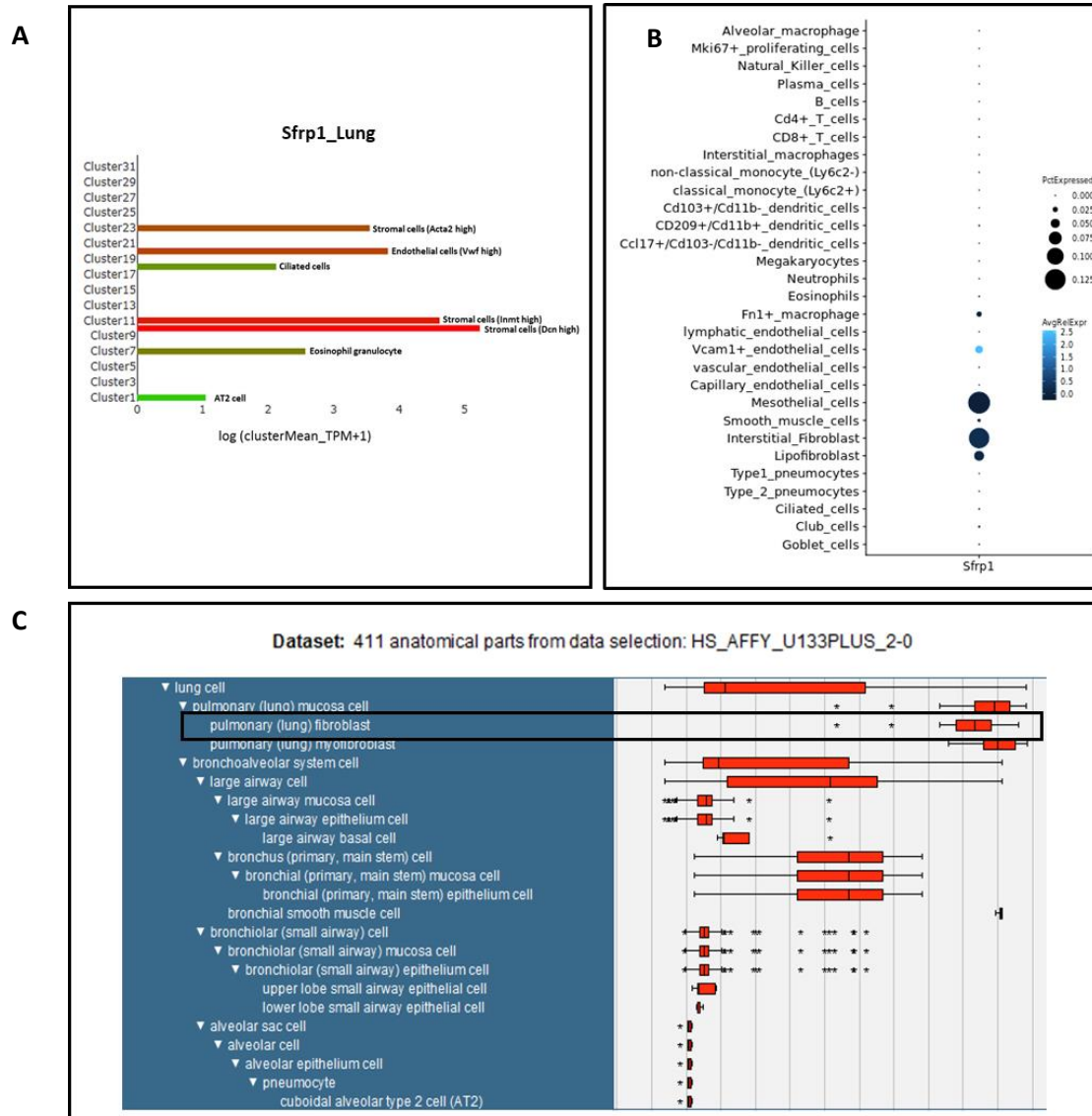
Collectively, my data advocates a novel molecular mechanism of SFRP1 in the framework of RhoA signaling with consequences for cell shape as well as cellular invasion.

### 4.2.3. Part III: SFRP1 expression in distinct fibroblast sub-populations

#### 4.2.3.1. In the lung mostly fibroblasts exclusively express SFRP1

An upregulation of SFRP1 during lung fibrosis was reported in several studies before, like in [45] and [39]. But, the specific cell-type exceedingly expressing SFRP1 still remains elusive. To further investigate this, first online-based datamining in lung databases was applied. Recent advances in single-cell gene expression analysis allowed us to have an enhanced view on cell identification and classification. A group led by Xiaoping Han established a “mouse cell atlas” using Microwell sequencing data covering 800 major cell types and more than 1000 subtypes [170]. In this web-based atlas, SFRP1 was found to be mainly

expressed in stromal cell populations in healthy mice (Fig. 4.26 A). As, lung fibrosis is an age-related disease, SFRP1 expression was next checked in the recently published “Lung Aging Atlas” [171]. This database clearly depicted SFRP1 expression limited to interstitial fibroblasts, lipofibroblasts and mesothelial cells in the aged mouse (Fig. 4.26 B). To further confirm these results within a human dataset, the Genevestigator software tool encompassing different types of curated expression datasets was used. The whole human genome expression array was investigated which covered 411 anatomical parts. Overall, lung fibroblasts were found as the primary cell type in the lung that expressed SFRP1 (Fig. 4.26 C).

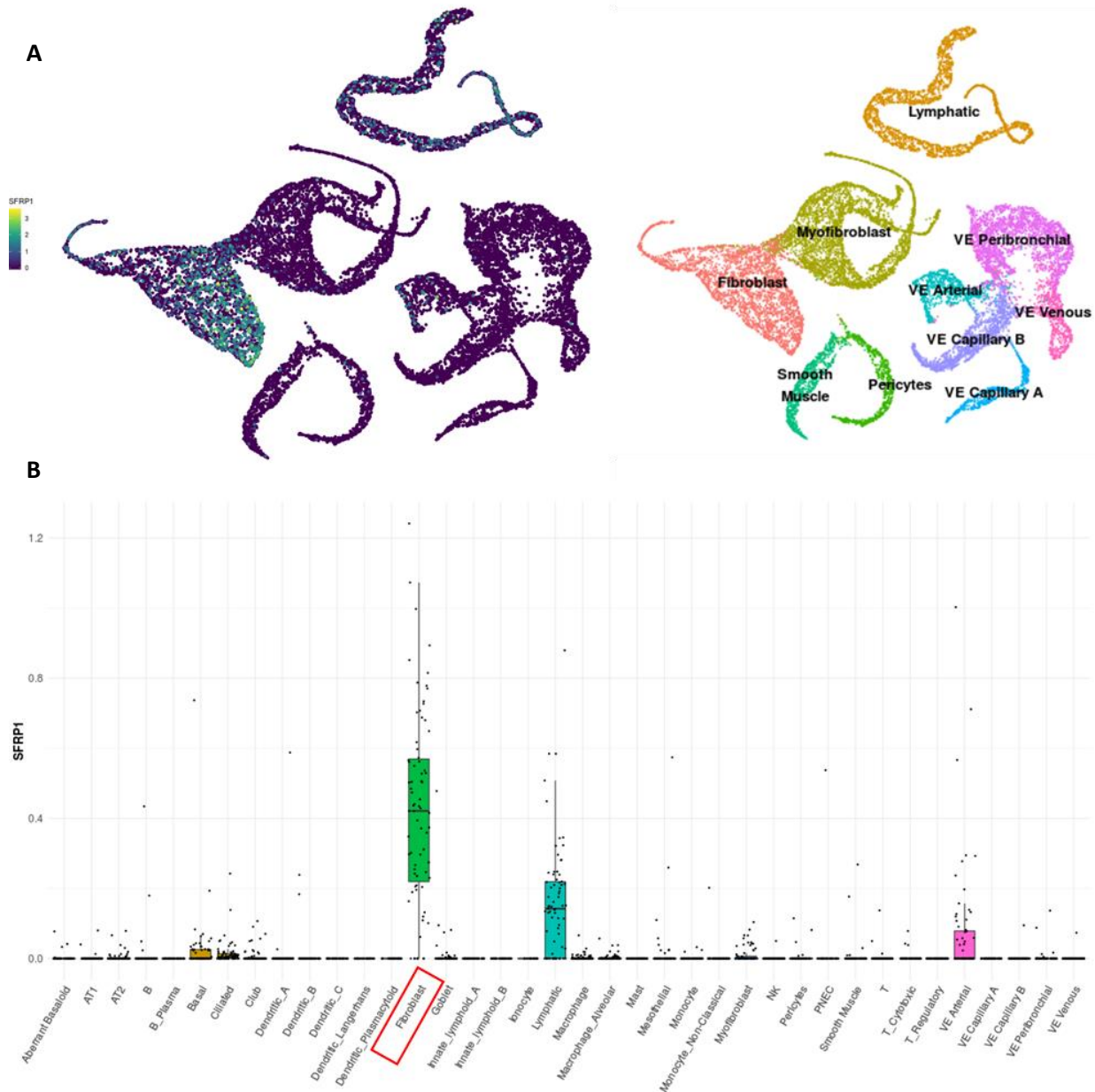


**Figure 4.26: SFRP1 is primarily expressed by fibroblasts**

Screenshot of different cell clusters of healthy mouse lungs showing mean expression levels of SFRP1 (<http://bis.zju.edu.cn/MCA/>) (A). Dot plot visualization of each cell type in the aging lung single-cell data [171]. The size of the dots encodes the percentage of cells within a cell type, and the color encodes the average expression levels ([http://146.107.176.18:3838/MLAA\\_backup/](http://146.107.176.18:3838/MLAA_backup/)) (B). Visualization of SFRP1 anatomical expression across different lung cell types (Genevestigator tool: <https://genevestigator.com/gv/>). The plot is sorted from highest to lowest expression (C).



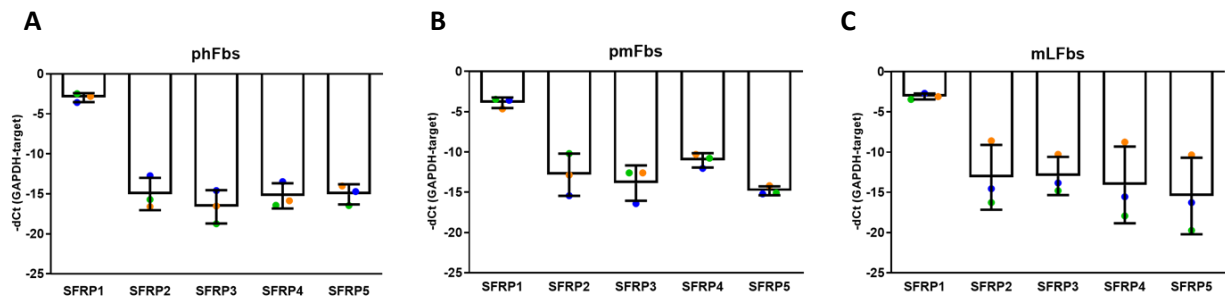
The recently established IPF cell atlas ([ipfcellatlas.com](http://ipfcellatlas.com)), provided a database profile of 312,928 cells from 32 IPF, 29 healthy control and 18 chronic obstructive pulmonary disease (COPD) lungs (TS Adams et al., 2019). Among the stromal cell populations, fibroblasts were found to express SFRP1 the most. (Fig.4.27 A-B).



**Figure 4.27: Identification of SFRP1 enriched cell population in lungs**

UMAP analysis of various stromal cell populations: fibroblasts, myofibroblasts, lymphatic, smooth muscle, pericytes, VE arterial, VE venous, VE peribronchial, VE capillary A and B, labelled according to cell type. High to low expression of SFRP1 in the UMAP is indicated by yellow and purple respectively (A). Boxplot representing in percent the distribution of SFRP1 among all the different cell types in the lung. Fibroblasts (marked with a red box) showed the highest SFRP1 expression (B). **Note:** Data obtained from IPFCellatlas.com.

Sfrp1 belongs to a family of secreted frizzled-related proteins that consist of five isoforms namely Sfrp1, Sfrp2, Frzb (Sfrp3), Sfrp4, and Sfrp5. To validate the *in-silico* results described before and to investigate the specificity of Sfrp1 expression in fibroblasts, total mRNA harvested from primary human fibroblasts (phFbs), primary mouse fibroblasts (pmFbs) and mouse lung fibroblast cell line (mLFbs; CCL206™, ATCC) were analyzed by qPCR. The results clearly indicated that SFRP1 was the most expressed among all isoforms in mouse and human lung fibroblasts (Fig. 4.28 A-C), demonstrating SFRP1's unique and exclusive expression in fibroblasts.

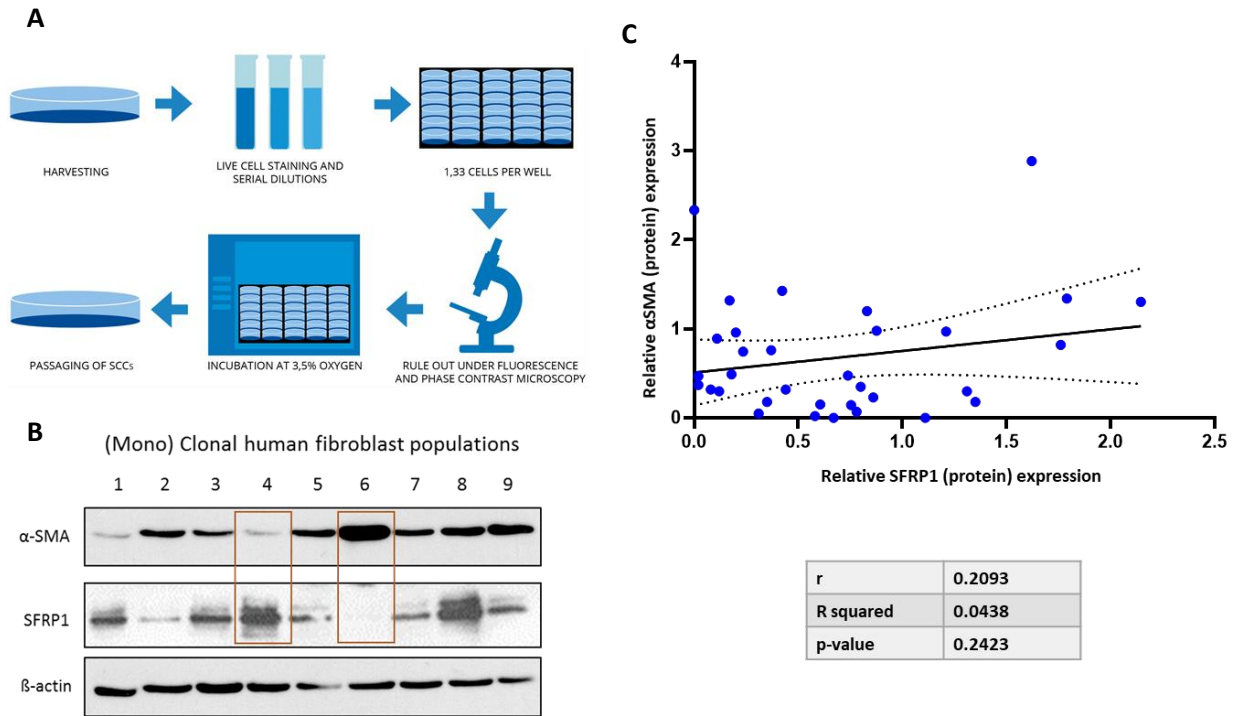


**Figure 4.28: Transcript levels of SFRP isoforms in lung fibroblasts**

qRT-PCR analyses displaying normalized mRNA expression of SFRP1, SFRP2, SFRP3, SFRP4 and SFRP5 in phFbs (A), pmFbs (B) and mLFbs (C). GAPDH served as a housekeeping gene. Bars are represented as mean  $\pm$  SEM from three independent biological experiments.

#### 4.2.3.2. Single cell clones derived from healthy primary human fibroblasts can be classified according to their SFRP1 expression

Fibroblast clonal heterogeneity previously was reported for protein synthesis and growth [172]. Single-cell clone isolation has recently gained increasing attention as a tool to study clonal functional heterogeneity. Single cell clones (SCCs) of phFbs were isolated using serial dilutions and then expanded under hypoxic culture conditions (Fig. 4.29 A). As, a pure clonal isolation from a single progenitor cell is of utmost importance, hence monoclonality was visually confirmed by fluorescence microscopy (data not shown). After expansion in low oxygen culture, fibroblast populations derived from one single cell were further passaged and expanded. Strikingly, fibroblasts derived from single cells of the same primary cell line revealed a differential protein expression of  $\alpha$ SMA and SFRP1 as revealed by western blotting. Interestingly, three different phFb subtypes were observed from the immunoblot: SFRP1<sup>high</sup> $\alpha$ SMA<sup>low</sup>, SFRP1<sup>low</sup> $\alpha$ SMA<sup>high</sup> and SFRP1<sup>med</sup> $\alpha$ SMA<sup>med</sup> (med: medium expression) (Fig. 4.29 B). Next, a correlation study of SFRP1 and  $\alpha$ SMA protein expression with 33 monoclonal samples of fibroblast clones (from 4 phFb cell lines) was performed. Yet, statistical analysis revealed no significant association between SFRP1 and  $\alpha$ SMA protein levels in phFb SCCs (Fig. 4.29 C). In summary, existence of three distinct lung fibroblast subtypes based on their characteristic SFRP1 expression was revealed here.



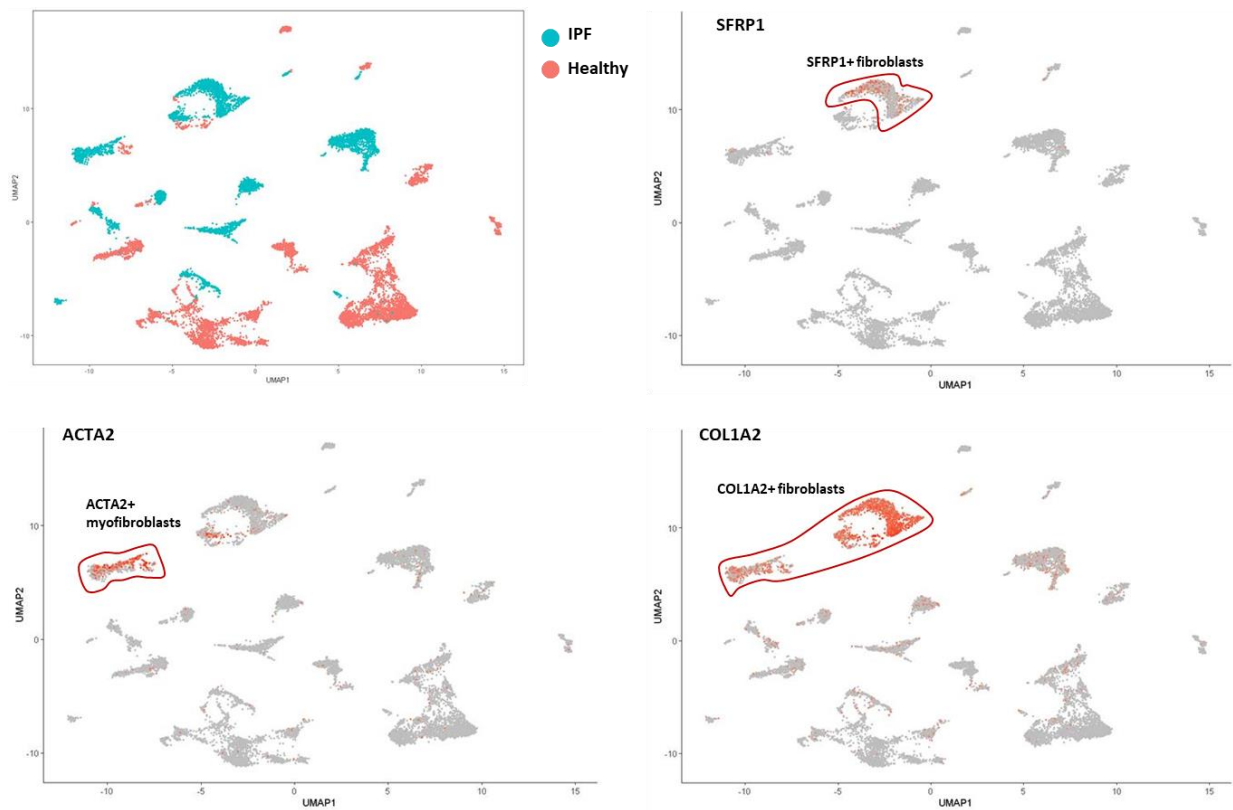
**Figure 4.29: Single-cell clones (SCCs) from phFbs show differential expression of SFRP1 and αSMA**

Experimental workflow for single cell clone isolation (A). Representative western blot from one phFb cell line (n=4) out of four independent biological experiments are shown. Total cell lysates obtained from different clones of the same cell line have been used for immunoblotting and probed for SFRP1 and αSMA. The differential relationship between SFRP1 and αSMA protein expression within SCCs in the Western blot is highlighted with red boxes. (B). SCCs from 33 individual monoclonal populations were analyzed for SFRP1 and αSMA expression. Statistical analysis: linear regression; r-value = 0.2093; p-value = 0.2423;  $R^2 = 0.0438$ . Dashed lines represent a confidence interval of 95%. **Note:** Single-cell cloning performed by M.Gerckens, Helmholtz Zentrum Munich.

#### 4.2.3.3. Single cell RNA sequencing validates SFRP1 expression in αSMA negative fibroblast subtypes in the diseased lung

In recent years, a rapid progress in the development of single cell methodology allowed researchers to uncover rare cell populations, new cell types and discover novel regulatory relationships among different genes. A “single cell atlas” of pulmonary fibrosis recently reported differential expression of genes between healthy and IPF lung biopsies and identified a novel senescent cell population emerging during fibrosis [173]. Due to our analysis of single fibroblast clones, we identified different subtypes such as  $\text{SFRP1}^{\text{high}}\alpha\text{SMA}^{\text{low}}$ ,  $\text{SFRP1}^{\text{low}}\alpha\text{SMA}^{\text{high}}$  and  $\text{SFRP1}^{\text{med}}\alpha\text{SMA}^{\text{med}}$ . To further investigate these fibroblast subtypes in the context of fibrosis, single cell droplet-based RNA sequencing (Dropseq) of lung resections obtained from healthy tumor-free lung tissue sections and IPF diagnosed patients was performed. Using Dropseq technology [174], single cells were sequenced and analyzed in the context of cell heterogeneity and disease-specific aspects as compared to control tissue. After alignment of sequencing reads and data

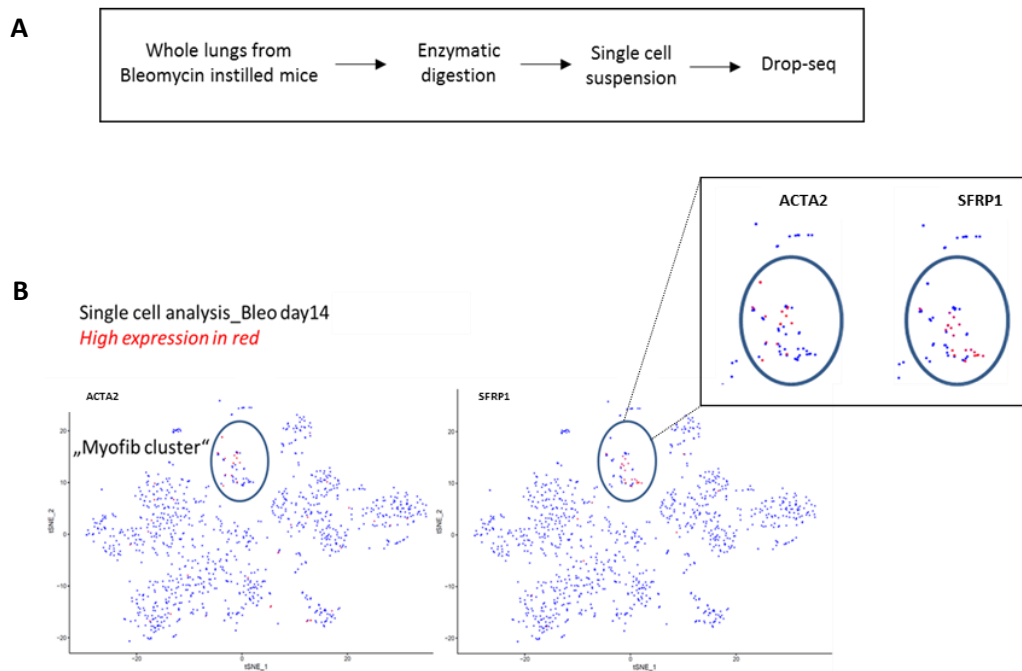
normalization following the Dropseq pipeline v2 (McCarroll Lab, 2019), data was represented in the uniform manifold approximation projection (UMAP) embedding (Fig. 4.30 A-D). Each dot in the plot represented a single cell. Different cell populations were clustered together and were represented in two different colors - either healthy (red) or diseased (blue). Batch corrections between the subjects were not performed. Gene expression overlaid to the UMAP embedding suggested that SFRP1 expressing cell populations were ACTA2 ( $\alpha$ SMA) negative (Fig. 4.30 B-C) but positive for COL1A2 (collagen 1a2) confirming a relation to fibroblasts (Fig. 4.30 D).



**Figure 4.30: Single cell sequencing confirmed SFRP1 expression by a distinct human (fibrotic) fibroblast sub-population** UMAP plot is shown with colored cell clusters as red and blue to indicate cells from healthy and IPF lung biopsies respectively (A). SFRP1<sup>high</sup> (B), ACTA2<sup>high</sup> (C) and COL1A2<sup>high</sup> (D) expressing cells are indicated by red dots encircled with red boundaries in the UMAP projections. Values are shown as log2 (density). **Note:** Single-cell RNA sequencing performed by Dr. M. Strunz and Dr. H.B. Schiller, Helmholtz Zentrum Munich.

Likewise, to identify similar SFRP1 related cell populations in the fibrotic mouse lungs, Dropseq of whole fibrotic and healthy mouse lungs were performed. After enzymatic and mechanical disruption of whole lung tissue, dead cells were removed and samples subjected to Dropseq. Transcript abundance is indicated in red, whereas each dot represents one analyzed cell. Concomitantly, SFRP1<sup>high</sup> IPF fibroblasts were found to be mostly ACTA2<sup>low</sup>. Our results with mouse and human tissues further corroborates the existence of the distinct fibroblast subtypes observed in single cell clones like: SFRP1<sup>high</sup>  $\alpha$ SMA<sup>low</sup>,

SFRP1<sup>low</sup>  $\alpha$ SMA<sup>high</sup> and SFRP1<sup>med</sup>  $\alpha$ SMA<sup>med</sup> and firmly advocate their presence during fibrosis. (Fig. 4.31 B).

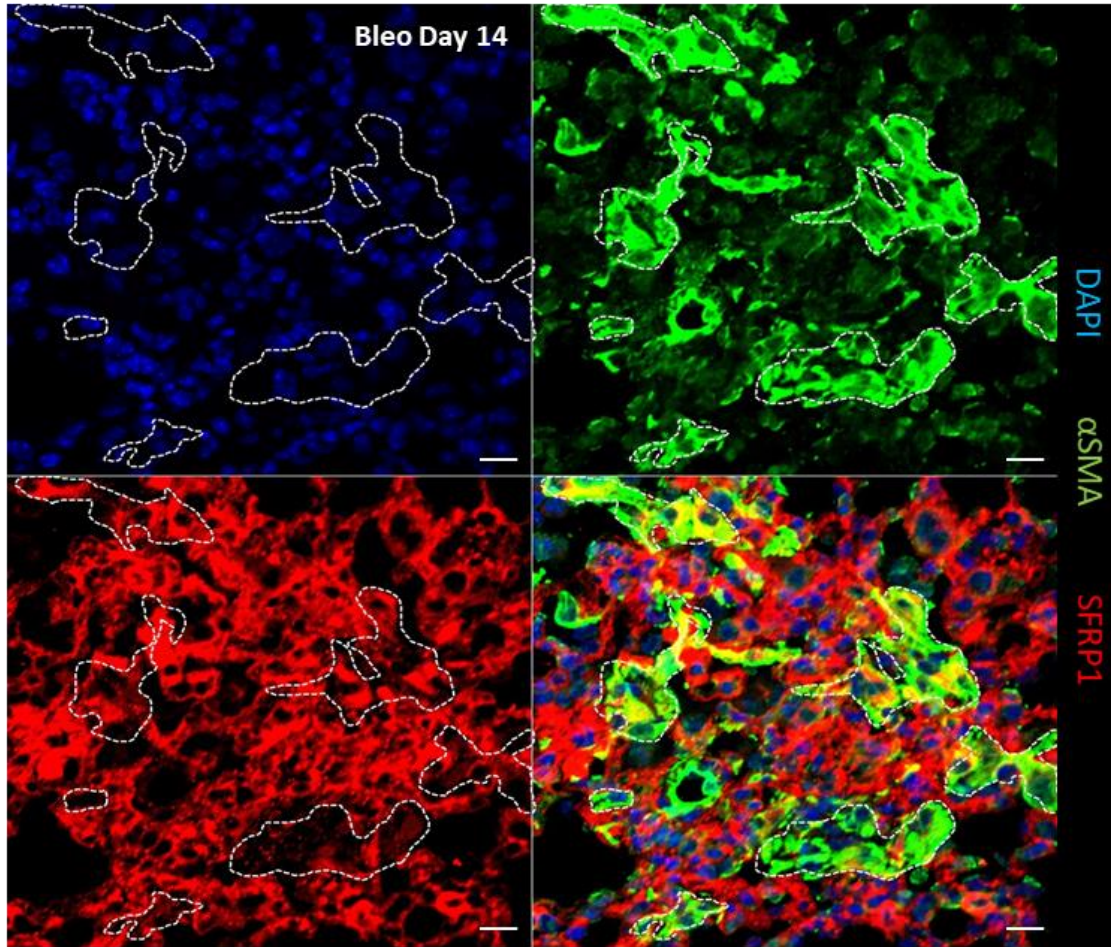


**Figure 4.31: Single cell sequencing show mutual exclusion of SFRP1 and ACTA2 expression.**

Schematic workflow of the study (A). t-SNE projection of the dataset showing ACTA2 and SFRP1 expression. Magnified view of the myofibroblast cluster for ACTA2 and SFRP1 expressing cells are shown on the right (B). **Note:** Single-cell RNA sequencing performed by Dr. M. Strunz and Dr. H.B. Schiller, Helmholtz Zentrum Munich.

Although here only a limited number of cells were obtained from these early scRNAseq experiments, there was a clear indication that SFRP1 and  $\alpha$ SMA expressing cells were largely mutual exclusive. For in situ validation of the presented single cell data, protein staining by immunofluorescence in fibrotic mouse lung tissue sections from day 14 after bleomycin injury were performed. The confocal z stack images obtained were represented as maximum intensity projections. Subsequently, regions of high density  $\alpha$ SMA positive myofibroblasts were encircled with white dotted lines. Density of SFRP1 positive cells were observed to be very low within these encircled  $\alpha$ SMA<sup>high</sup> regions. Therefore, similar to the scRNAseq data, SFRP1 and  $\alpha$ SMA protein expression were found to be largely mutually exclusive in fibrotic (day 14 Bleo) mouse lung tissues (Fig. 4.32).





**Figure 4.32: SFRP1 and  $\alpha$ SMA show mutually exclusive staining in fibrotic mouse lung tissues**

Representative immunofluorescent staining of fibrotic mouse lung tissue (day 14) double stained for  $\alpha$ SMA (in green) and SFRP1 (in red). Cell nuclei were counterstained with DAPI (in blue). Scale bar: 20  $\mu$ m.

### 4.3. Discussion

Fibroblasts are characterized as the primary effector cells in IPF and fibrosis. Inflammatory mediators, such as TGF $\beta$ 1, trigger the activation of fibroblasts and their trans-differentiation into myofibroblasts. Due to this activation, fibroblasts migrate into the intra-alveolar space, proliferate and subsequently deposit massive amounts of extracellular matrix (ECM) which ultimately results in impairment of gas exchange and death by asphyxiation. Hence, activation and invasion of fibroblasts are key pathomechanism in fibrosis progression. In an unbiased transcriptome analysis of the invading mouse lung fibroblasts, our lab previously identified SFRP1, an important regulator of the Wnt pathway to be significantly reduced in invading fibroblasts [144]. Additionally, SFRP1 is reported to be upregulated in IPF [154] and in bleomycin induced fibrotic mouse lungs at fibrosis day 14 [145]. However, given its importance, the function of SFRP1 in regards to fibrosis has not been characterized yet. Here, SFRP1

specific mechanisms in lung fibroblasts and their role in the context of lung fibrosis was analyzed for the first time.

Here, upregulation of SFRP1 was confirmed from IPF lung tissue as well as in fibrotic mouse lungs. Additionally, I performed experiments which demonstrated increased SFRP1 protein expression in *ex vivo* mouse and human injury and fibrosis models for the first time. Furthermore, a potential crosstalk between SFRP1 and TGF $\beta$ 1 in lung fibroblasts could be disclosed. Pathway inhibition studies revealed that TGF $\beta$ 1 reduced SFRP1 expression via an unknown Smad-independent pathway. Moreover, contrary to popular studies in different types of cancer, the expression of SFRP1 not regulated epigenetically in lung fibroblasts. Additionally, transcriptomics and proteomics of SFRP1 depleted human lung fibroblasts displayed a deregulation of RhoA and in its signaling network. Importantly, SFRP1 depleted fibroblasts displayed decreased RhoA expression as well as a decreased GTPase activity, which could advocate a novel and until now unknown molecular function of SFRP1. Consequently, SFRP1 depleted fibroblasts exhibited morphological changes towards a more elongated cell-type which could be a direct consequence of reduced RhoA expression and activity.

SFRP1 was largely expressed by fibroblasts in the lung. Furthermore, lung fibroblasts' clonal heterogeneity was studied by the isolation of single-cell clonal populations. SFRP1<sup>high</sup>, SFRP1<sup>low</sup> and SFRP1<sup>med</sup> fibroblast populations were identified for the first time in distinct fibroblast populations. These data delineate for the first time a comprehensive characterization of SFRP1 in healthy and fibrotic lung conditions, and delineate a pivotal role of SFRP1 in specific fibroblast subpopulation during fibrogenesis.

#### **4.3.1. Regulation of SFRP1 in fibrosis models**

The high need for novel IPF biomarkers and the lack of reproducibility and validation of established markers pose a constant challenge in the field [175]. Ongoing studies have identified various genes that are specifically associated with IPF. A study in 2007 characterized for the first-time variations in gene expression in different stages of IPF compared to healthy lungs [176]. Therefore, understanding drivers of fibrogenesis that are capable of discriminating between intermediate stages of fibrosis is crucial. Secreted and surface proteins represent easily accessible targets for various pharmacological compounds compared to intracellular molecules [96]. SFRP1 is a secreted antagonist of the Wnt signaling pathway and was identified in a couple of gene expression studies with IPF patient samples [45, 154]. Recently a group reported increased SFRP1 gene expression in bleomycin-induced fibrotic mouse lungs. The authors showed increased SFRP1 mRNA levels at day 7, day 14 and day 21 Bleo induced mouse lungs. However, the authors did not confirm this upregulation of SFRP1 observed in the bleomycin-induced mouse fibrosis model in human fibrosis [177]. Another study utilizing quantitative detergent solubility profiling (QDSP) and systemic analysis of the transcriptomic profiles identified SFRP1 as a novel constituent of the provisional extracellular repair matrix in the Bleo-induced fibrotic mouse model at day

14 [145]. But despite these findings, there has been no exclusive study characterizing SFRP1 in the context of lung fibrosis in detail. Here, protein expression of SFRP1 was investigated at various time-points in the course of Bleo injury in mice. For the first time, an early upregulation of SFRP1 was noted from day 3 (inflammatory phase) onwards peaking at day 7 and 14 (fibrogenic phase) and gradual reduction of expression was observed with the resolution of the disease. In addition, the IPF cohorts from Munich and Gießen showed a trend of SFRP1 upregulation compared to healthy controls. However, the coherence to mouse studies could not be verified probably due to the low power of the study. The observed heterogeneity of SFRP1 expression among different patient samples might stem from the fact that the lung resections were collected from different areas within the lungs. Also, the tissue sections were from patients at different stages of the disease, although I did not have direct insight into clinical data. In general, smaller clinical cohorts display greater variation depending upon sex, age, ethnicity and environmental effects [178]. Hence, in order to normalize the heterogeneity and to obtain a better understanding of SFRP1 expression in IPF, a larger cohort study will be required.

Our *ex vivo* mouse and human fibrosis-mimicking models indicated increased SFRP1 protein expression under pro-fibrotic perturbation conditions. Precision-cut lung slices (PCLS) add an additional dimensionality compared to 2D tissue culture models, and provide a unique platform for disease modeling. *Ex vivo* PCLS models largely retain the native cellular environment and cell-cell and cell-matrix interactions, as well as mechanobiological conditions which all closely resemble the *in situ/in vivo* situation [147]. Recently, the potential therapeutic compounds for IPF were validated in a human PCLS fibrosis model. The authors reported a similar expression of certain fibrotic markers in the PCLS on stimulation with a pro-fibrotic cocktail (same composition as used in our study) as reported *in vivo*. In a follow-up experiment, the group recruited Nintedanib and Pirfenidone for their study, which are the only 2 drugs approved for IPF clinical treatment. They showed that Nintedanib and Pirfenidone effectively recapitulated their anti-fibrotic effects confirmed by suppressing pro-fibrotic Wisp1 expression, reduced collagen deposition and increased pro-SPC secretion in the PCLS treated with the fibrotic cocktail [179]. Therefore, the PCLS platform opens up new areas for multitude drug testing and thereby highlight the potential importance of validating gene or protein expression in such disease-mimicking scaffolds. In light of this, SFRP1 could also act as a novel and attractive biomarker for these models indicating ongoing fibrosis, and, due to the fact that it is a secreted factor, furthermore could be tested as an early biomarker for fibrosis in the clinics.

#### **4.3.2. SFRP1 as a modulator of fibroblast invasion**

Parenchymal invasion of activated fibroblasts represents a critical pathomechanism in fibrosis [150]. Invasion of fibroblasts into three-dimensional matrices has recently garnered a lot of attention. A three-dimensional collagen-based invasion assay was established previously in our lab. The assay allowed



extensive profiling of invading and non-invading fibroblast fractions [180]. Utilizing this tool, the invading fibroblasts embedded in the gel and the non-invading fibroblast fractions were isolated and subjected to a whole transcriptome analysis. A strong reduction of SFRP1 gene expression was seen in the invasome of fibroblasts detected by microarray analyses.

A study with cervical cancer cells reported that overexpression of SFRP1 along with SFRP2 suppressed invasive capacity of these cells in a Matrigel-based Transwell assay [181]. Another group presented that overexpression of SFRP1 suppressed migration and invasion, whereas knockdown of SFRP1 resulted in enhanced migration and invasion of the colorectal cancer cells [182]. Additionally, restoration of SFRP1 expression in the otherwise low SFRP1 expressing nasopharyngeal carcinoma cells subdued their invasive capacity [183]. Of note, not much is known about SFRP1 expression in fibroblasts, fibrosis and its relation to fibrotic diseases. Hence, to get some mechanistic and functional insight, loss-of-function studies were accomplished by siRNA knock-down of SFRP1 in phFbs. Indeed, and in line with the cancer studies, a substantially increased invasive capacity of SFRP1 depleted fibroblasts was demonstrated.

Interestingly, the matrix metallo-proteinases (MMPs), MMP13, MMP3, MMP14 and MMP10 were found to be up-regulated in the invading cellular subpopulation in the before mentioned microarray analyzes (Bettina Oehrle, Ph.D. thesis). In the context of lung fibrosis, MMP13 along with MMP1 and MMP7 were upregulated in IPF lung tissue homogenates [184, 185]. Increased MMP14 protein levels is reported in experimental models of fibrosis and is a major proteolytic effector for invasion by degrading collagen fibers and matrices [186, 187]. Furthermore, MMP13 expression in cancer associated fibroblasts was shown to induce also the invasion of other neighboring carcinoma cells [188, 189]. In addition, MMP3 was found to be upregulated in both IPF lungs and fibrotic mouse lungs. Moreover, MMP3 expressed from fibroblasts play a crucial role in the pathogenesis of IPF by inducing epithelial-mesenchymal transition (EMT) [190]. Thus, our group previously performed Ingenuity pathway analysis (IPA) from the microarray dataset (discussed in section 4.2.2.1) and predicted a causal network of the invasome which included SFRP1 and MMPs. Interestingly, the pathway analysis predicted that the downregulation of SFRP1 could contribute to higher expression of MMP3 and MMP9 (Bettina Oehrle, Ph.D. thesis, 2015). Based on this conjecture, it might be promising to investigate further crosstalk and regulation of MMPs with SFRP1 in the context of fibroblast invasion.

TGF $\beta$ 1 was found differentially regulated in the invading fibroblasts. Considering TGF $\beta$ 1 as the master regulator in fibrosis, the upregulation of this growth factor in the invasome might be of particular interest. TGF $\beta$ 1 might potentially induce a forward loop of fibroblast activation. Conversely, one member of the TGF $\beta$ -superfamily, bone morphogenic protein 4 (BMP4) was found to be one of the most downregulated genes in invading fibroblasts. BMP4 has been associated mainly with cartilage and bone formation [191, 192] so far. Additionally, BMP4 was recently noted to reduce TGF $\beta$ 1 mediated extracellular matrix production in human lung fibroblasts [193]. Reports have established a cross talk between TGF $\beta$ 1-BMP4

and Wnt signaling via the Smad/ $\beta$ -catenin/Lef protein complex in the nucleus [194]. Moreover, BMP4 induces trans-differentiation of hepatic stellate cells increasing  $\alpha$ SMA expression *in vitro* and subsequently exert a pro-fibrotic role in liver fibrosis [195]. Based on this collective data, TGF $\beta$ 1 might crosstalk with BMP4 and SFRP1 in the regulation of fibroblast invasion and thereby serve as an interesting candidate to investigate further.

In conclusion, data from my thesis and from others strongly support that SFRP1 acts as a negative regulator of fibroblast invasion.

#### **4.3.3. Epigenetic regulation of SFRP1 expression in lung fibroblasts**

Epigenetic alterations via DNA methylation and histone modifications play an important role in the regulation of gene expression. Interestingly, SFRP1 is considered as one of the promising candidates for epigenetic therapy in several forms of cancer. Vincent and Postovit in 2017 have shown a consistent loss of SFRP1 in a pan-study with 29 different types of cancer cells [155]. In situ hybridization studies have confirmed a striking correlation between decreased SFRP1 mRNA levels and SFRP1 promoter hypermethylation in several cancer cell lines [164, 196, 197]. Apart from cancer, IPF patient samples as well demonstrated higher DNA methyltransferase expression and various genes with altered methylation status in a genome-wide DNA methylation study [198]. Moreover, IPF fibroblasts in comparison to healthy fibroblasts demonstrated global-wide differences in DNA methylation patterns which might as well contribute to fibrogenesis [199]. However, epigenetic regulation of SFRP1 in lung fibroblasts have not been investigated so far. 5-aza-2'-deoxycytidine or decitabine has been shown to restore SFRP1 expression in numerous cancer cell studies [197, 200]. Hence, decitabine was employed in my studies to repress DNA methyl transferase (DNMTs) activities in phFbs. Interestingly and quite surprisingly, contrary to numerous cancer studies, decitabine treated lung fibroblasts did not demonstrate any changes in SFRP1 expression compared with untreated vehicle controls. A recent study in 2015 indicated that decitabine treatment in lung fibroblasts attenuated TGF $\beta$ 1 induced Collagen1a1 and  $\alpha$ SMA gene and protein expression [201]. Subsequently, in line with this study, phFbs used in my experiments were concomitantly stimulated with TGF $\beta$ 1 and decitabine. However, our data did not indicate any alterations in TGF $\beta$ 1 induced SFRP1 expression following decitabine treatment in phFbs.

Next to methylation, acetylation of histones presents another classical epigenetic mechanism in gene expression regulation [203]. The dynamic acetylation and deacetylation cycles are regulated by the activity of histone acetylation transferases (HAT) and histone deacetylases (HDAC) respectively [202]. Importantly, histone acetylation has been demonstrated as an important regulator of gene expression in pulmonary fibrosis. Also, an involvement of histone deacetylation via HDAC4 during the early inflammatory phase and histone acetylation via HDAC2 during the late repair phase in lung fibrosis is discussed [204]. Interestingly, inhibition of histone deacetylation subdued TGF $\beta$ 1-mediated  $\alpha$ SMA and

Collagen 1 mRNA induction and thereby confirmed that lung fibroblast to myofibroblast differentiation might be HDAC dependent [205]. In line with this study, I applied the pan-HDAC Inhibitor Trichostatin A (TSA) in my experiments. Although previous studies have reported an important role of histone deacetylation for the regulation of SFRP1 expression [206, 207], my experiments in phFbs brought forth contrary results. Neither protein nor mRNA levels of SFRP1 were affected in TSA stimulated primary human fibroblast. Although our studies could not demonstrate any significant regulation of SFRP1's expression by investigating two major epigenetic regulatory mechanisms, there still might exist rare chromatin remodeling or histone post-translational modifications. Thus, apart from histone acetylation/deacetylation, histone lysine methylation has also been reported to occur infrequently in cancer via histone lysine demethylases and histone lysine methyl-transferases [208]. Dynamic chromatin structure remodeling along with their interaction with various transcription factors might also be of particular interest here [209]. Hence further investigations are required to fully get a clear mechanistic insight into SFRP1 regulation by epigenetic modifications in primary human fibroblasts.

#### **4.3.4. TGFβ1-induced regulation of SFRP1 expression**

The SFRPs are the largest family of antagonists known to inhibit the binding of Wnt ligands with their respective Frizzled receptors and thereby antagonize the signaling pathway during development [210]. Recent studies have indicated that SFRP1 is not merely a specific Wnt binding protein, but can interact with different receptors and matrix molecules [211]. A cross-regulation of Wnt and TGFβ1 pathways have been reported several times. This cross-talk activates a complex regulatory network that finally orchestrates fibrotic reactions at cellular and organ level [212]. Moreover, the TGFβ1 molecule has been ascribed as the central mediator of fibrogenesis and hence termed as the “master regulator of fibrosis”. Studies also provided evidence for TGFβ1 upregulation in various organ fibrosis and their role in regulating fibroblast function and trans-differentiation into myofibroblasts [213].

Very little information exists about the regulation of SFRP1 expression in fibrotic diseases. Our group has previously observed a reduced SFRP1 gene expression in the TGFβ1-activated invading fibroblast transcriptome signature (Bettina Oehrle, Ph.D. thesis, 2015) and hinted a potential crosstalk between the master regulator TGFβ1 and SFRP1. This was further confirmed in my thesis with *in vitro* TGFβ1-activated mouse and human fibroblasts displaying reduced SFRP1 gene and protein expression (Fig. 4.10). Gauger et al., and colleagues reported that silencing of SFRP1 resulted in an increased TGFβ1- mediated activity including its downstream transcriptional targets in breast cancer cells *in vitro* [214]. Furthermore, SFRP1 has been found to inhibit epithelial-mesenchymal transition (EMT) in TGFβ1- activated A549 lung cancer cell line. The authors further presented a downregulation of SFRP1 protein expression on upon TGFβ1 stimulation and simultaneous inactivation of GSK3β and increased β-catenin expression including its downstream effectors c-myc and Cyclin D1 [215]. Of note, all of these existing studies were

performed with cancer cells. Hence, for the first time a downregulation of SFRP1's gene and protein expression levels in TGF $\beta$ 1-stimulated mouse and human primary lung fibroblasts was demonstrated.

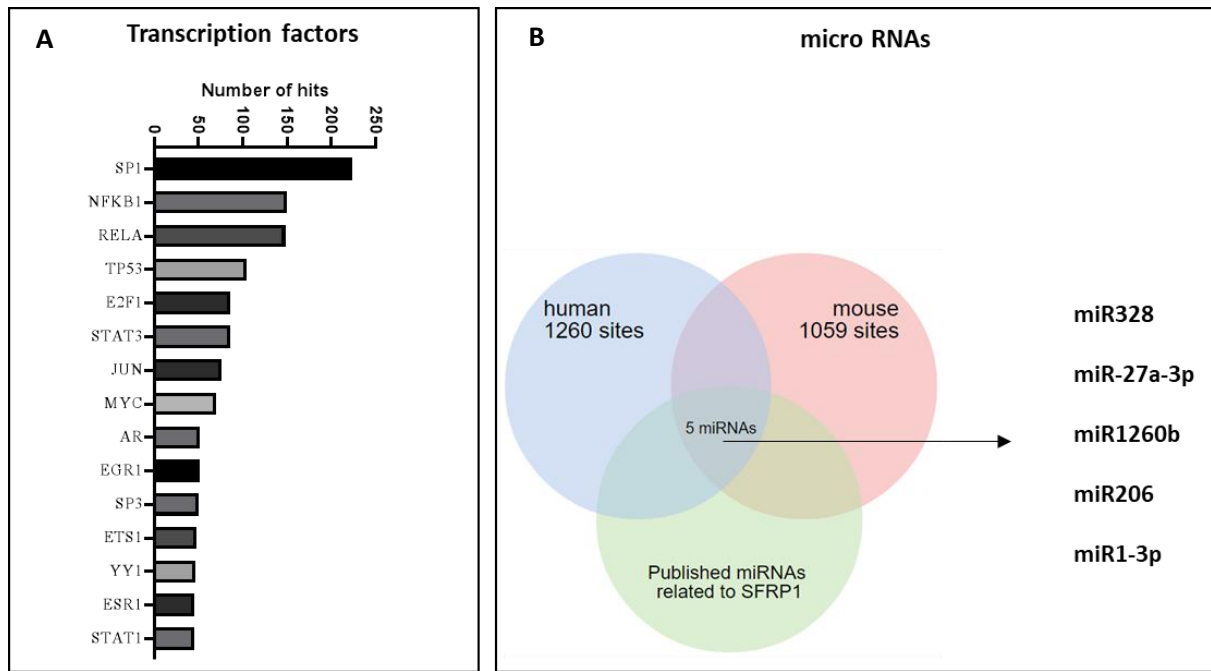
In general, the “differentiated myofibroblast” phenotype is characterized by *de novo* expression of  $\alpha$ -smooth muscle actin ( $\alpha$ -SMA) [96]. Here, I produced evidence that lack of SFRP1 expression might be a valid marker during fibroblast transdifferentiation. This observation accords well with a previous study by Matsuyama et al., where the authors reported increased  $\alpha$ SMA expression in SFRP1<sup>-/-</sup> mice which was shown to exacerbate progression of renal fibrosis [216]. TGF $\beta$ 1 exert its downstream cellular functions via the classical Smad-dependent signaling pathway, or via several non-canonical SMAD-independent signaling, which includes the Ras-Erk-MAPK, JNK/p38, and PI3K/Akt pathways [217, 218, 219]. In my experiments, TGF $\beta$ 1 was shown to regulate SFRP1 expression in pHFs neither via canonical nor via non-Smad3, or MAPK or JNK pathway, but potentially reduced SFRP1 levels via some unknown mechanism. In recent years several components of the ubiquitin–proteasome system (UPS) have been shown to act upon different factors of the TGF $\beta$  pathway. Ubiquitin-specific protease 15 (USP15) binds with Smad7-SMURF2 (Smad specific E3 ubiquitin protein ligase 2) complex and stabilizes type 1 TGF $\beta$  receptor thereby amplifying TGF $\beta$  activity [220]. In the same context, U-box E3 ubiquitin ligases either directly or via adaptors promote R-Smad phosphorylation to enhance TGF $\beta$  signaling [221]. In total, these ubiquitin enzymes undergo post translational modifications that affects their catalytic activity, which ultimately influences the TGF $\beta$  pathway [222]. Furthermore, knockdown of UHRF1 (RING-finger type E3 ubiquitin ligase) leads to demethylation at the SFRP1 loci [223]. Thereby, TGF $\beta$ 1 mediated regulation of SFRP1 might potentially be a proteasome-dependent mechanism

Over the past years, transcription factors (TFs) have been identified to act together with Smads or independently to regulate expression of target genes of the TGF $\beta$  pathway [224]. Using the TRANSFAC® database containing eukaryotic transcription factors and their genomic DNA binding sites, the potential TF binding sites within the promoter region of SFRP1 were excavated (Fig. 4.33 A). Among them, Sp1 is a key transcription factor that is known to regulate the expression of numerous fibrotic genes. Chen et al., in 2012 has shown that the Inhibition of Sp1 by decoy oligonucleotides halted progression of liver fibrosis [225]. The inflammation-associated TFs NF $\kappa$ B1 (nuclear factor kappa-light-chain-enhancer of activated B cells), RELA (nuclear factor NF-kappa-B p65 subunit), STAT1 (Signal transducer and activator of transcription 1) and STAT3 (Signal transducer and activator of transcription 3) were found among the top 15 predicted TFs. RELA and NF $\kappa$ B1 are involved in the NF $\kappa$ B heterodimer formation and are part of the NF $\kappa$ B superfamily [226]. NF $\kappa$ B pathway can cross-regulate with the Wnt signaling pathway by inhibiting  $\beta$ -catenin which thereby influences progression of inflammation [227]. Hence, NF $\kappa$ B is considered as a central link between injury and fibrosis. Moreover MYC, one of the predicted TFs in the list shown in Fig. 4.33A is a central mediator of (cancer) cell proliferation and is reported to regulate TGF $\beta$ 1 induced invasion of SFRP1 expressing breast cancer cells [228]. Thus, in future experiments the investigation of

the above mentioned and predicted TFs could shed some light on the yet unknown mechanism of SFRP1's expression driven by TGF $\beta$ 1 in primary human lung fibroblasts.

MicroRNAs or miRNAs are small 22 nucleotides long regulatory RNAs that are important downstream components of the TGF $\beta$  pathway [229]. In addition, the IPA from the microarray dataset (discussed in section 4.2.2.1) found a cluster of miRNA precursors like miR130, miR143, miR10, miR181 let7, and miR145 that were downregulated in the fibroblast invasion signature (Bettina Oehrle, Ph.D. thesis, 2015). Hence, utilizing a genome-wide miRNA target prediction tool named as miRDB (<http://www.mirdb.org/>) based on an integrated machine learning framework, over 1260 and 1059 miRNA binding sites were identified respectively in human and mouse SFRP1 gene. To narrow down important miRNAs, common binding sites in mouse and human obtained from the prediction tool were matched for experimental validation in published scientific literature and five miRNAs were identified in this process (Fig. 4.33 B). The miR328 was shown to directly target and inhibit SFRP1, activated Wnt pathway which contributed to an invasive glioma cell phenotype in the early stages of glioma progression [230]. Additionally, miR-27a-3p was reported to promote proliferation and invasion of colon cancer cells and squamous carcinoma stem cells by targeting SFRP1 and modulating Wnt signaling [231]. Interestingly, miR-27a-3p was also found significantly upregulated after TGF $\beta$ 1 stimulation in a miRNA-targetome study with primary human lung fibroblasts [232] and thereby could potentially regulate the expression of SFRP1.

Therefore, the downregulation of SFRP1 gene and protein expression upon TGF $\beta$ 1 stimulation in fibroblasts was presumably caused by either differential expression of ubiquitin enzymes, transcription factors, miRNAs or by a complex combination of these situations. Hence, this important mechanistic regulation has to be investigated further in order to delineate a detailed crosstalk between SFRP1 and TGF $\beta$ 1 pathway.



**Figure 4.33: Transcription factor and miRNA target prediction analysis in SFRP1 gene**

The TRANSFAC® database provides a positional weight matrix that displays the frequency of each transcription factor binding site occurrence in a gene. The top 15 transcription factor binding sites enriched in the SFRP1 gene are shown here (A). Venn diagram representing the number of miRNA binding sites in human and mouse SFRP1 gene predicted by the miRDB database and combined with those listed in published literature (B).

#### 4.3.5. Potential role of RhoA activation in regulation of cellular morphology and invasion of SFRP1 depleted fibroblasts

Mechanical stimuli and TGFβ1 stimulation are known to activate RhoA in fibroblasts [233, 234]. In an extension, a detailed study in 2014 reported that inhibition of RhoA signaling subdued matrix stiffness as well as TGFβ1-induced fibrosis in human colonic activated fibroblasts via an SRF (serum response factor) – MRTF-A (myocardin-related transcription factor A) pathway [235]. Increased RhoA - ROCK (Rho-associated, coiled-coil-containing protein kinase) activity has been reported in experimental models of fibrosis and in IPF patients [54]. Importantly, inhibition of RhoA-ROCK signaling demonstrated a noticeable amelioration of lung fibrosis within the mouse fibrosis model [55, 56] thereby suggesting the importance of RhoA in the regulation of IPF. Initially, our unbiased transcriptomic and proteomic screens, by using SFRP1 loss-of-function experiments, pointed towards a RhoA mediated regulation of SFRP1 in lung fibroblasts. RhoA mRNA expression was validated and found to be significantly reduced in SFRP1 depleted phFbs. Reduced RhoA expression has been reported to correlate with reduced FN (fibronectin), collagen and αSMA levels, while restoration of RhoA expression was demonstrated to revive the IPF phenotype in lung fibroblasts [57].

As Rho GTPase act as molecular switches that alternate between a GTP-bound active state and a GDP-bound inactive conformation. Here, the activity of RhoA was quantified by using a RhoA G-LISA assay. RhoGTPase activity was demonstrated to be significantly lowered in SFRP1 depleted pHFs compared to scramble and untreated controls. RhoA expression and activation has been reported to maintain the phenotype of various cells. RhoA expression and activation has been reported to maintain the phenotype of various cells and have been frequently linked to organization of actin cytoskeleton of the cells with direct impact on cellular morphology changes [236, 237]. Therefore, RhoA might be one of the important potential regulators for the morphological switch that we have observed in the SFRP1<sup>low</sup> pHFs. In connection, the smaller, spindle-shape of the SFRP1<sup>low</sup> fibroblasts having potentially reduced expression of several MMPs might presumably facilitate their invasive phenotype. This observation goes in line with a previous study, where reduced RhoA activity was shown to correlate with increased invasion of breast cancer cells in a 3D Matrigel assay. The authors further reported an imminent role of  $\beta$ 1 integrin which modulated the FAK (focal adhesion kinase)-RhoA-actomyosin signaling axis for the regulation of cell invasion in complex physiologically relevant 3D environments [238]. Since  $\beta$ -integrins are highly expressed in invasive tumor cells [239], these could be of particular interest for further research concerning fibroblast invasion in relation to SFRP1.

Numerous studies have associated RhoA small GTPase family as key mediators for cytoskeletal dynamics [240, 241, 242]. Therefore, to further delineate the crosstalk between RhoA and SFRP1 and investigate potential cytoskeletal changes, SFRP1 depleted pHFs were utilized to assess changes associated with cell shape. SFRP1 knockdown in pHFs produced elongated cell bodies with a possible reduced number of actin stress fibers. Therefore, reduced RhoA expression and activity in the SFRP1 silenced fibroblasts might act as the potential reason behind the associated morphological changes. This is in agreement to previous studies where RhoA expression was found highest in round mesenchymal cells and significantly declined in elongated cells [240, 243]. Moreover, RhoA gene knockout in foreskin fibroblasts has demonstrated reduced stress fibers and loss of  $\alpha$ SMA expression [244] which is also in line with our observations.

The Rho associated kinases specifically ROCK1 and ROCK2 are the major downstream effectors of RhoA [245]. The ROCKs have been reported to be involved in stress fiber formation, cell contractility as well as regulation of cell size [247], which points towards an alternative downstream regulation mechanism for RhoA in the SFRP1 depleted fibroblasts. Although ROCKs are known downstream effectors of RhoA, they are not the only ones. A study in 1997 first identified formin mDia1 as a downstream effector of Rho [246]. The active formin family members were demonstrated to polymerize actin filaments and moderate cytoskeletal rearrangements. Apart from formin mDia1, the multifaceted formin family encompasses various mDia like proteins such as the Dishevelled-associated activator of morphogenesis 1 (Daam1) and the “Formin-like” (FMNL) protein 1-3 [248] that might be of particular interest in this context. Hence and

in a future study, alternative downstream effectors of RhoA need to be further investigated to delineate the influence of SFRP1 on RhoA and vice versa.

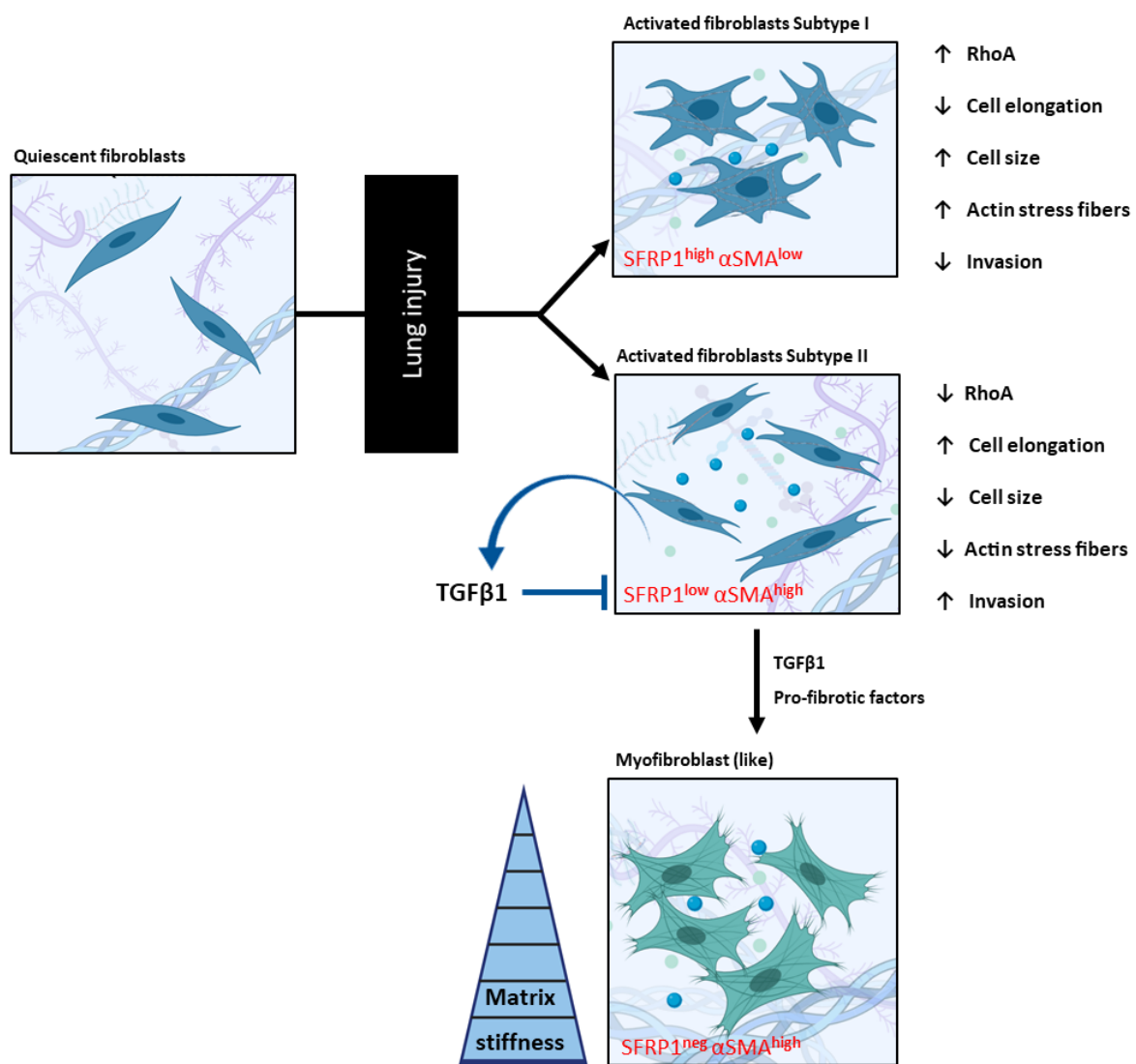
#### **4.3.6. SFRP1 expression in distinct fibroblast sub-populations**

Cellular heterogeneity has been well documented over the years both theoretically [249] and experimentally [250]. Cell to cell differences always existed in different cell populations and hence the overall collective behavior of the cell population does not truly represent the nature of an individual cell. Therefore, interpretation of cellular heterogeneity became essential for accurate identification of cell-based modulations of a gene. Fibroblasts have been reported to exhibit clonal heterogeneity for growth and protein synthesis [172]. In my experiments, a pure clonal population was generated from a single cell isolated from a multiclonal population by serial dilution. The single cell clones isolated from patient lung fibroblasts presented differential expression of SFRP1 and  $\alpha$ SMA. On careful investigation of numerous single cell clones, three different fibroblast subtypes were recognized: SFRP1<sup>high</sup> $\alpha$ SMA<sup>low</sup>, SFRP1<sup>low</sup> $\alpha$ SMA<sup>high</sup> and SFRP1<sup>med</sup> $\alpha$ SMA<sup>med</sup>. This exciting finding was further examined in the context of lung fibrosis. In recent years, rapid progress and development in the field have allowed researchers to perform single cell RNA (Dropseq) sequencing from tissue resections. Tissue explants were harvested from healthy tumor-free lung resections and IPF patients. The SFRP1<sup>high</sup> expressing cells in IPF tissues were interestingly found to be mostly  $\alpha$ SMA<sup>low</sup>, possibly indicating an activated fibroblast subtype which is substantially different from the myofibroblast genotype and phenotype. In accordance with the human lung tissues, the whole lung tissues isolated from Bleo and PBS mice displayed a similar enrichment of the SFRP1<sup>high</sup> $\alpha$ SMA<sup>low</sup> fibroblast populations in the fibrotic conditions (as discussed in section 4.2.3.3). The myofibroblast signature gene  $\alpha$ SMA has been reported to be highly expressed during fibrogenesis [251]. Moreover, the  $\alpha$ SMA<sup>low</sup> expressing collagen1<sup>high</sup> expressing cells have been defined as the matrix fibroblast subtype. This subtype was reported to increase from ~30% in healthy population to ~50% in fibrotic mesenchymal cell population [252]. This goes in line with our observation from human and mouse single cell RNA sequencing results. One could speculate that the SFRP1<sup>high</sup>Col1<sup>high</sup> matrix fibroblast subtypes are potentially enriched in early fibrosis, representing an activated fibroblast subtype. Such an activated SFRP1<sup>high</sup> subtype could be a valid progenitor of myofibroblasts, which gets transdifferentiated by TGF $\beta$ 1 treatment. Furthermore, lipofibroblasts have also been reported as a source for activated myofibroblasts in lung fibrosis [117]. Moreover, knockdown of SFRP1 in the cancer cells have reported to enhance invasion of these cells [182]. This goes in line with our observations where SFRP1<sup>low</sup> pHFs was demonstrated to invade the collagen gel significantly more than untreated or negative control cells. Additionally, the SFRP1<sup>low</sup> fibroblasts have been shown to acquire a smaller and slender phenotype which might be consequential of the reduced RhoA expression and activation within these cells. Although, a functional role for the SFRP1<sup>med</sup> expressing fibroblasts could not be deduced here, it might be still worth



to further characterize the novel SFRP1<sup>high</sup>, SFRP1<sup>low</sup> and SFRP1<sup>med</sup> expressing fibroblast populations in the background of pulmonary fibrosis.

In summary, three new fibroblast sub-populations determined by SFRP1 expression were identified in my thesis. It can be speculated that the quiescent or resident fibroblasts in the lung, upon injury differentiated into SFRP1<sup>low</sup>αSMA<sup>low</sup> invading cells and SFRP1<sup>high</sup>αSMA<sup>low</sup> non-invading, probably matrix producing, (synthetic) cells. TGFβ1 derived from an autocrine/paracrine loop is required to inhibit the SFRP1 expression in the activated fibroblast subtype and thereby potentially moderate a trans-differentiation to SFRP1<sup>neg</sup>αSMA<sup>high</sup> myofibroblast (like) cells. The trans-differentiation process into myofibroblasts is concerted by pro-fibrotic growth factors like TGFβ1 and/or matrix stiffness (Fig. 4.34).



**Figure 4.34: Schematic illustration of fibroblast subtypes expressing distinct levels of SFRP1**

Resident fibroblasts upon lung injury trans-differentiated into SFRP1<sup>high</sup>αSMA<sup>low</sup> and SFRP1<sup>low</sup>αSMA<sup>high</sup> fibroblast subtypes. The SFRP1<sup>low</sup>αSMA<sup>high</sup> subtype can transform into myofibroblast (like) phenotype upon stimulation with pro-fibrotic mediators like TGFβ1 and stiff matrices.

## **5. Chapter B: Validation of a pre-clinical *ex vivo* tool to confirm novel targets in IPF**

### **5.1. Introduction**

According to the world health organization (WHO), chronic respiratory diseases such as chronic obstructive pulmonary disease (COPD), idiopathic pulmonary fibrosis (IPF), and asthma are major causes of death globally [253]. One of the primary reasons behind the limited success in identifying successful drug therapies is the lack of translatable disease models which could efficiently predict and test drug targets and efficacies [142]. While, *in vitro* model systems have been largely used to mimic respiratory diseases by stimulation in culture or isolation, their analysis is mostly limited to one or two cell populations in two-dimensional cell culture systems. Additionally, due to the complexity of representing an *in vivo* like fibrosis, *in vitro* 2D and 3D assays could only depict single processes within fibrosis such as fibroblast migration or invasion, collagen deposition or myofibroblast differentiation. Although micro-physiological model systems and microfluidics have stretched the boundaries of *in vitro* assay design capabilities, the reliance on artificial scaffolds still presents a notable drawback [146, 254, 255]. Yet apart from the use of animal models, there is the need for relevant human disease models that could depict the complex nature of the cells and tissues in their 3D native microenvironment and still allow a straightforward investigation. To address this issue, tissue slices of various thicknesses have presented a potential solution for mechanistic understanding of disease-associated complexities and also reduce the number of animal use for experimentation. Such a 3D tissue-culture system allows for the analysis and visualization of potential therapeutic strategies in a spatio-temporal resolution within the native three-dimensional lung microenvironment.

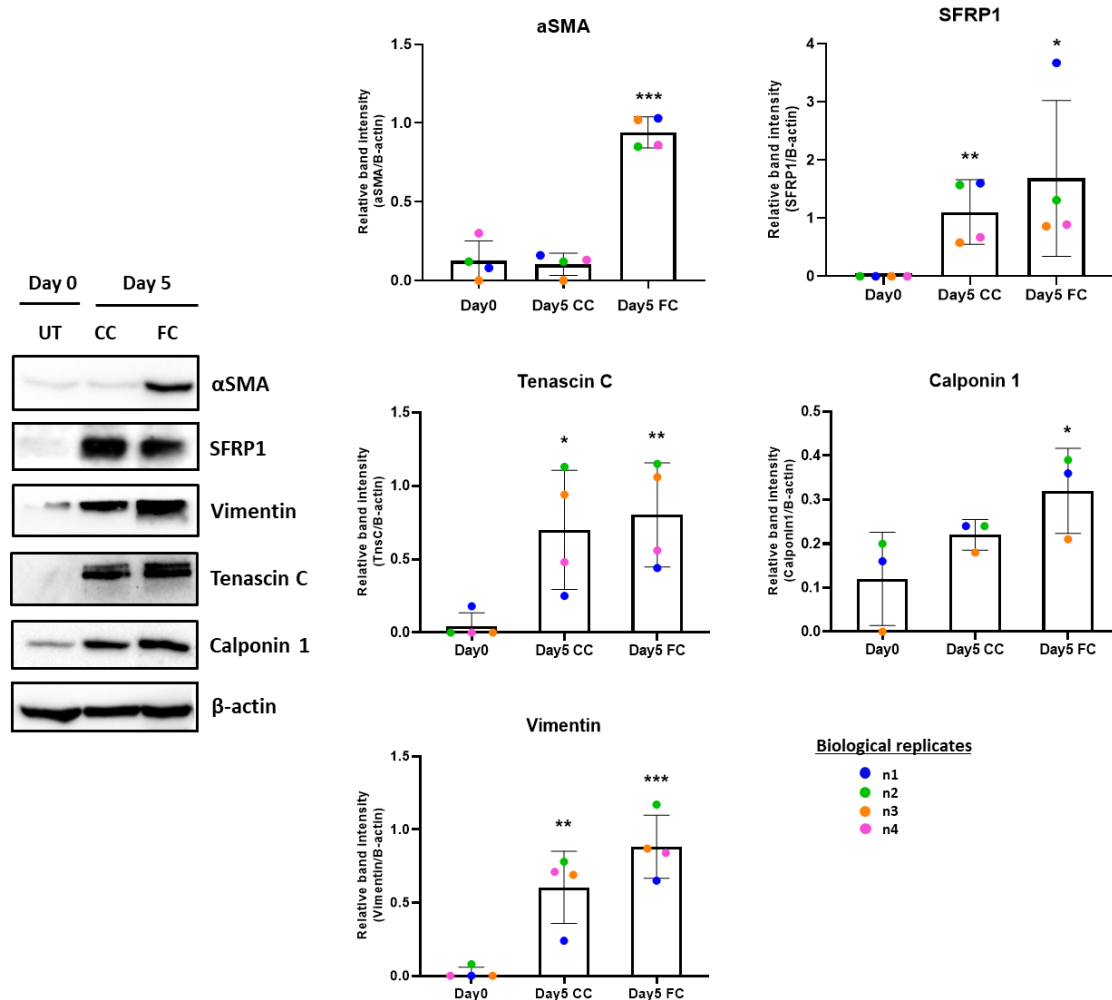
In this chapter, I demonstrate the implementation of a *ex vivo* fibrosis-mimicking model using mouse PCLS (mPCLS).

### **5.2.Results**

#### **5.2.1. Enrichment of fibrosis-related markers in mPCLS injury model**

Recapitulation of a number of developmental pathways have been established to cause the maladaptive repair processes in IPF [9]. To account for the activation of different signalling pathways, the mPCLS harvested from healthy C5BL6/7 mouse lungs were stimulated with a combination of pro-fibrotic and pro-inflammatory signalling molecules such as TGF $\beta$ 1, tumor necrosis factor alpha (TNF $\alpha$ ), platelet derived growth factor AB (PDGF-AB) and lysophosphatidic acid (LPA). This mixture was named “fibrotic cocktail” (FC) [91]. The combination of the control vehicles for the following signaling factors was termed “control cocktail” (CC). Fibrotic cocktail treatment for 5 days in the mPCLS induced protein expression levels of the well-established factors for (myo)fibroblast transdifferentiation in IPF namely

$\alpha$ SMA, vimentin, SFRP1, tenascin C and calponin 1 (Fig. 5.1). Interestingly, SFRP1, tenascin C and vimentin protein expression were upregulated in the mPCLS treated with CC at day 5 compared to samples taken immediately after slicing (day 0), which speaks for an induction of stress induced by the injury caused from slicing or culturing conditions. Thus, even unstimulated mPCLS might act as a valid injury model upregulating pro-fibrotic marker proteins.

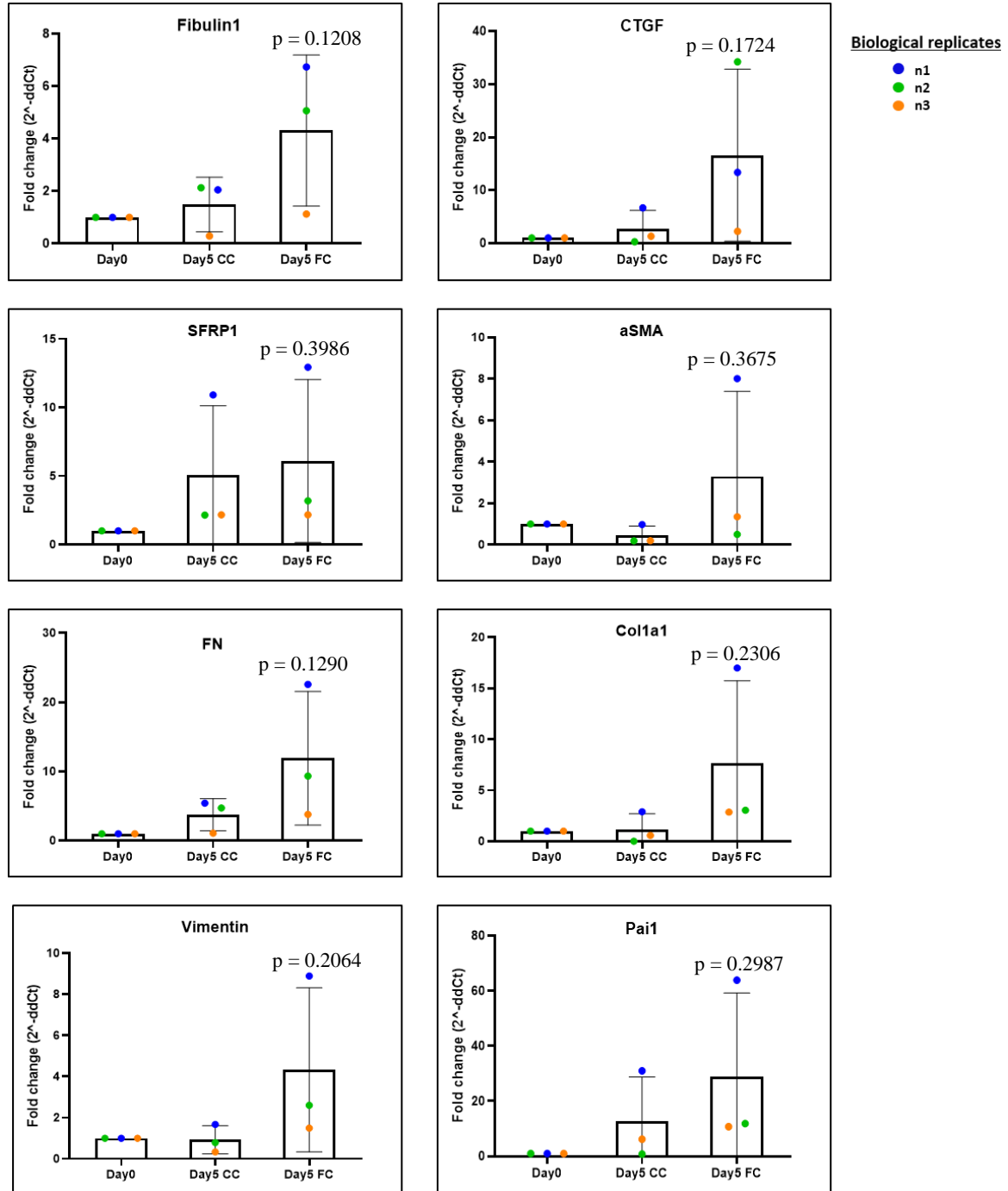


**Figure 5.1: Elevated expression of fibrosis-associated proteins in fibrotic cocktail treated mPCLS**

Immunoblot analysis of  $\alpha$ SMA, SFRP1, vimentin, and calponin1 from whole protein lysates of mPCLS immediately after slicing: day 0 controls and after 5 days of treatment with control cocktail (CC) and fibrotic cocktail (FC). One of the representative blots out of four independent biological experiments is shown (n=4) here. Densitometric quantification of all targets normalized with  $\beta$ -actin ratio is shown as mean  $\pm$  SEM. Statistical analysis: Paired two-tailed t-test. \*\*\*p-value < 0.001, \*\*p-value < 0.01, \*p-value < 0.05.

Furthermore, gene expression of fibrosis-associated genes was quantified and validated in mPCLS. The mPCLS were treated with CC and FC for 5 days and compared to day 0 freshly sliced mPCLS as controls. qRT-PCR analysis showed elevated gene expression levels, although all observed changes were found to be statistically non-significant: fibulin 1 (fold change: 2.9), connective tissue growth factor (CTGF) (fold change: 16.6), SFRP1 (fold change: 6.1),  $\alpha$ SMA (fold change: 3.3), fibronectin (FN)

(fold change: 11.9), collagen1a1 (Col1a1) (fold change: 7.6), vimentin (fold change: 4.3) and plasminogen activator inhibitor type 1 (Pai1) (fold change: 28.8) in the mPCLS treated with FC compared to day 0 controls (Fig. 5.2).



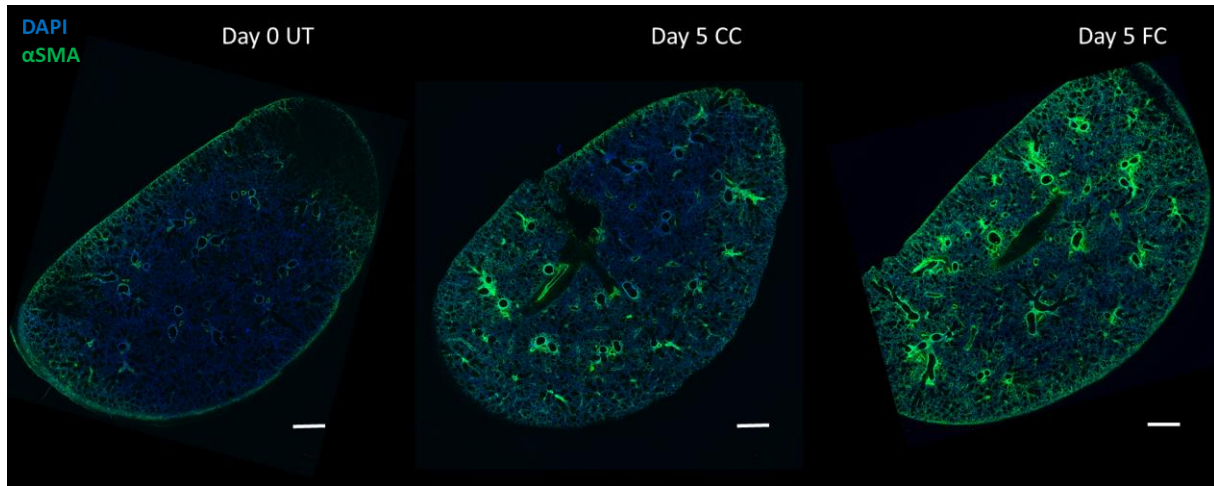
**Figure 5.2: Fibrotic cocktail treatment in mPCLS induce enhanced expression of fibrosis-related genes**

qRT-PCR analysis of fibulin1, CTGF, SFRP1, αSMA, FN, col1a1, vimentin and Pai1 gene expression from mPCLS untreated at day 0 and treated with the CC and FC for 5 days. GAPDH was used as a housekeeping gene. Data are depicted as mean ± SEM from three independent biological experiments. Statistical analysis: Paired two-tailed t test.

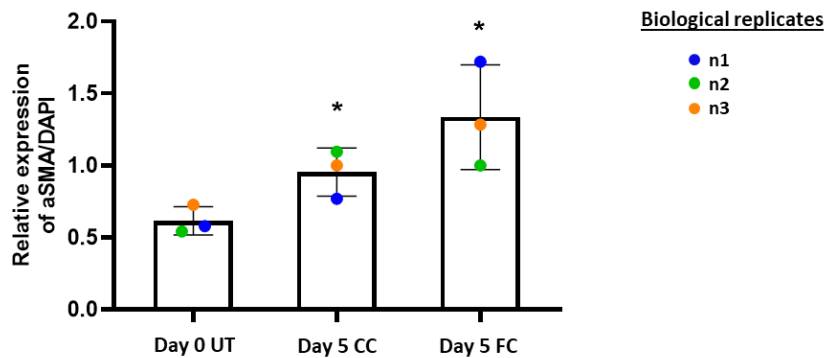
One of the classical hallmarks of IPF is the accumulation of αSMA expressing myofibroblasts in clusters termed fibrotic foci which are indicative of fibrosis progression and degree of tissue remodeling process

[45]. Hence, mPCLS treated with CC and FC were examined for  $\alpha$ SMA protein expression via immunofluorescence stainings. On treatment with FC healthy mPCLS showed an increased expression of  $\alpha$ SMA positive myofibroblasts compared to the day 0 and day 5 control mPCLS (Fig. 5.3 A-B). Interestingly, the culture conditions or the control cocktail might have provoked some kind of stress in the mPCLS, as noted from the significant increase in  $\alpha$ SMA positive IF-staining at day 5 CC treated mPCLS compared to day 0 conditions (Fig. 5.3 A).

A



B



**Figure 5.3: Immunofluorescent stainings show an increased expression of  $\alpha$ SMA in fibrotic cocktail treated mPCLS**

Representative (n=3) maximum intensity projections of confocal immunofluorescence microscopy images of mPCLS: day 0 untreated (UT), day 5 control cocktail (CC) treated and day 5 fibrotic cocktail (FC).  $\alpha$ SMA expression is shown in green and DAPI in blue. Scale bar 20  $\mu$ m.  $\alpha$ SMA and DAPI staining were quantified in the Zen software. Expression of  $\alpha$ SMA were normalized with DAPI to obtain relative expression of  $\alpha$ SMA. Data are represented as mean  $\pm$  SEM from three independent biological experiments (n=3). Statistical analysis: Paired two-tailed t-test with reference to day 0 UT. \*p-value < 0.05.

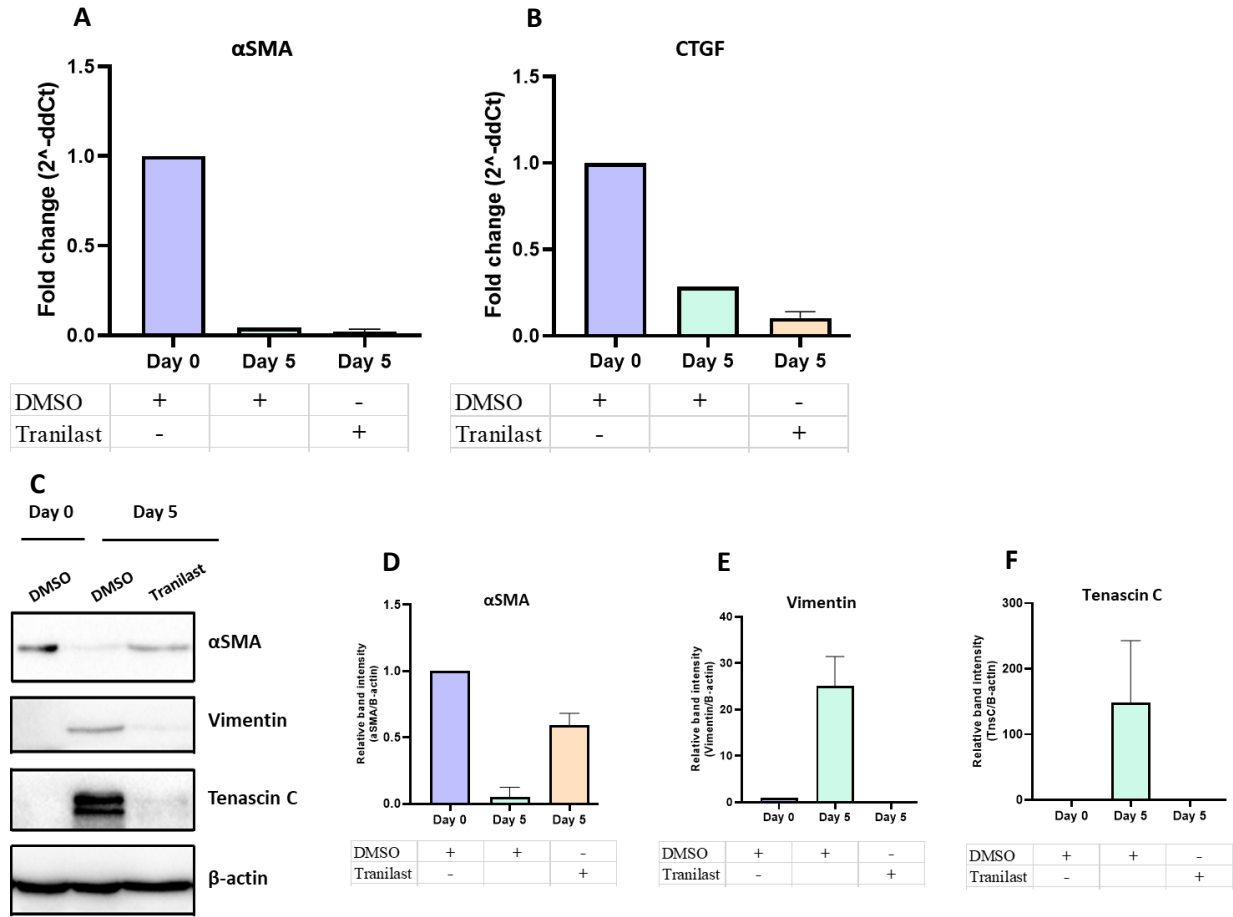
In summary, these data indicate that by injury due to cutting as well as by treatment with a pro-fibrotic cocktail, fibrosis-like processes can be triggered in mPCLS. Thus, this ex vivo model might be useful as

an injury model investigating fibrogenesis in general, as well as being used for testing anti-fibrotic compounds in drug discovery and development.

### **5.2.2. Analysis of an anti-fibrotic drug in the mPCLS injury model**

Nintedanib and Pirfenidone have both been reported to reduce fibrotic gene expressions in human PCLS stimulated with the fibrotic cocktail [179]. Tranilast has been well established as an anti-fibrotic and anti-inflammatory drug [256, 257]. Tranilast have been additionally reported to suppress TGF $\beta$ -mediated ECM production and thereby reduce pulmonary fibrosis in mice [258]. Hence, in our study, the mPCLS were treated with Tranilast for 5 days, whereas DMSO treated slices were used as controls. The gene expression analysis found reduced  $\alpha$ SMA (fold change: 0.02; p-value: <0.0001) and CTGF (fold change: 0.10; p-value: <0.0001) levels after 5 days in culture with Tranilast. Interestingly,  $\alpha$ SMA (fold change: 0.04) and CTGF transcripts (fold change: 0.27) were decreased in DMSO controls after 5 days in culture (Fig. 5.4 A-B), which might hint at several stress factors acting alongside in culture conditions.

In the next step, protein expression of fibrosis-associated markers was analyzed from the mPCLS treated with Tranilast. Although, the protein levels for  $\alpha$ SMA (fold change: 0.58; p-value: 0.0018) remained unchanged on treatment with Tranilast compared to controls, but, Tranilast somehow inhibited the stress-induced protein expression of vimentin (fold change: 0.01; p-value: 0.010) and tenascin C (fold change: 0.01; p-value: 0.115) in day 5 treated mPCLS (Fig. 5.4 C-F).



**Figure 5.4: Tranilast treatment in FC-unstimulated mPCLS leads to differential gene and protein expression of pro-fibrotic markers**

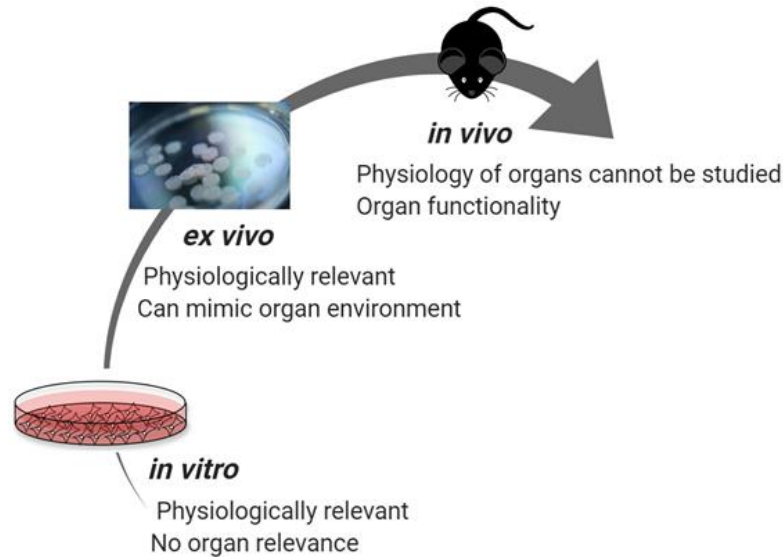
qRT-PCR analysis (n=1-2) of  $\alpha$ SMA (**A**) and CTGF (**B**) gene expression from mPCLS untreated at day 0 and treated with DMSO, Tranilast for 5 days. GAPDH was used as a housekeeping gene. Immunoblot analysis performed with whole protein lysates from mPCLS immediately after slicing at day 0 and after 5 days of treatment with DMSO and Tranilast and probed for  $\alpha$ SMA, vimentin and tenascin C. One representative blot out of two independent biological experiments is shown (n=2) here. Data are depicted as mean  $\pm$  SEM. N=1-2.

In summary, mPCLS as an *ex vivo* 3D-tissue culture tool provides a new valid and complex platform to test and analyze anti-fibrotic compounds in drug discovery and development procedures.

### 5.3. Discussion

Slicing of tissues for studying organ metabolism came to existence in the early 1920s. Initially liver tissues were sliced manually with varied thickness and limited viability and reproducibility [259]. From there onwards, the 1950s saw the development of tissue slices cut with a microtome equipped with a razor blade [260]. Enhanced versions of the microtome have been able to completely reduce variability among thickness of the slices and these tissue slices have come to be known as precision cut slices

(PCS). These *ex vivo* precision cut tissue slices should connect laboratory in vitro models closely to the pre-clinical in vivo models (Fig. 5.5).



**Figure 5.5: *Ex vivo* PCLS as bridging the gap between *in vitro* cell culture and pre-clinical *in vivo* animal models**

The schematic representation demonstrates the *ex vivo* PCS model as a translational tool which can efficiently connect the research performed in *in vitro* cell culture models with those applied to pre-clinical *in vivo* studies.

Precision-cut lung slices (PCLS) have been extensively studied with respect to IPF. PCLS production from IPF tissue explants have been shown to be possible [261]. However, IPF tissue explants are very rare and typically represent the end stage of the disease. For this, Alsafadi in 2018 have reported a novel model to study early changes of fibrosis in human PCLS stimulated with the fibrotic cocktail [91]. But importantly, several pulmonologists still rely on mouse models as they are more readily available than human tissues. Additionally, gene targeting in mice with resultant knockin, knockout and transgenic models have been reported to provide diverse information about the events occurring in human diseases [262].

Taken together, it was important to develop an early fibrosis mimicking and/or injury model using mouse PCLS. For the first time, substantial deregulations in fibrosis-associated markers on protein and gene expression levels were demonstrated upon stimulation with a fibrotic cocktail in mPCLS. In addition, immunofluorescence stainings in mPCLS were quantified to obtain statistically relevant data. Interestingly, tenascin C, SFRP1,  $\alpha$ SMA and vimentin were found to be higher expressed in mPCLS day 5 controls when compared to d0 controls (= tissue immediately lysed after slicing). It was revealed previously that cells in culture conditions can experience a variety of stress factors including oxidation, heat, chemical reactions or some unknown contaminations [263, 264]. Furthermore,  $\alpha$ SMA expression has been frequently associated with mechanical stress [265]. Increased levels of vimentin have been



indicated in cells bared to oxidative, biochemical and mechanical stress [266, 267]. Also, Tenascin C was found to be a marker for mechanical stress [268]. In addition, hypoxia and reactive oxygen species were demonstrated to induce Tenascin C expression in cells [269]. Hence, the increase of stress markers at day 5 CC treated mPCLS might hint at a couple of possible stress factors within the PCLS culture conditions. Biomarkers for oxidative, redox and mechanical stress should be further analyzed in the cultured PCLS to get a clearer idea about this model. In a preliminary study, the basal effects of an anti-inflammatory and anti-fibrotic drug Tranilast was tested in mouse PCLS under standard culture conditions. Although Tranilast treated mPCLS were demonstrated to withstand the stress-associated by culturing conditions.

Tranilast was reported in a previous study to attenuate expression of oxidative stress indicators like 4-hydroxynonenal (4-HNE)–modified proteins and thiobarbituric acid-reactive substances in liver fibrosis [270]. Moreover, recently Tranilast was noted to alleviate mechanical stress with regards to tumor blood vessel compression and accumulation of ECM components like collagen and hyaluron in solid tumors *in vivo* [271]. But none of these studies was performed by applying *ex vivo* lung slices. Therefore, for the first time Tranilast was demonstrated to actively reduce upregulation of stress-associated markers in mouse PCLS. However, further studies combining fibrotic cocktail treatment needs to be done to further confirm the anti-fibrotic potential of Tranilast in mouse PCLS.

In conclusion, the *ex vivo* mouse PCLS model presented here prospectively will provide an important pre-clinical platform to successfully test anti-fibrotic compounds in a straightforward manner.

## 6. Chapter C: Studying instructiveness of ECM in 3D-LTCs

Parts of this chapter have previously been published as: Burgstaller, G., Sengupta, A., Vierkotten, S., Preissler, G., Lindner, M., Behr, J., Königshoff, M. and Eickelberg, O. (2018). Distinct niches within the extracellular matrix dictate fibroblast function in (cell free) 3D lung tissue cultures. *American Journal of Physiology-Lung Cellular and Molecular Physiology*, 314(5), pp.L708-L723 [278].

### 6.1. Introduction

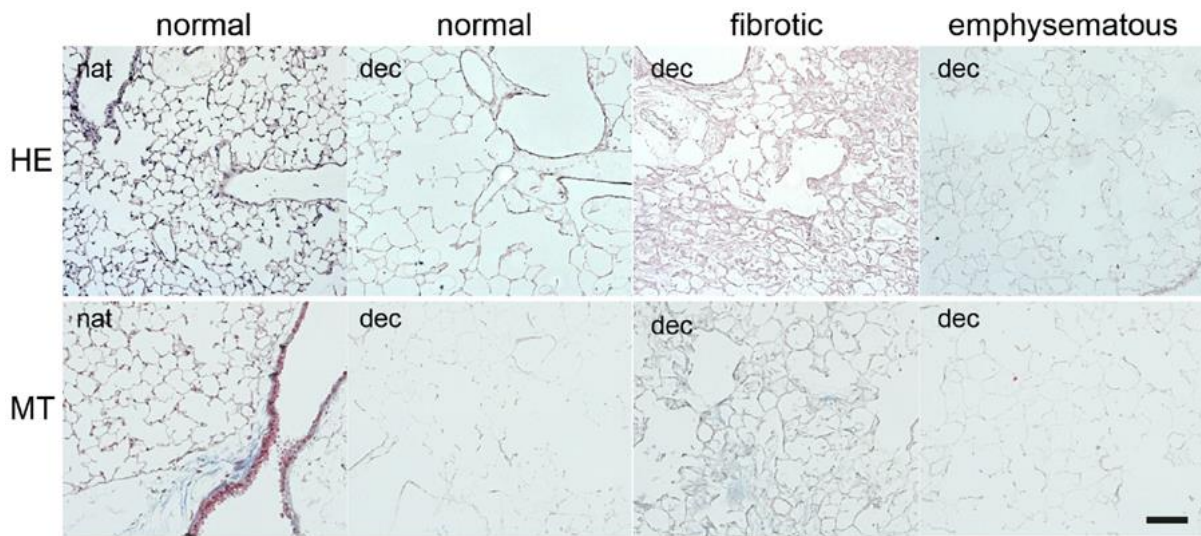
Extracellular matrix has been defined as the “non-cellular portion of a tissue” consisting of a meshwork of extracellular macromolecules to provide structural and biochemical support to the cells [272]. The ECM is ubiquitously present in all tissues and undergoes dynamic remodeling to control homeostasis. A wide range of tissue defects and embryonic lethality have been observed in cases of mutation of the genes encoding ECM components [273], which speaks for a functional importance of the ECM. Two types of ECM have been classified based on their composition and location. One is the interstitial connective tissue matrix which surrounds cells and provides a scaffolding platform for the tissues and, secondly, basement membranes which are specialized ECM that separates the epithelium from the neighboring stroma [274]. Excessive deposition of extracellular collagen especially type I and III have been reported from patients diagnosed with IPF and adult respiratory distress syndrome (ARDS) [275]. Given its functional importance in disease pathogenesis, a better understanding of ECM regulation and remodeling is required. Hynes and colleagues have comprehensively defined the “core matrisome” comprising of around 300 proteins (~ 43 collagen subunits, ~ 36 proteoglycans and ~ 200 complex glycoproteins) [276]. The ECM for long has been considered as a mere support system for the cells and tissues, but recent studies have uncovered additional functional roles. ECM related signals have been indicated to instruct cellular behaviors like adhesion, differentiation, survival, proliferation and migration [277].

Artificial two-dimensional (2D) culture conditions lead to abnormal cellular behaviors with altered cell morphology, migration, polarization and/or differentiation. Although three-dimensional (3D) cell culture platforms provide better biochemical and biomechanical properties, they still fail to recapitulate the molecular composition, structure and topology of the native ECM. In recent times, precision cut lung slices (PCLS) as 3D lung tissue cultures (3D-LTCs) have emerged as a powerful *ex vivo* tool to study cells and matrix in their native environment. Reports in bioengineering and regenerative medicine have stated the use of acellular biological tissue scaffolds as the key to mitigate the shortage of donor lungs for transplantation [148, 149]. Hence an improved understanding of the resident cells and their interaction with the ECM has become crucial. Fibroblasts are the primary effector cells and play a key role in wound healing and inflammation in the context of lung fibrosis [150]. Thus, we have investigated here the altered functional behavior of the engrafted mouse and human fibroblasts in decellularized 3D-LTCs (d3D-LTCs).

## 6.2. Results

### 6.2.1. Validating effective decellularization of *ex vivo* mouse 3D-Lung tissue cultures (LTCs)

Efficient decellularization of PCLS are required to obtain acellular scaffolds. Since, any remaining cells in the lung slices might cause a negative impact and hinder our analysis of the repopulated cells, control experiments were performed to demonstrate the effective removal of cellular material. To extract all nuclear and cellular components, the native 3D-LTCs were sequentially incubated in sterile deionized water (for 16 hours), 0.1% SDS solution (for 4 hours), 1M NaCl (for 16 hours) and DNase (for 3 hours) with washing steps in between. Initially, Hematoxylin-Eosin (HE) and Masson Trichrome (MT) histological stainings were performed with paraffin-embedded d3D-LTCs. Fibrotic lung tissues were obtained from bleomycin treated mice and emphysematous tissues from elastase treated mice. Lung tissues obtained from PBS treated control mice were termed “normal”. The stainings notably revealed an intact ECM lung architecture with complete alveoli and alveolar ducts (Fig. 6.1). This initial study demonstrated complete extraction of all cells from the normal and diseased PCLS.

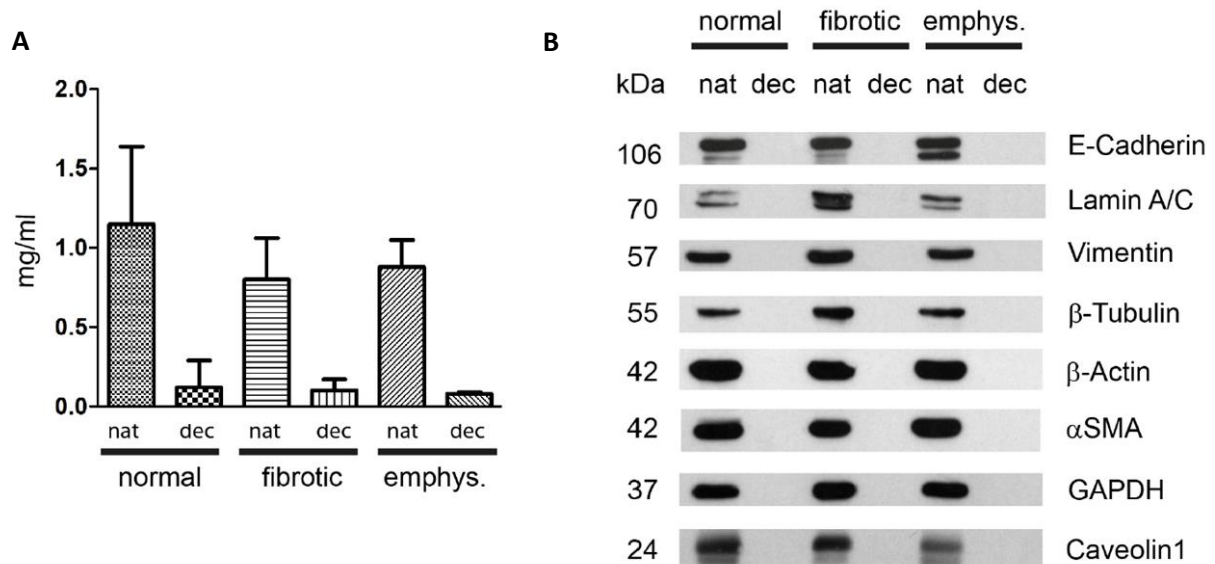


**Figure 6.1: Immunostaining of mouse native and decellularized PCLS**

Hematoxylin-Eosin (HE) and Masson Trichrome (MT) staining demonstrate effective decellularization (dec) of 3D-LTCs derived from normal, fibrotic and emphysematous mouse lung tissues in compared to native (nat) control 3D-LTCs. Scale bar = 100  $\mu$ m. [278]

To further verify the removal of total cellular components on a molecular level, the overall amount of soluble proteins was quantified by BCA assay and the amount of cell-specific proteins from western blots. The total amount of soluble proteins was strongly reduced by almost 90% in the PCLS (Fig. 6.2 A). In addition, the cell-specific proteins (E-cadherin, Lamin A/C, Vimentin,  $\beta$ -Tubulin,  $\beta$ -Actin,  $\alpha$ SMA,

GAPDH and Caveolin 1) from native healthy and diseased (fibrotic and emphysematous) PCLS displayed noticeable signal at their respective molecular weights (kDa), but were undetectable from d3D-LTCs (Fig. 6.2 B).



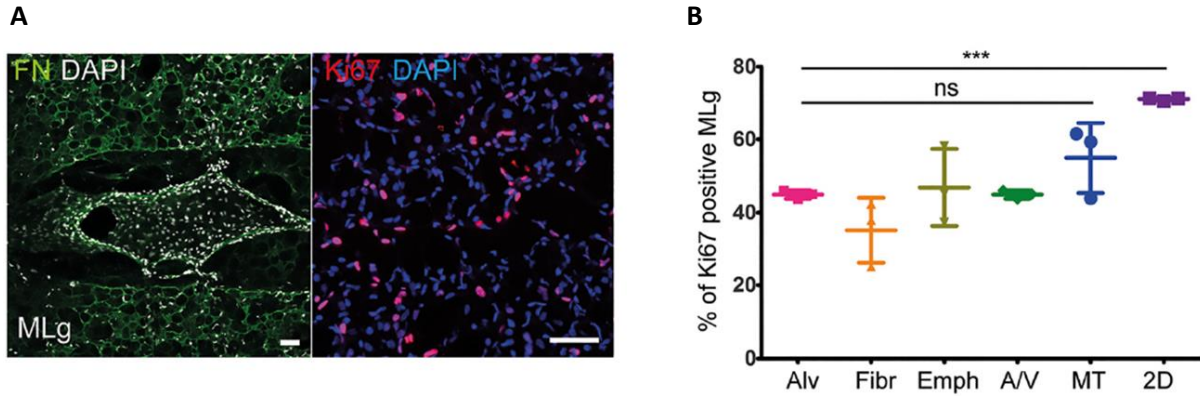
**Figure 6.2: Reduced cell-specific protein levels in d3D-LTCs confirms effective decellularization**

Total protein quantification by BCA assay confirming a reduced protein amount in d3D-LTCs (dec) compared to native (nat) 3D-LTCs (A). Western blot analysis exhibiting lack of cell-specific proteins after decellularization (dec) of 3D-LTCs derived from PBS (normal), Bleomycin (fibrotic) and Elastase (emphysematous) treated mice, compared to native (nat) control 3D-LTCs. [278]

In summary, we have demonstrated here an effective decellularization of mouse PCLS by a specific decellularization protocol.

### 6.2.2. Fibroblasts engrafted into decellularized ECM show a different protein expression profile

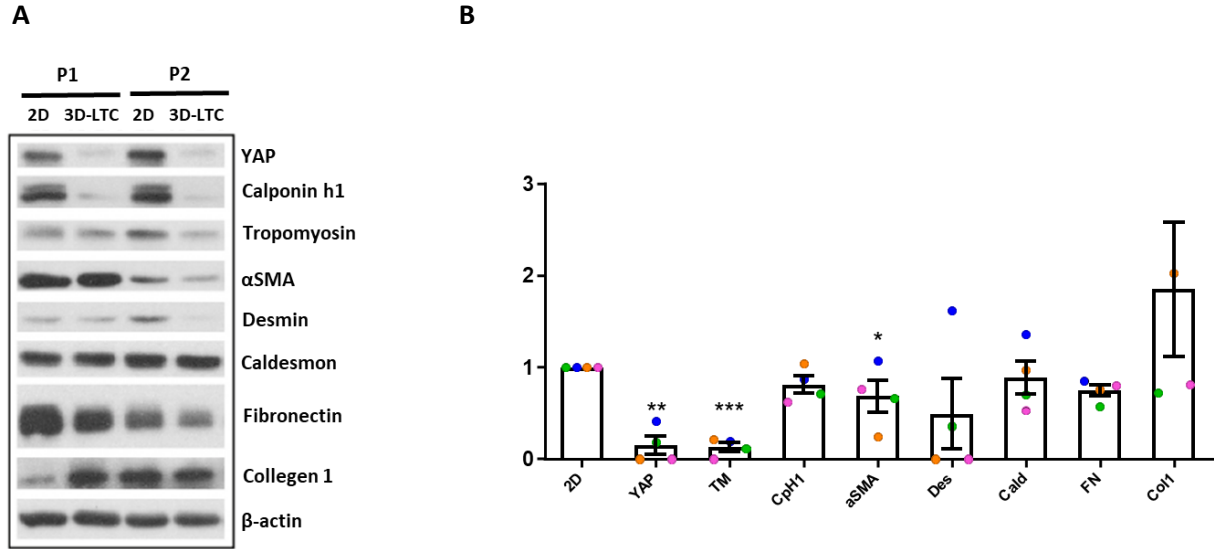
Next, the proliferation capacity of engrafted fibroblasts in the d3D-LTCs were investigated. Various ECM niches in the decellularized PCLS from alveolar (Alv), fibrotic (Fibr), emphysematous (Emph), airway/vessel (A/V) and mesothelium (MT) demonstrated structural and compositional differences. Hence, our hypothesis suggested that the different ECM niches might distinctly affect the proliferative capacity of the engrafted fibroblasts. To investigate this hypothesis, Ki-67 immunofluorescence stainings were performed. Quantification of the Ki-67 positive fibroblasts presented significantly decreased proliferative capacity when compared to the fibroblasts cultured on 2D plastic dishes (2D). However, among the different ECM niches in 3D-LTCs, proliferation was not statistically significant (Fig. 6.3 A-B).



**Figure 6.3: Fibroblasts engrafted in the 3D-LTCs show reduced proliferative capacity compared to 2D plastic dishes**

Immunofluorescent staining with Ki-67 (in red) in mouse lung fibroblasts demonstrates lower proliferation when cultured in 3D-LTCs than normal 2D- plastic dishes. ECM protein FN was stained in green and cell nuclei stained by DAPI in blue. Scale bars: 100µm (A). Confocal high-resolution images from three technical replicates (n=3) were quantified using Imaris software. Statistics used: One-way ANOVA with Bonferroni's multiple comparison test (B).

The previous study implicated that initial attachment of the fibroblasts might potentially differ in accordance with the type of ECM found in special niches. Next, we wanted to investigate if protein expression of in 3D-LTCs engrafted fibroblasts was substantially different from fibroblasts cultured on 2D cell culture dishes. For this experiment, ECM proteins like fibronectin (FN), collagen 1 (Col1) along with established mechanotransducers like yes-associated protein 1 (YAP) and tropomyosin (TM), cellular markers for (myo) fibroblast trans-differentiation like  $\alpha$ SMA, calponin h1 (Cph1) and desmin (Des) and markers involved in cell contractility like calponin h1 and caldesmon (Cald) were chosen. Immunoblotting along with subsequent densitometric analyses revealed substantial decrease in the protein expression of YAP, TM and FN in the 3D-LTC engrafted human fibroblasts compared to the cells grown in 2D plastic dishes. The remaining cellular markers demonstrated insignificant protein expression changes compared to 2D cell culture dishes (Fig. 6.4 A-B).



**Figure 6.4: Differential protein expression of cellular markers in phFbs engrafted in 3D-LTCs**

Protein lysates were harvested from human fibroblasts reseeded in 3D-LTCs. Immunoblots were probed for YAP, Calponin h1, tropomyosin, αSMA, desmin, caldesmon, fibronectin and collagen 1. β-actin was used as a loading control. Two representative blots out of four independent experiments are shown here (A). Densitometric quantification of the markers normalized to β-actin levels from four experiments were performed. Data are represented as  $\pm$  SEM. Statistics: Two-tailed paired t tests, \*\*\* $p < 0.001$ , \*\* $p < 0.01$  and \* $p < 0.05$ . [278]

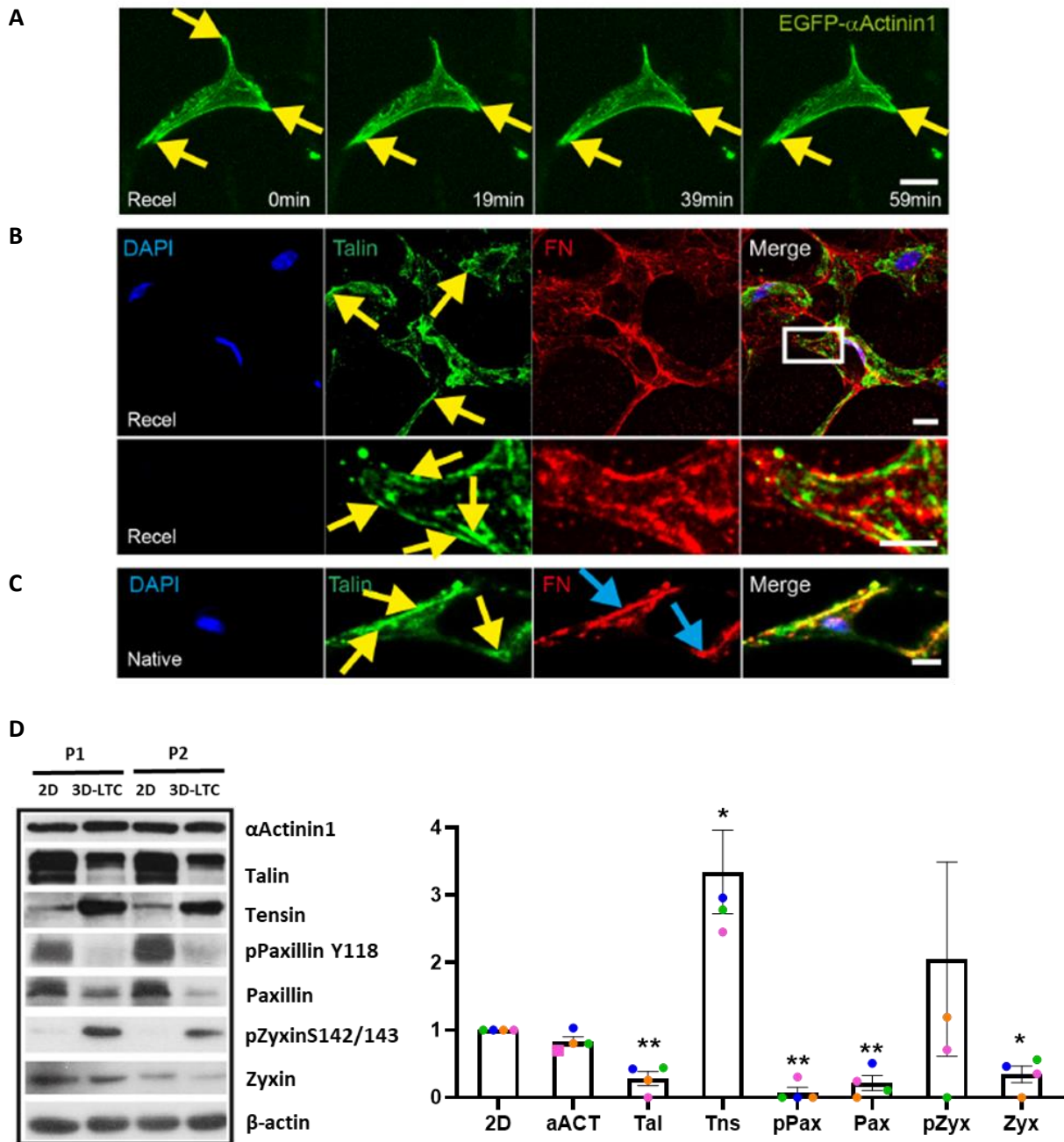
In summary, the results indicated an interesting reduction in the proliferation of fibroblasts engrafted in d3D-LTCs compared to the ones cultured in plastic dishes. Moreover, distinct protein expression for cellular markers like YAP, TM and FN was demonstrated in phFbs reseeded in d3D-LTCs compared to cells in 2D.

### 6.2.3. Repopulated fibroblasts adhere to d3D-LTCs by forming focal adhesion contacts

Focal adhesions (FAs) are multi-protein complexes connecting cells with the ECM matrix. FAs contain integrin clusters that directly bind to components of the ECM [279]. Recently, it was reported that fibroblasts externally added to native, meaning non-decellularized 3D-LTCs, integrated and adhered with the ECM by formation of FAs [137]. Hence, attachment of the engrafted fibroblasts to d3D-LTCs via focal adhesions was investigated in more detail. For that purpose, mouse lung fibroblasts were transfected with a construct ectopically expressing a marker for FAs, namely α-actinin1 which additionally is involved in cross-linking of actin filaments within stress fibers. Time-lapse microscopy pointed out to streak like structures reminiscent of FAs (highlighted with yellow arrows; Fig. 6.5 A).



Next, 3D-LTCs were repopulated with pHFs for 3 days and immunostained for the FA factor talin and ECM protein fibronectin. Talin positive streak like structures of FAs partially colocalized with fibronectin fibers (Fig.6.5 B). Confirmatively, talin and fibronectin staining in native 3D-LTCs likewise showed a partial overlap of the fibers (Fig 6.5 C). To investigate further which components of FAs are differentially regulated in the engrafted pHFs, immunoblotting and subsequent densitometric analyses were performed. Talin, paxillin and zyxin were found to be significantly reduced when the pHFs were engrafted in 3D-LTCs. Interestingly, phosphorylation of paxillin was significantly deregulated as well. On the other hand, tensin protein levels were upregulated in the reseeded pHFs (Fig 6.5 D).



**Figure 6.5: Fibroblast attachment to 3D-LTCs mediated by focal adhesions (FA)**

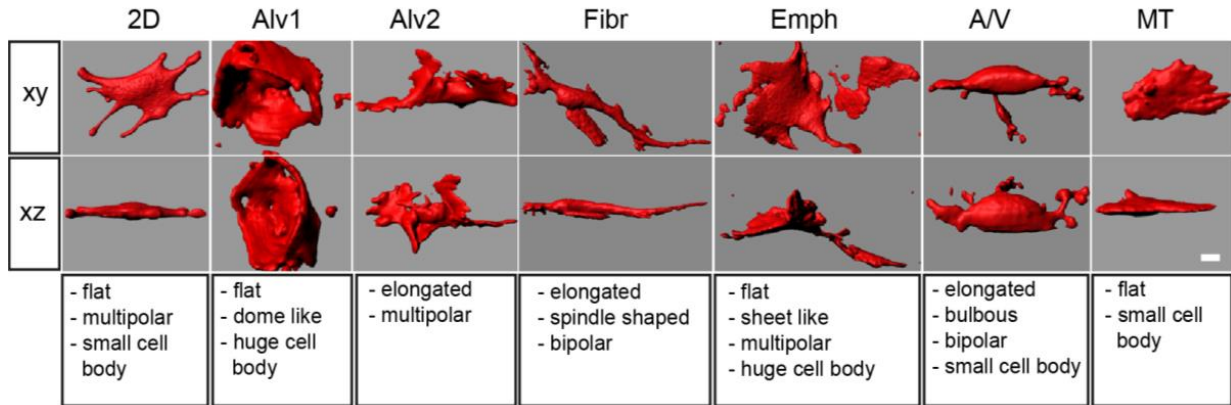
Confocal live cell imaging of mouse lung fibroblasts that ectopically expressed EGFP- $\alpha$ -actinin1 reseeded in d3D-LTCs. Four different time frames (0, 19, 39 and 59 mins) as maximum intensity projections are shown here. Yellow arrows point to band like structures reminiscent of FAs (A). Immunofluorescent staining was performed with fixed d3D-LTCs repopulated with phFbs for 3 days. The fibroblasts were stained for talin (green) and fibronectin (red) and the cell nuclei were stained with DAPI (blue). Magnified view of the interior cell region within the white rectangle box is presented in the bottom panel. The confocal z stack images are shown as maximum intensity projections (B). Confocal immunofluorescent staining of native 3D-LTCs. Yellow arrows point to talin positive FA fibers and blue arrows to fibronectin fibers. The confocal z stack images are shown as maximum intensity projections. All scale bars: 10 $\mu$ m (C). Two representative immunoblots out of four independent experiments (n=4) are shown here. Densitometric analyses demonstrate significant changes in specific FA protein expression.  $\alpha$ -Act,  $\alpha$ -actinin 1; Tal, Talin; Tns, Tensin; pPax, pPaxillin Y118; Pax, Paxillin; pZyx, pZyxinS142/143; Zyx, Zyxin. Data are represented as  $\pm$  SEM. Statistics: Two-tailed paired t tests, \*\*\*p<0.001, \*\*p<0.01 and \*p<0.05 (D). [278]

Taken together, the engrafted fibroblasts were reported to form focal adhesion contacts while adhering to the ECM d3D-LTCs. Moreover, a differential regulation of the focal adhesion proteins was demonstrated for fibroblasts reseeded in d3D-LTCs compared to the 2D plastic dishes.

#### **6.2.4. Specific niches within the microenvironment of 3D-LTCs modulate the morphology of repopulated fibroblasts**

Alterations in the three-dimensional ECM microenvironment have been reported to substantially affect fibroblast signaling [141]. Therefore, alterations in cellular morphology induced by various ECM niches were investigated next. EGFP expressing mLFbs were engrafted in 2D culture dishes as well as healthy or diseased d3D-LTCs. Subsequently, confocal live-cell imaging along with software (Imaris)-based isosurface rendering was performed. Surprisingly, the mLFbs were observed to display various distinct morphologies by apparently adopting to their surrounding ECM microenvironment. Fibroblasts in the mesothelium presented a flat surface with an overall smaller cell body. Correspondingly, the ECM niche of the airway/vessels (A/V) induced elongated, bipolar and bulbous looking fibroblast morphologies. In contrary, within the emphysematous regions, the fibroblasts were flat, multipolar along with huge cellular bodies unlike the dome-shaped phenotype demonstrated within Alv regions. Fibroblasts cultured in 2D plastic dishes gave rise to flat multipolar elliptical cellular shape, similar to those found in the emphysematous niche. Lastly, fibrotic ECM niches persuaded an elongated, bipolar and spindle-shaped fibroblast morphology (Fig. 6.6).





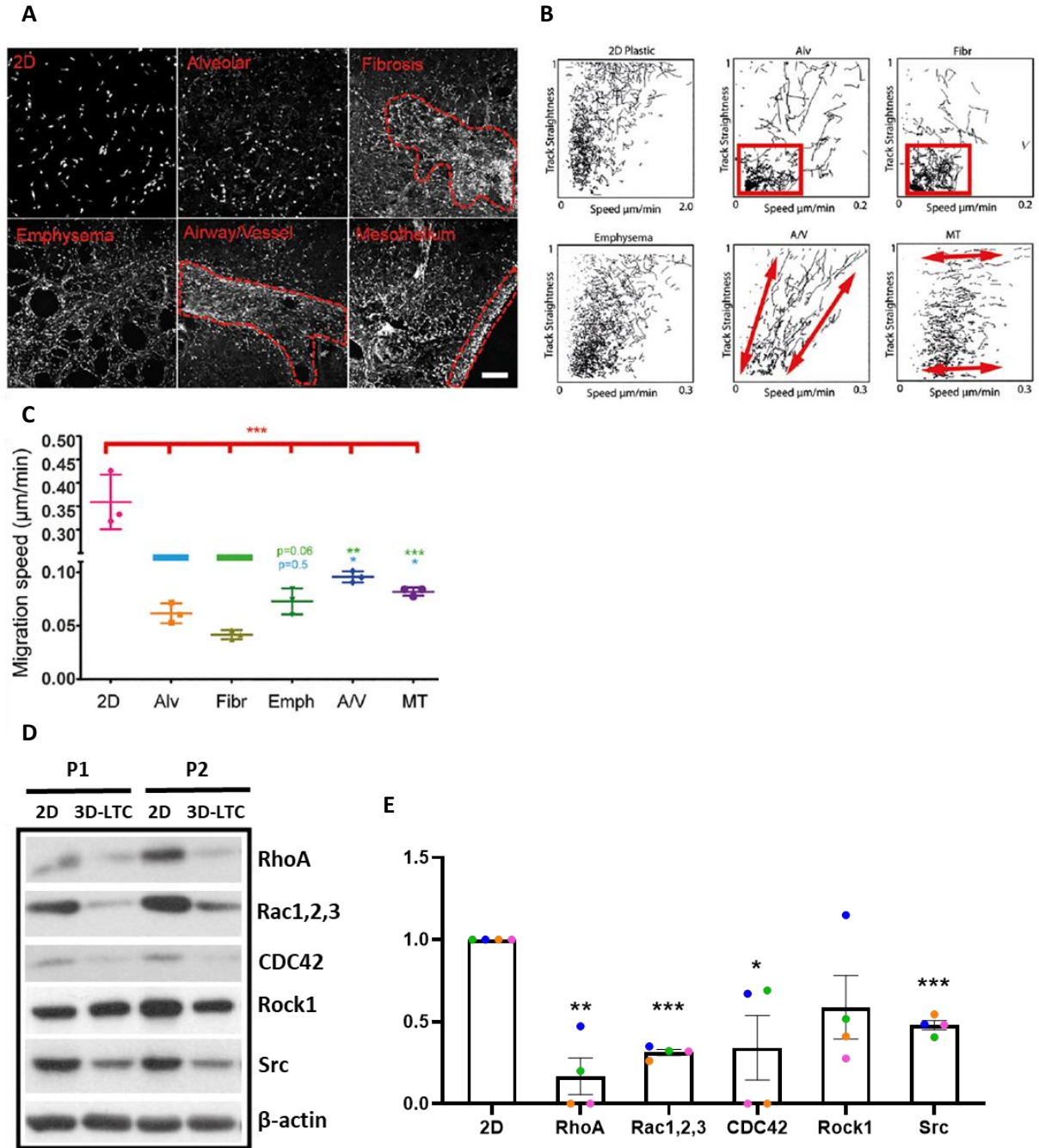
**Figure 6.6: EMC engrafted mLFbs adopt their morphology according to ECM niches**

The different ECM microenvironments; 2D plastic dish (2D), alveolar 1 and 2 regions (Alv1 / Alv2), fibrotic (Fibr), emphysematous (Emph), airway/vessel (A/V), and mesothelium (MT) alter the mLFb morphology. The EGFP-mLFbs were imaged by confocal 3D live-cell imaging. The subsequent z stacks produced were isosurface rendered and shown from xy and xz angles. Scale bar: 10  $\mu$ m.[278]

To summarize, mLFbs populating distinct niches within the d3D-LTCs displayed morphological flexibility, meaning that the cells adopted to their specific surrounding ECM microenvironment.

### 6.2.5. Engrafted fibroblasts demonstrate altered 3D migration in distinct ECM niches

Next, the role of the ECM microenvironment regarding fibroblast migration was investigated. For that, mLFbs were repopulated in decellularized healthy (PBS), fibrotic (bleomycin) and emphysematous (elastase) lung scaffolds. Fibroblasts were stained with Hoechst and was investigated by 4D confocal live-cell imaging for 24 hours to check for their migration. The measured migration speed was then plotted against the track straightness. Different migration patterns were observed in the engrafted mLFbs. Surprisingly, fibroblasts in the alveolar and fibrotic regions were mostly non-migratory. However, fibroblasts within emphysematous ECM regions showed a diverse migration pattern similar to fibroblasts cultured on 2D plastic dishes. Interestingly, fibroblasts in the A/V and mesothelium migrated in parallel or anti-parallel manner (Fig. 6.7 A-B). Generally, fibroblasts in 3D-LTCs demonstrated all together a significantly slower migration speed of 0.07  $\mu$ m/min compared to the cells seeded in 2D plastic dishes (0.4  $\mu$ m/min). Even when engrafted into distinct ECM niches of 3D-LTCSs, like for instance A/V or MT, fibroblasts demonstrated a significantly higher migration rate in comparison to alveolar or fibrotic areas (Fig. 6.7 C). Interestingly, immunoblotting with subsequent densitometric analyses have indicated a significant deregulation of the protein expression of migratory regulators like RhoA, Rac1,2,3, Cdc42, Rock1 and Src kinase (Fig.6.7 D-E) in phFbs engrafted within d3D-LTCs when compared to 2D cultured control cells.



**Figure 6.7: Lung fibroblasts in various ECM niches of d3D-LTCs show a different migration behaviour**

The migration of Hoechst stained mLFbs engrafted on d3D-LTCs was assessed by 4D confocal live-cell imaging. The different ECM niches chosen were 2D plastic dish (2D), alveolar (Alv), fibrotic (Fibr), emphysematous (Emph), airway/vessel (A/V), and mesothelium (MT). Parts of the fibrotic, A/V and MT are encircled by red-dashed line (A). The migration speed plotted against the track straightness demonstrated different migration modes. The red rectangles indicate stationary or slow migrating cells whereas the red arrows illustrate the overall direction of migration of the fibroblasts. Scale bar: 100  $\mu\text{m}$  (B). Quantification of the migration speed of the fibroblasts in different ECM niches reported an overall reduction in cell migration compared to plastic dishes. Statistics. One-way ANOVA with Bonferroni's multiple-comparison test;  $n=3$  (biological replicates) (C). Two of the representative blots (out of 4;  $n=4$ ) are shown here. Protein lysates were harvested from reseeded pHFs in 3D-LTCs (D). The protein expression of the migration regulators were normalized with the  $\beta$ -actin expression. Statistics: Two-tailed paired t-tests; \*\*\* $p<0.001$ , \*\* $p<0.01$  and \* $p<0.05$ . [278]

In conclusion, pHFs reseeded in different healthy and diseased d3D-LTCs demonstrated significantly reduced migration speed compared to the pHFs cultured in 2D plastics dishes. Moreover, among distinct lung scaffolds, pHFs within alveolar and fibrotic regions were mostly non-migratory, whereas pHFs in A/V and MT displayed higher migration speed in comparison. Consistently, differential protein expression of migration-related cellular markers like RhoA, Rac1,2,3, CDC42 and Src kinase were revealed in pHFs in 3D-LTCs compared to the cells in plastic dishes.

### **6.3. Discussion**

Our understanding of the interaction between cells and their ECM microenvironment has grown considerably within the last decade. ECM consist of an intricate network of macromolecules with varying bio-chemical and physiological properties that represent the non-cellular facet of the tissues in our body [280]. The synergy of cells and ECM underlay the basic foundation for various critical cellular functions such as growth, differentiation, adhesion, gene expression, morphogenesis and essentially survival [281]. The ever-growing regenerative medicine field have been working towards renovation of the impaired tissues and organs with natural bio-mimicking materials. For this, decellularized tissue scaffolds with its intact lung architecture and preserved ECM components have been highly investigated [282]. Although, functional studies have been reported previously which portray the precise nature of the cell-ECM communication processes [283, 284], but none of the earlier reports characterized an overall comparison of the instructive cues produced from the ECM of healthy and diseased 3D-LTCs compared to cells cultured on 2D plastic dishes. This bi-directional signalling interplay between the cells and their surrounding ECM microenvironment were studied in detail here in this chapter. To recapitulate the ECM in its “native” molecular composition, architecture, topology, and mechanobiology, *ex vivo* 3D-LTCs were utilized. Firstly, healthy and diseased decellularized mouse lung 3D-LTCs were utilized and mouse and human lung fibroblasts from various sources were reseeded in them. Importantly morphology, migration and protein expression in the engrafted fibroblasts were comprehensively investigated. Most cell types in the body have been reported to interact with their surrounding ECM which was reported to have direct repercussions in cellular behaviors [285]. With this hypothesis in mind, mLFbs and pHFs were engrafted in decellularized PCLS as harvested from healthy (PBS instilled) and diseased (elastase and bleomycin instilled) mouse lungs. Preceding the central experimental studies, sufficient decellularization of the tissue was validated at first by immunohistological stainings and quantification of total soluble proteins from the decellularized 3D-LTCs. This initial examination demonstrated successful clearance of the cellular components from the 3D-LTCs as evidenced from the HE and MT stainings and protein analyses by immunoblots.

Recent investigations have reported fibroblast-derived extracellular matrices to affect attachment, proliferation, migration and differentiation of the adipose tissue derive mesenchymal cells *in vitro* [286]. Moreover, informative signals from bone-derived extracellular matrix has been noted to stimulate

osteogenic differentiation of the embedded embryonic stem cells [287]. In line with these studies, the differential cellular behaviors of the engrafted lung fibroblasts were investigated in discrete healthy and diseased ECM niches including cell culture plastic dishes. The results indicated reduced proliferation of the fibroblasts when embedded in 3D-LTCs compared to when cultured in 2D plastic dishes. This goes in line with previous studies showing slower breast cancer proliferation within 3D synthetic scaffolds compared to 2D dishes [288] which confirm strongly that the ECM niche controls the proliferation of seeded cells. Moreover, divergent protein expression, especially substantial reduction of the mechano-transduction and ECM-related markers in fibroblasts within 3D-LTCs, verified our findings. The reduced expression of mechanotransducers like YAP and TM was predictive, as 2D plastic dishes have higher stiffness than the d3D-LTCs (~3GPa). Interestingly, fibroblast proliferation as detected by the Ki-67 positive cells did not reveal any statistical significance for the stiffer fibrotic regions and the maximal proliferation was observed only within the mesothelium. Therefore, along with stiffness, other factors like adhesion of the fibroblasts within the distinct ECM niches might also affect the rate of cell proliferation.

FAs have been reported to relay important information from the surrounding extracellular environment to the cytoskeleton of the cell, thus acting like a “mechanical link” between them [289]. Although, the turnover rate of FAs and in general their overall existence in 3D matrices have been highly controversial [289, 290], our group has previously demonstrated the definite existence of FAs in 3D lung scaffolds and have subsequently reported their involvement in the dynamic interaction of fibroblasts with their native ECM [137]. Moreover, the size of FAs has been directly linked to cellular migration capacity previously [291]. Therefore, the size and number along with the turnover rate of FAs in the fibroblasts engrafted within different 2D and 3D-LTCs might be an interest for further related studies.

Fibroblasts in general have been defined as elongated, spindle-shaped cells [93]. However, changes in their surrounding ECM microenvironment have been demonstrated to alter their cellular behaviors including morphology [141]. Surprisingly, fibroblasts reseeded in different ECM niches were found to adopt distinct shapes that might account for the altered migration pattern of these cells. Highest migration speeds were found for fibroblasts cultured in 2D plastic dishes compared to the 3D-LTCs. Recently, the ability of the cancer cells to migrate, along with their migration speed and net distance was shown to correlate in 2D and 3D cell culture systems [292], but it will be important to understand here the differences between the use of standard 3D hydrogel-based culture systems and *in vivo*-like tissue scaffolds. Although the differential migration of alveolar epithelial cells at different stages of alveogenesis was demonstrated in mPCLS [293], none of the previous studies have precisely compared cellular migration between 2D plastic dishes and lung tissue scaffolds. Interestingly, protein expression of cytoskeletal proteins, as well as migration and cytoskeletal regulatory proteins, was demonstrated to be significantly deregulated in fibroblasts in 3D-LTCs compared to 2D plastic dishes.

In conclusion, prominent changes in lung fibroblast migration speed and pattern along with eminent protein expression changes of migration-related cellular markers were successfully demonstrated here. Moreover, for the first-time lung fibroblasts were shown to adopt different cellular morphology based on their distinct occupied ECM niche. Also, lung fibroblasts were noted to have reduced proliferative capacity in 3D-LTCs compared to 2D plastic dishes with differential protein expression of mechanotransduction-related and ECM cell markers. Therefore, the protrusive changes in cellular behaviors have been demonstrated as a repercussion for the dynamic ever-changing instructiveness of the surrounding ECM.

## 7. Conclusion and future directions

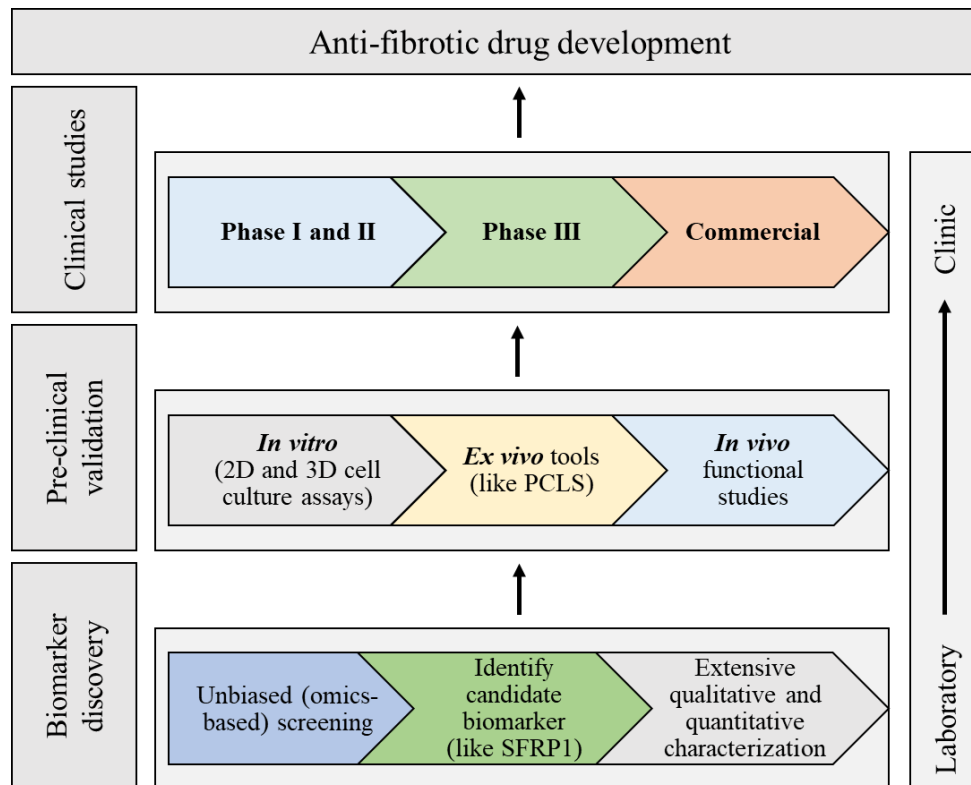
In the presented thesis, the functional role of SFRP1 was assessed in healthy and fibrotic lungs with particular focus on providing mechanistic evidence during fibrogenesis. Besides, a 3D-lung tissue injury model was developed and validated by using precision cut lung slices (PCLS) with the intention to utilize it for the ex-vivo 3D tissue validation of novel compounds in drug discovery and development.

Three fibroblast subtypes, determined by their characteristic SFRP1 expression emerged from the first chapter of the study. Using single cell clones and single cell RNA seq, the existence of at least three distinct SFRP1<sup>low</sup>, SFRP1<sup>med</sup> and SFRP1<sup>high</sup> fibroblast populations were confirmed. In addition, strong evidence was provided to establish the SFRP1<sup>low</sup> fibroblast subtype as an invading cell population. Transcriptomic screening, followed by gene expression analysis and activation assays revealed significantly reduced RhoA expression and activation in the SFRP1<sup>low</sup> fibroblasts, which might have consequential effect for the observed morphology changes and increased invasiveness of these cells. Furthermore, upregulation of SFRP1 expression in mouse and human fibrotic tissues was successfully confirmed which provided evidence for involvement of SFRP1 in lung fibrosis. Interestingly, the expression of SFRP1 was shown to be upregulated in the early phase of the bleomycin-induced lung fibrosis in mice which could be a hint for SFRP1's role during fibrogenesis rather than for the resolution phase. As, fibrosis can aggressively progress ending in organ failure it is crucial to find early biomarkers of fibrosis.

In the second chapter, regulation of fibrosis-related cellular markers was investigated in response to a pro-fibrotic cocktail in mPCLS. Here, a strong effect of the markers were demonstrated on both protein and gene level. This is an exciting finding as upregulation of the pro-fibrotic genes and proteins including SFRP1 was demonstrated in the healthy mPCLS without inducing lung fibrosis. Moreover, the anti-inflammatory and anti-fibrotic drug Tranilast was also tested in the setup. A strong reduction of the investigated fibrotic markers such as  $\alpha$ SMA, CTGF, Vimentin and Tenascin C were observed following Tranilast treatment. This establishes the mPCLS system as an important pre-clinical tool for validating potential therapeutics, especially as the availability of human tissue for the production of huPCLS can be a limiting factor.

The third chapter revealed that cultured mouse and human lung fibroblasts engrafted on native d3D-LTCs led to altered cellular behaviors especially in their proliferation rate, morphology, migration and expression of specific proteins, altogether apparently directed by the ECM's instructive cues. Furthermore, for the first time the repopulated fibroblasts were demonstrated to attach to decellularized lung scaffold ECM via FAs, as confirmed by positive Talin expression. This exciting finding sheds new light on the controversial existence of focal adhesions in 3D matrices (Fraley et al., 2010; Doyle and Yamada, 2016).

In conclusion, the results obtained in my thesis advocate SFRP1 as a possible early biomarker for lung fibrosis. Moreover, novel crosstalk pathways between SFRP1 and TGF $\beta$ 1 and RhoA were revealed that could provide further evidence for altered signaling mechanisms in fibrotic conditions. Importantly, the SFRP1 expression-based fibroblast populations discovered in this study could play an important during fibrogenesis and might be a target for therapeutic intervention in the future. Even the secreted SFRP1 itself might be a promising drug target. Lastly, *ex vivo* culture tools developed and validated in this current study might bring the basic research analyses a little closer to pre-clinical applications (Fig. 7.1).



**Figure 7.1: Schematic overview of laboratory to clinic anti-fibrotic drug development pipeline**

Step 1: Search for a novel biomarker or a drug-target which starts in the basic research and development area. Step2: Validation of the biomarker/drug target in *in vitro*, *ex vivo* and *in vivo* studies until confirmed with a strong biological effect. Step 3: Clinical phase studies in patients and final commercial production.

Although the present studies have contributed to a better understanding of the role of SFRP1 in lung biology, there still remains some open questions. One important question arises to the fate and trajectory of the SFRP1<sup>high</sup> and SFRP1<sup>low</sup> fibroblasts during fibrosis. For this, a SFRP1 reporter mouse could be potentially used to trace the expression of SFRP1 after bleomycin-induced injury. In particular, characterization of the SFRP1 expressing fibroblast population via single cell RNA sequencing might provide a better understanding about the function of these distinct subtypes. Additionally, huPCLS stimulated with FC could also provide a supplementary platform to investigate the nature of the SFRP1

expressing fibroblasts. Furthermore, functional *in vivo* studies testing the lung function in fibrotic SFRP1 knockout mice could also provide substantial evidence for the involvement of SFRP1. Furthermore, an *ex vivo* invasion assay could as well be utilized to investigate the invading SFRP1<sup>low</sup> fibroblasts and compare the results with that obtained from the 3D collagen gel (section 4.2.2.5). On a molecular level, signaling crosstalk between the SFRP1<sup>high</sup> fibroblasts and the epithelial cells during injury and the consequential impact on the Wnt activity of the epithelial cells could be of particular interest and could provide evidence for specific function of this fibroblast population. In addition, the precise regulatory mechanism for TGFβ1-mediated downregulation of SFRP1 needs to be examined which might potentially occur via transcription factors or miRNAs. Furthermore, as SFRP1 depletion in the fibroblasts did not affect the canonical Wnt pathway, but surprisingly altered the RhoA mediated non-canonical signaling, it remains an intriguing question about which RhoA downstream components are deregulated further.

The *ex vivo* mouse PCLS tool, although in the preliminary stages, have already provided substantial proof that it can effectively mimic fibrotic conditions as seen *in vivo*. But there are still open questions regarding the nature of the stress experienced by the mPCLS in culture which needs to be studied in detail before deducing further conclusions from the model. On the other hand, decellularized mouse scaffolds provide a more open ended, user-oriented approach to solve lung biology related questions. Although, more robust than the mPCLS fibrosis model, some questions remain still unanswered with this 3D ECM model. It could be interesting to understand which properties of the ECM whether micro-topographical differences, stiffness or other ECM factors are responsible for the directional migration patterns observed in the reseeded fibroblasts within the A/V and mesothelium regions. Furthermore, as specific niches of the ECM were demonstrated to alter fibroblast behaviors, one could speculate that the secretome of the fibroblasts could also be altered. A further proteomic investigation of the altered fibroblast secretome in response to differential ECM cues could provide novel evidence for cell-ECM interactions.



## References

1. Richard M. Effros. Anatomy, development, and physiology of the lungs. *Nature*. 2006; 10.1038.
2. Ferng, A. and Mytilinaios, D., 2020. *Bronchi*. Kenhub. Available at: <https://www.kenhub.com/en/library/anatomy/bronchi>.
3. Ward, H. And Nicholas, T. (1984). Alveolar Type I AND Type II cells. *Australian and New Zealand Journal of Medicine*, 14, pp.731-734.
4. Bourke, S. (2006). Interstitial lung disease: progress and problems. *Postgraduate Medical Journal*, 82(970), pp.494-499.
5. Grippi, M., Elias, J., Fishman, J., Kotloff, R., Pack, A., Senior, R. And Siegel, M. (1984). Fishman's pulmonary diseases and disorders.
6. Eickelberg, O. And Selman, M. (2010). Update in Diffuse Parenchymal Lung Disease 2009. *American Journal of Respiratory and Critical Care Medicine*, 181(9), pp.883-888.
7. Nalysnyk, L., Cid-Ruzafa, J., Rotella, P. And Esser, D. (2012). Incidence and prevalence of idiopathic pulmonary fibrosis: review of the literature. *European Respiratory Review*, 21(126), pp.355-361.
8. Wolters, P., Collard, H. And Jones, K. (2014). Pathogenesis of Idiopathic Pulmonary Fibrosis. *Annual Review of Pathology: Mechanisms of Disease*, 9(1), pp.157-179.
9. King, T., Pardo, A. And Selman, M. (2011). Idiopathic pulmonary fibrosis. *The Lancet*, 378(9807), pp.1949-1961.
10. Raghu, G., Remy-Jardin, M., Myers, J., Richeldi, L., Ryerson, C., Lederer, D., Behr, J., Cottin, V., Danoff, S., Morell, F., Flaherty, K., Wells, A., Martinez, F., Azuma, A., Bice, T., Bouros, D., Brown, K., Collard, H., Duggal, A., Galvin, L., Inoue, Y., Jenkins, R., Johkoh, T., Kazerooni, E., Kitaichi, M., Knight, S., Mansour, G., Nicholson, A., Pipavath, S., Buendía-Roldán, I., Selman, M., Travis, W., Walsh, S. And Wilson, K. (2018). Diagnosis of Idiopathic Pulmonary Fibrosis. An Official ATS/ERS/JRS/ALAT Clinical Practice Guideline. *American Journal of Respiratory and Critical Care Medicine*, 198(5), pp.e44-e68.
11. Gross, T. And Hunninghake, G. (2001). Idiopathic Pulmonary Fibrosis. *New England Journal of Medicine*, 345(7), pp.517-525.
12. Raghu, G. (2011). Idiopathic pulmonary fibrosis: guidelines for diagnosis and clinical management have advanced from consensus-based in 2000 to evidence-based in 2011. *European Respiratory Journal*, 37(4), pp.743-746.
13. Pulmonaryfibrosis.org. (2019). Treatment Options | Pulmonary Fibrosis Foundation. [online] Available at: <https://www.pulmonaryfibrosis.org/life-with-pf/pulmonary-fibrosis-treatment-options>.
14. Umei, N., Ichiba, S. And Sakamoto, A. (2018). Idiopathic pulmonary fibrosis patient supported with extracorporeal membrane oxygenation for 403 days while waiting for a lung transplant: A case report. *Respiratory Medicine Case Reports*, 24, pp.86-88.
15. Karampitsakos, T., Vraha, A., Bouros, D., Liossis, S. And Tzouvelekis, A. (2019). Biologic Treatments in Interstitial Lung Diseases. *Frontiers in Medicine*, 6.
16. Nhs.uk (2019). Idiopathic pulmonary fibrosis - Treatment. Available at: <https://www.nhs.uk/conditions/idiopathic-pulmonary-fibrosis/treatment/>.

17. Kotloff, R. and Thabut, G., (2011). Lung Transplantation. *American Journal of Respiratory and Critical Care Medicine*, 184(2), pp.159-171.
18. Cavazza, A., Rossi, G., Carbonelli, C., Spaggiari, L., Paci, M. And Roggeri, A. (2010). The role of histology in idiopathic pulmonary fibrosis: An update. *Respiratory Medicine*, 104, pp.S11-S22.
19. Hansell, D., Bankier, A., macmahon, H., mcloud, T., Müller, N. And Remy, J. (2008). Fleischner Society: Glossary of Terms for Thoracic Imaging. *Radiology*, 246(3), pp.697-722.
20. Daccord, C. And Maher, T. (2016). Recent advances in understanding idiopathic pulmonary fibrosis. *F1000Research*, 5, p.1046.
21. Coward, W., Saini, G. And Jenkins, G. (2010). The pathogenesis of idiopathic pulmonary fibrosis. *Therapeutic Advances in Respiratory Disease*, 4(6), pp.367-388.
22. Sakai, N. And Tager, A. (2013). Fibrosis of two: Epithelial cell-fibroblast interactions in pulmonary fibrosis. *Biochimica et Biophysica Acta (BBA) - Molecular Basis of Disease*, 1832(7), pp.911-921.
23. Seibold, M., Wise, A., Speer, M., Steele, M., Brown, K., Loyd, J., Fingerlin, T., Zhang, W., Gudmundsson, G., Groshong, S., Evans, C., Garantziotis, S., Adler, K., Dickey, B., du Bois, R., Yang, I., Herron, A., Kervitsky, D., Talbert, J., Markin, C., Park, J., Crews, A., Slifer, S., Auerbach, S., Roy, M., Lin, J., Hennessy, C., Schwarz, M. And Schwartz, D. (2011). A commonmuc5bpromoter Polymorphism and Pulmonary Fibrosis. *New England Journal of Medicine*, 364(16), pp.1503-1512.
24. Van Moorsel, C., Hoffman, T., van Batenburg, A., Klay, D., van der Vis, J. And Grutters, J. (2015). Understanding Idiopathic Interstitial Pneumonia: A Gene-Based Review of Stressed Lungs. *Biomed Research International*, 2015, pp.1-13.
25. Ahn, M., Park, B., Lee, S., Park, S., Park, J., Kim, D., Jang, A., Park, J., Shin, H., Uh, S., Kim, Y., Kim, Y., Han, S., Jung, K., Lee, K., Jeong, S., Park, J., Choi, B., Park, I., Chung, M., Shin, H., Song, J., Kim, D., Park, C. And Shim, Y. (2011). A promoter SNP rs4073t>A in the common allele of the interleukin 8 gene is associated with the development of idiopathic pulmonary fibrosis via the IL-8 protein enhancing mode. *Respiratory Research*, 12(1).
26. Richards, T., Kaminski, N., Baribaud, F., Flavin, S., Brodmerkel, C., Horowitz, D., Li, K., Choi, J., Vuga, L., Lindell, K., Klesen, M., Zhang, Y. And Gibson, K. (2012). Peripheral Blood Proteins Predict Mortality in Idiopathic Pulmonary Fibrosis. *American Journal of Respiratory and Critical Care Medicine*, 185(1), pp.67-76.
27. Fingerlin, T., Murphy, E., Zhang, W., Peljto, A., Brown, K., Steele, M., Loyd, J., Cosgrove, G., Lynch, D., Groshong, S., Schwarz, M. And Schwartz, D. (2013). Genome-wide association study identifies multiple susceptibility loci for pulmonary fibrosis. *Nature Genetics*, 45(6), pp.613-620.
28. Kaur, A., Mathai, S. And Schwartz, D. (2017). Genetics in Idiopathic Pulmonary Fibrosis Pathogenesis, Prognosis, and Treatment. *Frontiers in Medicine*, 4.
29. Whitsett, J., Wert, S. And Weaver, T. (2010). Alveolar Surfactant Homeostasis and the Pathogenesis of Pulmonary Disease. *Annual Review of Medicine*, 61(1), pp.105-119.
30. Maitra, M., Wang, Y., Gerard, R., Mendelson, C. And Garcia, C. (2010). Surfactant Protein A2 Mutations Associated with Pulmonary Fibrosis Lead to Protein Instability and Endoplasmic Reticulum Stress. *Journal of Biological Chemistry*, 285(29), pp.22103-22113.

31. Wang, Y., Kuan, P., Xing, C., Cronkhite, J., Torres, F., Rosenblatt, R., dimaio, J., Kinch, L., Grishin, N. And Garcia, C. (2009). Genetic Defects in Surfactant Protein A2 Are Associated with Pulmonary Fibrosis and Lung Cancer. *The American Journal of Human Genetics*, 84(1), pp.52-59.
32. Yamano, G., Funahashi, H., Kawanami, O., Zhao, L., Ban, N., Uchida, Y., Morohoshi, T., Ogawa, J., Shioda, S. And Inagaki, N. (2001). ABCA3 is a lamellar body membrane protein in human lung alveolar type II cells. *FEBS Letters*, 508(2), pp.221-225.
33. Tsakiri, K., Cronkhite, J., Kuan, P., Xing, C., Raghu, G., Weissler, J., Rosenblatt, R., Shay, J. And Garcia, C. (2007). Adult-onset pulmonary fibrosis caused by mutations in telomerase. *Proceedings of the National Academy of Sciences*, 104(18), pp.7552-7557.
34. Kropski, J., Mitchell, D., Markin, C., Polosukhin, V., Choi, L., Johnson, J., Lawson, W., Phillips, J., Cogan, J., Blackwell, T. And Loyd, J. (2014). A Novel Dyskerin ( DKC1 ) Mutation Is Associated With Familial Interstitial Pneumonia. *Chest*, 146(1), pp.e1-e7.
35. Alder, J., Stanley, S., Wagner, C., Hamilton, M., Hanumanthu, V. And Armanios, M. (2015). Exome Sequencing Identifies Mutant TINF2 in a Family With Pulmonary Fibrosis. *Chest*, 147(5), pp.1361-1368.
36. Kim, S., Kaminker, P. And Campisi, J. (1999). TIN2, a new regulator of telomere length in human cells. *Nature Genetics*, 23(4), pp.405-412.
37. Cogan, J., Kropski, J., Zhao, M., Mitchell, D., Rives, L., Markin, C., Garnett, E., Montgomery, K., Mason, W., mckean, D., Powers, J., Murphy, E., Olson, L., Choi, L., Cheng, D., Blue, E., Young, L., Lancaster, L., Steele, M., Brown, K., Schwarz, M., Fingerlin, T., Schwartz, D., Lawson, W., Loyd, J., Zhao, Z., Phillips, J. And Blackwell, T. (2015). Rare Variants in TINF2 are Associated with Familial Interstitial Pneumonia. *American Journal of Respiratory and Critical Care Medicine*, 191(6), pp.646-655.
38. Tummala, H., Walne, A., Collopy, L., Cardoso, S., de la Fuente, J., Lawson, S., Powell, J., Cooper, N., Foster, A., Mohammed, S., Plagnol, V., Vulliamy, T. And Dokal, I. (2015). Poly(A)-specific ribonuclease deficiency impacts telomere biology and causes dyskeratosis congenita. *Journal of Clinical Investigation*, 125(5), pp.2151-2160.
39. Rabinovich, E., Kapetanaki, M., Steinfeld, I., Gibson, K., Pandit, K., Yu, G., Yakhini, Z. and Kaminski, N., (2012). Global Methylation Patterns in Idiopathic Pulmonary Fibrosis. *PLoS ONE*, 7(4), p.e33770.
40. Kulkarni, T., O'Reilly, P., Antony, V., Gaggar, A. And Thannickal, V. (2016). Matrix Remodeling in Pulmonary Fibrosis and Emphysema. *American Journal of Respiratory Cell and Molecular Biology*, 54(6), pp.751-760.
41. Booth, A., Hadley, R., Cornett, A., Dreffe, A., Matthes, S., Tsui, J., Weiss, K., Horowitz, J., Fiore, V., Barker, T., Moore, B., Martinez, F., Niklason, L. And White, E. (2012). Acellular Normal and Fibrotic Human Lung Matrices as a Culture System for in vitro investigation. *American Journal of Respiratory and Critical Care Medicine*, 186(9), pp.866-876.
42. Nho, R. And Hergert, P. (2014). IPF Fibroblasts Are Desensitized to Type I Collagen Matrix-Induced Cell Death by Suppressing Low Autophagy via Aberrant Akt/mTOR Kinases. *Plos ONE*, 9(4), p.e94616.
43. Baarsma, H. And Königshoff, M. (2017). 'WNT-er is coming' : WNT signalling in chronic lung diseases. *Thorax*, 72(8), pp.746-759.
44. Nayeem, S., Arfuso, F., Dharmarajan, A. And Keelan, J. (2016). Role of Wnt signalling in early pregnancy. *Reproduction, Fertility and Development*, 28(5), p.525.

45. Selman, M., Pardo, A. And Kaminski, N. (2008). Idiopathic Pulmonary Fibrosis: Aberrant Recapitulation of Developmental Programs? *Plos Medicine*, 5(3), p.e62.
46. Königshoff, M., Balsara, N., Pfaff, E., Kramer, M., Chrobak, I., Seeger, W. And Eickelberg, O. (2008). Functional Wnt Signaling Is Increased in Idiopathic Pulmonary Fibrosis. *Plos ONE*, 3(5), p.e2142.
47. Königshoff, M., Kramer, M., Balsara, N., Wilhelm, J., Amarie, O., Jahn, A., Rose, F., Fink, L., Seeger, W., Schaefer, L., Günther, A. And Eickelberg, O. (2009). Wisp1 mediates pulmonary fibrosis in mice and is upregulated in humans with idiopathic pulmonary fibrosis. *Journal of Clinical Investigation*.
48. Chilosì, M., Poletti, V., Murer, B., Lestani, M., Cancellieri, A., Montagna, L., Piccoli, P., Cangi, G., Semenzato, G. And Doglioni, C. (2002). Abnormal Re-epithelialization and Lung Remodeling in Idiopathic Pulmonary Fibrosis: The Role of  $\Delta N$ -p63. *Laboratory Investigation*, 82(10), pp.1335-1345.
49. Pfaff, E., Becker, S., Guenther, A., Eickelberg, O. and Königshoff, M., 2010. Dickkopf proteins influence lung epithelial cell proliferation in idiopathic pulmonary fibrosis. *Pneumologie*, 64(01).
50. Lam, A., Herazo-Maya, J., Sennello, J., Flozak, A., Russell, S., Mutlu, G., Budinger, G., dasgupta, R., Varga, J., Kaminski, N. And Gottardi, C. (2014). Wnt coreceptorlrp5 is a Driver of Idiopathic Pulmonary Fibrosis. *American Journal of Respiratory and Critical Care Medicine*, 190(2), pp.185-195.
51. Sennello, J., Misharin, A., Flozak, A., Berdnikovs, S., Cheresch, P., Varga, J., Kamp, D., Budinger, G., Gottardi, C. And Lam, A. (2016). Lrp5/ $\beta$ -catenin Signaling Controls Lung Macrophage Differentiation and Inhibits Resolution of Fibrosis. *American Journal of Respiratory Cell and Molecular Biology*.
52. Vuga, L., Ben-Yehudah, A., Kovkarova-Naumovski, E., Oriss, T., Gibson, K., Feghali-Bostwick, C. And Kaminski, N. (2009). WNT5A Is a Regulator of Fibroblast Proliferation and Resistance to Apoptosis. *American Journal of Respiratory Cell and Molecular Biology*, 41(5), pp.583-589.
53. Martin-Medina, A., Lehmann, M., Behr, J. And Königshoff, M. (2018). Increased Extracellular Vesicles Mediate WNT5A Signaling in Idiopathic Pulmonary Fibrosis. *American Journal of Respiratory and Critical Care Medicine*, 198(12), pp.1527-1538.
54. Zhou, Y., Huang, X., Hecker, L., Kurundkar, D., Kurundkar, A., Liu, H., Jin, T., Desai, L., Bernard, K. And Thannickal, V. (2013). Inhibition of mechanosensitive signaling in myofibroblasts ameliorates experimental pulmonary fibrosis. *Journal of Clinical Investigation*, 123(3), pp.1096-1108.
55. Bei, Y., Hua-Huy, T., Duong-Quy, S., Nguyen, V., Chen, W., Nicco, C., Batteux, F. And Dinh-Xuan, A. (2013). Long-term treatment with fasudil improves bleomycin-induced pulmonary fibrosis and pulmonary hypertension via inhibition of Smad2/3 phosphorylation. *Pulmonary Pharmacology & Therapeutics*, 26(6), pp.635-643.
56. Jiang, C., Huang, H., Liu, J., Wang, Y., Lu, Z. And Xu, Z. (2012). Fasudil, a Rho-Kinase Inhibitor, Attenuates Bleomycin-Induced Pulmonary Fibrosis in Mice. *International Journal of Molecular Sciences*, 13(7), pp.8293-8307.
57. Monaghan-Benson, E., Wittchen, E., Doerschuk, C. And Burridge, K. (2018). A Rnd3/p190rhogap pathway regulates rhoa activity in idiopathic pulmonary fibrosis fibroblasts. *Molecular Biology of the Cell*, 29(18), pp.2165-2175.
58. Kawano, Y. (2003). Secreted antagonists of the Wnt signalling pathway. *Journal of Cell Science*, 116(13), pp.2627-2634.

- 
59. Melkonyan, H., Chang, W., Shapiro, J., Mahadevappa, M., Fitzpatrick, P., Kiefer, M., Tomei, L. And Umansky, S. (1997). Sarps: A family of secreted apoptosis-related proteins. *Proceedings of the National Academy of Sciences*, 94(25), pp.13636-13641.
  60. Bafico, A., Gazit, A., Pramila, T., Finch, P. W., Yaniv, A. And Aaronson, S. A. (1999). Interaction of frizzled related protein (FRP) with Wnt ligands and the frizzled receptor suggests alternative mechanisms for FRP inhibition of Wnt signaling. *J. Biol. Chem.* 274, 16180 -16187.
  61. Selman, M., Pardo, A., Barrera, L., Estrada, A., Watson, S., Wilson, K., Aziz, N., Kaminski, N. And Zlotnik, A. (2006). Gene Expression Profiles Distinguish Idiopathic Pulmonary Fibrosis from Hypersensitivity Pneumonitis. *American Journal of Respiratory and Critical Care Medicine*, 173(2), pp.188-198.
  62. Selman, M., Pardo, A. And Kaminski, N. (2008). Idiopathic Pulmonary Fibrosis: Aberrant Recapitulation of Developmental Programs? *Plos Medicine*, 5(3), p.e62.
  63. Zhou, J., Yi, Z. And Fu, Q. (2019). Dynamic decreased expression and hypermethylation of secreted frizzled-related protein 1 and 4 over the course of pulmonary fibrosis in mice. *Life Sciences*, 218, pp.241-252.
  64. Moore, B. And Hogaboam, C. (2008). Murine models of pulmonary fibrosis. *American Journal of Physiology-Lung Cellular and Molecular Physiology*, 294(2), pp.L152-L160.
  65. Roberts, S., Howie, S., Wallace, W., Brown, D., Lamb, D., Ramage, E. And Donaldson, K. (1995). A novel model for human interstitial lung disease: Hapten-driven lung fibrosis in rodents. *The Journal of Pathology*, 176(3), pp.309-318.
  66. Beach, T., Johnston, C., Groves, A., Williams, J. And Finkelstein, J. (2017). Radiation induced pulmonary fibrosis as a model of progressive fibrosis: Contributions of DNA damage, inflammatory response and cellular senescence genes. *Experimental Lung Research*, 43(3), pp.134-149.
  67. Seifirad, S. (2013). Pirfenidone could decrease paraquat-induced pulmonary fibrosis in rats. *Tzu Chi Medical Journal*, 25(2), p.130.
  68. Barbarin, V., Nihoul, A., Misson, P., Arras, M., Delos, M., Leclercq, I., Lison, D. And Huaux, F. (2005). The role of pro- and anti-inflammatory responses in silica-induced lung fibrosis. *Respiratory Research*, 6(1).
  69. Hammar, S. And Abraham, J. (2015). Commentary on pathologic diagnosis of asbestosis and critique of the 2010 Asbestosis Committee of the College of American Pathologists (CAP) and Pulmonary Pathology Society's (PPS) update on the diagnostic criteria for pathologic asbestosis. *American Journal of Industrial Medicine*, 58(10), pp.1034-1039.
  70. Kishimoto, K., Arakawa, H., Ashizawa, K., Inai, K. And Takeshima, Y. (2011). Clinical, Radiological, and Pathological Investigation of Asbestosis. *International Journal of Environmental Research and Public Health*, 8(3), pp.899-912.
  71. Sime, P., Xing, Z., Graham, F., Csaky, K. And Gauldie, J. (1997). Adenovector-mediated gene transfer of active transforming growth factor-beta1 induces prolonged severe fibrosis in rat lung. *Journal of Clinical Investigation*, 100(4), pp.768-776.
  72. Lee, C., Cho, S., Kang, M., Chapoval, S., Lee, P., Noble, P., Yehualaeshet, T., Lu, B., Flavell, R., Milbrandt, J., Homer, R. And Elias, J. (2004). Early Growth Response Gene 1-mediated Apoptosis Is Essential for Transforming Growth Factor  $\beta$ 1-induced Pulmonary Fibrosis. *The Journal of Experimental Medicine*, 200(3), pp.377-389.

73. Ouyang, X., Gulliford, T., Huang, G. And Epstein, R. (1999). Transforming growth factor- $\alpha$  short-circuits downregulation of the epidermal growth factor receptor. *Journal of Cellular Physiology*, 179(1), pp.52-57.
74. Lee, C., Homer, R., Zhu, Z., Lanone, S., Wang, X., Koteliansky, V., Shipley, J., Gotwals, P., Noble, P., Chen, Q., Senior, R. And Elias, J. (2001). Interleukin-13 Induces Tissue Fibrosis by Selectively Stimulating and Activating Transforming Growth Factor  $\beta$ 1. *The Journal of Experimental Medicine*, 194(6), pp.809-822.
75. Fujita M, Shannon JM, Morikawa O, Gauldie J, Hara N, Mason RJ. Overexpression of tumor necrosis factor- $\alpha$  diminishes pulmonary fibrosis induced by bleomycin or transforming growth factor- $\beta$ . *Am J Respir Cell Mol Biol* 2003;29:669–676.
76. Kolb, M., Margetts, P., Anthony, D., Pitossi, F. And Gauldie, J. (2001). Transient expression of IL-1 $\beta$  induces acute lung injury and chronic repair leading to pulmonary fibrosis. *Journal of Clinical Investigation*, 107(12), pp.1529-1536.
77. Sundarakrishnan, A., Chen, Y., Black, L., Aldridge, B. And Kaplan, D. (2018). Engineered cell and tissue models of pulmonary fibrosis. *Advanced Drug Delivery Reviews*, 129, pp.78-94.
78. Polacheck, W. And Chen, C. (2016). Measuring cell-generated forces: a guide to the available tools. *Nature Methods*, 13(5), pp.415-423.
79. Pezzulo, A., Starner, T., Scheetz, T., Traver, G., Tilley, A., Harvey, B., Crystal, R., mccray, P. And Zabner, J. (2011). The air-liquid interface and use of primary cell cultures are important to recapitulate the transcriptional profile of in vivo airway epithelia. *American Journal of Physiology-Lung Cellular and Molecular Physiology*, 300(1), pp.L25-L31.
80. Yu, W., Fang, X., Ewald, A., Wong, K., Hunt, C., Werb, Z., Matthay, M. And Mostov, K. (2007). Formation of Cysts by Alveolar Type II Cells in Three-dimensional Culture Reveals a Novel Mechanism for Epithelial Morphogenesis. *Molecular Biology of the Cell*, 18(5), pp.1693-1700.
81. Evard, S., D'udigier, C., Mauge, L., Israel-Biet, D., Guerin, C., Bieche, I., Kovacic, J., Fischer, A., Gaussem, P. And Smadja, D. (2012). The profibrotic cytokine transforming growth factor- $\beta$ 1 increases endothelial progenitor cell angiogenic properties. *Journal of Thrombosis and Haemostasis*, 10(4), pp.670-679.
82. Smithmyer, M., Sawicki, L. And Kloxin, A. (2014). Hydrogel scaffolds as in vitro models to study fibroblast activation in wound healing and disease. *Biomater. Sci.*, 2(5), pp.634-650.
83. Cukierman, E., Pankov, R. And Yamada, K. (2002). Cell interactions with three-dimensional matrices. *Current Opinion in Cell Biology*, 14(5), pp.633-640.
84. Abbott, A. (2003). Biology's new dimension. *Nature*, 424(6951), pp.870-872.
85. Arora, P., Narani, N. And mcculloch, C. (1999). The Compliance of Collagen Gels Regulates Transforming Growth Factor- $\beta$  Induction of  $\alpha$ -Smooth Muscle Actin in Fibroblasts. *The American Journal of Pathology*, 154(3), pp.871-882.
86. Rodin, S., Antonsson, L., Hovatta, O. and Tryggvason, K., (2020). Monolayer Culturing And Cloning Of Human Pluripotent Stem Cells On Laminin-521–Based Matrices Under Xeno-Free And Chemically Defined Conditions.
87. Hafemann, B., Ensslen, S., Erdmann, C., Niedballa, R., Zühlke, A., Ghofrani, K. and Kirkpatrick, C., (1999). Use of a collagen/elastin-membrane for the tissue engineering of dermis. *Burns*, 25(5), pp.373-384.

88. Pelham, R. And Wang, Y. (1997). Cell locomotion and focal adhesions are regulated by substrate flexibility. *Proceedings of the National Academy of Sciences*, 94(25), pp.13661-13665.
89. Damljjanovic, V., Christoffer Lagerholm, B. And Jacobson, K. (2005). Bulk and micropatterned conjugation of extracellular matrix proteins to characterized polyacrylamide substrates for cell mechanotransduction assays. *Biotechniques*, 39(6), pp.847-851.
90. Lin, C. And Anseth, K. (2008). PEG Hydrogels for the Controlled Release of Biomolecules in Regenerative Medicine. *Pharmaceutical Research*, 26(3), pp.631-643.
91. Alsafadi, H., Staab-Weijnitz, C., Lehmann, M., Lindner, M., Peschel, B., Königshoff, M. And Wagner, D. (2017). An ex vivo model to induce early fibrosis-like changes in human precision-cut lung slices. *American Journal of Physiology-Lung Cellular and Molecular Physiology*, 312(6), pp.L896-L902.
92. Kendall, R. And Feghali-Bostwick, C. (2014). Fibroblasts in fibrosis: novel roles and mediators. *Frontiers in Pharmacology*, 5.
93. Ravikanth, M., Manjunath, K., Ramachandran, C., Soujanya, P. And Saraswathi, T. (2011). Heterogeneity of fibroblasts. *Journal of Oral and Maxillofacial Pathology*, 15(2), p.247.
94. Li, B. And Wang, J. (2011). Fibroblasts and myofibroblasts in wound healing: Force generation and measurement. *Journal of Tissue Viability*, 20(4), pp.108-120.
95. P. Bainbridge. (2013). Wound healing and the role of fibroblasts. *Journal of Wound Care*, 22(8), pp.407-412.
96. Hinz B, Phan SH, Thannickal VJ, Galli A, Bochaton-Piallat ML, Gabbiani G. (2007); The myofibroblast: one function, multiple origins. *The American journal of pathology* 170(6):1807-16.
97. Kirsner, R. (2007). Wound Healing. *Archives of Dermatology*, 143(10).
98. Sorrell, J. (2004). Fibroblast heterogeneity: more than skin deep. *Journal of Cell Science*, 117(5), pp.667-675.
99. Selman, M., López-Otín, C. and Pardo, A., (2016). Age-driven developmental drift in the pathogenesis of idiopathic pulmonary fibrosis. *European Respiratory Journal*, 48(2), pp.538-552.
100. Midwood, K., Williams, L. And Schwarzbauer, J. (2004). Tissue repair and the dynamics of the extracellular matrix. *The International Journal of Biochemistry & Cell Biology*, 36(6), pp.1031-1037.
101. Phan, S., (2008). Biology of Fibroblasts and Myofibroblasts. *Proceedings of the American Thoracic Society*, 5(3), pp.334-337.
102. Willis, B. (2006). Epithelial Origin of Myofibroblasts during Fibrosis in the Lung. *Proceedings of the American Thoracic Society*, 3(4), pp.377-382.
103. Abu El-Asrar, A. (2016). Endothelial-to-mesenchymal transition contributes to the myofibroblast population in proliferative diabetic retinopathy. *Saudi Journal of Ophthalmology*, 30(1), pp.1-2.
104. Zhang, P., Guan, Y., Chen, J., Li, X., mcconnell, B., Zhou, W., Boini, K. And Zhang, Y. (2018). Contribution of p62/SQSTM1 to PDGF-BB-induced myofibroblast-like phenotypic transition in vascular smooth muscle cells lacking Smpd1 gene. *Cell Death & Disease*, 9(12).
105. Ashley, S., Wilke, C., Kim, K. And Moore, B. (2016). Periostin regulates fibrocyte function to promote myofibroblast differentiation and lung fibrosis. *Mucosal Immunology*, 10(2), pp.341-351.
106. Chang, F., Chou, Y., Chen, Y. And Lin, S. (2012). Novel insights into pericyte–myofibroblast transition and therapeutic targets in renal fibrosis. *Journal of the Formosan Medical Association*, 111(11), pp.589-598.

107. Cieslik, K., Trial, J. and Entman, M., (2011). Defective Myofibroblast Formation from Mesenchymal Stem Cells in the Aging Murine Heart. *The American Journal of Pathology*, 179(4), pp.1792-1806.
108. Scotton, C. and Chambers, R., (2007). Molecular Targets in Pulmonary Fibrosis. *Chest*, 132(4), pp.1311-1321.
109. Tomasek, J., Gabbiani, G., Hinz, B., Chaponnier, C. and Brown, R., (2002). Myofibroblasts and mechano-regulation of connective tissue remodelling. *Nature Reviews Molecular Cell Biology*, 3(5), pp.349-363.
110. Hinz, B., Celetta, G., Tomasek, J., Gabbiani, G. and Chaponnier, C., (2001). Alpha-Smooth Muscle Actin Expression Upregulates Fibroblast Contractile Activity. *Molecular Biology of the Cell*, 12(9), pp.2730-2741.
111. Vu, T., Chen, X., Foda, H., Smaldone, G. And Hasaneen, N. (2019). Interferon- $\gamma$  enhances the antifibrotic effects of pirfenidone by attenuating IPF lung fibroblast activation and differentiation. *Respiratory Research*, 20(1).
112. Greenberg, R., Bernstein, A., Benezra, M., Gelman, I., Taliana, L. And Masur, S. (2006). FAK-dependent regulation of myofibroblast differentiation. *The FASEB Journal*, 20(7), pp.1006-1008.
113. Liguori, T., Liguori, G., Moreira, L. And Harmsen, M. (2018). Fibroblast growth factor-2, but not the adipose tissue-derived stromal cells secretome, inhibits TGF- $\beta$ 1-induced differentiation of human cardiac fibroblasts into myofibroblasts. *Scientific Reports*, 8(1).
114. García-Cuesta, E., Santiago, C., Vallejo-Díaz, J., Juarranz, Y., Rodríguez-Frade, J. and Mellado, M., (2019). The Role of the CXCL12/CXCR4/ACKR3 Axis in Autoimmune Diseases. *Frontiers in Endocrinology*, 10.
115. Maher, T., Evans, I., Bottoms, S., Mercer, P., Thorley, A., Nicholson, A., Laurent, G., Tetley, T., Chambers, R. And meanulty, R. (2010). Diminished Prostaglandin E2Contributes to the Apoptosis Paradox in Idiopathic Pulmonary Fibrosis. *American Journal of Respiratory and Critical Care Medicine*, 182(1), pp.73-82.
116. Bozyk, P. And Moore, B. (2011). Prostaglandin e2and the Pathogenesis of Pulmonary Fibrosis. *American Journal of Respiratory Cell and Molecular Biology*, 45(3), pp.445-452.
117. El Agha, E., Moiseenko, A., Kheirollahi, V., De Langhe, S., Crnkovic, S., Kwapiszewska, G., Szibor, M., Kosanovic, D., Schwind, F., Schermuly, R., Henneke, I., mackenzie, B., Quantius, J., Herold, S., Ntokou, A., Ahlbrecht, K., Braun, T., Morty, R., Günther, A., Seeger, W. And Bellusci, S. (2017). Two-Way Conversion between Lipogenic and Myogenic Fibroblastic Phenotypes Marks the Progression and Resolution of Lung Fibrosis. *Cell Stem Cell*, 20(4), p.571.
118. Saito, A., Horie, M. And Nagase, T. (2018). TGF- $\beta$  signaling in Lung Health and Disease. *International Journal of Molecular Sciences*, 19(8), p.2460.
119. Hoyt DG, Lazo JS. (1988); Alterations in pulmonary mrna encoding procollagens, fibronectin and transforming growth factor-beta precede bleomycin-induced pulmonary fibrosis in mice. *The Journal of pharmacology and experimental therapeutics* 246 (2), pp.765-71.
120. Leppäranta O, Sens C, Salmenkivi K, Kinnula VL, Keski-Oja J, Myllärniemi M, Koli K. (2012); Regulation of TGF- $\beta$  storage and activation in the human idiopathic pulmonary fibrosis lung. *Cell and tissue research* 348 (3), pp.491-503.
121. Tatler, A. And Jenkins, G. (2012). TGF- $\beta$  Activation and Lung Fibrosis. *Proceedings of the American Thoracic Society*, 9(3), pp.130-136.



122. Henderson, N. and Sheppard, D., (2013). Integrin-mediated regulation of TGF $\beta$  in fibrosis. *Biochimica et Biophysica Acta (BBA) - Molecular Basis of Disease*, 1832(7), pp.891-896.
123. Stetler-Stevenson WG, Aznavoorian S, Liotta LA. (1993); Tumor cell interactions with the extracellular matrix during invasion and metastasis. *Annual review of cell biology* 9:541-73.
124. Wipff P. J., Hinz B. (2008); Integrins and the activation of latent transforming growth factor beta1 - an intimate relationship. *European journal of cell biology* 87 (8-9):601-15.
125. Lyons RM, Keski-Oja J, Moses HL. (1988); Proteolytic activation of latent transforming growth factor-beta from fibroblast-conditioned medium. *The Journal of cell biology* 106 (5):1659-65.
126. Barcellos-Hoff MH, Dix TA, Chatterjee A. (1996); Redox-mediated activation of latent transforming growth factor-beta 1. *Molecular endocrinology (Baltimore, Md.)* 10 (9):1077-83.
127. Jakowlew, S., (2006). Transforming growth factor- $\beta$  in cancer and metastasis. *Cancer and Metastasis Reviews*, 25(3), pp.435-457.
128. Derynck R, Zhang YE. (2003); Smad-dependent and Smad-independent pathways in TGF-beta family signalling. *Nature* 425 (6958):577-84.
129. Fabregat I, Caballero-Díaz D. (2018); Transforming Growth Factor- $\beta$ -Induced Cell Plasticity in Liver Fibrosis and Hepatocarcinogenesis. *Frontiers in oncology* 8:357.
130. Robert Lanza and Anthony Atala "Handbook of stem cells" (2014) Pg 952.
131. Gattazzo F, Urciuolo A, Bonaldo P. (2014); Extracellular matrix: a dynamic microenvironment for stem cell niche. *Biochimica et biophysica acta* 1840 (8), pp.2506-19.
132. Rosińczuk J, Taradaj J, Dymarek R, Sopel M. (2016); Mechanoregulation of Wound Healing and Skin Homeostasis. *Biomed research international* 2016, pp.3943481.
133. Rangarajan S, Kurundkar A, Kurundkar D, Bernard K, Sanders YY, Ding Q, Antony VB, Zhang J, Zmijewski J, Thannickal VJ. (2016); Novel Mechanisms for the Antifibrotic Action of Nintedanib. *American journal of respiratory cell and molecular biology* 54 (1):51-9.
134. Janson IA, Putnam AJ. (2015); Extracellular matrix elasticity and topography: material-based cues that affect cell function via conserved mechanisms. *Journal of biomedical materials research. Part A* 103 (3), pp.1246-58.
135. Naba A, Clauser KR, Hoersch S, Liu H, Carr SA, Hynes RO. (2012); The matrisome: in silico definition and in vivo characterization by proteomics of normal and tumor extracellular matrices. *Molecular & cellular proteomics: MCP* 11 (4), pp.M111.014647.
136. Pedersen JA, Swartz MA. (2005); Mechanobiology in the third dimension. *Annals of biomedical engineering* 33 (11), pp.1469-90.
137. Burgstaller, G., Vierkotten, S., Lindner, M., Königshoff, M. And Eickelberg, O. (2015). Multidimensional immunolabeling and 4D time-lapse imaging of vital ex vivo lung tissue. *American Journal of Physiology-Lung Cellular and Molecular Physiology*, 309(4), pp.L323-L332.
138. Fernandez IE, Eickelberg O. (2012); New cellular and molecular mechanisms of lung injury and fibrosis in idiopathic pulmonary fibrosis. *Lancet (London, England)* 380 (9842):680-8.
139. Lindahl GE, Chambers RC, Papakrivopoulou J, Dawson SJ, Jacobsen MC, Bishop JE, Laurent GJ. (2002); Activation of fibroblast procollagen alpha 1(I) transcription by mechanical strain is transforming growth factor-beta-dependent. *Jbc*, 277 (8):6153-61.

140. Liu F, Mih JD, Shea BS, Kho AT, Sharif AS, Tager AM, Tschumperlin DJ. (2010); Feedback amplification of fibrosis through matrix stiffening and COX-2 suppression. *The Journal of cell biology* 190 (4):693-706.
141. Green, J. And Yamada, K. (2007). Three-dimensional microenvironments modulate fibroblast signaling responses☆. *Advanced Drug Delivery Reviews*, 59(13), pp.1293-1298.
142. Kola, I. And Landis, J. (2004). Can the pharmaceutical industry reduce attrition rates?. *Nature Reviews Drug Discovery*, 3(8), pp.711-716.
143. Ng, B., Dong, J., D'Agostino, G., Viswanathan, J., Jiang, D., Noble, P., Schafer, S. And Cook, S. (2019). Interleukin-11 is a therapeutic target in idiopathic pulmonary fibrosis. *Science Translational Medicine*, 11(511), pp. 1237.
144. Oehrle, B., Burgstaller, G., Irmeler, M., Dehmel, S., Grün, J., Hwang, T., Krauss-Etschmann, S., Beckers, J., Meiners, S. And Eickelberg, O. (2015). Validated prediction of pro-invasive growth factors using a transcriptome-wide invasion signature derived from a complex 3D invasion assay. *Scientific Reports*, 5(1).
145. Schiller, H., Fernandez, I., Burgstaller, G., Schaab, C., Scheltema, R., Schwarzmayer, T., Strom, T., Eickelberg, O. And Mann, M. (2015). Time- and compartment-resolved proteome profiling of the extracellular niche in lung injury and repair. *Molecular Systems Biology*, 11(7), p.819.
146. Liu, G., Betts, C., Cunoosamy, D., Åberg, P., Hornberg, J., Sivars, K. And Cohen, T. (2019). Use of precision cut lung slices as a translational model for the study of lung biology. *Respiratory Research*, 20(1).
147. Gerckens, M., Alsafadi, H., Wagner, D., Lindner, M., Burgstaller, G. And Königshoff, M. (2019). Generation of Human 3D Lung Tissue Cultures (3D-ltcs) for Disease Modeling. *Journal of Visualized Experiments*, (144).
148. Balestrini, J., Gard, A., Gerhold, K., Wilcox, E., Liu, A., Schwan, J., Le, A., Baeovova, P., Dimitrievska, S., Zhao, L., Sundaram, S., Sun, H., Rittié, L., Dyal, R., Broekelmann, T., Mecham, R., Schwartz, M., Niklason, L. And White, E. (2016). Comparative biology of decellularized lung matrix: Implications of species mismatch in regenerative medicine. *Biomaterials*, 102, pp.220-230.
149. Rosmark, O., Åhrman, E., Müller, C., Elowsson Rendin, L., Eriksson, L., Malmström, A., Hallgren, O., Larsson-Callerfelt, A., Westergren-Thorsson, G. And Malmström, J. (2018). Quantifying extracellular matrix turnover in human lung scaffold cultures. *Scientific Reports*, 8(1).
150. Wynn TA. (2008); Cellular and molecular mechanisms of fibrosis. *The Journal of pathology* 214(2):199-210.
151. Mosmann, T. (1983). Rapid colorimetric assay for cellular growth and survival: Application to proliferation and cytotoxicity assays. *Journal of Immunological Methods*, 65(1-2), pp.55-63.
152. Uhl, F., Vierkotten, S., Wagner, D., Burgstaller, G., Costa, R., Koch, I., Lindner, M., Meiners, S., Eickelberg, O. and Königshoff, M., (2015). Preclinical validation and imaging of Wnt-induced repair in human 3D lung tissue cultures. *European Respiratory Journal*, 46(4), pp.1150-1166.
153. Grosche, A., Hauser, A., Lepper, M., Mayo, R., von Toerne, C., Merl-Pham, J. and Hauck, S., (2015). The Proteome of Native Adult Müller Glial Cells From Murine Retina. *Molecular & Cellular Proteomics*, 15(2), pp.462-480.
154. Kusko, R., Brothers, J., Tedrow, J., Pandit, K., Huleihel, L., Perdomo, C., Liu, G., Juan-Guardela, B., Kass, D., Zhang, S., Lenburg, M., Martinez, F., Quackenbush, J., Sciurba, F., Limper, A., Geraci, M., Yang, I., Schwartz, D., Beane, J., Spira, A. And Kaminski, N. (2016). Integrated Genomics Reveals Convergent

- Transcriptomic Networks Underlying Chronic Obstructive Pulmonary Disease and Idiopathic Pulmonary Fibrosis. *American Journal of Respiratory and Critical Care Medicine*, 194(8), pp.948-960.
155. Vincent, K. And Postovit, L. (2017). A pan-cancer analysis of secreted Frizzled-related proteins: re-examining their proposed tumour suppressive function. *Scientific Reports*, 7(1).
  156. Liu, T., Gonzalez De Los Santos, F. And H. Phan, S. (2017). The Bleomycin Model of Pulmonary Fibrosis. *Methods in Molecular Biology*, 1627.
  157. Adamson IY, Bowden DH. The pathogenesis of bleomycin-induced pulmonary fibrosis in mice. *Am J Pathol* (1974);77(2):185-97.
  158. Selman, M., King, T. And Pardo, A. (2001). Idiopathic Pulmonary Fibrosis: Prevailing and Evolving Hypotheses about Its Pathogenesis and Implications for Therapy. *Annals of Internal Medicine*, 134(2), p.136.
  159. Rabeyrin, M., Thivolet, F., Ferretti, G., Chalabreysse, L., Jankowski, A., Cottin, V., Pison, C., Cordier, J. And Lantuejoul, S. (2015). Usual interstitial pneumonia end-stage features from explants with radiologic and pathological correlations. *Annals of Diagnostic Pathology*, 19(4), pp.269-276.
  160. Hesse, C., Mang, S., Hoymann, H., Niehof, M., Braubach, P., Jonigk, D., Warnecke, G., Pfennig, O., Fieguth, H., Braun, A. and Sewald, K., 2016. Induction of pro-fibrotic biomarkers in precision-cut lung slices (PCLS). 1.5 Diffuse Parenchymal Lung Disease..Bérubé, K., Prytherch, Z., Job, C. And Hughes, T. (2010). Human primary bronchial lung cell constructs: The new respiratory models. *Toxicology*, 278(3), pp.311-318.
  161. Negmadjanov, U., Godic, Z., Rizvi, F., Emelyanova, L., Ross, G., Richards, J., Holmuhamedov, E. And Jahangir, A. (2015). TGF- $\beta$ 1-Mediated Differentiation of Fibroblasts Is Associated with Increased Mitochondrial Content and Cellular Respiration. *PLOS ONE*, 10(4), p.e0123046.
  162. Dees, C., Schlottmann, I., Funke, R., Distler, A., Palumbo-Zerr, K., Zerr, P., Lin, N., Beyer, C., Distler, O., Schett, G. and Distler, J., (2013). The Wnt antagonists DKK1 and SFRP1 are downregulated by promoter hypermethylation in systemic sclerosis. *Annals of the Rheumatic Diseases*, 73(6), pp.1232-1239.
  163. Liu, J., Zhu, H., Wang, H., Li, J., Han, F., Liu, Y., Zhang, W., He, T., Li, N., Zheng, Z. and Hu, D., (2018). Methylation of secreted frizzled-related protein 1 (SFRP1) promoter downregulates Wnt/ $\beta$ -catenin activity in keloids. *Journal of Molecular Histology*, 49(2), pp.185-193.
  164. Veeck, J., Niederacher, D., An, H., Klopocki, E., Wiesmann, F., Betz, B., Galm, O., Camara, O., Dürst, M., Kristiansen, G., Huszka, C., Knüchel, R. And Dahl, E. (2006). Aberrant methylation of the Wnt antagonist SFRP1 in breast cancer is associated with unfavourable prognosis. *Oncogene*, 25(24), pp.3479-3488.
  165. Liang, G., Gonzales, F., Jones, P., Orntoft, T. and Thykjaer, T., (2002). Analysis of Gene Induction in Human Fibroblasts and Bladder Cancer Cells Exposed to the Methylation Inhibitor 5-aza-2'-deoxycytidine. *Cancer Res.*, 15(62(4)), pp.961-6.
  166. Gopalsamy, A., Shi, M., Stauffer, B., Bahat, R., Billiard, J., Ponce-de-Leon, H., Seestaller-Wehr, L., Fukayama, S., Mangine, A., Moran, R., Krishnamurthy, G. and Bodine, P., (2008). Identification of Diarylsulfone Sulfonamides as Secreted Frizzled Related Protein-1 (sFRP-1) Inhibitors. *Journal of Medicinal Chemistry*, 51(24), pp.7670-7672.
  167. Pseaquant.scripps.edu. (2019). PSEA-Quant: Protein set enrichment analysis on label-free and label-based protein quantification data. [online] Available at: <http://pseaquant.scripps.edu/>.

168. Ihara, K., Muraguchi, S., Kato, M., Shimizu, T., Shirakawa, M., Kuroda, S., Kaibuchi, K. And Hakoshima, T. (1998). Crystal Structure of Human rhoa in a Dominantly Active Form Complexed with a GTP Analogue. *Journal of Biological Chemistry*, 273(16), pp.9656-9666.
169. Cellprofiler-manual.s3.amazonaws.com. (2019). Measurement — CellProfiler 3.0.0 documentation, Broad Institute.
170. Han X, Wang R, Zhou Y, Fei L, Sun H, Lai S, Saadatpour A, Zhou Z, Chen H, Ye F, Huang D, Xu Y, Huang W, Jiang M, Jiang X, Mao J, Chen Y, Lu C, Xie J, Fang Q, Wang Y, Yue R, Li T, Huang H, Orkin SH, Yuan GC, Chen M, Guo G. Mapping the Mouse Cell Atlas by Microwell-Seq. *Cell* (2018);173(5):1307.
171. Angelidis, I, Simon, LM, Fernandez, IE, Strunz, M, Mayr, CH, Greiffo, FR, ... & Schiller, HB. An atlas of the aging lung mapped by single cell transcriptomics and deep tissue proteomics. *Nature communications* (2019);10(1):963.
172. Falanga, V., Zhou, L. H., Takagi, H., Murata, H., Ochoa, S., Martin, T. A., & Helfman, T. (1995). Human Dermal Fibroblast Clones Derived from Single Cells Are Heterogeneous in the Production of mrnas for  $\alpha 1(I)$  Procollagen and Transforming Growth Factor- $\beta$  1. *Journal of Investigative Dermatology*, 105(1), 27-31.
173. Reyfman PA, Walter JM, Joshi N, Anekalla KR, mcquattie-Pimentel AC, Chiu S, Fernandez R, Akbarpour M, Chen CI, Ren Z, Verma R, Abdala-Valencia H, Nam K, Chi M, Han S, Gonzalez-Gonzalez FJ, Soberanes S, Watanabe S, Williams KJN, Flozak AS, Nicholson TT, Morgan VK, Winter DR, Hinchcliff M, Hrusch CL, Guzy RD, Bonham CA, Sperling AI, Bag R, Hamanaka RB, Mutlu GM, Yeldandi AV, Marshall SA, Shilatifard A, Amaral LAN, Perlman H, Sznajder JI, Argento AC, Gillespie CT, Dematte J, Jain M, Singer BD, Ridge KM, Lam AP, Bharat A, Bhorade SM, Gottardi CJ, Budinger GRS, Misharin AV. (2019); Single-Cell Transcriptomic Analysis of Human Lung Provides Insights into the Pathobiology of Pulmonary Fibrosis. *American journal of respiratory and critical care medicine* 199(12):1517-36.
174. Macosko, E., Basu, A., Satija, R., Nemesh, J., Shekhar, K., Goldman, M., Tirosh, I., Bialas, A., Kamitaki, N., Martersteck, E., Trombetta, J., Weitz, D., Sanes, J., Shalek, A., Regev, A. And mccarroll, S. (2015). Highly Parallel Genome-wide Expression Profiling of Individual Cells Using Nanoliter Droplets. *Cell*, 161(5), pp.1202-1214.
175. Zhang Y, Kaminski N. (2012); Biomarkers in idiopathic pulmonary fibrosis. *Current opinion in pulmonary medicine* 18(5):441-6.
176. Selman M, Carrillo G, Estrada A, Mejia M, Becerril C, Cisneros J, Gaxiola M, Pérez-Padilla R, Navarro C, Richards T, Dauber J, King TE, Pardo A, Kaminski N. (2007); Accelerated variant of idiopathic pulmonary fibrosis: clinical behavior and gene expression pattern. *Plos one* 2(5):e482.
177. De Langhe E, Aznar-Lopez C, De Vooght V, Vanoirbeek JA, Luyten FP, Lories RJ. (2014); Secreted frizzled related proteins inhibit fibrosis in vitro but appear redundant in vivo. *Fibrogenesis & tissue repair* 7:14.
178. Dahan M, Scemama C, Porcher R, Biau DJ. (2018); Reporting of heterogeneity of treatment effect in cohort studies: a review of the literature. *BMC medical research methodology* 18(1):10.
179. Lehmann M, Buhl L, Alsafadi HN, Klee S, Hermann S, Mutze K, Ota C, Lindner M, Behr J, Hilgendorff A, Wagner DE, Königshoff M. (2018); Differential effects of Nintedanib and Pirfenidone on lung alveolar epithelial cell function in ex vivo murine and human lung tissue cultures of pulmonary fibrosis. *Respiratory research* 19(1):175.

180. Burgstaller, G., Oehrle, B., Koch, I., Lindner, M. and Eickelberg, O., (2013). Multiplex Profiling of Cellular Invasion in 3D Cell Culture Models. *PLoS ONE*, 8(5), p.e63121.
181. Chung MT, Lai HC, Sytwu HK, Yan MD, Shih YL, Chang CC, Yu MH, Liu HS, Chu DW, Lin YW. (2009); SFRP1 and SFRP2 suppress the transformation and invasion abilities of cervical cancer cells through Wnt signal pathway. *Gynecologic oncology* 112(3):646-53.
182. Wang Z, Li R, He Y, Huang S. (2018); Effects of secreted frizzled-related protein 1 on proliferation, migration, invasion, and apoptosis of colorectal cancer cells. *Cancer cell international* 18:48.
183. Ren XY, Zhou GQ, Jiang W, Sun Y, Xu YF, Li YQ, Tang XR, Wen X, He QM, Yang XJ, Liu N, Ma J. (2015); Low SFRP1 Expression Correlates with Poor Prognosis and Promotes Cell Invasion by Activating the Wnt/ $\beta$ -Catenin Signaling Pathway in NPC. *Cancer prevention research (Philadelphia, Pa.)* 8(10):968-77.
184. Rosas IO, Richards TJ, Konishi K, Zhang Y, Gibson K, Lokshin AE, Lindell KO, Cisneros J, Macdonald SD, Pardo A, Sciurba F, Dauber J, Selman M, Gochuico BR, Kaminski N. (2008); MMP1 and MMP7 as potential peripheral blood biomarkers in idiopathic pulmonary fibrosis. *Plos medicine* 5(4):e93.
185. Bauer Y, Tedrow J, de Bernard S, Birker-Robaczewska M, Gibson KF, Guardela BJ, Hess P, Klenk A, Lindell KO, Poirey S, Renault B, Rey M, Weber E, Nayler O, Kaminski N. (2015); A novel genomic signature with translational significance for human idiopathic pulmonary fibrosis. *American journal of respiratory cell and molecular biology* 52(2):217-31.
186. Cabrera S, Selman M, Lonzano-Bolaños A, Konishi K, Richards TJ, Kaminski N, Pardo A. (2013); Gene expression profiles reveal molecular mechanisms involved in the progression and resolution of bleomycin-induced lung fibrosis. *American journal of physiology. Lung cellular and molecular physiology* 304(9):L593-601.
187. Peng R, Sridhar S, Tyagi G, Phillips JE, Garrido R, Harris P, Burns L, Renteria L, Woods J, Chen L, Allard J, Ravindran P, Bitter H, Liang Z, Hogaboam CM, Kitson C, Budd DC, Fine JS, Bauer CM, Stevenson CS. (2013); Bleomycin induces molecular changes directly relevant to idiopathic pulmonary fibrosis: a model for "active" disease. *Plos one* 8(4):e59348.
188. Lederle, W., Hartenstein, B., Meides, A., Kunzelmann, H., Werb, Z., Angel, P. And Mueller, M. (2009). MMP13 as a stromal mediator in controlling persistent angiogenesis in skin carcinoma. *Carcinogenesis*, 31(7), pp.1175-1184.
189. Lecomte, J., Masset, A., Blacher, S., Maertens, L., Gothot, A., Delgaudine, M., Bruyère, F., Carnet, O., Paupert, J., Illemann, M., Foidart, J., Lund, I., Høyer-Hansen, G. And Noel, A. (2012). Bone Marrow-derived Myofibroblasts Are the Providers of Pro-invasive Matrix Metalloproteinase 13 in Primary Tumor. *Neoplasia*, 14(10), pp.943-951.
190. Yamashita CM, Dolgonos L, Zemans RL, Young SK, Robertson J, Briones N, Suzuki T, Campbell MN, Gauldie J, Radisky DC, Riches DW, Yu G, Kaminski N, mcculloch CA, Downey GP. (2011); Matrix metalloproteinase 3 is a mediator of pulmonary fibrosis. *The American journal of pathology* 179(4):1733-45.
191. Tsumaki, N., Nakase, T., Miyaji, T., Kakiuchi, M., Kimura, T., Ochi, T. And Yoshikawa, H. (2002). Bone Morphogenetic Protein Signals Are Required for Cartilage Formation and Differently Regulate Joint Development During Skeletogenesis. *Journal of Bone and Mineral Research*, 17(5), pp.898-906.
192. Cao, X. And Chen, D. (2005). The BMP signaling and in vivo bone formation. *Gene*, 357(1), pp.1-8.

193. Pegorier, S., Campbell, G., Kay, A. and Lloyd, C., (2010). Bone Morphogenetic Protein (BMP)-4 and BMP-7 regulate differentially Transforming Growth Factor (TGF)- $\beta$ 1 in normal human lung fibroblasts (NHLF). *Respiratory Research*, 11(1).
194. Guo, X. and Wang, X., (2008). Signaling cross-talk between TGF- $\beta$ /BMP and other pathways. *Cell Research*, 19(1), pp.71-88.
195. Herrera, B., Aránzazu, c. and Sánchez, A., (2017). BMP Signalling at the Crossroad of Liver Fibrosis and Regeneration. *International Journal of Molecular Sciences*, 19(1), p.39.
196. Inai (2010). Aberrant promoter methylation of WIF-1 and SFRP1, 2, 4 genes in mesothelioma. *Oncology Reports*, 24(2).
197. Taguchi, Y., Iwadate, M. And Umeyama, H. (2016). SFRP1 is a possible candidate for epigenetic therapy in non-small cell lung cancer. *BMC Medical Genomics*, 9(S1).
198. Sanders, Y., Ambalavanan, N., Halloran, B., Zhang, X., Liu, H., Crossman, D., Bray, M., Zhang, K., Thannickal, V. and Hagood, J., (2012). Altered DNA Methylation Profile in Idiopathic Pulmonary Fibrosis. *American Journal of Respiratory and Critical Care Medicine*, 186(6), pp.525-535.
199. Huang, S., Scruggs, A., mceachin, R., White, E. And Peters-Golden, M. (2014). Lung Fibroblasts from Patients with Idiopathic Pulmonary Fibrosis Exhibit Genome-Wide Differences in DNA Methylation Compared to Fibroblasts from Nonfibrotic Lung. *Plos ONE*, 9(9), p.e107055.
200. Cooper, S., von Roemeling, C., Kang, K., Marlow, L., Grebe, S., Meneffee, M., Tun, H., Colon-Otero, G., Perez, E. And Copland, J. (2012). Reexpression of Tumor Suppressor, *sfrp1*, Leads to Antitumor Synergy of Combined HDAC and Methyltransferase Inhibitors in Chemoresistant Cancers. *Molecular Cancer Therapeutics*, 11(10), pp.2105-2115.
201. Neveu, W., Mills, S., Staitieh, B. and Sueblinvong, V., (2015). TGF- $\beta$ 1 epigenetically modifies Thy-1 expression in primary lung fibroblasts. *American Journal of Physiology-Cell Physiology*, 309(9), pp.C616-C626.
202. Crump, N., Hazzalin, C., Bowers, E., Alani, R., Cole, P. And Mahadevan, L. (2011). Dynamic acetylation of all lysine-4 trimethylated histone H3 is evolutionarily conserved and mediated by p300/CBP. *Proceedings of the National Academy of Sciences*, 108(19), pp.7814-7819.
203. Farhan, M., Ullah, M., Faisal, M., Farooqi, A., Sabitaliyevich, U., Biersack, B. And Ahmad, A. (2019). Differential Methylation and Acetylation as the Epigenetic Basis of Resveratrol's Anticancer Activity. *Medicines*, 6(1), p.24.
204. Li, M., Zheng, Y., Yuan, H., Liu, Y. And Wen, X. (2017). Effects of dynamic changes in histone acetylation and deacetylase activity on pulmonary fibrosis. *International Immunopharmacology*, 52, pp.272-280.
205. Guo, W., Shan, B., Klingsberg, R., Qin, X. And Lasky, J. (2009). Abrogation of TGF- $\beta$ 1-induced fibroblast-myofibroblast differentiation by histone deacetylase inhibition. *American Journal of Physiology-Lung Cellular and Molecular Physiology*, 297(5), pp.L864-L870.
206. Quan, H., Zhou, F., Nie, D., Chen, Q., Cai, X., Shan, X., Zhou, Z., Chen, K., Huang, A., Li, S. And Tang, N. (2013). Hepatitis C virus core protein epigenetically silences SFRP1 and enhances HCC aggressiveness by inducing epithelial-mesenchymal transition. *Oncogene*, 33(22), pp.2826-2835.
207. Tang, Y., Wen, W., Chang, J., Wei, T., Tan, Y., Salunke, S., Chen, C., Chen, C. And Wang, Y. (2010). A Novel Histone Deacetylase Inhibitor Exhibits Antitumor Activity via Apoptosis Induction, F-Actin Disruption and Gene Acetylation in Lung Cancer. *Plos ONE*, 5(9), p.e12417.

208. Bryant, R., Winder, S., Cross, S., Hamdy, F. And Cunliffe, V. (2008). The polycomb group protein EZH2 regulates actin polymerization in human prostate cancer cells. *The Prostate*, 68(3), pp.255-263.
209. Felsenfeld, G. And Groudine, M. (2003). Controlling the double helix. *Nature*, 421(6921), pp.448-453.
210. Xu, Q., A. D'Amore, P. and Y. Sokol, S., (1998). Functional and biochemical interactions of Wnts with FrzA, a secreted Wnt antagonist. *Development*, 125, pp.4767-4776.
211. Häusler, K., Horwood, N., Chuman, Y., Fisher, J., Ellis, J., Martin, T., Rubin, J. and Gillespie, M., (2004). Secreted Frizzled-Related Protein-1 Inhibits RANKL-Dependent Osteoclast Formation. *Journal of Bone and Mineral Research*, 19(11), pp.1873-1881.
212. Działo, E., Tkacz, K. and Błyszczuk, P., (2018). Crosstalk between TGF- $\beta$  and WNT signalling pathways during cardiac fibrogenesis. *Acta Biochimica Polonica*, 65(3), pp.341-349.
213. Meng, X., Nikolic-Paterson, D. and Lan, H., (2016). TGF- $\beta$ : the master regulator of fibrosis. *Nature Reviews Nephrology*, 12(6), pp.325-338.
214. Gauger, K., Chenausky, K., Murray, M. and Schneider, S., (2011). SFRP1 reduction results in an increased sensitivity to TGF- $\beta$  signaling. *BMC Cancer*, 11(1).
215. Ren, S., Johnson, B., Kida, Y., Ip, C., Davidson, K., Lin, S., Kobayashi, A., Lang, R., Hadjantonakis, A., Moon, R. and Duffield, J., (2013). LRP-6 is a coreceptor for multiple fibrogenic signaling pathways in pericytes and myofibroblasts that are inhibited by DKK-1. *Proceedings of the National Academy of Sciences*, 110(4), pp.1440-1445.
216. Matsuyama, M., Nomori, A., Nakakuni, K., Shimono, A. and Fukushima, M., (2014). Secreted Frizzled-related Protein 1 (Sfrp1) Regulates the Progression of Renal Fibrosis in a Mouse Model of Obstructive Nephropathy. *Journal of Biological Chemistry*, 289(45), pp.31526-31533.
217. Massagué, J., (2012). TGF $\beta$  signalling in context. *Nature Reviews Molecular Cell Biology*, 13(10), pp.616-630.
218. Mulder, K., (2000). Role of Ras and Mapks in TGF $\beta$  signaling. *Cytokine & Growth Factor Reviews*, 11(1-2), pp.23-35.
219. Zhang, L., Zhou, F. and ten Dijke, P., (2013). Signaling interplay between transforming growth factor- $\beta$  receptor and PI3K/AKT pathways in cancer. *Trends in Biochemical Sciences*, 38(12), pp.612-620.
220. Eichhorn, P., Rodón, L., González-Juncà, A., Dirac, A., Gili, M., Martínez-Sáez, E., Aura, C., Barba, I., Peg, V., Prat, A., Cuartas, I., Jimenez, J., García-Dorado, D., Sahuquillo, J., Bernards, R., Baselga, J. and Seoane, J., (2012). USP15 stabilizes TGF- $\beta$  receptor I and promotes oncogenesis through the activation of TGF- $\beta$  signaling in glioblastoma. *Nature Medicine*, 18(3), pp.429-435.
221. Pray, T. R., Parlati, F., Huang, J., Wong, B. R., Payan, D. G., Bennett, M. K., ... Demo, S. D. (2002). Cell cycle regulatory E3 ubiquitin ligases as anticancer targets. *Drug Resistance Updates*, 5(6), 249–258.
222. Iyengar, P., (2017). Regulation of Ubiquitin Enzymes in the TGF- $\beta$  Pathway. *International Journal of Molecular Sciences*, 18(4), p.877.
223. Felle, M., Joppien, S., Németh, A., Diermeier, S., Thalhammer, V., Dobner, T., Kremmer, E., Kappler, R. and Längst, G., (2011). The USP7/Dnmt1 complex stimulates the DNA methylation activity of Dnmt1 and regulates the stability of UHRF1. *Nucleic Acids Research*, 39(19), pp.8355-8365.
224. Watanabe, M. and Whitman, M., (1999). The role of transcription factors involved in TGF $\beta$  superfamily signaling during development. *Cell Mol Biol*, 45(5), pp.537-43.

225. Chen, S., Xu, D., Jiang, H., Xi, Z., Zhu, P. and Liu, Y., (2012). Trans-Platinum/Thiazole Complex Interferes with Sp1 Zinc-Finger Protein. *Angewandte Chemie International Edition*, 51(49), pp.12258-12262.
226. Nolan, G., Ghosh, S., Liou, H., Tempst, P. and Baltimore, D., (1991). DNA binding and I $\kappa$ B inhibition of the cloned p65 subunit of NF- $\kappa$ B, a rel-related polypeptide. *Cell*, 64(5), pp.961-969.
227. Du, Q., Zhang, X., Cardinal, J., Cao, Z., Guo, Z., Shao, L. and Geller, D., (2009). Wnt/ $\beta$ -Catenin Signaling Regulates Cytokine-Induced Human Inducible Nitric Oxide Synthase Expression by Inhibiting Nuclear Factor- $\kappa$ B Activation in Cancer Cells. *Cancer Research*, 69(9), pp.3764-3771.
228. Cichon, M., Moruzzi, M., Shqau, T., Miller, E., Mehner, C., Ethier, S., Copland, J., Radisky, E. and Radisky, D., (2016). MYC Is a Crucial Mediator of TGF-Induced Invasion in Basal Breast Cancer. *Cancer Research*, 76(12), pp.3520-3530.
229. Ebert, M. and Sharp, P., (2012). Roles for MicroRNAs in Conferring Robustness to Biological Processes. *Cell*, 149(3), pp.515-524.
230. Delic, S., Lottmann, N., Stelzl, A., Liesenberg, F., Wolter, M., Götze, S., Zapatka, M., Shiao, Y., Sabel, M., Felsberg, J., Reifenberger, G. and Riemenschneider, M., (2013). MiR-328 promotes glioma cell invasion via SFRP1-dependent Wnt-signaling activation. *Neuro-Oncology*, 16(2), pp.179-190.
231. Ba, S., Xuan, Y., Long, Z., Chen, H. and Zheng, S., (2017). MicroRNA-27a Promotes the Proliferation and Invasiveness of Colon Cancer Cells by Targeting SFRP1 through the Wnt/ $\beta$ -Catenin Signaling Pathway. *Cellular Physiology and Biochemistry*, 42(5), pp.1920-1933.
232. Ong, J., Timens, W., Rajendran, V., Algra, A., Spira, A., Lenburg, M., Campbell, J., van den Berge, M., Postma, D., van den Berg, A., Kluiver, J. and Brandsma, C., (2017). Identification of transforming growth factor-beta-regulated microRNAs and the microRNA-targetomes in primary lung fibroblasts. *PLOS ONE*, 12(9), p.e0183815.
233. Lessey, E., Guilluy, C. And Burridge, K. (2012). From Mechanical Force to rhoa Activation. *Biochemistry*, 51(38), pp.7420-7432.
234. Vardouli, L., Moustakas, A. And Stournaras, C. (2005). LIM-kinase 2 and Cofilin Phosphorylation Mediate Actin Cytoskeleton Reorganization Induced by Transforming Growth Factor-. *Journal of Biological Chemistry*, 280(12), pp.11448-11457.
235. Johnson, L., Rodansky, E., Haak, A., Larsen, S., Neubig, R. And Higgins, P. (2014). Novel Rho/MRTF/SRF Inhibitors Block Matrix-stiffness and TGF- $\beta$ -Induced Fibrogenesis in Human Colonic Myofibroblasts. *Inflammatory Bowel Diseases*, 20(1), pp.154-165.
236. Tkach, V., Bock, E. and Berezin, V. (2005). The role of RhoA in the regulation of cell morphology and motility. *Cell Motility and the Cytoskeleton*, 61(1), pp.21-33.
237. Katoh, K., Kano, Y. and Ookawara, S. (2007). Rho-kinase dependent organization of stress fibers and focal adhesions in cultured fibroblasts. *Genes to Cells*, 12(5), pp.623-638.
238. Costa, P., Scales, T., Ivaska, J. And Parsons, M. (2013). Integrin-Specific Control of Focal Adhesion Kinase and rhoa Regulates Membrane Protrusion and Invasion. *Plos ONE*, 8(9), p.e74659.
239. Guo, W. and Giancotti, F., (2004). Integrin signalling during tumour progression. *Nature Reviews Molecular Cell Biology*, 5(10), pp.816-826.
240. Hall, A. (1998). Rho gtpases and the Actin Cytoskeleton. *Science*, 279(5350), pp.509-514.
241. Nayak, R., Chang, K., Vaitinadin, N. And Cancelas, J. (2013). Rho gtpases control specific cytoskeleton-dependent functions of hematopoietic stem cells. *Immunological Reviews*, 256(1), pp.255-268.



242. Moorman, J., Luu, D., Wickham, J., Bobak, D. And Hahn, C. (1999). A balance of signaling by Rho family small gtpases rhoa, Rac1 and Cdc42 coordinates cytoskeletal morphology but not cell survival. *Oncogene*, 18(1), pp.47-57.
243. Bishop, A. And Hall, A. (2000). Rho gtpases and their effector proteins. *Biochemical Journal*, 348(2), p.241.
244. Alkasalias, T., Alexeyenko, A., Hennig, K., Danielsson, F., Lebbink, R., Fielden, M., Turunen, S., Lehti, K., Kashuba, V., Madapura, H., Bozoky, B., Lundberg, E., Balland, M., Guvén, H., Klein, G., Gad, A. And Pavlova, T. (2017). Rhoa knockout fibroblasts lose tumor-inhibitory capacity in vitro and promote tumor growth in vivo. *Proceedings of the National Academy of Sciences*, 114(8), pp.E1413-E1421.
245. Street CA, Bryan BA. (2011); Rho kinase proteins--pleiotropic modulators of cell survival and apoptosis. *Anticancer research* 31(11), pp.3645-57.
246. Watanabe, N. (1997). P140mdia, a mammalian homolog of *Drosophila* diaphanous, is a target protein for Rho small gtpase and is a ligand for profilin. *The EMBO Journal*, 16(11), pp.3044-3056.
247. Riento, K. and Ridley, A., (2003). ROCKs: multifunctional kinases in cell behaviour. *Nature Reviews Molecular Cell Biology*, 4(6), pp.446-456.
248. Kühn, S. and Geyer, M., (2014). Formins as effector proteins of Rho GTPases. *Small GTPases*, 5(3), p.e983876.
249. Elsasser, W. (1984). Outline of a theory of cellular heterogeneity. *Proceedings of the National Academy of Sciences*, 81(16), pp.5126-5129.
250. Altschuler, S. And Wu, L. (2010). Cellular Heterogeneity: Do Differences Make a Difference?. *Cell*, 141(4), pp.559-563.
251. Xie, T., Liang, J., Liu, N., Huan, C., Zhang, Y., Liu, W., Kumar, M., Xiao, R., D'Armiento, J., Metzger, D., Chambon, P., Papaioannou, V., Stripp, B., Jiang, D. and Noble, P., (2016). Transcription factor TBX4 regulates myofibroblast accumulation and lung fibrosis. *Journal of Clinical Investigation*, 126(8), pp.3063-3079.
252. Xie, T., Wang, Y., Deng, N., Huang, G., Taghavifar, F., Geng, Y., Liu, N., Kulur, V., Yao, C., Chen, P., Liu, Z., Stripp, B., Tang, J., Liang, J., Noble, P. and Jiang, D., (2018). Single-Cell Deconvolution of Fibroblast Heterogeneity in Mouse Pulmonary Fibrosis. *Cell Reports*, 22(13), pp.3625-3640.
253. Who.int. (2019). The top 10 causes of death. [online] Available at: <https://www.who.int/en/news-room/fact-sheets/detail/the-top-10-causes-of-death>.
254. Huh, D., Fujioka, H., Tung, Y., Futai, N., Paine, R., Grotberg, J. And Takayama, S. (2007). Acoustically detectable cellular-level lung injury induced by fluid mechanical stresses in microfluidic airway systems. *Proceedings of the National Academy of Sciences*, 104(48), pp.18886-18891.
255. Stucki, J., Hobi, N., Galimov, A., Stucki, A., Schneider-Daum, N., Lehr, C., Huwer, H., Frick, M., Funke-Chambour, M., Geiser, T. And Guenat, O. (2018). Medium throughput breathing human primary cell alveolus-on-chip model. *Scientific Reports*, 8(1).
256. Weiskirchen, R., (2016). Hepatoprotective and Anti-fibrotic Agents: It's Time to Take the Next Step. *Frontiers in Pharmacology*, 6.
257. Swiderski, K., Todorov, M., Gehrig, S., Naim, T., Chee, A., Stapleton, D., Koopman, R. and Lynch, G., (2014). Tranilast administration reduces fibrosis and improves fatigue resistance in muscles of mdx dystrophic mice. *Fibrogenesis & Tissue Repair*, 7(1), p.1.

258. Kato, M., Takahashi, F., Mitsuishi, Y., Tajima, K., Ihara, H., Hidayat, M., Wirawan, A., Koinuma, Y., Hayakawa, D., Yagishita, S., Ko, R., Sato, T., Harada, N., Kodama, Y., Nurwidya, F., Sasaki, S., Niwa, S. And Takahashi, K. (2013). Tranilast inhibits pulmonary fibrosis by suppressing tgfb-mediated extracellular matrix protein production 42: pp 2330.
259. Warburg, O. And Minami, S. (1923). Versuche an Überlebendem Carcinom-gewebe. Klinische Wochenschrift, 2(17), pp.776-777.
260. Majno, G. And Bunker, W. (1957). Preparation of tissue slices for metabolic studies: A hand microtome especially suitable for brain. Journal of Neurochemistry, 2(1), pp.11-14.
261. Wasnick, R., Korfei, M., Piskulak, K., Königshoff, M., Eickelberg, O. and Guenther, A., (2019). Restored alveolar epithelial differentiation and reversed human lung fibrosis upon Notch inhibition. BioRxiv.
262. Baron, R., Choi, A., Owen, C. And Choi, A. (2012). Genetically manipulated mouse models of lung disease: potential and pitfalls. American Journal of Physiology-Lung Cellular and Molecular Physiology, 302(6), pp. L485-L497.
263. Halliwell, B. (2003). Oxidative stress in cell culture: an under-appreciated problem? FEBS Letters, 540(1-3), pp.3-6.
264. Murray, J., Whitfield, M., Trinklein, N., Myers, R., Brown, P. And Botstein, D. (2004). Diverse and Specific Gene Expression Responses to Stresses in Cultured Human Cells. Molecular Biology of the Cell, 15(5), pp.2361-2374.
265. Shaw, A. and Xu, Q., (2003). Biomechanical Stress-induced Signaling in Smooth Muscle Cells: An Update. Current Vascular Pharmacology, 1(1), pp.41-58.
266. Tanaka, H., Goto, H., Inoko, A., Makihara, H., Enomoto, A., Horimoto, K., Matsuyama, M., Kurita, K., Izawa, I. And Inagaki, M. (2015). Cytokinetic Failure-induced Tetraploidy Develops into Aneuploidy, Triggering Skin Aging in Phosphovimentin-deficient Mice. Journal of Biological Chemistry, 290(21), pp.12984-12998.
267. Danielsson, F., Peterson, M., Caldeira Araújo, H., Lautenschläger, F. And Gad, A. (2018). Vimentin Diversity in Health and Disease. Cells, 7(10), p.147.
268. Chiquet, M., Gelman, L., Lutz, R. And Maier, S. (2009). From mechanotransduction to extracellular matrix gene expression in fibroblasts. Biochimica et Biophysica Acta (BBA) - Molecular Cell Research, 1793(5), pp.911-920.
269. Midwood, K. And Orend, G. (2009). The role of tenascin-C in tissue injury and tumorigenesis. Journal of Cell Communication and Signaling, 3(3-4), pp.287-310.
270. Uno, M., Kurita, S., Misu, H., Ando, H., Ota, T., Matsuzawa-Nagata, N., Kita, Y., Nabemoto, S., Akahori, H., Zen, Y., Nakanuma, Y., Kaneko, S. And Takamura, T. (2008). Tranilast, an antifibrogenic agent, ameliorates a dietary rat model of nonalcoholic steatohepatitis. Hepatology, 48(1), pp.109-118.
271. Papageorgis, P., Polydorou, C., Mpekris, F., Voutouri, C., Agathokleous, E., Kapnissi-Christodoulou, C. And Stylianopoulos, T. (2017). Tranilast-induced stress alleviation in solid tumors improves the efficacy of chemo- and nanotherapeutics in a size-independent manner. Scientific Reports, 7(1).
272. Theocharis, A., Skandalis, S., Gialeli, C. And Karamanos, N. (2016). Extracellular matrix structure. Advanced Drug Delivery Reviews, 97, pp.4-27.
273. Bateman, J., Boot-Handford, R. And Lamandé, S. (2009). Genetic diseases of connective tissues: cellular and extracellular effects of ECM mutations. Nature Reviews Genetics, 10(3), pp.173-183.

274. Bonnans, C., Chou, J. And Werb, Z. (2014). Remodelling the extracellular matrix in development and disease. *Nature Reviews Molecular Cell Biology*, 15(12), pp.786-801.
275. Raghu G, Striker LJ, Hudson LD, Striker GE. (1985); Extracellular matrix in normal and fibrotic human lungs. *The American review of respiratory disease* 131(2):281-9.
276. Hynes, R. And Naba, A. (2011). Overview of the Matrisome--An Inventory of Extracellular Matrix Constituents and Functions. *Cold Spring Harbor Perspectives in Biology*, 4(1), pp.a004903-a004903.
277. Baker, B. And Chen, C. (2012). Deconstructing the third dimension – how 3D culture microenvironments alter cellular cues. *Journal of Cell Science*, 125(13), pp.3015-3024.
278. Burgstaller, G., Sengupta, A., Vierkotten, S., Preissler, G., Lindner, M., Behr, J., Königshoff, M. and Eickelberg, O., (2018). Distinct niches within the extracellular matrix dictate fibroblast function in (cell free) 3D lung tissue cultures. *American Journal of Physiology-Lung Cellular and Molecular Physiology*, 314(5), pp.L708-L723.
279. Scherzer, M., Waigel, S., Donniger, H., Arumugam, V., Zacharias, W., Clark, G., Siskind, L., Soucy, P. And Beverly, L. (2015). Fibroblast-Derived Extracellular Matrices: An Alternative Cell Culture System That Increases Metastatic Cellular Properties. *PLOS ONE*, 10(9), p.e0138065.
280. Özbek, S., Balasubramanian, P., Chiquet-Ehrismann, R., Tucker, R. And Adams, J. (2010). The Evolution of Extracellular Matrix. *Molecular Biology of the Cell*, 21(24), pp.4300-4305.
281. Rozario, T. and DeSimone, D., (2010). The extracellular matrix in development and morphogenesis: A dynamic view. *Developmental Biology*, 341(1), pp.126-140.
282. Lee JS, Choi YS, Cho SW. (2018); Decellularized Tissue Matrix for Stem Cell and Tissue Engineering. *Advances in experimental medicine and biology* 1064, pp.161-80.
283. Elowsson Rending, L., Löfdahl, A., Isaksson, H., Malmström, J. And Westergren-Thorsson, G. (2019). Matrisome Properties of Scaffolds Direct Fibroblasts in Idiopathic Pulmonary Fibrosis. *International Journal of Molecular Sciences*, 20(16), p.4013.
284. Cole, M., Quan, T., Voorhees, J. and Fisher, G., (2018). Extracellular matrix regulation of fibroblast function: redefining our perspective on skin aging. *Journal of Cell Communication and Signaling*, 12(1), pp.35-43.
285. Lu, P., Takai, K., Weaver, V. And Werb, Z. (2011). Extracellular Matrix Degradation and Remodeling in Development and Disease. *Cold Spring Harbor Perspectives in Biology*, 3(12), pp.a005058-a005058.
286. Dzobo, K., Turnley, T., Pepper, M. and Parker, M. (2016). Fibroblast-Derived Extracellular Matrix Induces Chondrogenic Differentiation in Human Adipose-Derived Mesenchymal Stromal/Stem Cells in Vitro. *International Journal of Molecular Sciences*, 17(8), p.1259.
287. Evans, N., Gentleman, E., Chen, X., Roberts, C., Polak, J. and Stevens, M. (2010). Extracellular matrix-mediated osteogenic differentiation of murine embryonic stem cells. *Biomaterials*, 31(12), pp.3244-3252.
288. Hongisto, V., Jernström, S., Fey, V., Mpindi, J., Kleivi Sahlberg, K., Kallioniemi, O. and Perälä, M. (2013). High-Throughput 3D Screening Reveals Differences in Drug Sensitivities between Culture Models of JIMT1 Breast Cancer Cells. *PLoS ONE*, 8(10), p.e77232.
289. Doyle, A. and Yamada, K., (2016). Mechanosensing via cell-matrix adhesions in 3D microenvironments. *Experimental Cell Research*, 343(1), pp.60-66.

- 290. Fraley, S., Feng, Y., Krishnamurthy, R., Kim, D., Celedon, A., Longmore, G. and Wirtz, D., (2010). A distinctive role for focal adhesion proteins in three-dimensional cell motility. *Nature Cell Biology*, 12(6), pp.598-604.
- 291. Kim, D. and Wirtz, D., (2013). Focal Adhesion Size Uniquely Predicts Cell Migration. *Biophysical Journal*, 104(2), p.319a.
- 292. Galarza, S., Kim, H., Atay, N., Peyton, S. R., & Munson, J. M. (2019). 2D or 3D? How in vitro cell motility is conserved across dimensions, and predicts in vivo invasion. doi: 10.1101/627281, *BioRxiv* pre-print.
- 293. Akram, K., Yates, L., Mongey, R., Rothery, S., Gaboriau, D., Sanderson, J., Hind, M., Griffiths, M. and Dean, C. (2019). Live imaging of alveologenesis in precision-cut lung slices reveals dynamic epithelial cell behaviour. *Nature Communications*, 10(1).

## Abbreviations

### A

ANOVA	Analysis of variance
APS	Ammonium peroxodisulfate
AT I / II	Alveolar type I / II
ATS	American thoracic society
$\alpha$ SMA	Alpha Smooth Muscle Actin

### B

BAL	Bronchoalveolar lavage
Bleo	Bleomycin
BMP4	Bone morphogenic protein 4
BSA	Bovine serum albumin

### C

°C	Degrees Celsius
CDC42	Cell division cycle 42 protein
cDNA	Complementary DNA
CRD	Cysteine-rich domain

### D

D	Dimensional
DAPI	4',6-diamidino-2-phenylindole
ddCt	Delta-delta- cycle threshold value
DMEM	Dulbecco's Modified Eagle's Medium
dNTP	Deoxy-nucleotide-tri-phosphate

### E

ECM	Extracellular matrix
EDTA	Ethylenediaminetetraacetic acid
EGF	Epidermal growth factor
EMT	Epithelial-Mesenchymal transition
ERS	European Respiratory society

### F

FBS	Fetal Bovine Serum
FGF	Fibroblast growth factor
FFPE	Formalin-Fixed Paraffin-Embedded

**G**

G Gram

**H**

HRP Horseradish peroxidase

**I**

IL1 $\beta$  Interleukin 1  $\beta$

ILD Interstitial Lung Disease

inv Invading

IPF Idiopathic Pulmonary Fibrosis

**L**

L Liter

LTC Lung tissue culture

**M**

m<sup>2</sup> Square meter

Min(s) Minutes

mL Milliliter

MMP Matrix metalloproteinase

mRNA Messenger RNA

MTT 3-(4,5-dimethylthiazol-2-yl)-2,5 diphenyl tetrazolium bromide

$\mu$  Micro

**N**

neg Negative

ninv Non-invading

NIV Non-invasive

**P**

PBS Phosphate buffered saline

PAGE Polyacrylamide gel electrophoresis

PDGF Platelet-derived growth factor

PF Pulmonary Fibrosis

PFA Paraformaldehyde

**Q**

QDSP Quantitative detergent solubility profiling

qRT-PCR	Quantitative real-time Polymerase chain reaction
<b>R</b>	
RIPA	Radio-Immunoprecipitation Assay
ROCK	Rho-associated, coiled-coil-containing protein kinase 1
RNA	Ribonucleic acid

**S**

SDS	Sodium dodecyl sulphate
sec	Seconds
SFRP1	Secreted Frizzled Related Protein 1

**T**

TBS	Tris-buffered saline
TBS-T	Tris-buffered saline with TWEEN®20
TEMED	N,N,N',N'-Tetramethylenediamine
TGFβ1	Transforming growth factor, beta 1
TNFα	Tumor necrosis factor alpha
TRIS	Tris(hydroxymethyl)-aminomethane

**U**

UIP	Usual Interstitial Pneumonia
-----	------------------------------

**W**

Wnt	Wingless/integrase-1
-----	----------------------

## Acknowledgements

I would like to express my deepest appreciation for Dr. Gerald Burgstaller for his exemplary guidance and for providing me with this opportunity to work on interesting and challenging projects and gain valuable experience. His constant motivation along with his prompt “over a coffee” feedbacks helped me to complete this thesis successfully. I would especially like to thank him for providing me the platform for presenting my data at numerous conferences.

I am very grateful to PD Dr. Silke Meiners for her excellent supervision and her constant encouraging support. I am thankful to Prof. Dr. Oliver Eickelberg, Dr. Ali Önder Yildirim and Dr. Markus Rehberg for serving as my thesis committee members, for all the fruitful discussions and the great advices.

I am also very thankful for the support and training that I received from the CPC research school “Lung Biology and Disease” and especially want to thank PD Dr. Claudia Staab-Weijnitz and Dr. Doreen Franke for their constant involvement.

I am grateful to all former and current members of the Burgstaller team, Bettina Oehrle, Jessica Grün, Kyra Peters, Marisa Neuman, Armando-Marco Dworsky, Severine Cranz Somlo, Mahesh Gouda and Michael Gerckens for their contribution of ideas, their kind support and for outstanding technical assistance.

Furthermore, I am very thankful for all the support that I received from my collaboration partners from CPC & ILBD (Dr. Isis E. Fernandez, Dr. Herbert Schiller, Maximilian Strunz, Christoph Mayr, Dr. Otmar Schmid and Lin Yang) and from the Helmholtz Zentrum München (Dr. Juliane Merl-Pham and Dr. Martin Irmeler).

I am thankful to all members of CPC and ILBD for their kind support and technical advices.

I furthermore highly appreciated the companionship of my fellow PhD students. In particular Carmela Morrone, Gizem Güneş, Pushkar Ramesh, Shruthi Kalgudde, Ashesh Chakraborty, Vijay Rajendran, Valeria Viteri, Erika Gonzalez, Maximilian Strunz, Ilias Angelidis, Ceylan Onursal, Mario Pepe, Stephanie Weiß and Salome Rehm have supported me in many ways and highly contributed in making my time at the CPC memorable. I am especially grateful to Dr. Prajakta Oak for her constant support and motivation.

I dearly thank my parents, my in-laws and my brother for their unconditional help and support, for always encouraging me, and for understanding me at difficult times. My deepest thanks to Ankita Pal, Durba Mukherjee and Sayantani Bhattacharjee for always being a phone call away.

Finally, I would like to thank my husband Ritaja for always standing beside me and keeping me sane throughout these years.